Mechanisms and prediction of climate variability in tropical North Africa

Abebe Yeshanew

Department of Environmental Studies
Faculty of Science
University of Zululand

Thesis submitted to the Faculty of Science in the fulfillment of the requirement for the degree of
Doctor of Philosophy

June 2003

Abstract

One of the monsoon regions of the world is the tropical North Africa. The Sahara Desert lies in contrast with the cool South Atlantic. The monsoon systems control the mean circulation of this region. Superimposed on this basic state, large-scale variability dictates the life of the people and their socio-economic activities. The tropical North Africa climate exhibits a spectral energy mainly in the ENSO and decadal temporal band as revealed by wavelet transform. The lowland Sahelian climate swing reveals low frequency signals. The mountainous regions of tropical Northeast Africa exhibit higher frequency variability. This variability has one common factor: a large-scale east-west overturning that connects the Pacific and Atlantic. An upper-level velocity dipole is established that induces convection polarity between tropical North Africa and South America. The strength and the sign of opposing poles are determined by the Atlantic and Walker Circulations. This is verified using correlation based on longer timeseries (1950-2000). ENSO signal modulates tropical North Africa climate by surpassing other tropical SST through these Circulations. Tropical Atlantic SST modes and Indian Ocean SST dipole influence tropical North Africa climate variability through the connection of Atlantic Circulation. The impacts of these SSTs are more pronounced during non-ENSO years as their influences are masked by global ENSO mode of variability.

The modulation of transverse Monsoon Circulation (in Indian Ocean where Tropical Easterly Jet is the upper limb) on this part of Africa climate operates in phase with Atlantic Circulation. More than 80% of the variance of the Sahelian climate variability is associated to this circulation. It as well imparts equally the Brazilian rainfall following the sign of the Atlantic Circulation velocity potential. One of the aspects that the Indian Ocean differs from other east-west Circulations is that the Monsoon Circulation leads the global ENSO in coherent mode and it explains 60% of the Indo-Pacific SST variation. Locally, the African Easterly Jet determines the north-south moisture and convection between Sahel and Guinea through Hadley Circulation.

To understand the ocean's role in the tropical North Africa and South America convection polarity, subsurface thermocline temperature and heat content are analysed using singular value decomposition, correlation and composite analyses. One of the main results that come from these analyses is that the convection over tropical North Africa and South America are closely tied to subsurface properties of the tropical oceans. The most important ocean signal that is sensitive to Atlantic Zonal Circulation convection is the east-west sea–saw of the equatorial thermocline. The east-west upper-ocean dipole is manifested in the leading EOF modes in thermocline temperature and in heat content anomaly (HCA) in the Pacific Ocean and Indian Ocean. In the Atlantic however, the main climate signal is in the kinematic fields.

In developing predictive equations for tropical North Africa climate variability, stable predictors were found: lower-level Atlantic and Pacific zonal wind. The key factor that leads to high hit rates in the prediction models is the 'memory' and stability of the equatorial ocean winds. The kinematic predictors outperform SST in hindcast fit by 33% with respect to Sahelian climate and river flow. The multi-decadal oscillation of angular momentum is shown to play a role in the predictability.

The study therefore contributes to understanding of the climate variability and prediction of tropical North Africa climate by inclusion of the kinematic component of the climate system that is the means of ENSO transmission to Africa.

DECLARATION

The whole thesis is my original work, unless specifically indicated for the contrary in the text, and has not been submitted in part or whole to any university for a degree purpose. The research work is carried out in the Department of Environmental Studies in the Faculty of Science in the University of Zululand.

University of Zululand, 2002

To my mother, sisters and brothers

Acknowledgment

I am indebted to supervisor Professor Mark Jury for sharing me his knowledge in the subject and always having an open door for discussion. I thank him for awarding a bursary during PhD studies. I thank the staffs of the Department for their support, particularly to Dr. Lawrence T. Dube and Mr. Amos T. Mthembu. I greatly appreciate Anna G. Kozakiewicz, the computer expert of the Department, who has helped me in solving computer-related problems. I also thank Pamela Phkamile, the Secretary of the Department. My thanks also go to my friends Emmanuel Mpeta and Muhammad Matitu who help me to get started. A word of thanks goes to Eliakim Matari and Lukiya Tazalika who share their experience in life.

Special warm words of thanks go to Yeshemebet Ayalew (my mother), Bezaw Endale, Tilaye Yeshanew, Mekuria Yeshanew (my brothers), Arefaine Yeshanew, Tiruwork Yeshanew and Mame Yeshanew (my sisters) who encourage and support me throughout my life. Special thanks go to Mame and Mekuria who have taken the responsibility of the family during my absence. I am grateful to Ato Lemma Guggessa who has given me inspiration to purse my study.

The National Meteorological Services Agency of Ethiopia is thanked for providing study leave.

The data used in this study are obtained from National Center for Environmental Prediction, National Oceanic and Atmospheric Administration, International Research Institute for Climate Prediction, Food and Agriculture Organization, United Nation Environmental Programme, and Indian Institute of Tropical Meteorology.

PREFACE

Climate variability in tropical North Africa influences all walks of life. To tap the available resources optimally it is important to consider an early warning system that ameliorates the impact of climate variability. Understanding the causes of climate variability plays a vital role in a sound mitigation strategy. Our present state of advancement in climate prediction is insufficient to this end. International climate centres are only able to provide a climate outlook after the rainy season has started. A gap exists in understanding of the mechanisms and prediction of the tropical North Africa climate. It is this research problem that drives this is study.

The main goals of this research thesis are to describe and investigate the causes and prediction of the interannual-decadal climate variability in tropical North Africa. To understand the climate fluctuation of this part of Africa, the following objectives are considered:

(i) To identify the mode of variability atmospheric circulation that most affect of the climate of tropical North Africa.

(ii) To unravel the mechanisms responsible for it.

(iii) To identify how the tropical oceans relate to the circulation system influencing tropical North Africa climate.

(iv) To develop prediction models for climate, stream flow and agricultural production over tropical North Africa.

(v) To document the contribution of this study to the advancement of climate and allied sciences.

The thesis entails ten chapters. The first chapter provides a concise account of the background of the research problem, justification, hypothesis, research objectives and motivation of the study. Chapter two is dedicated to a review of present knowledge on climate regimes, mode of variability, mechanisms and state-of-the-art statistical climate prediction. Chapter three documents the

temporal and spatial density of the multi-dimensional data set assembled for this research: observed rainfall and sea surface temperatures, reanalysed atmospheric data, and model assimilated subsurface thermocline temperature and heat content. A hierarchy of methods (multivariate analysis, wavelet based spectral analysis, eigenvector-based analysis) are used to uncover the mechanisms of climate variability in this Chapter. In Chapter four, mean structures of boreal summer circulations are described. Here, the dominant mean upper-level divergent velocity potential circulation pattern is identified. The co-spectral character of the mean circulation and climate in tropical North Africa are also perused in this chapter. The interplay between various kinematics features is studied, mainly with regard to the annual cycle. The interplay between this variability and ocean-atmosphere coupling is revealed in Chapter five through the analysis of interannual residuals in both space and time. The connection between Pacific and Atlantic Circulations is also revealed in this chapter in relation to regional convection patterns.

In Chapter six, the modulation of tropical sea surface temperatures on tropical North Africa climate is studied using composite analysis, correlation analysis and wavelet transform. It is found that ENSO influences tropical North African climate variability not through the thermodynamic, but rather the kinematics component of climate system. Tropical North Africa climate is sensitive to the Atlantic and Indian Ocean through perturbation of Atlantic Zonal Circulation. Two key issues are unlocked. The principal east-west divergent circulations are tuned to ENSO at interannual timescale. The Atlantic Zonal Circulation, Pacific Walker Circulation and transverse Indian Monsoon Circulation contribute to an east-west convection dipole between tropical North Africa/ west Pacific and South America.

In Chapter Seven, modes of variability of equatorial subsurface temperature are investigated using global ocean assimilation data from 1950 to 1999. The most dominant modes of variability are identified using singular value decomposition for the first 250-metre depth of Pacific, Atlantic and Indian oceans. The temporal

component is decomposed into seasonal / annual cycles and interannual timescales using wavelet transform. The interannual timescale of the subsurface ocean temperature is analysed co-spectrally.

In Chapter eight, the prediction models in linear mode are developed for climate, stream flow and agricultural production. Skilful prediction schemes are developed that provide sufficient time for mitigation strategy. It is also found that surface winds in the equatorial oceans have longer memory than sea surface temperature and can be used in climate prediction models. Chapter ten summarises the findings of the study and places its contribution in the context of understanding and prediction of climate variability in tropical North Africa.

TABLE OF CONTENTS

LIST OF FIGURES

LIST OF TABLES

TABLE **PAGE**

CHAPTER 1
INTRODUCTION

1.1 General

The continent of Africa is the largest of all tropical landmasses with a surface area of 30, 313, 000 km^2 and a population of 793, 626 (FAO, 2002 (http://apps.fao.org/page/collections)). It stretches from 39°N to 35°S. The continent includes some of the driest deserts, largest tropical rain forests and highest equatorial mountains in the world (Fig. 1.1). But key natural resources are unevenly distributed. For example, more than 20 per cent of the remaining tropical forest resides in the Democratic Republic of the Congo, while a major share of the continent's water resources are in a few large basins such as the Congo, Niger, Nile and Zambezi Rivers (UNEP, 2000) (Fig. 1.2). These rivers along Senegal River are main African rivers and their mean discharge is shown in Table 1.1. This natural wealth is not however tapped in such a way that it reflects the welfare of the region's inhabitants. One of the major problems common to African countries is the limited benefit accruing from the use of its natural resources such as water, energy, and agriculture potential. In this equation, the disparity in exploiting of these resources is a perplex problem. Striking a balance between economic development and sustainability for the growing population is a major environmental and development challenge (UNEP, 2000). One of the main solutions in sustainable development for agricultural fed economies is to tap the scientific technology reached at present time and to do in-depth studies on climate variability and predictability. Climate predictions can help to use natural resources in a sound way. Some countries and regions are using climate prediction for applications to agriculture and water resources (WCRP, 1997).

In Africa, subsistence agriculture is the foundation of the economy and the major employment sector. It is estimated that more than 50% gross domestic product (GDP) and two-thirds of the jobs are attribute to rain-fed agriculture (Jury,

2001c). Recurrent drought in Africa influences food production, energy and water supply. Food production over Africa has declined since 1970s as illustrated in Fig. 1.3 (UNEP, 2000). This declining trend can be attributed to government mismanagement, political instability, economy of scale (subsides), and to recurrent drought. Declining stream flows (Jury, 2001b); impose pressure on energy and water resources. The shortage of hydropower and rotation of electricity supplies is common practice over this part of the world. What has been happening in Northeast Africa is a typical example of the impact of climate variability on water resources, hydropower energy and agriculture as given in Fig. 1.4. To improve the life of people of Africa, to sustain the limited resources and to tap the vulnerable resources such as agriculture, water and hydropower, an understanding and predicting of hydro-climate and agricultural production variability is a viable solution. Through this, a stable supply of food and water, as well as prosperous economy can be secured. Making use of scientific advances in understanding and predicting the swings of African climate can mitigate half the costs incurred (Jury, 2001b and c).

1.2 Background to the research problem

North of the Equator, rainfall occurs in the June to September as the monsoons encroach and upper easterlies develop. The monsoon systems pump moisture from the Atlantic and to West Africa. For moisture to produce convection and hence rainfall, there must be a low-level convergence and upper level divergence. The Inter-tropical convergence (ITCZ) zone provides the low-level kinematics while at upper level; the Tropical Easterly Jet (TEJ) generates the necessary upper-level dynamics.

The African climate is governed by monsoon circulations extending across large parts of the Atlantic and Indian Oceans. The potential for adequate rainfall depends on the response of the African atmosphere to prevailing global Circulation patterns.

The Atlantic SST dipole, warm in the north and cold in the south, generates an inter-hemispheric pressure gradient and strong monsoon by weakening the Azores High and building up the St. Helena Anticyclone. This hemispheric pressure gradient is conducive for moisture flux to tropical North Africa. Yet we know little about the global circulation and regional ocean patterns interaction.

On this background, notable climate fluctuations are present over tropical North Africa. Decadal rhythms and prolonged drought characterise the climate of sub-Saharan West Africa. The thermal structure of the tropical Atlantic and Pacific Oceans are thought to be the causes for the variability over this part of the globe (Lamb and Pepper, 1978; Lough, 1986; Folland, et al., 1986; Palmer, 1986; Semazzi et al., 1996; Camberlin, 1995). Other studies have also shown that dipole modes of Atlantic (Servain, et. al., 1998) and east-west dipole over Indian Ocean (Saji, et. al., 1999) are determinants of Africa climate variability.

ENSO is thought to be one of the factors that influence African climate and stream flows. ENSO is a phenomenon that is inherently due to the coupling between the atmosphere and ocean (Battisti and Sarachik, 1995). Eltahir and Wang (1999) found a correlation of -0.54 between Nile flow and Nino 3 SST using a longer record from 1871 to 1997. Other studies on the Nile flow also corroborate the effect of ENSO on the natural variability of flow of the Nile (Wang and Eltahir, 1999; Eltahir, 1996; Eltahir and Wang, 1999; Amarasekera, et al., 1997, Quinn, 1992). Rainfall variability over the main source region of Nile is also influenced by ENSO (Camberlin, 1997). According to these studies, warm phases of east Pacific Ocean result into the reduction of the Nile flow. The process that makes this reduction possible is through the atmospheric systems. Jury and Melice (2000) found that the warming in the equatorial east Pacific causes an indirect circulation and sinking motion over much of Africa, including the source of Nile. They also have revealed a common spectral peak at 2.2- 4 years between summer Nile flow and November-March Durban (South Africa) rainfall.

1.3 Justification for research scope

Many African regions are coming to be recognised as having climates that are among the most variable in the world on time-scales of intraseasonal to decadal (Jury, 2001d). However, large gaps exist in the understanding of many features of African Climate (WCRP, 1999; Jury 2001d). In this regard, the plausible physical mechanisms for climate and stream flow swings over tropical North Africa are not yet fully established. There is a considerable scope in understanding, modelling, predicting and developing skill in climate variability over tropical North Africa. The extent of Pacific, Atlantic and Indian SST influence on tropical North Africa climate requires further research (Jury, 2001d). A comprehensive understanding of the role of tropical jet streams and the modulation of regional and global SST on the hydroclimate of tropical North Africa deserve in-depth research. Knowledge of the processes involved in the tropical North Africa climate and the surrounding oceans enhances predictability. Skilful seasonal predictions of rainfall depend largely upon the ability to model the atmospheric response over Africa to global features (Hastenrath et al., 1995; Mason et al., 1996).

In 1995, the World Meteorological Organisation introduced an International research programme called CLIVAR to investigate climate variability and predictability on time-scales from months to decades. The programme addresses key questions pertaining to African Climate variability and predictability that need solutions and attention. The relevant key questions are:

- What coupling processes drive African climate variability?
- How is the global ENSO signal transmitted to Africa and at what lead-time?

Jury (2001d) also reviewed the gaps that exist in the understanding of African climate. Of the issues addressed, paramount points to this study are:

- Circulation over and around Africa remains an important, but inadequately studied component of the global matrix. Several global and regional teleconnection links are to be uncovered.
- Predictability on seasonal to interannual timescale requires a solid understanding of the space-time characterisation of the major climate processes in the African regions.

This study attempts to address these issues to better understand the climate and stream flow over tropical North Africa towards the development of prediction models. This research will advance and contribute to the physical mechanisms and prediction of hydroclimate variability across tropical North Africa. A better understanding of the swings of African hydroclimate contributes to better management of agriculture and water resources. Mitigation of impacts, stemming from hydroclimate (drought, flood, and extreme temperatures), can be achieved through predicting the variability over the region. The socio-economic sectors where hydroclimate variability prediction can contribute are in national planning, water resource, agriculture, industry, health, safety, transport, town planning, communication, tourism and recreation. Environmental prediction is also vital for proper tapping of natural resources towards sustainable development. To achieve and promote these aspects to a high-level, the study of teleconnection mechanisms, ocean-atmosphere coupling and upper-ocean thermocline variability with respect to Africa climate variability and prediction are required. This study sheds light along this line.

1.4 Hypotheses

The central offing of this research lies on testing the hypotheses and meeting the objectives stated in Section 1.5. The hypotheses to be tested are:

a) Anomalous, strong upper level easterly flow and anomalous low-level westerly flow over the equatorial Atlantic produce the necessary dynamics for abundant rainfall and hence excessive stream flow over tropical North Africa during boreal summer.

b) Atlantic East-west over-turning between tropical North Africa and tropical South America drives rainfall in opposing manner during boreal summer.

c) The Walker Circulation over the Pacific Ocean couples with anomalous sea surface temperatures over the East Pacific to create the necessary dynamics for Northern Hemisphere Summer rainfall and flow augmentation over tropical North Africa regions through the upper circulation of the Atlantic Zonal Circulation.

d) The north-south tropical North Africa boreal summer rainfall dipole is controlled by the African Easterly Jet through the north-south overturning.

1.5 Research objectives

The research objectives are classified into the overall and specific. The overall objective of the research and the frame of the objective are summarised in Fig. 1.5.

Overall Objectives

The overall objective is to:

- Understand the mode of variability of boreal summer hydroclimate across tropical North Africa.
- Unravel the physical mechanisms of the major mode of hydro-climate variability across tropical North Africa.
- Develop the hydro-climate predictive models across tropical North Africa at different lead-time.

If the main mode of hydro- climate variability can be revealed, it helps to unfold the physical mechanisms leading to a better understanding of the climate variability. These too proffer the foundation for climate prediction as illustrated in Fig. 1.5.

Specific objectives

The specific objectives of the study for tropical North Africa are:

- Identify the mode of inter-annual variability of wet rainfall activity and high river flow versus dry spells and low river flow in northern hemisphere summer.
- Study the atmospheric circulation, processes and atmospheric-oceanic couplings responsible for inter-annual co-variability of hydro-climate over the Nile Basin.
- Investigate the role of tropical jets disposition and intensity on North Africa hydroclimate.
- Conceptualise the regional/global atmospheric connections (physical links) and processes governing to the inter-annual variability of the hydro-climate across tropical North Africa during boreal summer.
- Investigate the predictability of climate over the tropical North Africa at longer time lead times.

1.6 Motivation

It is apparent that the swing of climate typifies tropical Africa and imposes on various socio-economic sectors. Climate variability causes many multi-faceted problems over this region and predicting this is crucial for a sound mitigation strategy.

The circulation, processes and teleconnection over North African rivers; role of African climate systems in the global circulation, and the influence of temperature anomalies over Atlantic, Indian and Pacific Oceans are not fully understood. The teleconnection between tropical North Africa climate and the tropical jet streams is yet to be examined.

Inter-annual variability of African climate and river flows stream flows is challenging to understand (Servat et al., 1998). One of the problems is that

hydrological fluctuations are not seen in the context of climate that is driving the variability.

These issues identified in Sections 1.2 and 1.3 and the socio-economic implications of understanding the mode of variability and developing skilful prediction models over tropical North Africa drive this research.

1.7 Outline

Chapter 2 provides background on the present state of climate research on tropical Africa and results achieved so far in developing climate prediction models. Chapter 3 gives a space-time overview of the data used in this study and the multitude of techniques in the quest for understanding and predicting the hydroclimate of tropical North Africa. The analysis of the basic state of the atmospheric systems is presented in Chapter 4. The mode of hydroclimate variability and its physical causes are studied in Chapter 5. The modulation of regional and global SST on hydroclimate over tropical North Africa is covered in Chapter 6. The influences and teleconnections of tropical circulations with respect to tropical North Africa climate variability are documented in this Chapter 6. Chapter 7 reports on exciting new research with regard to subsurface tropical ocean structure with respect to North Africa rainfall, using ocean data assimilation products. Chapter 8 dwells on the statistical linear prediction models developed for tropical North Africa climate variability at longer lead times. The overall results of the study and its main contribution to science and socio-economic implications are reported in Chapter 9.

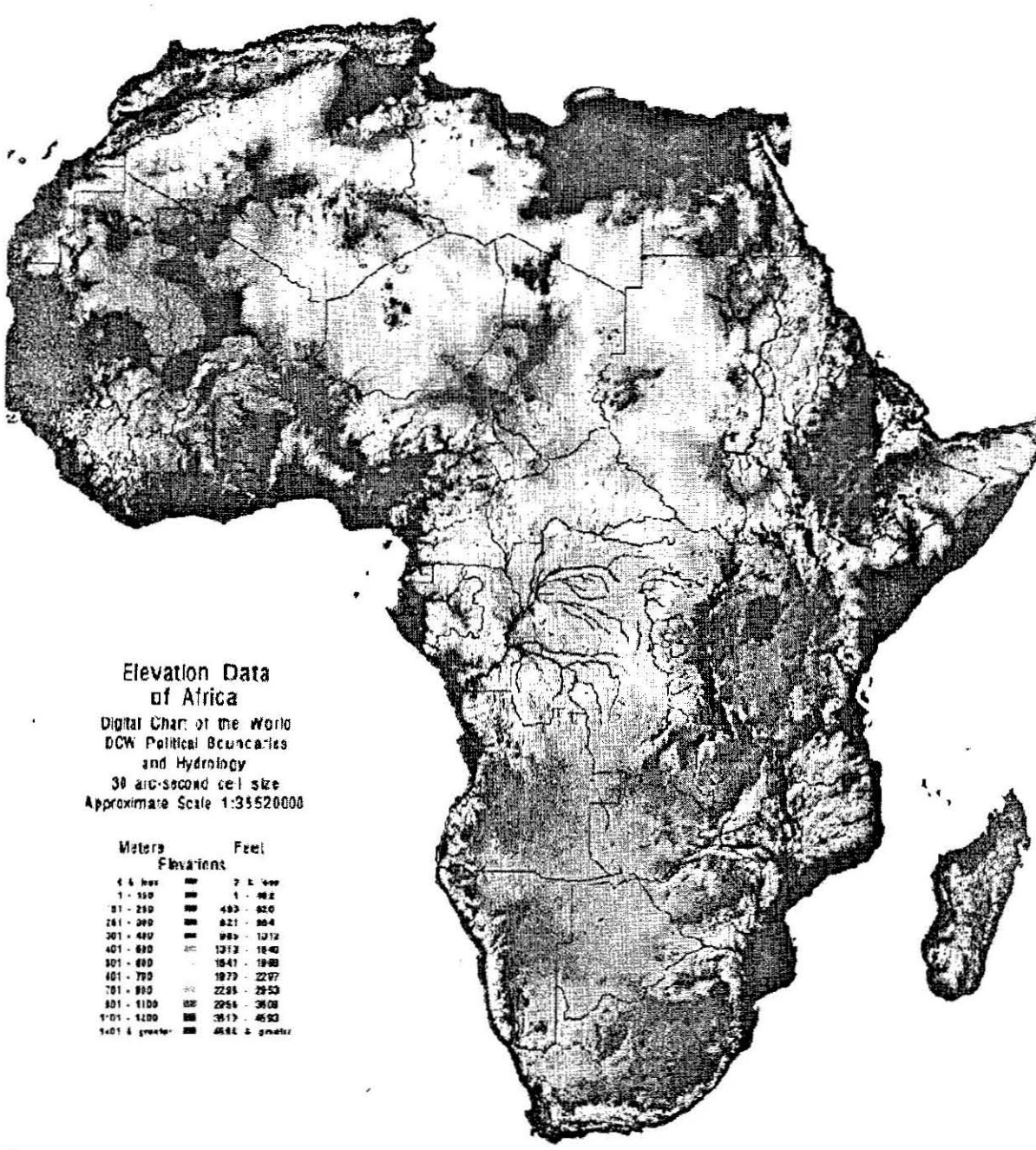

Fig. 1.1 Topography of Africa.

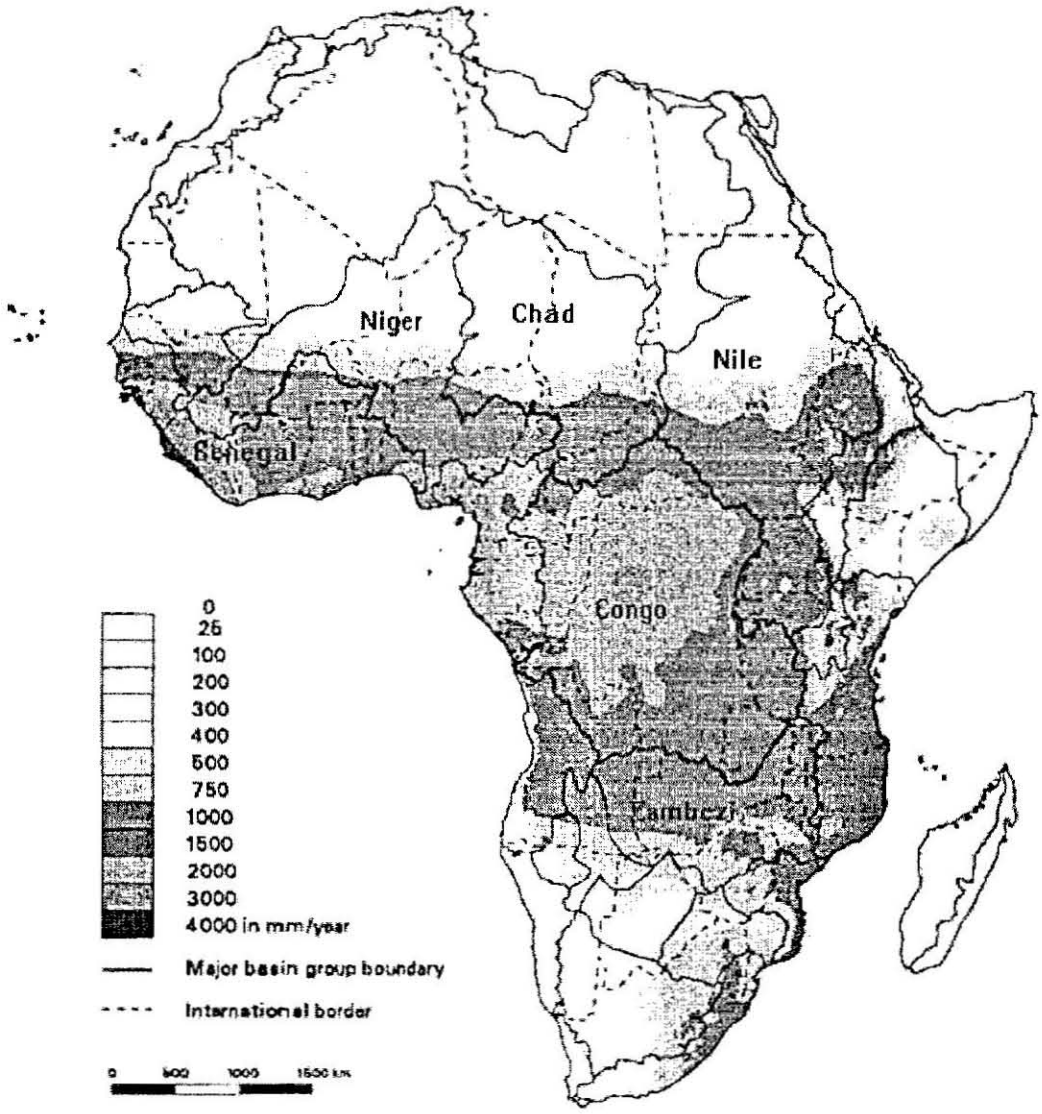

Fig.1.2 Major river basins of Africa and mean annual rainfall (mm/year). Mean discharge ($m^3 s^{-1}$)for the main rivers($mm\ yr^{-1}$) is shown in Table 1.1.

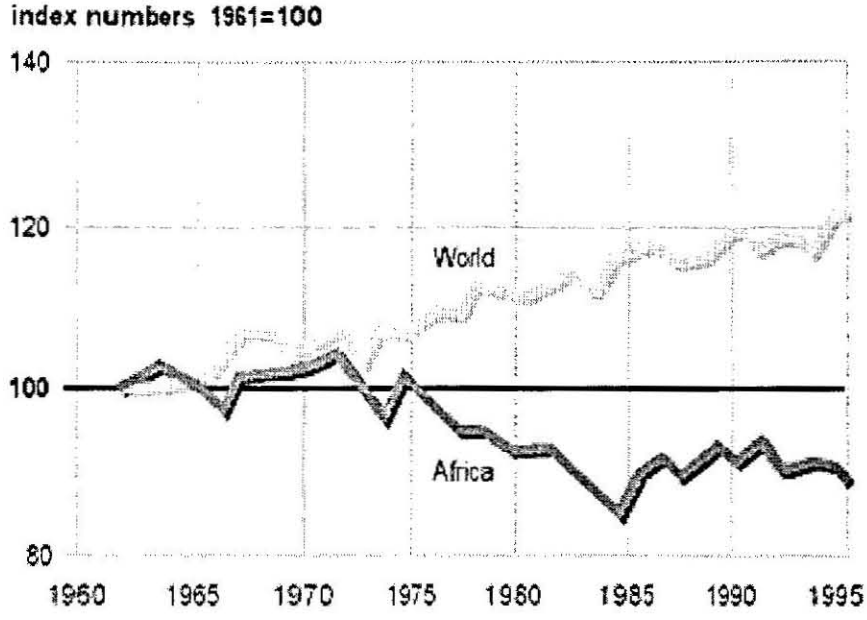

Sources: http://www.unep.org/geo2000/english/0053.htm

Fig.1.3 Food production (standardized with respect to 1961) per capita showing the decline of food production over Africa for the last three decades. This decline trend corresponds well with the decline rainfall trend of over most parts of Africa.

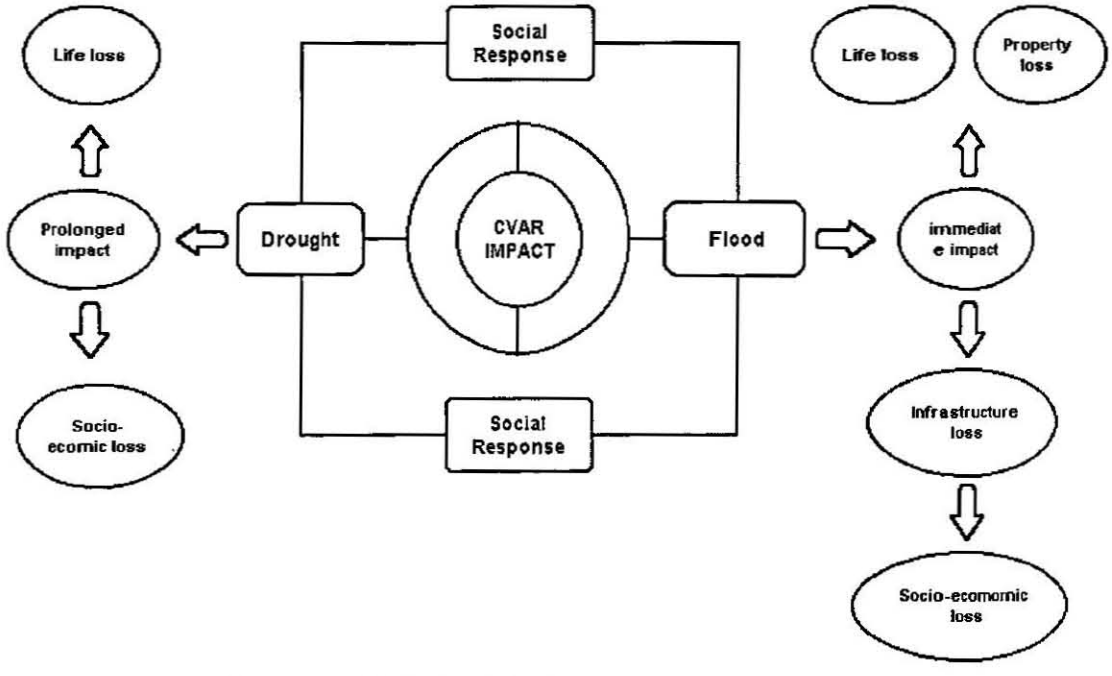

Fig. 1.4 Impacts of climate variability without climate prediction based mitigation strategy. The detail of this is given in Table 1.2

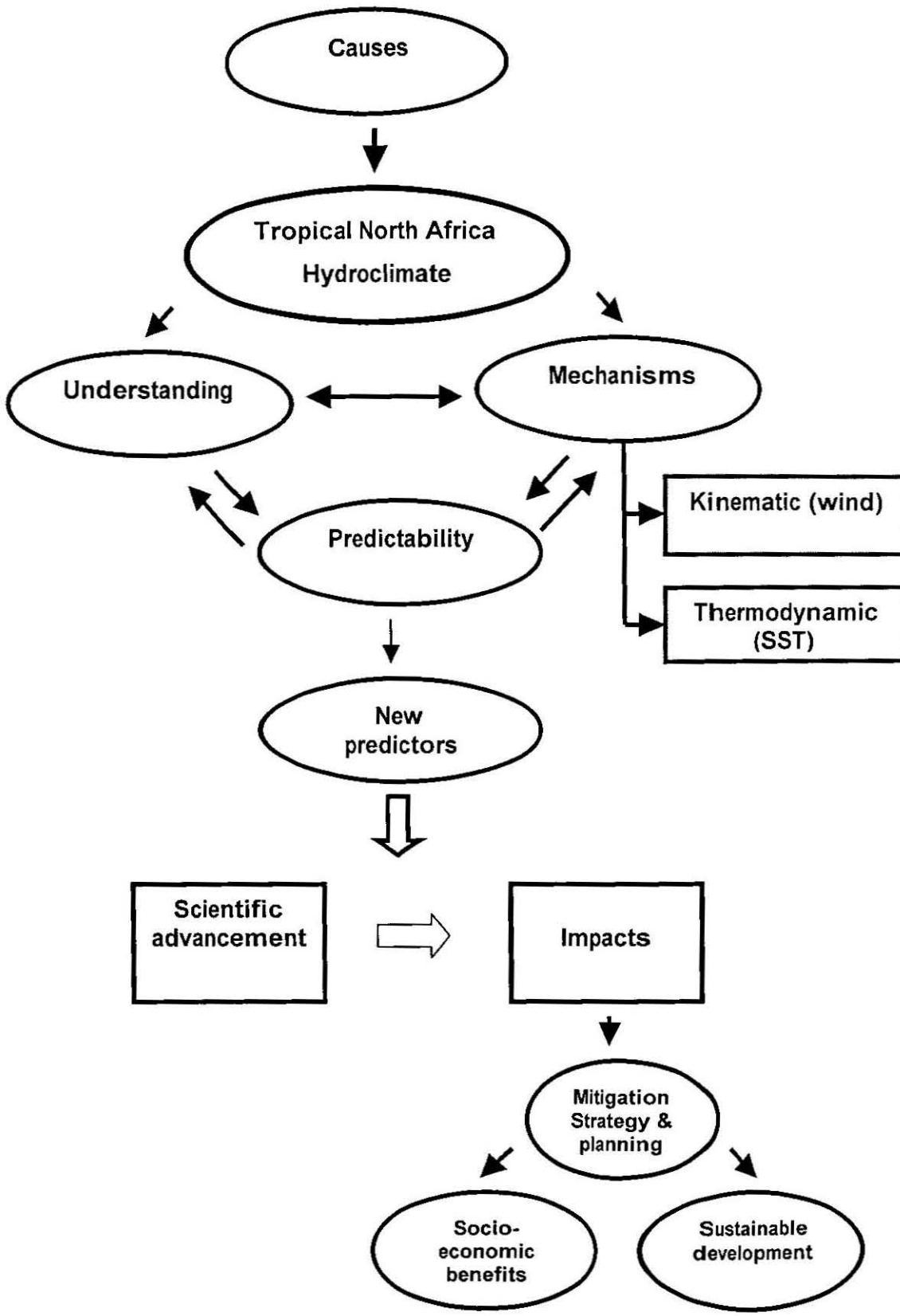

Fig. 1.5 The overall objects of the study and the expected contributions.

Table 1.1 Mean discharge (10^3 m^3/s) for main African rivers (Sources: Soil and Water Conservarion of Metro Halifax, 1998: http://lakes.chebucto.org /rivers.html)

MAIN AFRICAN RIVERS	MEAN DISCHARGE (10^3 m^3s^{-1})
Congo	39.7
Zambezi	7.1
Niger	6.1
Nile	2.8
Senegal	0.9

Table 1.2 Consequences of climate variability without the use of climate prediction in early warning and mitigation strategy in reference to Fig. 1.4.

1	DROUGHT TYPES	IMPACTS OF CLIMATE VARIABILITY
2	Meteorological drought	Persistent below normal rainfall leads to agriculture and hydrological drought.
3	Agriculture drought	Inadequate soil moistures leads to: • Crop failure and animals (cattle, sheep, goat) perish, • High prices for agriculture products, • Starvation and famine, and • Social upheavals.
4	Hydrological drought	a) Impacts on hydropower and industry • Reduced stream-flow and levels of reservoirs, • Inadequate performance of hydropower, • Limited time for electric power distribution, • Limited time for industrial production, and • High price for industrial goods. b) Water supply and health • Limited distribution of water in quotas drinking and washing; • Health epidemics and • Social upheavals.

CHAPTER 2
LITERATURE REVIEW

2.1 Introduction

A primary focus of this Chapter is to document previous studies done on tropical North Africa climate systems, their mode of climate variability and identified physical mechanisms. The various analysis methods used in climate prediction are recorded. The status of the representation of Africa climate by numerical simulation is discussed and a concise treatise on applications in climate is covered.

2.2 Climate regimes and climate systems

a) Climate regions

Over tropical North Africa, rainfall is a limiting factor for socio-economic activity and an indicator of climate variability. Over this region, maximum rainfall occurs during boreal summer (June to September). The main rainfall activity is confined between 15°N to 0° and 18°E to 40°E forming a V shape in the equatorial zone. Sahara Desert dominates north of 15°N. South of the equator, dry spell prevails during boreal summer.

Various researchers have mapped out the rainfall regions over tropical North Africa. Particular attention has been given in this regard to West Africa and Sahel regions. Nicholson (1998) delineated five rainfall regions over West Africa to understand the Interannual and inter-decadal rainfall variability (Fig. 2.1a). The rainfall timeseries from 1901-1990 for these regions is shown in Fig. 2.1a. Low frequency variability dominates the timeseries with rainfall decline in the 1960s and 1970s. Nicholson and Grist (2001) regionalised tropical North Africa into 90 rainfall regions. Regionalisation into small areas may conceal the uptake of remote teleconnections such as ENSO.

To predict rainfall over tropical North Africa UK (United Kingdome) Met Office uses four rainfall regions. These regions reflect the north-south rainfall gradients of West Africa. There the regionalisation does not incorporate the Northeast (Nile Basin) and northern Congo Basin. In view of this, the UK regionalisation is not consulted in this study.

Landsea et al. (1998) used Sahel and Guinea Coast rainfall. This classification incorporates the east - west and the north-south rainfall patterns (Fig. 2.2b). However, the rainfall delineation does not cover eastern and southern regions – as it was aimed at Atlantic Hurricane activity. Analysis based on wavelet transform based band-pass filter and a hundred years of record reveal a multi-decadal signal in Sahel rainfall (Fig. 2.1c).

Jury and Philipp (2002) identified fifteen rainfall regions of Africa using continuous monthly rainfall of the Climate Research Unit of University of East Angela gridded at 0.5° (latitude and longitude) resolution and varimax rotated principal component (Fig. 2.2a). The regionalisation is done in such a way that the uptake of remote influences is preserved. The rainfall regimes for tropical North Africa are considered in this study. The regions, which are given particular attention, are Region 1 (East Sahel), Region 3 (Guinea Coast), Region 8 (West Sahel), Region 9 (North Congo), and Region 11 (mainly Ethiopia). The rainfall timeseries are shown in Fig. 2.2b. It reveals the interannual timescale variability from 1950 to 1998.These timeseries data from Jury and Phillip (2002) are used to pursue an understanding of the variability of tropical North Africa climate.

b) Climate Systems

Tropical North Africa Climate system is characterised by a large-scale reversal of winds. This characteristic qualifies tropical North Africa to be part of the monsoon systems (Fig. 2.3). Monsoon systems are predominantly tropical phenomena. During boreal summer an inter-hemispheric sea-surface temperature gradient is

produced over the Atlantic Ocean. Warm SST in the northern part induces a thermal trough called the inter-tropical convergence zone. In the south due to cooling, the St. Helena high-pressure established as a quasi-permanent system. The thermal low over West Africa and the high- pressure the South Atlantic produce an inter-hemispheric pressure gradient. The pressure gradient pumps moistures to tropical North Africa. The moisture is lifted dynamically in the inter-tropical convergence zone supported by upper-level divergence in the generation of deep convection. The dynamical lifting is "pulsed" by Tropical Easterly Jet. Africa easterly jet contributes to the development of squall lines across West Africa. The principal climate systems of tropical North Africa are depicted in Fig. 2.4.

Over the other side of Africa, Indian Ocean along the Asian continent plays important roles in establishing the southwest Indian monsoon. During boreal summer, western parts of Asia are warm due to the overhead sun, while the tropical South Indian Ocean is cooled by evaporation. The South Indian Ocean becomes favourable for building up of the quasi-permanent Mascarene High-pressure system. The warm land surface over India establishes a low-pressure belt as an extension of the inter-tropical convergence zone. As a result, inter-hemispheric pressure gradient is developed to generate a strong monsoon flow at lower level transporting moisture from the Indian Ocean northwards. The strong low-level monsoon flow is called the Somali Jet. It produces subsidence over the Horn of Africa (Fig. 4.4a). The tropical systems tilt with height in the north-south direction. Baroclinic instability plays pivotal role in the development and characteristics of Africa Easterly Jet over West Africa (Thorncroft, 1995; Thorncroft and Hoskins, 1994).

2.3 Mode of climate variability

Modes of climate variability occur at various time-scales and involve either thermodynamic or kinematic process. Land interaction is a salient feature at the

decadal time-scale. In the ocean-atmospheric coupling, El Nino-Southern Oscillation (ENSO) is the most important signal (Philander, 1990).

A number of studies have been done on tropical North Africa in the context of Sahel rainfall characteristics. Nicholson (1998) studied the mode of rainfall variability over West Africa and Guinea from 1901-1996. The standardised time-evolution of the rainfall over these regions is presented in Fig. 2.1a. In all of these rainfall regions, the rainfall fluctuation is dominated by a decreasing trend starting around 1960. The period portrays the drought years of Sahel and the surrounding regions. The 1950s and early 1960s are considered the wet period for west and Guinea Coast. Landsea et al. (1998) also studied boreal summer rainfall variability over the Sahel-Guinea region.

The decadal rhythms and the prolonged drought in the sub-Saharan zone are well documented (Lamb 1978a,b; 1979, 1980,1982a,b, 1983; Nicholson 1981, 1993,1998). Since the end of the 1960s, the Sahel region has experienced a persistent downward trend in rainfall (Lamb 1978; Nicholson and Palao, 1993; Nicholson 1998). Recently this trend has reversed (e.g. 1999 onward).

2.4 Mechanisms of climate variability

Studies done on the causes of climate variability of tropical North Africa are reviewed below.

2.4.1 West Africa

Various ocean-atmosphere mechanisms and boundary forcing have been identified from observational and numerical model analyses. The causes of Sahel and West Africa rainfall variability are often attributed to the north-south Atlantic SST Pattern (Lough, 1986; Palmer, 1986; Semazzi et al., 1996). Fontaine et al. (1998) linked persistent dry condition over Sahel to warm phases of the global

SST mode that shows cold SST in the northern tropical Atlantic and warm in southern tropical Atlantic.

Fontaine (1998) found that the West African rainfall drought could be accounted due to the generation of subsidence in the mid-troposphere. A southward extension of upper level easterlies and a decrease of upper-level meridional diffulence in the Hadley Circulation are considered as cause for droughts over Sahelian and Guinea regions (Fontaine et al., 1995). The seasonal rainfall and associated convective heating are related to the seasonal anomalies of African Easterly Jet wave activity (Thorncroft et al., 1998). Grist et al. (2002) provided a new insight to explain the causes for wet episodes of Wet Africa. Their results show a fast growth rate and high phase speeds of the easterly wave in wet years over West Africa. In analysing the instability of the easterly waves, they also found a significant increase in the barotropic term of the instability in wet episodes. During the persistent dry period, the barotropic and baroclinic terms are comparable.

To get a better insight to the Sahel rainfall variability, general circulation model simulations have been given attention. Rowell et al. (1992) modelled the influence of global sea surface temperature on the variability and predictability of seasonal rainfall. The results of their experiment support the idea that ocean thermodynamic effects tend to dominate the forcing of both interannual and interdecadal variability of Sahel rainfall. They found the June SST anomaly to be a skilful predictor of boreal summer rainfall of Sahel. The relationship between Sahel and Guinea coast rainfall is a research problem in atmospheric sciences. Rowell et al. (1995) found a dipole structure between these two tropical North Africa regions. The spatial dipole configuration is the most common pattern in tropical North Africa west of 15°E (Nicholson and Grist, 2001; Jury, 2001d). The decade 1950-1959 was characterised by above-normal precipitation over most of Africa, although rainfall deficiencies prevailed over the near-equatorial region. This rainfall anomaly pattern dramatically reversed in sign in 1960-1969 while the

equatorial region experienced widespread abundance of rainfall. These two time periods also coincide with a reversal in the sign of the Sahelian rainfall anomalies (Lamb and Peppler, 1992). At interannual time-scale, Ward (1998) found the association between Guinea rainfall and equatorial Atlantic Sea surface temperature to be robust.

There is ample evidence that drought and wet periods are forced by global sea surface temperature changes. On a year to year basis, ENSO with its alterations of tropical Pacific sea surface temperature leads to drier Sahel rainfall conditions during warm events and more rain in cold events (Palmer et al., 1992; Ward 1992; Janicot, et al., 1988). Of note is the more frequent occurrence of moderate to strong El Niños (e.g. warm events) during the 1980s and 1990s, contributing both to decreased Sahel rainfall and lowers Atlantic basin hurricane activity. On a multidecadal time scale, a warmer southern and cooler northern Atlantic sea surface temperature leads to the long-term Sahel drought episodes (Folland et al., 1986; Follander et al., 1991). Sahelian rainfall variability is also closely linked to the latitudinal position of the inter-tropical convergence zone and the meridional SST gradient in tropical Atlantic (Tourre and Lamb, 1997 in http://www/clivar.org). Eltahir and Gong (1996) proposed entropy for describing the interannual variability of West Africa. This theory predicts that a large meridional gradient of boundary-layer entropy results in a strong monsoon circulation (hence wet condition) while a flat distribution of entropy leads to a weaker monsoon (dry condition). Sahel response to entropy is tantamount to the modulation of Atlantic meridional SST gradient to Sahel rainfall. Other studies also show that in boreal summer, El Nino events enhance the northeasterly trades over the tropical North Africa, weaker Guinea flow and upper level easterly. As a result, dry conditions prevail over West Africa (Camberlin et al., 2001; Hastenrath, 2000; Grist and Nicholson, 2001).

Ocean-atmosphere coupling systems do not provide the complete answer for the causes of drought that has been affecting Sahel to West Africa for the last three

decades. The idea of positive feedback mechanism between vegetation cover and albedo is gathering momentum to explain the interdecadal climate variability of Sahel. Charney (1975) and Charney et al (1977) initiated the hypothesis of positive feedback mechanisms between albedo-rainfall-vegetation cover. A number of researchers pursue in this line to unlock the mystery of the multidecadal Sahel rainfall mechanisms (Cunnington and Rowntree, 1986; Xue et al., 1990; Zeng and Eltahir, 1997, 1998; Zeng et al., 1999).

The rainfall over the West Africa Sahel region shows a multidecadal-drying trend (Zeng et al, 1999). Causes proposed to explain this dramatic trend include global sea surface temperature variation (Folland, et al.1986; Rowell, et al., 1995; Semazzi, 1996) and land use change, that is, deserification processes (Xue and Shukla, 1993; Dimeyer and Shukla, 1996). This trend could be part of an 80-1000-year cycle in African climate (Tyson, 2001).

Using a coupled climate-vegetation mode, Xue, et al. (1990) showed that the existence of a significant feedback in the climate system. The simulation responses to temperature and zonal wind agree with dry years of climate when the model is forced with an expanded desert. Studies on this line continue to further knowledge on the bio-geophysical feedback on Africa climate. Xue et al. (1993) run the general circulation model consists of five pairs of integration with different initial condition and SST boundary conditions that reduce the moisture flux convergence and rainfall over Sahel while increases occur over to the southern (Guinea Coast). The result of this simulation is consistent with the observed anomaly dipole pattern between Sahel and Guinea. The land surface change influenced the circulation over the region. As a result the tropical easterly jet was weaker and the Africa easterly jet was stronger than normal. Various scientists have been conducting series of general circulation experiments to explain the interdecadal climate variability of Sahel. Recently, Zeng et al. (1999) explored the role of naturally varying vegetation in influencing the Sahel rainfall using a coupled ocean-atmosphere-land-vegetation model. The atmospheric-

ocean coupling experiment explained the low frequency variability of Sahel rainfall (Fig. 2.5). The land-surface feedback is found to increase the interannual and decadal Sahel rainfall variability. Yet, the interactive vegetation simulation fails to be in phase relationship with the observed rainfall. Additionally the role of ocean-atmosphere coupling in the modulation of Sahel rainfall needs to be considered. In a similar line, Zeng et al. (2000) performed an experiment using a coupled atmosphere-land-vegetation model to find out the role of vegetation-climate interaction and interannual variability in shaping the Africa Savannah. When observed climatological SST forced the model, positive feedback from vegetation changes tends to increase the spatial gradient between the desert region along the gradient and forest regions. When the interannual variation of SST is included, the climate variability tends to reduce rainfall and vegetation in the wetter regions and increase in the drier regions.

Understanding the West African climate using the feedback between SST, albedo and the monsoon circulation is also gaining attention. A change in Atlantic sea surface temperature is shown to produce a positive feedback between West Africa monsoon, vegetation and albedo. Cooler SST in the north and warmer SST in the south Atlantic Basin shift the ITCZ south and weaken the West Africa monsoon circulation. This in turn perturbs the vegetation and as a result the surface assumes a higher albedo. The high albedo produces a weaker West Africa monsoon system. Several experiments have been conducted in the same line to investigate the role of vegetation distribution in the atmospheric dynamics of West Africa monsoon and to determine how the atmosphere responds to the changes in the lower boundary condition. In this regard, changes in vegetation cover along the southern coast of West Africa (deforestation) results in the weakening of the monsoon (Zeng and Eltahir, 1998). However, a vegetation perturbation along edge of the Sahara had a minor impact on the simulated monsoon circulation.

2.4.2 Northeast Africa

The impact of year-to-year climate fluctuations in Northeast Africa is one of the most publicised issues around the world. Pronounced variability is a fingerprint of Northeast Africa. Its impact is enormous and the entire population's livelihood and well-being suffers as a result.

This part of Africa is characterised by a diversified climate; high elevations (the Ethiopian mountains), and is the semi-arid in nature. It is over the Ethiopian mountainous that more than 80% of the Nile flow derives. In spite of this, limited attention is given to understand the climate variability and prediction of this region. In recent times, the fluctuation of Nile flow has been linked to ocean-atmosphere coupling (Quinn, 1992, Eltahir, 1996; Eltahir and Wang, 1999; Wang and Eltahir, 1999; Jury, 1999). According to Eltahir (1996) the global ENSO accounts for 30% the variance of Nile flow variability based on 127 years data. Based on this result, Wang and Eltahir (1999) established a 2-3 month prediction model with forecast index (FI) of 0.45. A perfect forecast has an FI of 1.0. Bliss (1925) first identified the association between the Nile in the context of the Southern Oscillation. Jury (1999) provided a new avenue to understand the Africa rainfall variability with respect to ocean-climate composite structures. This approach is very important to identify coherent features that govern the river fluctuations over Africa. He showed that Africa rivers stream flow variability is sensitive to the coupling between the quasi-zonal circulations over the tropical Atlantic, the global ENSO phase and the Atlantic dipole. According to this result, a warming in the equatorial east pacific causes sinking motion over the source of Nile and a reduction inflow for all major rivers in Africa.

It is only since 1990 has much research focused on Northeast Africa climate variability. Most of the research publications are due to Camberlin (1995, 1997, and 2001) and Seleshi (1991 and 1996). The results obtained from Camberlin (1995) show that the occurrence of drought over Ethiopia and Uganda is

attributed to El Nino and high-pressure over India. Camberlin (1997) established the association between the Southwestern monsoon and Northeast Africa rainfall variability and suggested that monsoon activity over India is a major trigger for boreal summer rainfall variability over the East Africa highlands. A study by Shanko and Camberlin associated the high frequency of occurrence of tropical cyclones in the Southwest Indian Ocean with Ethiopian drought, particularly during February - March rainy season. In the study on the teleconnection between tropical North Africa rainfall and SST variation over Atlantic and Pacific basins (Camberlin et al, 2001), the ENSO impact on boreal summer rainfall over Ethiopia is again corroborated. Teleconnection refers to the exertion of tropical SST anomalies on the climate remote from the source region through intermediary circulations.

2.5 Climate prediction and associated techniques

Statistical climate prediction involves diagnostic studies, selecting prediction candidates, developing the prediction model and validating the forecast. In this Section, the climate predictability and statistical climate prediction techniques are covered.

2.5.1 Climate predictability

It has been long realised that accurate observation of the initial atmospheric state is crucial for short and medium-range forecasting (Thompson, 1957; Lorenz, 1963,1984,1990; Shukla, 1981; Reinhold, 1987; Palmer and Anderson, 1994). For long-range forecasting, the initial boundary condition is important. When the thermal inertia of the upper ocean or the land surface are dynamically coupled to the atmosphere and allowed to evolve at a longer time scale, predictability can be attainable (Rosati et al, 1997; Zeng et al., 1999).

The tropical Pacific Ocean SST is widely used in Climate prediction. Over much of the tropical Pacific Ocean, the decorrelation time scale of SST variability is about one year, where ENSO events dominate the variability (Goddard et al, 2001). ENSO is the most prominent mode of climate variability at interannual timescale and is recognised as an important manifestation of tropical ocean-atmosphere-land coupled system (Yamagata, 2001). The highest amplitude of thermodynamic component of the ENSO signals is depicted in the Nino regions (east and central Pacific regions). The Kinematic component is represented by the pressure difference between Tahiti and Darwin, known as the Southern Oscillation.

All scales of atmospheric motion are involved in the transfer of energy between the ocean and the atmosphere, and most of the atmospheric phenomena respond (directly or indirectly) to the seas surface temperature (Wells, 1998). The ENSO response to atmospheric circulation is transmitted through redistribution of surface heating that drive tropical convection and subsequent atmospheric heating that drives anomalous atmospheric circulation at the global scale (Goddard et al, 2001). The ENSO signal or influence is transmitted to teleconnected regions via zonal winds.

Any perturbation in the atmospheric circulation due to warming or cooling of the central and east Pacific Ocean results in a re-orientation of rainfall characteristics over tropical regions. During an ENSO event, approximately one third of the land areas of the globe have predictable effect (http:/iri.columbi.edu/climate/toturial2/index.htm). Ropelewski and Halpert (1987, 1989) broadly identify ENSO sensitive regions of the world in respect to rainfall. The recognised effect of ENSO on Northeast Africa rainfall is not accommodated in the Ropelewski and Halpert findings.

Other SST Indices that reflects the ENSO signal over the Pacific Ocean are available. These are Nino 3.5 (5°N-5°S, 170°-120°W) (http://www.cpc.ncep.

noaa.gov/data/cddb/), Wright S index (http://www.csrl.ars.usda.gov/wewc/enso&ag/WrightsS.htm), cold tongue Index (6°S-6°N, 180°W, 90°W) (http://tao.atmos.Washington.edu/data_sets/cti/) and Multivariate ENSO index (tropical Pacific Ocean). These indices, like Nino 3 index, have been used to statistically predict climate and resources (agriculture and water).

Other tropical oceans play in the modulation of climate variability and predictability. A change in Atlantic meridional SST gradient shifts the ITCZ position north or south whether the sign of the gradient is positive or negative. Cooler tropical North Atlantic and warmer tropical South Atlantic shifts the ITCZ south to its mean conditions. In response to this, convection shifts south in favour of Brazil (Hasternrath and Lamb, 1977; Markham and McLain, 1977; Moura and Shukla, 1981) and Guinea Coast (Folland et al, 1986, Semazzi et al., 1988; Lamb and Pepper, 1992; Ward, 1998).

A second mode of variability in the tropical Atlantic is the equatorial Atlantic SST (eqaSST) and evolves similarly but independently to ENSO but independent of ENSO (Goddard et al, 2001). This mode is most pronounced in boreal summer and affects the Gulf of Guinea region (Wanger and da Silva, 1994), parts of central Africa (Hist and Hasternrath, 1983; Nicholson and Entekhabi, 1987) and southern Africa (Jury, 1996).

In the tropical Indian Ocean, a SST dipole between Sumatra and the western Indian Ocean has been shown to induce the rainfall variability over the east and west. The Indian Dipole mode index (IOD) has been introduced by Saji et al. (1999). Using a coupled GCM (General Circulation model), Iizuka (2001) showed that the IOD is characterised by anomalous cooling of sea surface temperature in the southeast tropical Indian Ocean and anomalous warming SST in the western tropical Indian Ocean. In association with this ocean-atmospheric coupling, an anomalous easterly wind develops in the equatorial Indian east Ocean. As a result convection is suppressed (enhanced) in the east (west).

The independence of the Indian SST dipole from ENSO has yet to be established. Yamagata and his collaborators (2001) stated that IOD is a physical mode involving dynamics over the tropical Ocean that may give birth to an inherent coupled mode. Modelling studies show evidence of atmospheric changes induced by ENSO events capable of affecting the Indian Ocean (Venzke, et al., 2000). Li et al. (2001) showed that IOD is damped air-sea coupled mode triggered by various external forcing such as ENSO and intra-seasonal oscillation (ISO). They simulated the IOD in the presence of realistic ENSO and ISO using coupled model. The IOD can be thought to be a Rossby wave that offers predictive potential for climate variability in the surrounding countries (Jury, 2001a and Xie et al., 2002).

2.5.2 Statistical climate prediction techniques

Progresses have been achieved in predicting climate variability over the tropics due to the high thermal inertia of the ocean that allows it to retain heat for a long period of time. Due to this long 'memory', prediction beyond the limit of general circulation model capacity is possible in the tropics.

To predict climate variability over different parts of the world, various statistical climate models have been used. The Indian Meteorological Department has been developing diversified models to predict boreal summer monsoon rainfall (http://www.met.reading.ac.uk/cag/MOL/Monsoon/year2000/imd2K.html). Power regression and parametric model are employed. Operationally, five different types of experimental model have been developed. These are multiple regression model, dynamic stochastic transfer models, power transfer models, principal component regression and artificial neural network. The principal component regression can be consulted in Vautard et al. (1999) and neural network is documented in Tangang el al (1998), Hsieh and Tang (1998) and Tang, et al., 1998.

A generalised multiple regression model, canonical correlation analysis (CCA), may be applied as a statistical forecast tool when observations of the predictor field precede the observation of predictand field in time (Barnston and Ropelewski, 1992; Barnston, 1994; Barnston and Smith, 1995, Barnston et al., 1996). CCA can be viewed as vector multiple regressions. A detailed inter-comparison of coupled eigenvector techniques entailing the CCA is documented by Bretherton et al. (1992).

Another eigenvector based multivariate technique used to forecast rainfall over Sahel and Northeast Brazil is discriminant analysis. Since the 1986 the United Kingdom Met office has been using discriminant analysis to forecast Sahel rainfall (Folland et al., 1991).

The above statistical climate model techniques require computational capacity and are run as a "black box". The selection of predictors is chosen automatically and the problem of collinearity does not arise. The alternative statistical climate prediction technique is stepwise regression that bases on set predictors. Stepwise regression is one of the most commonly used statistics in Africa climate variability prediction (Jury et al., 1997; Jury et al., 2001b; Camberlin et al., 2001). Stepwise regression is used in this study to construct climate, stream flow and agricultural production multivariate linear models.

2.5.3 Application of climate prediction

Climate prediction science has progressed in recent years in providing skilful prediction up to a year ahead. As result of this development, the application of climate prediction is growing enormously. Reliable prediction has far-reaching applications from saving life and property to planning to take alternative measures in mitigation the impact of extreme climate variability. In doing so the socio-economic cost of climate fluctuation can be reduces (Glanz et a, 1991; Glanz, 1996; Moura a and Sarachik, 1997; WCRP, 1999; Jury, 2001c). The uses

of the climate predictions increase as the prediction is tailored to area of application and resource specific (agriculture, water resource, health and the likes). Predicting onset of malaria using climate variable over malaria prone regions can save million of lives. Hydroclimate prediction has paramount importance in water resource management and in hydropower distribution. Offering agrometeorological prediction plays a decisive role in agricultural activity (in determination of the planting dates, delineating agroclimatic zones, providing agrometeorological information for intervention of farmers during adverse weather and the likes) (Hammer et al., 2000). Other socio-economic sectors that can benefit from climate prediction are construction, transport, tourism, and telecommunication. Moreover, an advance warning of drought risk and seasonal rainfall prospects are believed to improve the economic growth potential of a county and to provide additional security for food and water supply (Jury, 1999).

2.6 Summary

Boreal summer rainfall over tropical North Africa is dictated by monsoon systems. The people living over this part of the globe depend on the monsoon rainfall. However, the rainfall fluctuation has been showing a decline trend up to the mid-1990s. West Africa has been facing a persistent drought since 1968. Researches have been trying to understand the causes of the prolonged drought over Sahel. Possible explanations for this unprecedented below normal rainfall for the last three decades are given based observation studies, ocean-atmospheric general circulation model and -atmospheric-land interactions. At high frequency, enhanced northeasterly wind, strong Africa easterly jet, feeble tropical easterly jet and weak monsoon flow result into low rainfall during boreal summer. At low frequency, changes in global sea surface temperature, alternation in the meridional Atlantic SST dipole, and a flat distribution of entropy are thought to account for the Sahel rainfall variability. Simulation studies in ocean-atmosphere-land interaction produce multi-decadal rainfall variability. An example to this is the work of Zeng and Eltahir (1998), where a positive feedback

between the feeble monsoon, albedo and vegetation cover is established. The mechanisms attributed to climate variability of Sahel are schematically represented in Fig. 2.6. This reveals the key causes of Sahel at high and the low frequency variability identified in the literature.

A number of studies are done to understand the causes of Nile stream flow fluctuation. The results of these studies reveal that 30% the variability comes from ocean-atmospheric coupling from the east Pacific Ocean. The warm of phase of ENSO affects Northeast Africa rainfall variability. In El Nino years, the tropical easterly jet weakens consequently the rainfall over Northeast Africa is reduced. According to Camberlin (1997, 2001), the Atlantic and Indian monsoons play a role in modulating the rainfall over Northeast Africa.

Climate predictability over tropical North Africa comes from the boundary conditions while initial conditions are important for short range forecasting. The tropical ocean has high thermal inertia that renders climate prediction up to a year in advance. Using ENSO information and SST over the Atlantic and Indian Ocean, climate prediction over Africa is achieved. In recent time, it is recognised that atmosphere variables over tropical oceans are as skilful as SST indices (Jury, 1997). The presence of ocean Rossby waves is believed to enhance predictive in climate variability (Jury, 2001a; Xie et al., 2002).

Progress has been achieved to develop statistical climate prediction schemes. In climate science, use is made of multivariate linear models to develop prediction equations. Of this, a straightforward approach is the stepwise regression. Eigenvector based statistical prediction are widely used in climate prediction. CCA falls in this category. Non-linear models such as neural network are blooming to predict SST (Tang and Hsieh, 2002; Wu and Hsieh, 2002; Tang et al., 1998; Tangang et al., 1998). When the linear statistical model skill saturates non-linear models can provide is a solution towards improving climate prediction.

The principal issue is then what does this study contribute compared to what is already known. Climate variability and prediction is a cutting-edge research problem in the science. Understanding the mode of variability of tropical North Africa in the global and local context is not yet achieved. Here thermodynamic and kinematics predictors of tropical North Africa climate are established. Modes of teleconnection with respect to tropical North Africa climate are recognised through the use of quality data and robust methodologies underpinned by conceptualising the processes involved.

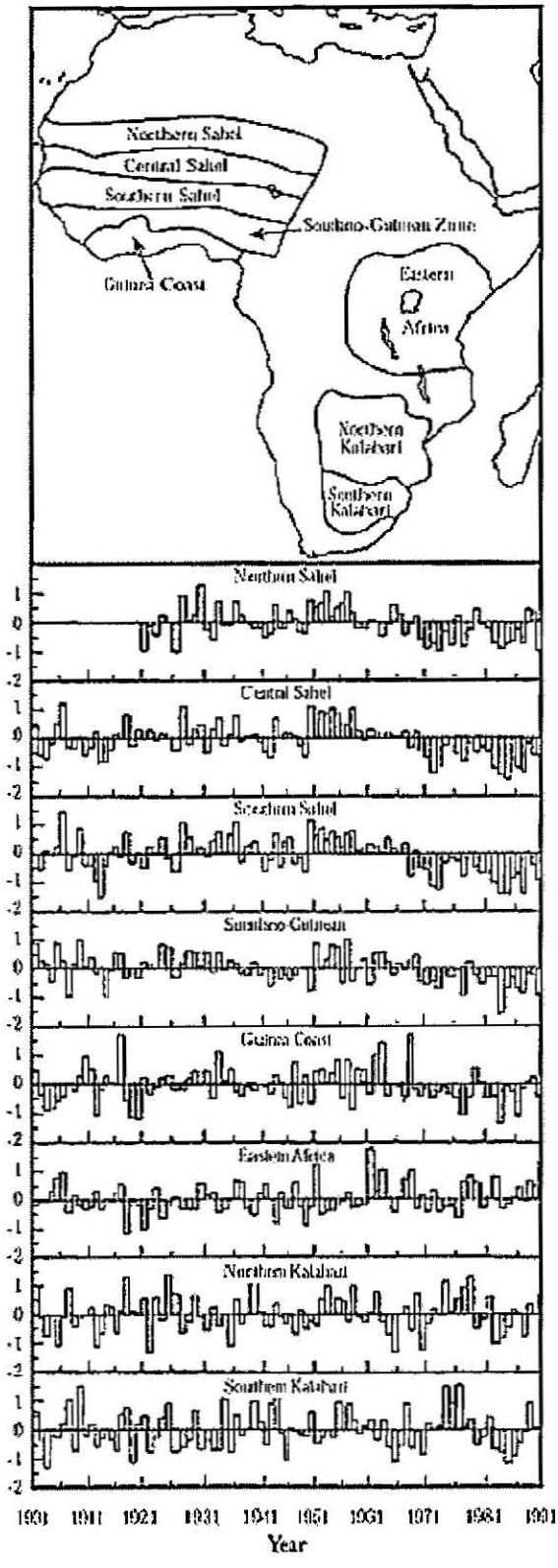

a) Rainfall regions of Africa and the corresponding standardised rainfall timeseries (After Nicholson, 1998).

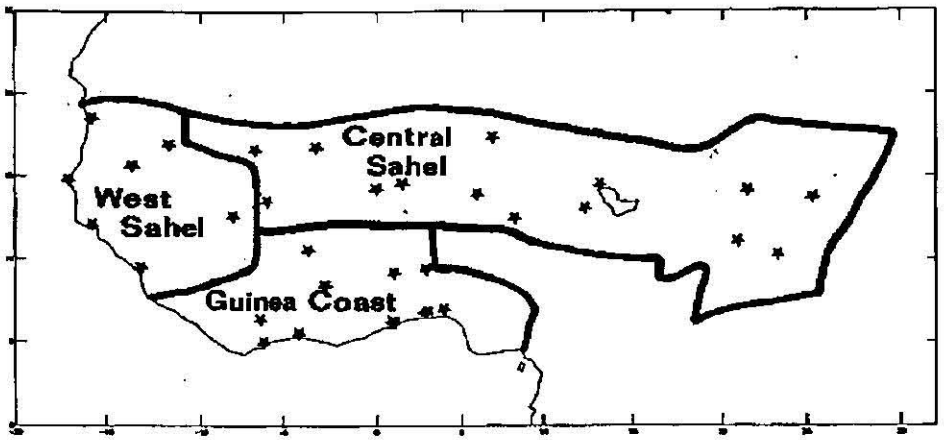

b) Rainfall regions used by Landsea et al (1998).

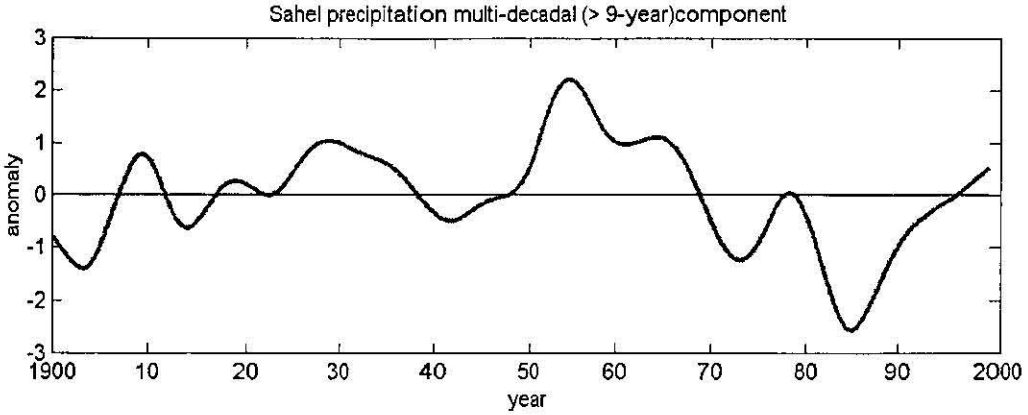

c) Multi-decadal rainfall of Sahel [(10W, 20E), (10N, 17N)] revealed by wavelet transform.

2.1 Rainfall regions of tropical North Africa used in climate studies.

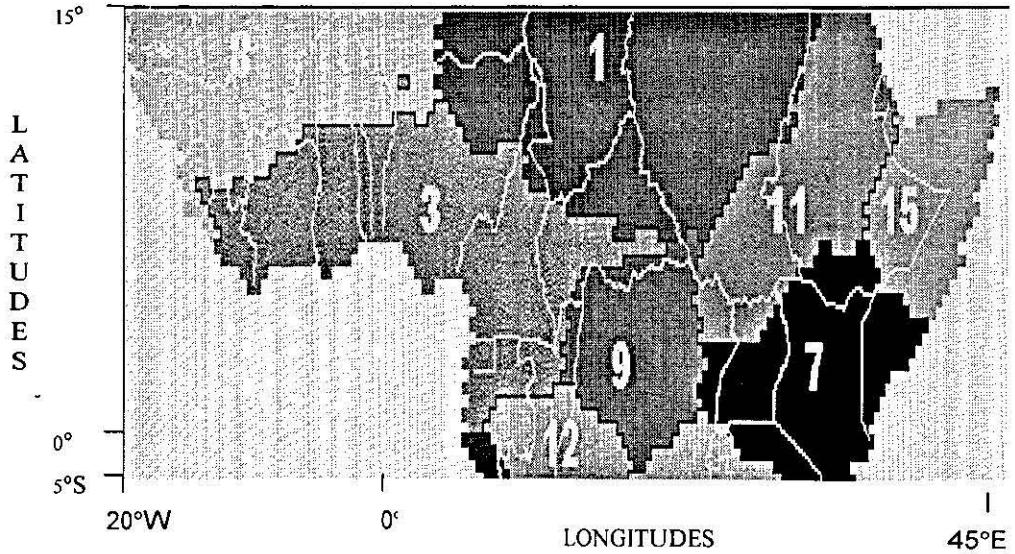

a) Rainfall regionalisation of tropical North Africa adopted in this study (Jury and Phillip, 2001). In this study, Region 1 (Northeast Africa), Region 3 (Guinea Coast) , Region 8 (West Africa) and Region 11 (mainly Western Ethiopia) are considered.

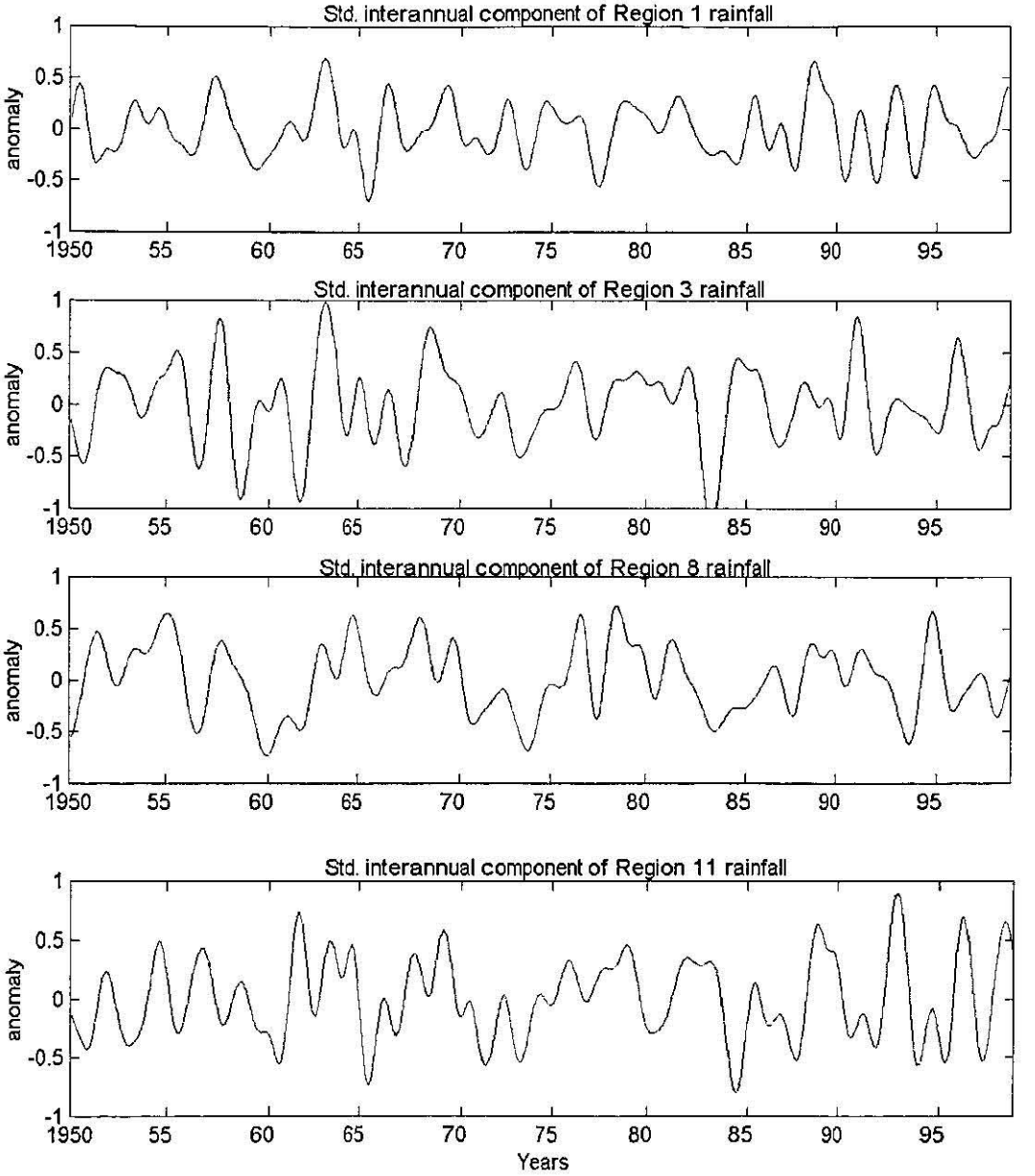

b) Standardised Interannual variability of tropical North Africa (see the regions in a)

Fig. 2.2 Rainfall regions and standardised rainfall variability of tropical North Africa used in this study.

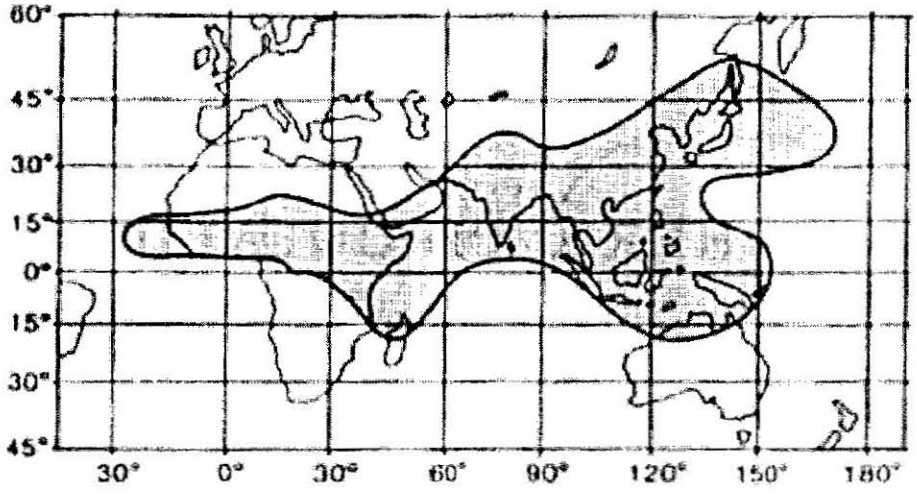

Fig. 2.3 The Monsoon regions (shaded areas). The shaded region, between 18°W and 50°E, is the tropical North Africa monsoon region.

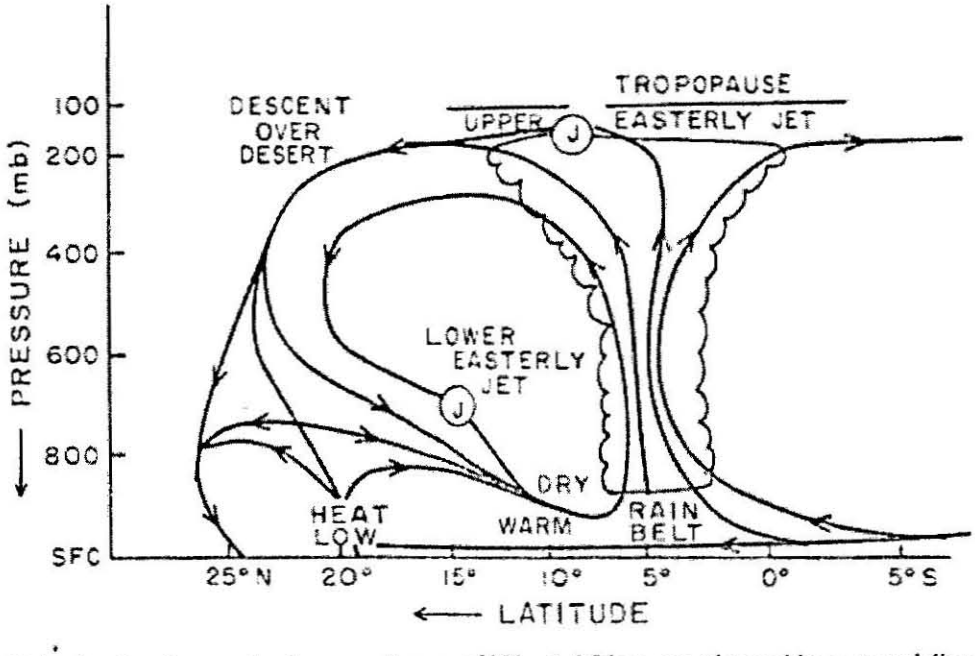

Fig. 2.4 Principal rain producing systems of West Africa as viewed in a meridional plane (After Krishnamurti, 1979). Note that J denotes the low-level African Easterly and Tropical Easterly Jet stream.

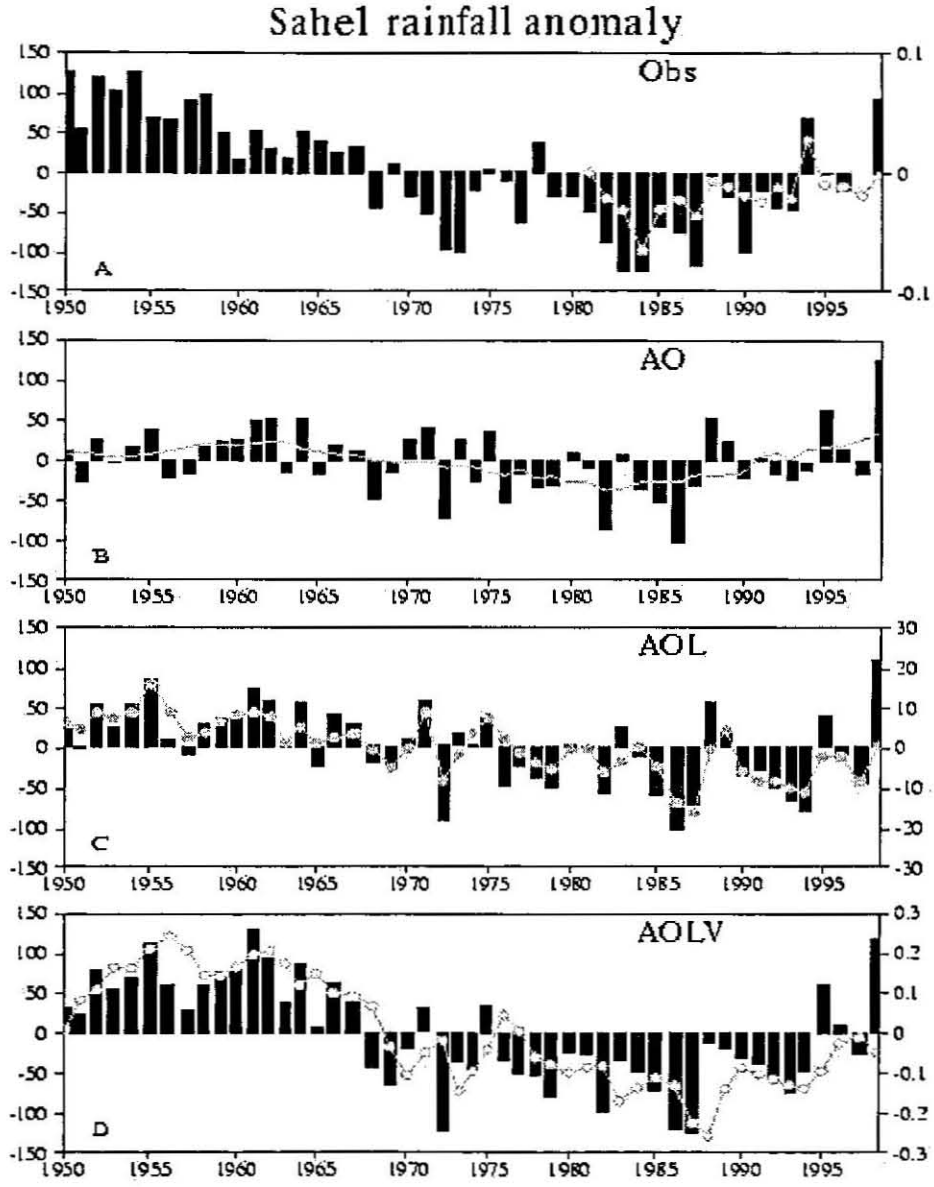

Fig. 2.5 The dramatic drying trend in the Sahel from the 1950s to the 1990s is initially forced by SST (A), but amplified by moisture(C) and vegetation (D). After Zeng, et al. (1999)

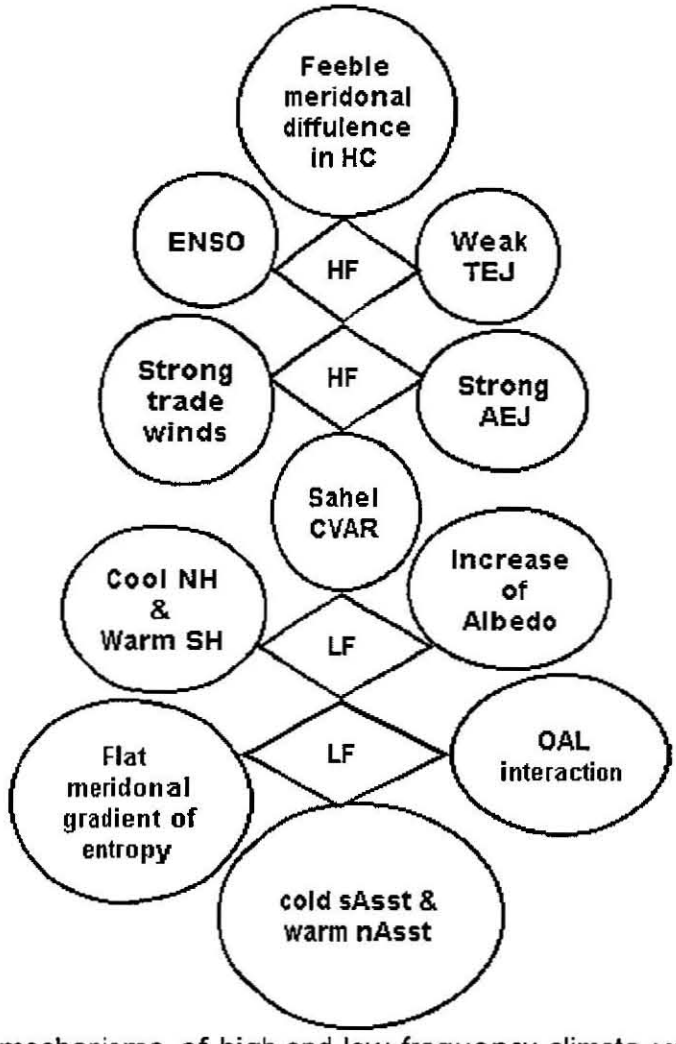

Fig. 2.6 Integrated mechanisms of high and low frequency climate variability (HF and LF) of Sahel identified so far in the literature. Here CVAR stands for Climate variability, HC is Hadley Circulation; NH and SH are northern and southern hemispheres, nAsst and sAsst represent for the tropical north and south Atlantic SST. OAL is the ocean-atmosphere-land-vegetation interaction simulation. AEJ and TEJ stand for Africa Easterly Jet and Tropical Easterly Jet in that order. ENSO is El Nino-Southern Oscillation. HF and LF refer to interannual oscillations of 2-8 years and decadal trends > 8 years, respectively.

CHAPTER 3
DATA AND METHODS

3.1 Introduction

In Chapter 1, a number of problems and hypothesis were put forward to better understanding physical mechanisms of the mode of tropical North African climate variability. To find the solutions for these problems, to attain the objectives stated and to contribute to our understanding, multifarious and multi-dimensional data sets are used. The temporal and spatial characteristics of these data sets are discussed in Section 3.2. The data ranges from observed to reanalysed data sets. The methods entail composite analysis, correlation analysis, wavelet transform, GCM numerical simulations, auto- and EOF analysis using singular value decomposition, cross-correlation, and stepwise linear regression. The details of these techniques are covered in Section 3.3.

3.2 Data used

The data set entails rainfall, stream flow, atmospheric variables, and sea surface temperature (SST). These data sets are grouped into: observed and re-analysed. Rainfall, stream flow, and SST data are part of the observed group. The latter is enhanced by satellite thermal infrared information. The atmospheric data (sea level pressure, wind, geopotential height, velocity potential and the likes) are in the re-analysed group. Model assimilated subsurface ocean thermocline temperature is also consulted to study thermocline variability with respect to tropical North Africa convection.

3.2.1 Observed

The observed data used in this study includes rainfall over tropical North Africa, Brazil and India, Nile flow at Aswan, and sea surface temperatures over the Atlantic, Indian and Pacific Oceans. The nature of each variable and the sources of the data are discussed below.

a) Tropical North Africa and India rainfall area indices

Fifteen optimal Africa rainfall regions are produced via rotated principal component analysis using continuous monthly rainfall departures at 0.5° longitude and latitude resolution, obtained from the Climate Research Unit (CRU) of University of East Anglia (Jury and Philipp, 2002). The optimal rainfall regionalisation of tropical North Africa rainfall is given in Fig. 2.3a. Continuous monthly rainfall indices are developed for each region over tropical North Africa from 1948 to 1998 (Fig. 2.4b). The rotated principal component analysis produced five homogeneous regions over unimodal rainfall regions of tropical North Africa. From this regionalisation, East Sahel (Region 1), Guinea region (Region 3), West Sahel (Region 8), and Ethiopia (Region 11) are considered. Monthly and seasonal rainfall indices of these regions from 1950-1998 are used.

Tropical North Africa and India get most of their rainfall during boreal summer (June to September). Besides, these regions are part of the largest monsoon region of the world with meridional flow at lower and upper levels. So it is necessary to study the common features that these regions share. India has a long rainfall record starting from 1871-2000. Of these rainfall records, Central Indian monthly and seasonal rainfall data from 1950-1998 is considered in this study. These data are obtained from the Indian Institute of Tropical Meteorology (web site: http://www.tropmet.res.in).

b) Stream flow data

Continuous monthly Nile flow data at Aswan from 1950-1997 is obtained from Wang G. (personal communication). These stream flow data are high quality and are naturalised from known human interference (for instance, dams). Using these data, a number of scientific publications have derived (Eltahir and Wang, 1999; Eltahir, 1996; Jury, 1999, 2001b).

Other stream flow data are also used in the study over tropical North Africa and South America. Over tropical North Africa, the Niger and Senegal rivers are considered. The Parana River flow from South America is used. The flow data for these rivers cover most of the period from 1950-1997 and have varying length. The stream flow data for Niger and Senegal Rivers are annual. These flow data are naturalised for anthropogenic effects and are quality checked (Jury, 1999). The drainage of these river basins is given in Fig. 3.1. The main characteristics of these river basins are shown in Table 3.1.

c) Sea surface temperature data

To understand the modulation of ENSO and related signals on tropical North Africa climate variability, sea surface temperature data over Pacific, Atlantic and Indian Oceans are used. Well-known SST indices like Nino 3 and Atlantic SST dipole mode are considered. The SST data for these indices, from 1950-1998, are obtained from http://cpc.noaa.gov web site. The Southern Oscillation Index (SOI), the atmospheric component of ENSO, is also taken into account. The SOI is the sea-saw of pressure between Tahiti and Darwin. This atmospheric index is also procured from http://cpc.noaa.gov web site (Table 3.2).

3.2.2 NCEP reanalysis data

The basic notion of the NCEP (National Centres for Environmental Prediction) reanalysis is in the use of a frozen state-of-the-art analysis / forecast system and performs data assimilation using all archived data, from 1948 to the present. The details of NCEP reanalysis can be consulted in Kalnay et al (1996) and Kistler et al (2001). One the most attracting characteristics of the NCEP reanalysis with respect to climate studies is its consistency. It is the best approach in depicting the three-dimensional atmospheric state from the past to the present.

The NCEP reanalysis can be classified into categories, depending on the relative influence of the observational data and the model on the gridded variable. Here,

variables underpinned by observations are used. The detail of category and the level available in NCEP are given in Table 3.3.

In this study, sea level pressure, out-going long wave radiation, air temperature, geopotential height, wind vector, stream function and velocity potential are used. These are used at regional and global scale as appropriate. The list of variables employed here and their vertical extents are shown in Table 3.4.

NCEP reanalysis data density

This section considers the spatial and temporal characteristic of the different sources of data used in NCEP reanalysis. The main sources of the data come from land surface, balloon sonde, and ship and buoy observations. Salient features of the temporal evolution and the spatial patterns of the observation density from these observational platforms are examined with respect to the impact of sparse and discontinuity of data density in NCEP reanalysis product.

Land surface observation density

To examine the temporal and spatial characteristics of observational density used in NCEP reanalysis, the web site for NCEP http://wesley.wwb.noaa.gov/cgi_bin /disp_m_obscnt.sh is consulted. Making use of the observation density incorporated in NCEP, the temporal and spatial characteristics of the surface and upper level observation are studied in context of the validity of NCEP reanalysis products. This is illustrated using examples.

The NCEP observation density over tropical North Africa ({20°W, 45°E}, {0°, 15°N}) is plotted in Fig. 3.2. The surface observation density is given in the upper panel. It depicts two distinct periods with low and high observational density. The period 1950 - 1967 is characterised by very low surface observation density. After 1967, meteorological observation platforms are widely introduced over tropical Africa, from east to west. The surface density over West and Central Africa after 1967 is

better than the East Africa (NEAF) observation density. Discontinuity and jumps in the observation density prior to and post 1967 produce sampling biases in NCEP reanalysis surface products. A gradual decline of surface observation in recent times is apparent in Fig. 3.2 and is most notable over West and Central Africa.

The year-to-year variation of surface observation density over tropical North Africa reveals low surface density prior to 1960s and a gradual rise since then. What does this say with respect to NCEP reanalysis products? That discontinuity and inhomogeneity produce biases with more weighting towards the high-density period. To normalise this density weighted variables could have gone into NCEP reanalysis to eliminate the jumps and discontinuity. On this issue, Poccard et al. (2000) and Camberlin et al (2001) have given a detail treatise in reference to rainfall structure in NCEP reanalysis over tropical Africa.

b) Sonde and aircraft observation

Rawindsonde, dropsonde and pibal, collectively called sonde, are commonly used to probe the vertical structure of the atmosphere. The data obtained from these instruments are used as inputs in NCEP reanalysis. Here, the temporal patterns of the observation density that go into the NCEP are examined.

The timeseries of sonde observation over tropical North Africa is given in Fig. 3.2. The observation density is low over Northeast Africa. A relatively better upper-level observation density is seen from the middle of 1955 to 1964. After 1994, the upper-level observation density over Central and West Africa exceeds Northeast Africa. Central and West Africa have similar sonde observation density. These regions show high year-to-year variability of sonde observation in the 1970s. After the 1990, the sonde observation density declines to the 1965 -1970 density-level.

The NCEP reanalysis also incorporate aircraft observation. The data from this platform suffers from consistency. The inconsistency is to all regions considered here (refer lower panel of Fig. 3.2). Observing the atmosphere using aircraft started

in 1965. In recent times, an increase of aircraft observation is shown over the regions considered.

c) Satellite wind observation

Space-based observing platforms become useful in atmospheric sciences to derive variables such as sea surface temperature, atmospheric surface temperature, wind speed, atmospheric moisture, rain rate, and long-wave radiation. Satellite derived wind and SST are used in NCEP reanalysis. In this section, the density of wind derived from the satellite is discussed.

Satellite contribution to NCEP reanalysis does not exceed two decades though the availability of geostationary satellite data goes back to 1970s (in a digital form). The contribution of satellite-derived wind is enormous over wide-areas of the ocean and tropical deep convective regions, where radiosonde observation is sparse. Consistent and reliable flow of information over large area can be obtained from satellite remote sensing. These attributes make the space-based observing systems superior to the conventional ones, but do not substitute the in situ observation. Space-based measurements complement the ground truth.

The satellite derived wind data used in NCEP reanalysis is bounded in space and time. Usage of satellite information in wind estimation for NCEP reanalysis started in January 1968. During this time, the global tropical latitudes were covered to some extent. It continues in this mode for a few years until 1975, where the coverage became limited to 180°W-15°W. Starting 1980, the spatial coverage and the pixels grow exponentially. The extended domain included western Pacific and the Maritime Continent. The satellite gaps remain over the central Indian Ocean. Satellite derived winds over tropical Africa deep convective regions become available starting the middle of 1980s. This trend continues in the 1990s (Fig. 3.3). Through these times, central Indian Ocean and India are satellite void regions with respect to geostationary Meteosat. Recently, Meteosat-5 Satellite has been

positioned over the Indian Ocean to provide Meteosat Imagery for the Indian Ocean to support the Indian Ocean Experiment (INDOEX).

d) Ship and Buoy observation

To understand the climate over the global ocean and their influence on global and regional climate, ship and buoy observation has played a major role. This is possible from Voluntary Observing Ships (VOS) of the World Weather Watch. A major limitation of ship observation is that only shipping lanes are covered. Buoys are also good sources of observation but limited to equatorial latitudes. Here, the spatial and temporal characteristics of the observation density from these observing platforms are discussed.

Spatial distribution

The spatial coverage of ship and buoy observations varies from time to time over the Atlantic and Indian Ocean. The observation density is concentrated along the ship lanes off coast of Africa and South America. In the 1950s, tropical Indian Ocean became essentially observation free region. The closing of Suez Canal from 1967 to 1975 favoured the Indian Ocean. In these periods, the ship observation density increased. In the late 1960s, a triangular ship lane is established over Indian Ocean, one along the coast, the second along southwest to northeast direction, from the tip of South Africa to northern tip of Indonesia. The third lane is established between Persian Gulf and the northern tip of Indonesia. In the middle of 1970s, ship observation density concentrated along the coastal regions of Africa and over the Red Sea. Ship observation density over the Indian and Atlantic Ocean is shown in Fig. 3.4.

Temporal distribution

The year-to-year variation of ship and buoy observation density over equatorial and tropical oceans is examined. Temporal characteristics are plotted over equatorial

oceans (5°S, 5°N) and topical oceans (5°N (S)-20°N (S)). These plots are given in Fig 3.5. The timeseries of the ship and buoy observation density for the tropical and south tropical oceans are shown in Fig. 3.5. Compared to the equatorial ocean regions, the south tropical ocean is the least observed. This is also very well reflected in the spatial distribution in Fig. 3.4. All of the profiles depict the increasing ocean observation network after the second half of the 1960s. Starting in the late 1980s, there exists another turning point, which reveals the opposing trend, namely a decreasing of ocean observation network. This is particularly well portrayed over the Atlantic and Indian oceans. The observation density over the equatorial and tropical Indian Ocean dropped from the second half of 1960 to 1975. Comparison of the observation density over these oceans leads to the conclusion that Atlantic is the better-observed ocean, the Indian Ocean the least observed. The other aspect that Fig. 3.5 demonstrates is that the South Pacific Ocean is poorly observed. In summary, drops, rise and jumps of observing network impacts the output elicited from NCEP reanalysis.

e) Satellite derived SST

In the previous section it has been noted that ship and buoy observations are insufficient NCEP reanalysis. A number of important regions of the oceanic world are void of data. To supplement this, satellite information is used in NCEP reanalysis to derive one of the most important basic ocean state variables, the SST. The use of the satellite derived SST started in1973 (Fig. 3.6). A notable increment of satellite derived SST and surface temperature is seen in the 1990s.

The global average temporal characteristics of the satellite derived SST coverage reveal (not shown) a slow increase until the 1980s. Then, a huge leap of satellite data usage for SST estimation continues to present. Hence NCEP products are much more accurate since the 1980 due to satellite data inputs.

f) Model assimilated upper ocean thermal data

A global assimilation of upper-ocean temperature for the period 1950-2000 is considered in the study of the coupling mechanisms (Table 3.2). The global ocean assimilation analysis relies on a first guess provided by a General Circulation Model of the oceans based on the GFDL MOM2 (coupled Ocean-general circulation model of Geophysical Fluid Dynamics Laboratory Modular Ocean Model) code. The assimilation algorithm is an extension of optimum interpolation. The horizontal grid resolution for the global analysis is 0.5x2.5 degree in the tropics expanding pole-ward of 10 degrees to a uniform 1.5x2.5 degree grid at mid-latitudes. The basin domain extends from 70°S to 60°N for a total of 146x91 horizontal grid-points. The vertical resolution is 15 m in the upper 150 m, expanding toward the deep ocean for a total of 20 vertical levels. Vertical mixing is Richardson Number dependent, while horizontal diffusion and viscosity are a constant $2x10^3$ m^2/s. The time step of the model is 2 hours. Updating is carried out over the upper 16 levels spanning the upper 400m. Details about the model-assimilated ocean data can be found in Carton et al. (1999).

3.3 Methods

In this Section, the techniques employed in this study are discussed.

3.3.1 Atmospheric equations

Geopotential heights

Geopotential height is useful in depicting the atmospheric waves and their evolution in time and space. Geopotential height (Z) is defined as

$$Z \equiv \frac{\phi(z)}{g_0} = \frac{1}{g_0}\int_0^z g\,dz \qquad (3.1)$$

Where g_0 is taken as 9.8 ms^{-1} and ϕ (z) = gdz.

Horizontal wind vector

Wind vector is one of the dynamical variables that carries mass (moisture and temperature and the likes) and shows atmospheric circulation. Wind is defined as the rate of change of air displacement along the parcel's motion. Wind vector can be represented as V=ui +vj, where i and j denote the unit vectors along x and y, u and v are zonal and meridional components of wind vector in that order. These are further defined as:

$$Zonal\ wind = u \equiv \frac{dx}{dt} \qquad (3.2a)$$

$$Meridional\ wind = v \equiv \frac{dy}{dx} \qquad (3.2b)$$

Specific humidity

Specific humidity, q, is defined as the mass of water vapour contained in a unit mass of moist air (dry air plus water vapour). It is expressed as water vapour per kilogram of air. Specific humidity is a function of vapour pressure and total pressure. This is given as

$$q = \frac{0.622e}{p - 0.378e} \qquad (3.3)$$

where e is vapour pressure and p is the air pressure.

Velocity potential and stream function

The two-dimensional wind vector, as Helmholtz theorem, can be decomposed into the gradients of stream function and velocity potential. That is,

$$V = k \times \nabla \psi - \nabla \chi \qquad (3.4)$$

The stream function (ψ) is the rotational (non-divergent) component of the wind fields while velocity potential (χ) is the divergent (iirotational) component of the horizontal wind vector. These two scalar variables can be determined using a Laplacian solution with appropriate boundary conditions.

The cross- and dot products of Eq. (3.4) gives

$$\nabla^2 \psi = \nabla \times V = \xi \qquad (3.5a)$$

$$\nabla^2 \chi = -\nabla \bullet V \qquad (3.5b)$$

Eq. (3.5) shows interesting relationship. The Laplacian of stream function is the relative vorticity. In a region where the Laplacian of stream function vanishes, maximum value of stream function is guaranteed.

In climate studies, Eq. 3.5 has paramount importance. About 80 % of the variance of motion field is described by the rotational part. All circulations in vertical planes such as the Hadley and east-west over-turning are divergent (Krishnamurti, 1971).

Eq. 3.5 can be rewritten as

$$\xi = k \bullet \nabla \times V = \frac{\partial v}{\partial x} - \frac{\partial u}{\partial y} = \textit{Relative vorticity} \qquad (3.6)$$

$$\nabla \bullet V = \frac{\partial u}{\partial x} + \frac{\partial v}{\partial y} = \textit{Horizontal divergence} \qquad (3.7)$$

Vertical motion

Omega is the term used to represent the vertical motion in pressure co-ordinate system. It is the rate of change pressure of the parcel along the motion and is mathematically expressed as

$$\omega = dp/dt = \partial p/\partial t + V_H \bullet \nabla_H p + w \bullet \partial p/\partial z \qquad (3.8a)$$

Where, the first term is the rate of change of pressure along the parcel's motion. The second term represents the pressure tendency. The third and the fourth term are the horizontal and vertical advection of pressure.

In large-scale motion, the second and the third term are small compared to the fourth term. Taking this into consideration and making use of the hydrostatic assumption, Eq. 3.8a is reduced to

$$\omega = -\rho g w \qquad (3.8b)$$

Where $w = \frac{dz}{dt}$ is the vertical velocity in (x, y, z, t) frame.

3.3.2 Composite analysis

A contingency analysis is employed to discern the co-variability of the rainfall, stream flow and ocean-atmospheric variables. The standardised hydro-climate variables across Northeast Africa (Ethiopia rainfall, East Sahel rainfall, Nile River flow) are used to identify wet/high flow and dry/low flow years. Identification of years that represent the extreme mode of variability have paramount importance to understand the atmospheric systems, processes and connections that drive hydro-climate variability of tropical North Africa. Using |0.5| sigma as an identifier for wet/flow and dry/low flow category, five years are selected in each category. For wet /high flow years 1958, 1961, 1964, 1975 and 1988 are identified; for dry/low flow years 1982, 1984, 1987, 1990 and 1991 are selected. These years are used as inputs in the composite analysis. The same procedure is followed to identify the modulation of tropical sea surface temperatures and the principal circulation deriving tropical North Africa climate variability.

Composite analysis is done on NCEP web site http:// www.cdc.noaa.gov/cgi-bin/composites to obtain seasonal ocean-atmospheric composite at different lags and levels.

3.3.3 Correlation analysis

Measure of association

The degree of association between two variables is computed using correlation analysis is expressed as

$$r = \frac{S_{xy}}{S_x S_y} \qquad (3.9)$$

where $S_x S_y = \frac{\sum (X - \bar{X})(Y - \bar{Y})}{N-1}$ is the product of the standard deviation of x and y.

In this study the correlation analysis is used to identify the temporal and spatial relationship between the rainfall/stream flow of tropical North Africa on one hand and the ocean-atmospheric variables on the other. Correlation mapping is also undertaken using the NCEP correlation web: http://www.cdc.noaa.gov/Correlation. Significant results obtained from this technique help establish the physical connection between hydroclimate and ocean-atmospheric coupling. The same procedure is followed to identify teleconnection and key predictors with respect to tropical North Africa climate variability.

Defining key areas

A key area is a region that drives or modulates the climate system of a certain region (e.g. equatorial Atlantic). A key area must be large enough to depict the uptake of remote ocean-atmosphere signals. Key areas are vital to the understanding and the prediction of the climate, water resource and food resource variability.

Key areas can be defined by principal component analysis, singular spectrum analysis, canonical analysis, correlation analysis and composite analysis. In this study, composite, correlation analysis and singular value decomposition are adopted. Key area indices that have been widely used are also considered (examples, Nino 3, Atlantic SST dipole, Indian Ocean SST dipole).

Autocorrelation functions

Autocorrelation function ($\rho(\tau)$) represents the correlation between pairs of values of {x(t)} separated by an interval of length τ. This is given as

$$\rho(\tau) = \frac{\mathrm{cov}\{x(t), x(t+\tau)}{[\mathrm{var}\{x(t)\} \bullet \mathrm{var}\{x(t+\tau)\}]^{0.5}} \qquad (3.10a)$$

Eq. 3.18a can be rewritten as

$$\rho(\tau) = \frac{R(\tau)}{R(o)} \qquad (3.10b)$$

Where $R(\tau) = E[\{x(t)-\mu\}\{ x(t+\tau)-\mu\}] = Cov\{x(t), x(t+\tau)\}$. This function is called autocovariance function. $R(0) = E[\{x(t)-\mu\}^2] = var\{x(t)\}=\sigma^2$, (all t).

The rate at which $\rho(\tau)$ decays to zero is interpreted as a measure of the "memory" (persistence) of the process. If the correlation function vanishes at all t (except t=0), then the process has no memory (persistence). This type of variable is purely random behaviour (white noise). Long memory timeseries have autocorrelations that decay slowly as lag increases.

The autocorrelation function is symmetric at the origin (τ=0), if x (t) is real valued, and has maximum at t=0. For all τ, the norm of $\rho(\tau)$ is bounded by 1.

The autocorrelation function at a given τ is evaluated based on degree of freedom and the value of the autocorrelation value. An estimate of the degree of freedom (df) for autocorrelation is provided as (Jury 2001, personal communication)

$$df = \frac{n}{\text{persistence}} \qquad (3.10c)$$

where n is the number timeseries points included in the autocorrelation. For instance, if the autocorrelation starts to decay below a significant levels at 9 months, and n= 180, then df = 180/9=20. The significance of the autocorrelation is evaluated as per df =20.

The cross- correlation is given as

$$\rho_{ij}(\tau) = \frac{\hat{\rho}_{ij}(\tau)}{\sqrt{\hat{\rho}_{ii}(0)\hat{\rho}_{jj}(o)}} \qquad (3.10c)$$

The cross-correlation function measures the correlation between x(t) and y(t+τ) and has the properties $\rho_{xy}(\tau) = \rho_{yx}(-\tau)$ and $|\rho_{xy}(\tau) < 1|$. To get reasonable result from

cross-correlation, the input timeseries need proper filtering (de-trending etc) to avoid spurious solutions. The significant result obtained after filtering will indicate the degree of association between two timeseries at various lags τ.

3.3.4 Wavelet transform

Wavelet transform is introduced in atmospheric sciences to detect multi-scale climate signals (Wang and Wang, 1996; Lau, and Weng, 1995) and to find the co-variability of climate and river flow (Jury and Melice, 2000).

Continuous wavelet transform (CWT) is here consulted to identify the mode of variability in a spectral domain, to understand the co-spectral characteristics, to compute phase differences between hydro-climate variables and key environmental indices. The other function of CWT is filtering for a certain band of variability.

Introduction

A time series signal has been applied to Fourier Transform to find out the integrated characteristics of the signal over period (frequency). But, this type of transform fails to proffer the local characteristics of the signal.

Wavelet analysis on the other hand analyses localised variations of power within a time series in time-frequency (time-localisation) mode. In wavelet transform, individual wavelet functions are *localised in space*. The localisation in space is a typical characteristic of CWT that makes it differ from Fourier transform.

CWT decomposes the signal x(t), mathematically, in terms of wavelets. The fundamental idea behind wavelets is to analyse according to scale. In wavelet analysis, the scale plays a special role. Wavelet algorithm processes data at different scales or resolutions. When signals are "viewed" with a large "window" gross features are noticed, with a small "window", then fine features are detected. The result in wavelet analysis is to see both the forest and the trees, so to speak.

The wavelet analysis procedure adopts a wavelet prototype function called an analysing wavelet or mother wavelet. Mother wavelets are scale varying basis functions. In window Fourier Transforms, a single window is used for all frequencies and hence the resolution of the analysis is the same at all locations in the time-frequency plane. A basis function, wavelet, varies in scale by chopping up the same function or data space using different scale sizes. The basis functions are localised in frequency, making mathematical tools such as power spectra and scale-grams, useful at picking out frequencies and calculating power distributions.

Temporal analysis is performed with a contracted (high frequency version of the prototype wavelet) while frequency analysis is performed with a dilated (low frequency version of the same wavelet). Because the original signal or function can be represented in terms of a wavelet expansion (using coefficients in a linear combination of the wavelet functions), data operations can be performed using just the corresponding wavelet coefficients.

Formulation

CWT of a signal $x(t)$ with wavelet ψ is defined as

$$W_x(b,a) = \frac{1}{a}\int_{-\infty}^{\infty} x(t)\psi^*\left(\frac{t-b}{a}\right)dt \qquad (3.11)$$

where a is the dilatation parameter, b is the time translation parameter and * denotes the complex conjugate. Morelet (1983) devised a continuous complex wavelet that is localized in frequency space, suitable for a relatively well-defined signal in frequency space. As a result, here, the complex Morlet wavelet is adopted. This Morlet wavelet is defined as:

$$\psi(t) = \pi^{-1/4}\exp(-t^2/2)\exp(i\omega_0 t) \qquad (3.12)$$

with $i = \sqrt{-1}$ and $\omega_0 = \sqrt{2/\ln 2} \cong 5.34$. With this wavelet, the transform coefficient $W_x(b,a)$ may be expressed in terms of real and imaginary parts, modulus and

phase, and the relation between the dilation parameter a and frequency f is $f(a) = \omega(a)/2\pi = 0.874/a$.

The cross-wavelet spectrum of two series $x(t)$ and $y(t)$ is defined as:

$$W_{xy}(b,a) = W_x(b,a)W_y^*(b,a) \qquad (3.13)$$

where $W_x(b,a)$ and $W_y(b,a)$ are the CWT of $x(t)$ and $y(t)$ respectively and * denotes the complex conjugate. The cross-wavelet coefficient $W_{xy}(b,a)$ is a complex number and may be expressed in terms of real and imaginary parts, modulus and phase difference. Recall that if $z_1 = \exp(i\theta_1)$ and $z_2 = \exp(i\theta_2)$ are two complex numbers with phases θ_1 and θ_2, then $z_1 z_2^* = c_1 c_2 \exp[i(\theta_1 - \theta_2)]$ is a complex number with phase: $\Delta\theta = \theta_1 - \theta_2$.

Consequently, the cross-wavelet spectrum provides an estimation of the local phase difference $\Delta\phi(b,a)$ between the two series for each point of the (b,a) time-frequency space. This local phase difference is independent of the amplitude of the series. These characteristics allow an estimate of the instantaneous phase difference between the two series $x(t)$ and $y(t)$. Keeping in mind that b corresponds to the time t, this phase difference is defined as:

$$\Delta\Phi(b) = \tan^{-1}\frac{\int_{a1}^{a2} \mathrm{Im}[W_{xy}(b,a)]da}{\int_{a1}^{a2} \mathrm{Re}[W_{xy}(b,a)]da} \qquad (3.14)$$

where $\mathrm{Re}[W_{xy}(b,a)]$ and $\mathrm{Im}[W_{xy}(b,a)]$ are the real and imaginary parts of $W_{xy}(b,a)$ and where $a_1 < a_2$ are the lower and upper limits of the dilation parameter. The instantaneous time-lag between $x(t)$ and (t) is then obtained from the relation:

$$T(b) = \frac{\Delta\Phi(b)}{2\pi F(b)} \qquad (3.15)$$

where $F(b)$ is the instantaneous frequency defined as the first normalized moment in frequency of $W_{xy}(b,a)$:

$$F(b) = \frac{\int_{a1}^{a2} f(a) \mid W_{xy}(b,a) \mid da}{\int_{a1}^{a2} \mid W_{xy}(b,a) \mid da} \qquad (3.16)$$

where $f(a)$ is the frequency corresponding to the dilation parameter a and where $|W_{xy}(b,a)|$ is the modulus of $W_{xy}(b,a)$. Here the data are filtered in the 1.5 to 16-year range and analysed for coherency between terrestrial climate and ocean monsoon.

3.3.5 EOF analysis

Singular value decomposition (SVD) is used to perform on the EOF (empirical orthogonal function) analysis of subsurface ocean fields. SVD can be used for a single set of data (say, subsurface temperature) to identify the dominant space-time structure of a geophysical field in a reduced dimension (Preisendorfer, 1988). It can also be applied on coupled fields (e.g., ocean subsurface thermal field and zonal wind velocity; SST and sea level pressure) to find out the common (coupled) mode of variability (Preisendorfer, 1988; Bretherton, Smith and Wallace, 1992; von Storch and Navarra, 1995; Björnsson and Venegas, 1997; Venegas, 2001). In this study, the SVD is applied on the thermal field, heat content anomaly and zonal wind stress separately (in "uncoupled" mode). The ocean-atmosphere coupling in this study is investigated using teleconnection and CWT.

The SVD has two advantages to perform EOF (empirical orthogonal function) analysis over other eigenvector techniques that use a covariance matrix (Venegas, 2001). It provides a one-step method to compute all the components of the eigenvalue problem (computationally efficient). The resulting decomposition is computationally stable and robust.

Let Z (s, t) represent anomaly of subsurface ocean property in time and space (x, y). Then, the spatial and temporal pattern of the property can be decomposed into space and time components. This decomposition represents the data fully if these components are summed up (or integrated if the data continuous) over all data

points and for all time. The question is however representing the date with few components without losing the dominant spatio-temporal structure of the data. This is possible in eigenvector representation.

Z (s, t) can be now decomposed into its temporal and spatial pattern as follows.

$$Z(s,t) = \sum_{k=1}^{p} PC_k(t) \bullet EOF_k(s); \qquad (3.17)$$

t: 1, ..., n and s=1, ...p.

Where, PC_k (t) is the amplitude (principal component) series. EOF_k(s) is the spatial structure.

The orthonormality (the independence of the adjacent space-time patterns of the SVD) are maintained in the following relationship:

$$\sum_{s=1}^{p} EOF_j(s)EOF_k(s) = \delta_{jk} \qquad (3.18)$$

Where δ_{ij} is Kronecker's delta and is unity for j=k otherwise zero.

The normalised principal component (dimensionless) is

$$\alpha_k(t) = \frac{PC_k(t)}{l_k^{1/2}} \; ; \; k = 1,\ldots,p; \; t: 1,\ldots,n. \qquad (3.19)$$

Where l is the eigenvalue.

It follows that

$$z(s,t) = \sum_{k=1}^{p} l^{1/2} \bullet \alpha_k(t) \bullet EOF_k(s); \qquad (3.20)$$

k = 1..,...,p; t: 1,...,n

Eq. constitutes a form of the singular value decomposition of the data set Z(s,T).

The question now is how to determine the 'signal' from the 'noise' retaining the salient space-time structure of Z(s,t). There are various selection rules (e.g. Scree Test). A detail account on the subject can be referred in Preisendorfer (1998). In this study, the first two or three are taken depends on the spatial modes of the EOF

structure. If the identified pattern corresponds to the known structures and exhibits ocean-atmosphere signals in the context of tropical North Africa climate, then that pattern is retained.

3.3.6 Multivariate linear prediction: stepwise regression

A stepwise regression model is developed in stages. A list of several potential explanatory variables is available and this list is repeatedly searched for variables, which should be included in the model. The best explanatory variable is used first, then the second best, and then the third; after which the procedure is halted and colinearity checks are applied.

Introducing basic concepts

In multiple regression, a variable selection procedure requires a criterion for deciding how many and which variables to select. Numerous selection procedures are available based on the problem and type of equations involved to answer a certain question. A detail discussion on stepwise regression can be referred to Afifi and Clark (1996).

Residual mean square (RMS)

The RMS about the regression plane is one of the most common in stepwise regression. The RMS is given by:

$$\text{RMS}= \frac{\sum\left(Y-\hat{Y}\right)^2}{N-P-1} \qquad (3.21)$$

Where $\hat{Y}$ is the predicted value for a given set of values, $X_1^* + X_2^* + ... + X_p^*$ is then calculated as $\hat{Y} = A + B_1X_1^* + B_2X_2^* + ... + BpX_p^*$.

The square root of the residual mean square is called the standard error (SE) of the estimate. It represents the variation unexplained by the regression plane and is given as

$$SE = \sqrt{\frac{\sum (Y - \hat{Y})^2}{N - P - 1}} \qquad (3.22)$$

The SE for the regression coefficient and constant is useful in computing the confidence interval and prediction intervals around the computed $\hat{Y}$.

Multiple correlation (R)

Multiple correlation coefficient describes the strength of the linear relationship between the Y (dependent) and set of X (independent) variables. It represents the correlation between the dependent and the corresponding point on the regression plane for all possible combinations of the independent variables. The maximum possible value for R is 1.0. R is explicitly expressed as

$$R^2 = 1 - \frac{S^2}{S_Y^2} \qquad (3.23)$$

where

$$S_y^2 = \frac{\sum (Y - \bar{Y})^2}{N - 1} = \frac{\text{total sum of square}}{\text{N-1}} \text{ and } S^2 = \frac{\sum (Y - \hat{Y})^2}{N - P - 1} = \frac{\text{residual sum of squares}}{\text{N - P - 1}}.$$

Here P is the number of independent variables in the regression equation, N is the number of the samples and N-P-1 is the degree of freedom. This may be "deflated" as outlined above.

The multiple correlation square provides the proportion of variance accounted for by the regression plane. In a simple linear regression, $100 \bullet \sqrt{(1 - R^2)}$ is the percentage unexplained by the independent variables.

Adjusted multiple correlation coefficient

Multiple regression can overestimate the population correlation coefficient, which leads to adding too many variables in the corresponding equation. To reduces this bias, the adjusted multiple correlation coefficient ($\overline{R}$) is used. The adjusted multiple correlation is given as

$$\overline{R}^2 = R^2 - \frac{P \bullet \left(1 - R^2\right)}{N - P - 1} \qquad (3.24)$$

where, P is the number of independent variables in the stepwise regression. If a constant is added in the regression model, then P' =P+1 will be the independent variables estimated. N is the sample size of the variables considered in the stepwise. $N - P - 1$ is the degree of freedom. And $\overline{R}^2$ is the adjusted multiple correlation coefficients square.

Partial correlation ($\rho_{ij,k}$)

The partial correlation coefficient is useful in measuring the degree of dependence between variables after adjusting (removing) for the linear effect of one or more of the other independent variables. It is given as

$$\rho_{ij,k} = \frac{\rho_{ij} - \rho_{ik}\rho_{jk}}{\left[\left(1-\rho_{ik}^2\right)\left(1-\rho_{jk}^2\right)\right]^{\frac{1}{2}}} \qquad (3.25)$$

where ρ is the correlation coefficient. The partial correlation is the simple correlation between residuals. In this case, the residual deviations from the regression plane on the variables whose linear effects are removed. Here the subscript *ij, k* shows that *ij* is possible provided (given) *k*.

Mean absolute errors (MAE)

MAE provides the average magnitude of the error of the predicted values with respect to the observed values. MAE is given as

$$MAE = \frac{1}{N}\left[\sum_{i=1}^{N}|F_i - O_i|\right] \qquad (3.26)$$

Where, N is the number of occasions, F_i is the i^{th} forecast and O_i is the i^{th} observation.

Multicollinearity

Multicollinearity is a problem in statistical prediction using multiple regression. Multicollinearity occurs when some independent variables are highly inter-correlated. When multicollinearity is present, the computed estimates of the regression coefficients are unstable and have large standard errors. As a result, the computation could be inaccurate. The higher the multiple correlation (R), the larger is the standard error square. As a result the standard error square becomes infinity. Hence, higher values of standard error square indicate collinearity. The standard error of the regression coefficient would be large. Multicollinearity is usually detected by examining tolerance. Tolerance is equal to 1-R_i^2. When the tolerance is small, say less than 0.01, then there is a problem of collinearity. The tolerance provides a warning of which variable is causing the problem when the forward stepwise selection method is used. A screening threshold variance for collinearity is $r^2 > 9\%$. Adjacent predictors that share more than this threshold are eliminated in the construction of prediction models.

A general F test

Suppose that the variables $X_1, X_2, \ldots, X_p$ are used in the regression. Suppose also that additional Q variables $X_{p+1}, X_{P+2}, \ldots, X_{p+q}$ are available. Prior to deciding to include these additional variables in the regression equation, it is required to test the hypothesis that, as a group, the Q variables do not improve the regression equation.

To perform the test, there should be an equation that includes all the P+Q variables, which is multiple regression within P+Q variables and constants. Then, the residual

sum of square (RSS_{P+Q}), which is equal to $\left\{RSS = \sum (Y - \bar{Y})^2 \left(1 - R^2\right)\right\}$, is obtained.

In the same way, the equation that includes only the first P variables and the corresponding RSS_P is elicited. The F test statistic is computed as

$$F = \frac{\left(RSS_P - RSS_{P+Q}\right)/Q}{RSS_{P+Q}/(N-P-Q-1)} \qquad (3.27)$$

The numerator measures the improvement in the equation from the additional Q variable. This quantity is always positive. The hypothesis is rejected if the computed F exceeds the tabled $F(1-\alpha)$ with Q and N-P-Q-1 degrees of freedom.

Stepwise regression

Stepwise regression is a widely used multiple linear regression technique to establish statistical prediction scheme in climate studies. The stepwise regression is a subset of multivariate regression equation, where variable selection is done in successive steps. The variable selection is done based on adjusted multiple correlation coefficient, partial correlation, standard error and F-test. Stepwise regression has backward elimination and forward stepwise methods. The stepwise procedure combines both of these two methods. The backward elimination method begins with all the variables in the equations and proceeds by eliminating the least useful variables one at time. In the forward selection method, it adds a variable in each step to the predictive equations. The standard stepwise regression programs such as Statgraphics do the forward selection with option of removing some variables already selected. To develop statistical hydroclimate prediction scheme, the stepwise procedure is used in this study.

Stepwise procedure

Stepwise procedure adds a variable to the prediction equation. At step 1 the program prints the computed F-to-enter for each variables. In next step, the variable with highest computed F-to-enter is entered. For a given equation, variables with

small enough computed F-to-remove values are removed, and the variables with large enough computed F-to-enter values are included. The process stops when no variables can be deleted or added. . The process goes back and forth until it establishes the 'final' prediction equation.

The choice of the minimum F-to-enter and the maximum F-to-remove affects both the nature of selection process and the number of selected. If the maximum F-to-remove is much smaller than the minimum F-to-enter, then the process is essentially forward selection. Minimum F-to-enter equals to 4.00 and maximum F-to-remove equals to 4.00 are used in establishing statistical prediction model for tropical North Africa climate variability.

Strategy in stepwise regression

In stepwise regression the possible strategy is to search the variables that maximise multiple R^2 when combined with the selected variables and selecting variables that minimise the residual sum of squares if retained in the equation. This procedure is equivalent to choosing the second variable to maximise the magnitude of the partial correlation after removing the linear effect of the selected variable. The variable thus selected maximises the F statistic. In short, maximising R^2, minimising RSS, maximising partial correlation and choosing stable predictors provide the optimal solution for hindcast prediction.

The other issue for consideration is artificial skill. Restricting predictors to three prevents over-fitting and artificial skill (Jury 2001 (personal communication)). The final selection of the model for each target (rainfall and stream flow) is based on optimal adjusted multiple correlation that gives a maximum hindcast fit with the lowest collinearity selected from a candidate pool that is as small as possible.

Skill test and validation of prediction

The first step to test the skill of the developed model is splitting the sample data into three-fourth and one-fourth. The three-four of the timeseries are used to develop the model (training) and one fourth are used for validation purpose, that is, these independent data sets are used to test the accuracy of the prediction system. The developed model is run to predict the independent values (one-fourth of the data). Then, the predicted and the observed values are aligned side by side according to ascending order to establish the tercile categories (above normal, normal and below normal). Values that fall in each category are tallied to compute the hit rate. A hit rate is the proportion of events for which a warning was provided correctly (Mason, 2000). The hit rate is computed by assigning points to each predicted value in the context of the observed. The hit rate is computed as $hit\ rate = \frac{\sum \text{points}}{\sum \text{forecasts}}$.

3.4 Summary

In this chapter various data and method topics have been covered. A detailed analysis is made of the data used in this study. The sources, the temporal characteristic, the spatial distribution of the conventional and remote sensed observation density of NCEP reanalysis are comprehensively examined. Impacts of the inconsistency of the observation density on the NCEP products are revealed.

The second topic dwelt in this chapter is the methods employed in reference to understanding the variability, causes and prediction of hydroclimate over tropical North Africa. To this end, multitudes of techniques are applied.

The whole procedures are summarised in Table 3.5. In this set-up, the first moment is used to compute the basic states of boreal summer circulation over Africa and the surrounding oceans. Mean circulation patterns such as the quasi-permanent pressure systems, monsoon flows and jet streams are identified. CWT is employed

to understand the mode of variability, co-spectral characteristics and phase relationships between hydroclimate, environmental indices and dynamical indices. Correlation analysis is used to establish the degree of association between key areas and targets (hydroclimate variables) and to identify teleconnection regions related to tropical North Africa climate. Composite analysis plays a part in revealing the cause of the extreme mode of variability over tropical North Africa hydroclimate, tropical circulation and SST indices over tropical oceans. SVD is applied to subsurface ocean thermal fields and zonal wind stress to characterise space-time mode of variability in the context of tropical ocean-atmosphere teleconnection. Using the results obtained, the statistical hydroclimate prediction models for tropical North Africa climate variability are developed. The skill of the prediction scheme is tested with independent data using hit rate. The stability of the predictors is also examined. This leads to physical mechanisms of tropical North Africa climate and conceptual models thereof.

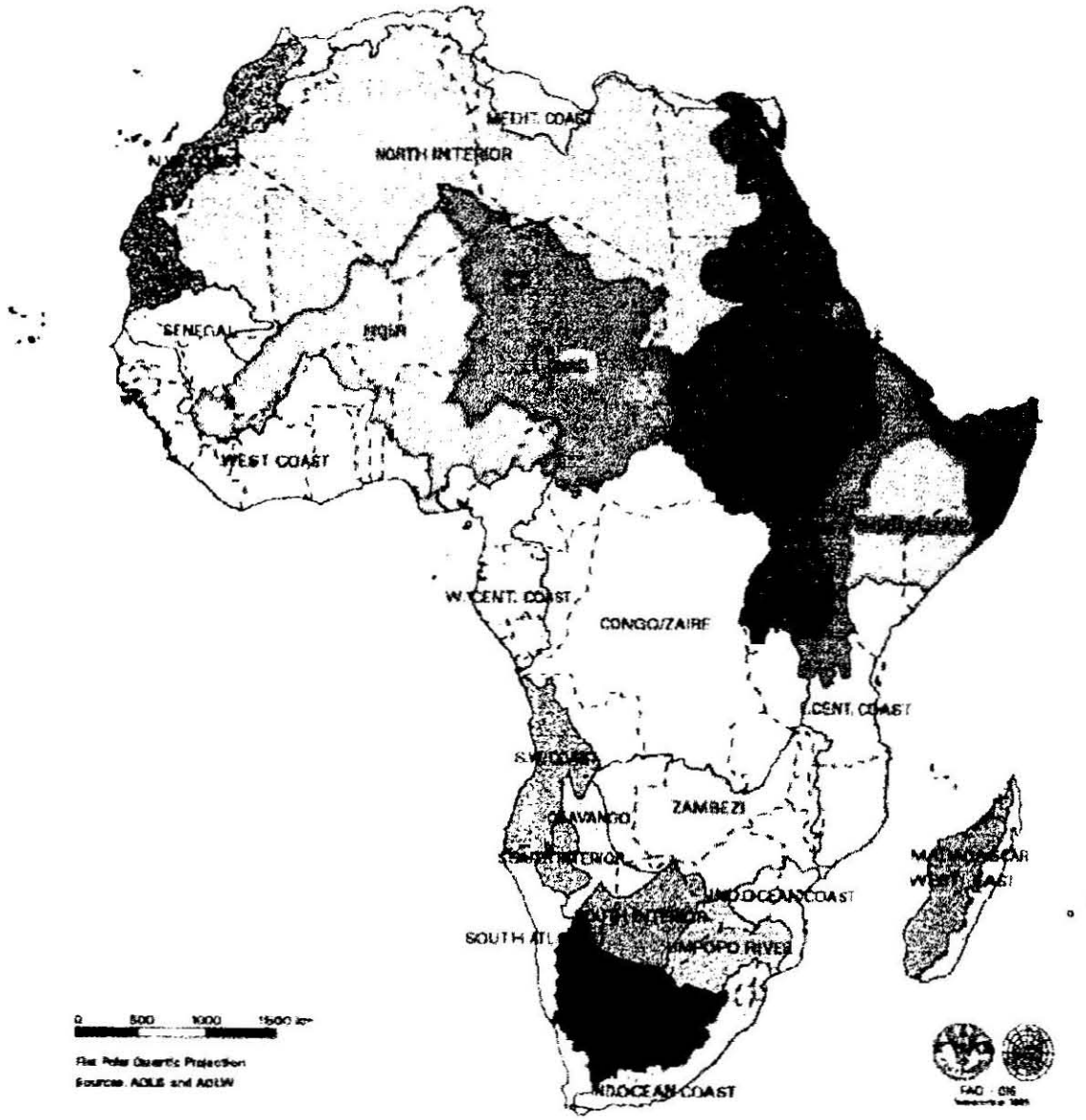

Fig. 3.1 Drainage of African Rivers. Tropical North Africa major rivers considered in this study are Blue Nile (dark blue), Niger (red) and Senegal (white).

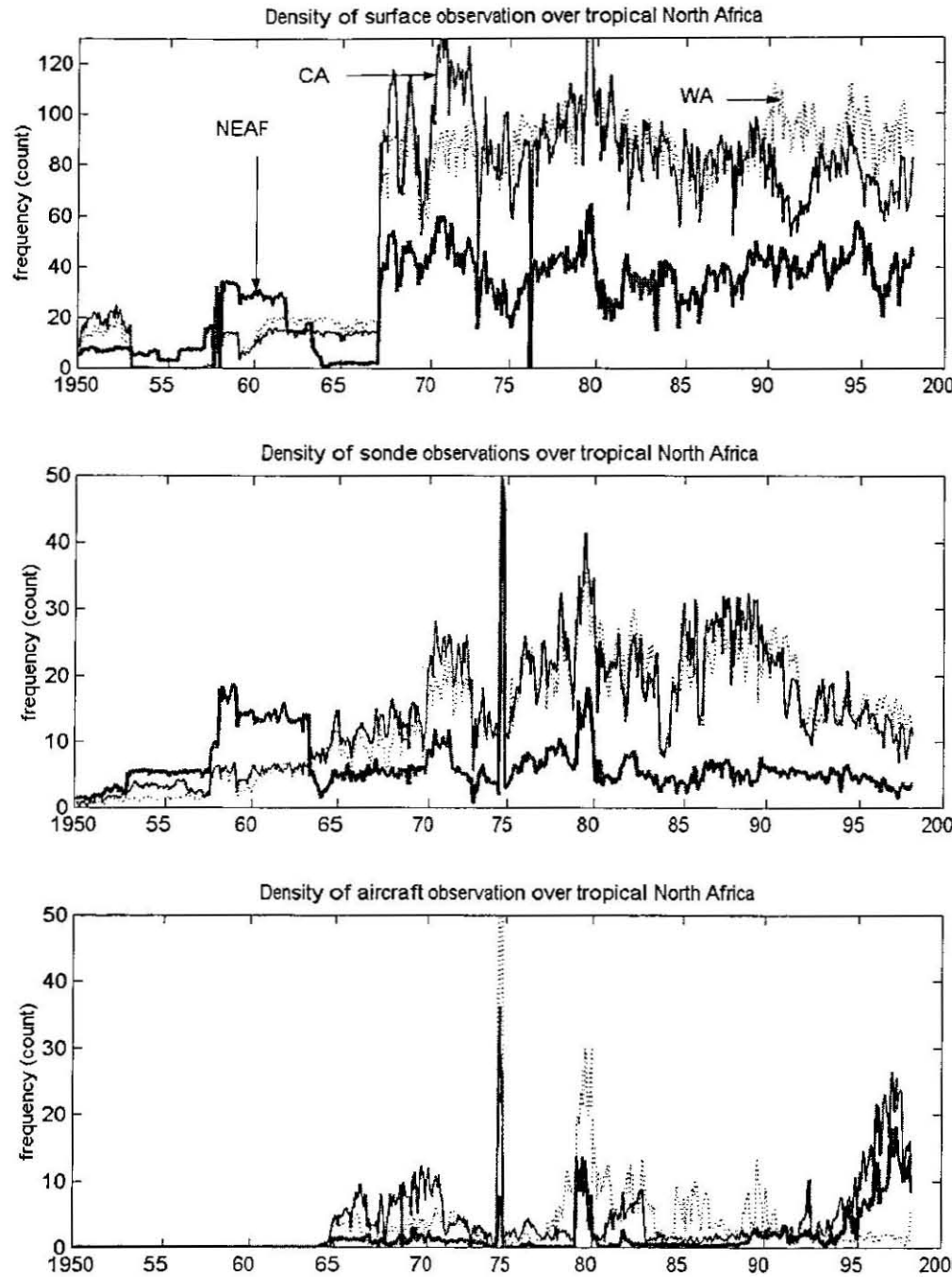

Fig. 3.2 Timeseries of surface and upper air observation density of tropical North Africa incorporated in NCEP reanalysis data. The abrupt increase in observation in 1975 can be associated to GARP (Global Atmospheric Research Program) Atlantic Tropical Experiment (GATE). Note that WA, CA and NEAF stand for West Africa, Central Africa and Northeast Africa, respectively and these labels apply for the other panels.

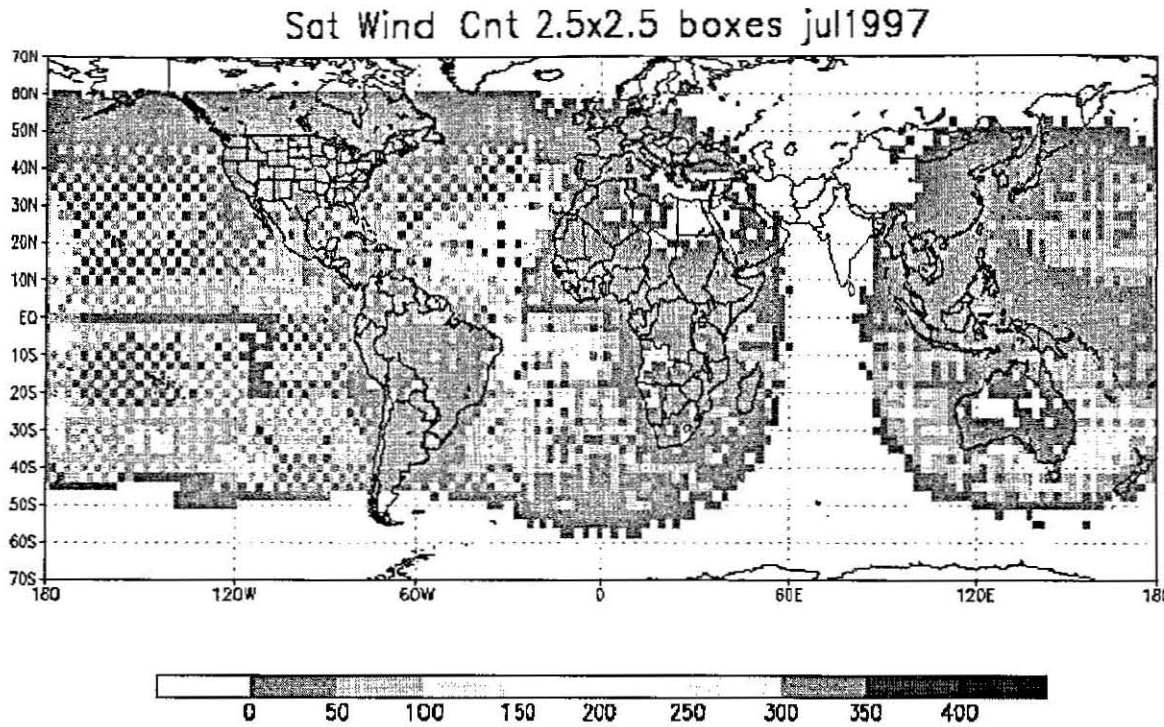

3.3 Satellite derived wind data density used in NCEP/NCAR reanalysis showing near-global coverage in the recent years.

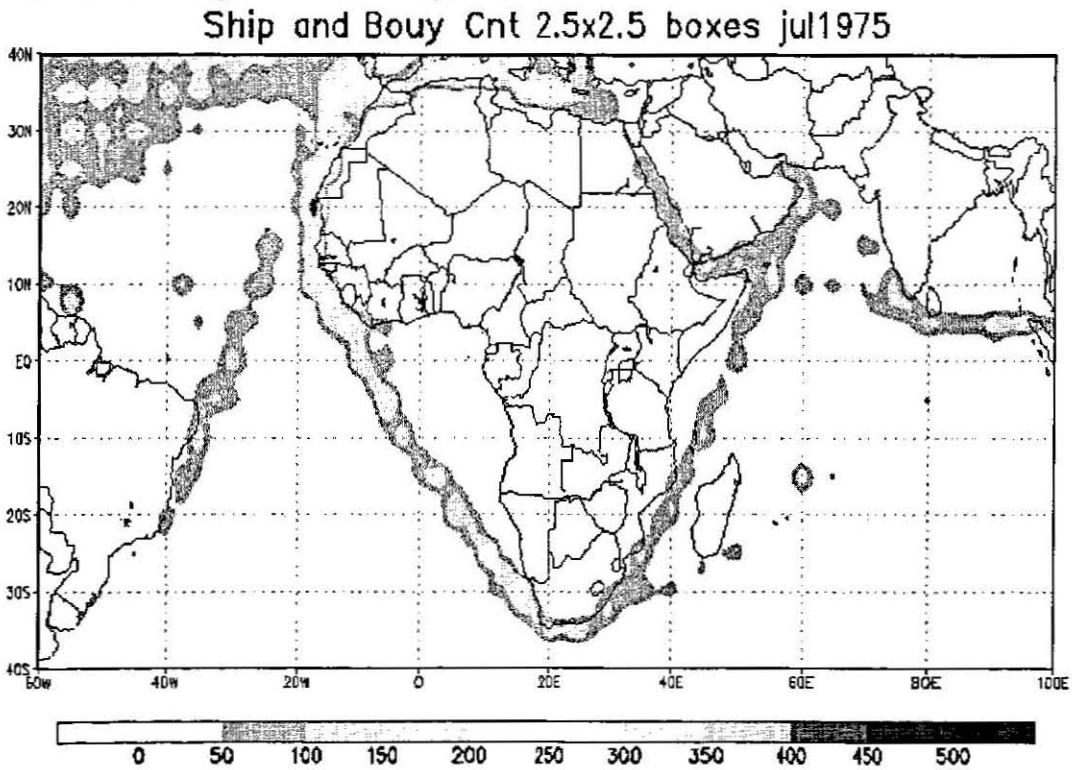

Fig. 3.4 Ship and buoy observation density circumventing the African continent.

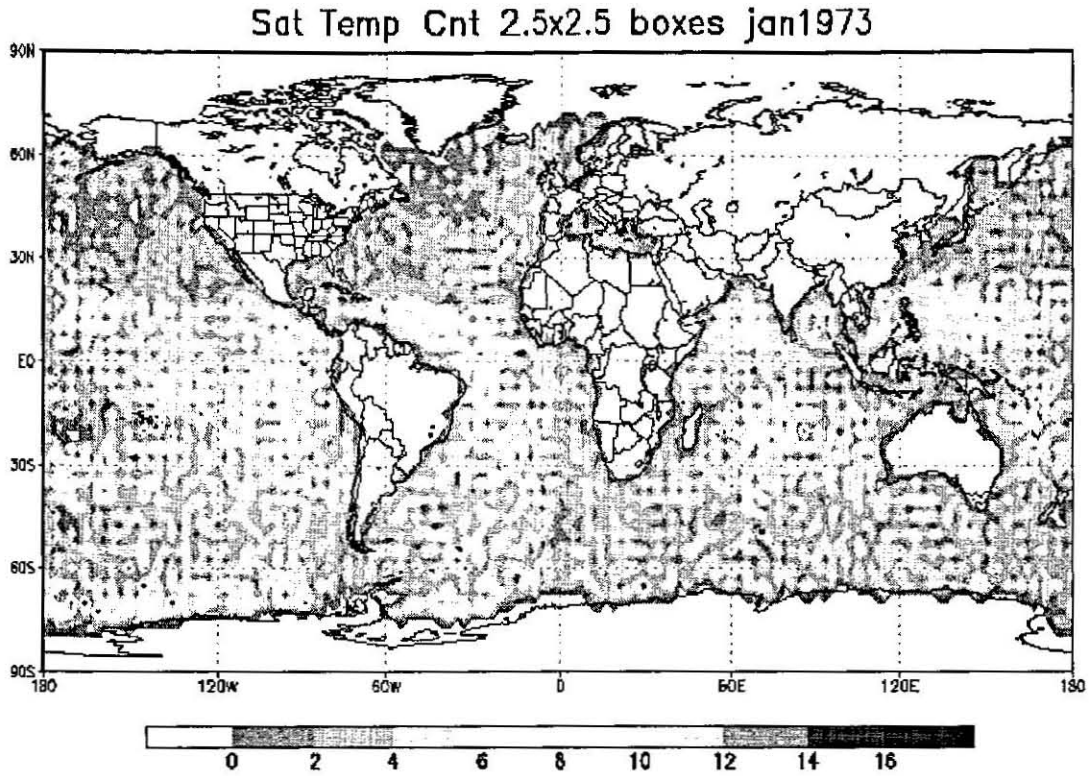

Fig. 3.6 Global coverage of Satellite derived SST (counts (density)) started in January 1973.

Table 3.1 Characteristics of the tropical North Africa and South America rivers.

				Percent of watershed that is:					
Major watersheds	Watershed area	CWW (number)	APD (km^{-2})	Crop-land	Forest	Irrigated area	Arid area	Wet-lands	WAP ($m^3/p/y$)
Nile	3 254 853	10	44	10.7	2.0	1.4	674	6.1	2 207
Niger	2 261 741	10	32	44	0.9	0.1	65.4	4.1	4 076
Senegal	419 575	4	10	48	0.1	0.0	82.0	3.6	5 775
Parana	2 582 704	4	27	43.3	18.1	0.5	9.9	10.9	8 025

CWW = Countries within the watershed area, APD = Average population density and WAP = Water available per person (m^3/person/yr). Source: World Resources 2000-2001-People and ecosystems: The fraying web of life (http://www.wri.org/wri/wr-00-01/).

Table 3.2 Temporal and area coverage of sea surface and ocean temperature data used in this study.

No.	Type	Area coverage	Period	Source and description
2	Nino 3 SST	(150°W, 5°N) (90°W, 5°S)	1950-1998	Sea surface temperature timeseries data are extracted from: Http://wesley.wwb.noaa.gov/ncep_data/index_sgi51_png.html. SOI data is accessed from http://www.cdc.noaa.gov/Correlation/ and http://www.cdc.noaa.gov/Climate/Indices/Analysis/. Temperature-depth of the upper-layer the ocean are obtained from: http://iridl.ldeo.columbia.edu/expert/SOURCES/.UMD/.Carton/.goa/.beta7/.
4	Southern Oscillation Index (SOI)	Darwin & Tahiti	Ditto	
5	Ocean Basin SSTs	Regional/ Global	Ditto	
6	Upper-layer temperature of Ocean Basin	Atlantic, Indian and Pacific Ocean	1950-2000	

Table 3.3 NCEP atmospheric variables used in this study categorised as per the influence of observational and model on the gridded variables.

No.	Atmospheric fields	Levels	Category
1	Temperature (K)	17	A
2	Geopotential height (gpm)	17	A
3	u-wind (m/s)	17	A
4	v-wind (m/s)	17	A
5	Pressure vertical velocity (Pa/s)	12	B
6	Specific humidity (g/kg)	8	B
7	Surface Pressure (Pa)	1	B
8	u-wind at the maximum wind level (m/s)	1	A
9	v-wind at the maximum wind level (m/s)	1	A

Note that an A indicates that the analysis variable is strongly influenced by observed data. The designation B indicates that the observational data and the model directly affect the value of the variable.

Table 3.4 Lists of meteorological elements used in this study from NCEP reanalysis.

NO.	NCEP REANALYSIS	COVERAGE	LEVELS
1	Surface pressure level	Regional	Surface
2	Geopotential height	Global	1000-100-hPa
3	Air temperature	Regional	Ditto
4	Wind vector (u,v)	Global	Ditto
5	Omega	Global	Ditto
6	Velocity potential	Global	Two sigma levels
7	Stream function	Global	Ditto
8	OLR	Regional	Single level
9	Specific Humidity (q)	Regional	1000-300-hPa
These data are used in this study (from 1950 to 2000) for composite, correlation and wavelet analyses, numerical simulation, and prediction studies.			

Table 3.5 Description of techniques used and expected results in this study.

Input	Technique	Role	Expected results
Ocean-atmospheric variables of NCEP	Mean	Compute mean boreal summer circulation.	Semi-permanent high-pressure systems, monsoon systems and jet streams.
Presented in Chapter 4	CA	Relate between key areas and hydroclimate variables.	Links between hydroclimate and basic state key areas.
Hydroclimate, Ocean-atmospheric variables	CMP	Investigate mechanisms for hydro- climate variability.	Causes for tropical North Africa variability.
	CA	Establish connection between hydroclimate & kinematic indices.	Regional & global ocean-atmosphere teleconnection.
Presented in Chapter 5	CWT	To identify mode of climate in tropical North Africa.	Common energy and predictability potential.
Thermodynamic, tropical North Africa rainfall and	CMP	Examine SST modulation on tropical North Africa climate.	Preferred atmospheric anomaly patterns.
atmospheric variables	CA	Unravel interplay between and thermodynamic and tropical North Africa.	Contribution of SST to Tropical North Africa rainfall variability.
Presented in Chapter 6	CCM3	Simulate responses of tropical SST.	Preferred local and region atmospheric circulations to tropical SST forcing.
	CWT	Uncover common mode of SST & Sahel rainfall variability.	Co-spectrum, phase diagram → prediction of Sahel rainfall.
Thermodynamic and kinematics of	CMP	Unravel upper-ocean signals coupled to Sahel climate.	Equatorial subsurface east-west oscillations
subsurface ocean indices & tropical	CA	Role & teleconnection of subsurface property	ENSO signals in ocean oscillation, global ocean-atmospheric teleconnection.
atmospheric indices	SVD	Identify spatial-temporal oscillation of subsurface property	Most dominant oscillatory signals of upper ocean.
Presented in Chapter 7	CWT	Determine spectral of upper and atmospheric indices.	Time varying frequency-phase spectrum of subsurface and atmospheric indices
Kinematics, SST, hydroclimate and agricultural	stepwise regression	Develop prediction models.	Climate Prediction models for tropical North Africa.
production indices	Hit rate	Cross-validate.	Skilful prediction models.
Presented Chapter 8	Stability analysis	Identify key predictors.	New kinematic predictors.
Results and discussion obtained from all Chapters **Presented in Chapter 9**	Integrate Concepts results & discussion	To document contribution to science and socio-economics of tropical North Africa.	Source of variability & predictability of North African climate, food & cash crops. Modes of subsurface ocean and their connection to African Monsoon climate.

Note: CWT= continuous wavelet transform analysis, CMP = composite analysis, CA = correlation analysis, CCM3= Community Climate Model. SVD = singular value decomposition.

CHAPTER 4
MEAN BOREAL SUMMER CIRCULATION FOCUSING ON TROPICAL NORTH AFRICA

4.1 Introduction

The tropical North Africa summer circulation is part of monsoon regime. Trade winds, the inter-tropical convergence zone, the Africa easterly jet, the Tropical Easterly Jet and the convection associated with these systems are integral parts of the monsoon that control the climate of tropical North Africa. In this Section, these components are discussed.

4.2 Tropical North Africa boreal summer rainfall

a) Annual cycle

The annual cycle of tropical Africa rainfall exhibits varied patterns. In equatorial Africa a double peak is recognised, having two rainfall seasons and a dry season during boreal summer (Fig. 4.1). The double rainfall region over the equatorial regions is the response of inter-tropical convergence zone crossing twice a year over these regions. Over tropical North Africa, the situation is different. During boreal summer the rainfall activity attains a maximum.

Nicholson and Grist (2001) have identified the annual rainfall pattern based on 78 years (1920-1997). 29 years show a dipole structures in rainfall between Sahel and the Guinea Coast, whilst in phase relation is observed for 25 years. On the mean annual rainfall cycle, the dipole is evident (Fig. 4.1).

The annual cycle precipitation over tropical North Africa exhibits interesting patterns. Equatorial regions show a broader rainfall pattern having a short dry period. The rainy season becomes shorter and the wet period becomes

concentrated from June to July within 7.5°N-12.5°N. Further North, the magnitude of rainfall diminishes in proximity to the Sahara Desert. The Sahel boundary region is where unprecedented drought has occurred in the 1970s - 1990s.

b) Boreal summer rainfall

The mean rainfall for August in tropical North Africa is given in Fig. 4.2. Enhanced convection over tropical North Africa is observed in July, August and September. The boreal summer convection covers a large part of the tropical Africa. In the north, it extends up to the northern limit of the inter-tropical convergence zone (ITCZ). In the South, it reaches into the Congo. The latter region is one of the most intense convection regions of the tropics. It is the northern half of the Congo basin that receives rainfall during boreal summer. The spatial structure of the boreal summer mean rainfall has a V-shaped configuration over this region. The southward penetration of the mean rainfall over the North Congo region can be attributed to the wind deformation field between the two quasi-anticyclones of the South Atlantic and South Indian Ocean (refer Section 4.3). The deformation field generates easterly waves over Zambia and Angola. The trough of the easterly waves interacts with the rainfall in the north and as a result the convection extends south to Namibia (Mulenga, 1998). Besides the deformation field, cold front incursion over southern Africa can maintain the boreal summer V-shaped mean rainfall pattern near of the equator.

During boreal summer, the maximum rainfall activity prevails over the Ethiopian highlands and Guinea Coast. The satellite rainfall estimation using thermal infrared identifies these regions as centres of maximum convection (refer Fig. 2.1). Over these convective regions, more than 450 mm/month is common. A relatively low value of rainfall is depicted over Sudan as shown in Fig. 4.1. This can be attributed to the Nile valley. In the northern and southern limits of the

boreal summer, strong rainfall gradient is found (a gradient of 100-mm within a few degrees of latitudes). Most of tropical North Africa is characterised by a single rainfall (refer Fig, 4.1) except the Southeastern regions. Example, Somali and Northern Kenya experience dry weather during boreal summer. These regions are where the Southwest Monsoon flow diverges (Fig. 4.4a) and are influenced by the associated subsidence (Fig.4.7). The detail dynamics of tropical North Africa is discussed in the following section.

4.3 Boreal summer circulation

Atmospheric circulations that influence the tropical North Africa during boreal summer are discussed in this Section. Mean structures of these circulations are computed based on 1950-1999 NCEP reanalysis data.

a) Mean SST

Over the tropical region of Atlantic, the mean SST pattern resembles the Pacific SST. The difference is the spatial scale of the two basins. The Pacific Basin has the largest east-west horizontal scale.

The mean SST over tropical Atlantic Ocean shows a range of SST values. The northern part of the Atlantic, north of 15°N, has mainly a mean SST temperature of less than 27°C, which is not conducive for initiation of tropical convection. The coldest part of the Atlantic is found in the southern sector where radiative cooling is important. It is over this region where the cold Benguela Current prevails and the strong southeasterly winds produce upwelling. Upwelling takes place in the coastal regions of Angola, Namibia and western coast of South Africa.

Over the northern equatorial Atlantic, a narrow warm pool exists east of 40°W. This warm pool (SST > 27°C) broadens along the routes of Atlantic Hurricanes. It is over this warm SST (north of the equator) that the ITCZ resides. The equatorial

warm pool is the genesis for convection and hurricanes in this part of the Atlantic Ocean.

Over the tropical Indian Ocean, the SST is relatively uniform. Along the track of the southwest monsoon, the SST ranges from 24°C-27°C. Over the equatorial Indian Ocean, east Arabian Sea and Bay of Bengal, the SST rises > 29°C. This high SST value is favourable for convection genesis. The warm Agulhas Current is prevalent over the Southeast coast of Africa. The southwesterly monsoon along the coast of Somali generates upwelling and radiative processes that modulate the variability. The amplitude of SST over these upwelling regions is higher.

b) Sea level pressure and stream flow

In boreal summer, the sea level pressure pattern shows the quasi-permanent anticyclonic gyres over the coldest regions of Atlantic and Indian Ocean. These quasi-permanent pressure systems are Azores high pressure (over North Atlantic), St. Helena High pressure (over South Atlantic) and the Mascarene High pressure (over South Indian Ocean). Over warm pool regions of equatorial Atlantic, a thermal low pressure resides. Over the monsoon regions, deep low-pressure system prevails and shown in pressure field (Fig. 4.3). The question is then what is the role of this type of spatial pressure configuration in setting the circulation? The high-pressure systems over South Atlantic and the thermal low over north equatorial Atlantic initiates pressure gradient force directed towards the equator. The pressure gradient along with friction and Coriolis forces derives the monsoon circulation. These forces balance in such a way so that the West Africa Monsoon system is established and maintained. The same forces work over the Indian Ocean to generate the strongest monsoon flow on the earth. However, the meridional pressure gradient between the two monsoon systems is quite different. Over the Atlantic, the pressure gradient between the thermal equator and the St. Helena High is 4.5-hPa per 10° latitude. In the Indian

Monsoon, the pressure gradient between the monsoon trough and the Mascarene High-pressure system is 10-hPa / 10° latitude. From this simple comparison, it can be visualised how strong the Indian monsoon is.

The degree of association between the monsoon pressure fields is identified as shown in Table 4.1. The annual cycle of the Azores high-pressure system of North Atlantic links feebly with the Southwest Monsoon system. Its relation within the Atlantic Basin pressure systems is very loose (Table 4.2). Therefore, the Azores high-pressure is not maintaining either the Southwest or the West Africa monsoon systems. However, it is important in establishing the ITCZ over north equatorial Atlantic. Equatorial Atlantic thermal low and the St. Helena High-pressure systems are highly linked to the pressure components of the Southwest Monsoon. The equatorial Atlantic thermal low and monsoon trough as well as monsoon pressure index are related negatively and the correlation coefficients are -0.76 and -0.83, respectively. A positive relationship exists between the annual cycle of the Atlantic thermal low and the Mascarene High (r=0.78). Subtropical Ocean high-pressure gyres covary. More than 60% variance goes to the common characteristics.

c) Wind vectors

Low-level circulation

The boreal summer wind flow at 925-hPa shows the following patterns (Fig. 4.4a):

a) Anticyclonic gyres in subtropical oceans.
b) Trade winds in the Sahara Desert and tropical oceans.
c) West Africa and Southwest monsoons.
d) Inter-tropical convergence zone (ITCZ).

Southeast trade winds emanate from the South Atlantic Anticyclone re-curves as southwesterly flow into West Africa. The trade winds from two hemispheres in this basin converge at 10°N and continue the ITCZ to this narrow latitudinal belt (Fig. 4.7) within the Africa monsoon region except the southeast lowland areas.

The ITCZ does not show large north-south movement in the Atlantic, West Africa and east Pacific. It is always north of the equator throughout the year due the presence of trades in southern latitudes. A larger meridional displacement of the ITCZ is shown in Northeast Africa, Indian Ocean and Asia due the reversal of the Indian monsoon winds. During boreal summer, the ITCZ assumes its northern position in Asia (near 30°N). In boreal winter, it propagates as far as 20°S.

Westerly monsoon winds propagate inland and impact the weather and climate of Northeast Africa. These winds impinge on the windward side of the Ethiopian Mountain to produce topographic lifting $\left(w = u\frac{dh}{dx} + v\frac{dh}{dy} \right)$. Support by the upper-level dynamics (Tropical Easterly Jet), results in deep convection (Fig. 4.5a and b). An easterly flow around 600-hPa (the African Easterly Jet) gains momentum to assume maximum strength over West Africa (Fig. 4.5). At the upper level the tropical easterly jet shows its presence with a core region over the Arabian Sea extending across Africa.

The Southwest monsoon drives the low tropospheric circulation. This monsoon flow is linked to the Southeast Pacific winds and winds from the Mascarene Anticyclone contribute to its strength. Its U-shaped structure due the balances of pressure gradient, friction and Coriolis forces reveals different flow pattern within tropical Indian Ocean. In the south, it reveals a 10°-latitude band of easterly flow. These winds as they arrive at 50°E become southerly at the equator near the East Africa coast. Further north, they become southwesterly and westerly east of 80°E. Westerly winds impinge the Western Ghats of India to produce orographic rainfall enhancement as in Fig. 4.5b. The wind in coastal regions of the Horn of

Africa are of low-level jet strength and are known by different names (the East Africa Low Level Jet (EALLJ) and the Somali Jet). The mean core speed of the Somali Jet is 16-18 ms^1 and is located in 5°N-15°N and 50°E-65°E.

The low-level jet produces subsidence and hence a dry climate over southern Ethiopia, Somali and East Africa during boreal summer. This can be seen in the OLR (Fig. 4.7).

Mid-tropospheric circulation

Near mid-tropospheric circulation at 600-hPa depicts easterly flow in tropical North Africa (Fig. 4.4b). Of these, the Africa Easterly Jet in West Africa is the most prominent. This strong easterly flow extends to equatorial South America. In West Africa, the warm Sahara Desert in the North and the cool tropical regions in the Gulf of Guinea generate a horizontal temperature gradient. This temperature gradient maintains the African Easterly Jet (Fig. 4.4b). At the core of jet, the speed is 12-13 ms^{-1}. Ascending motion prevails in the equatorial side of jet core; subsidence dominates on the northern side (Fig. 4.7a). A shallow secondary rising motion prevails from 15°N -20°N. Thorncroft and Blackburn (1999) have shown that latent heat release associated with deep moist convection on the equatorward side of the jet helps to maintain the AEJ. The feedback mechanism between the precipitation and the AEJ is an unsolved problem (Grist and Nicholson, 2001). Krishnamurti (1979) considers the cyclonic wind shear on the equatorial side of the jet as instrumental in the lower-tropospheric wave activity (the Africa Easterly Wave, AEW). Observational studies of AEWs indicate that baroclinic energy conversion is important over land (Burpee, 1972; Norquist et al., 1977), while the barotropic process dominates over the ocean (Thompson et al., 1989). GCM studies also signify the importance of baroclinic processes over land (Ross, 1991). Other GCM simulations under linear mode suggest the waves grow mainly through barotropic energy conversions, similar to the waves of the ocean (Kwon, 1989; Thorncroft

and Hoskins, 1994). Examining the vertical structure of the waves, Grist and Nicholson (2001) suggest that strong baroclinicity exits the north of AEJ, while the baroclinicity is feeble over the equatorial side of the jet.

Upper level circulation

The tropical regions (particularly the Atlantic) in upper level are sandwiched on either side of the subtropical westerly jet streams (Fig. 4.4c). The subtropical jet streams are planetary features and their wind speeds can exceeds 100 m s^{-1}.

In between these subtropical features, another planetary easterly wind flow of tropical origin is depicted in the upper tropospheric circulation (Koteswaram, 1958). Observations reveal the TEJ as a planetary scale feature that extends from Indonesia (west Pacific) to equatorial Atlantic where the tropical North Africa upper-level circulation is driven (Fig. 4.4c). This upper-level jet provides the dynamical lifting for rainfall enhancement for tropical North Africa. The stronger it is, the higher the rainfall in the West Africa Monsoon region.

Height-longitude cross-section of zonal wind

Zonal wind circulation within tropical North Africa is presented using height-longitude representation averaged over 0 to 20°N (Fig. 4.3d). In this cross-section, the main components of the Monsoon are identified. These are the westerly winds of monsoon from (30°W, 35°E) and the easterly flows of the AEJ and the TEJ.

In Fig. 4.5b, the West Africa Monsoon impinges on the Ethiopian Mountains and returns back as easterly flow in the mid-troposphere. The Southwest monsoon remains in the Indian Ocean and does not merge with the African Monsoon. Their influence on Northeast Africa climate is different. The West Africa Monsoon augments rainfall whereas Southwest Monsoon induces dry conditions.

c) Moisture distribution

Moisture is a 'fuel' for convection. Dynamic lifting is possible without the "fuel" but it remains a dry dynamics. It is hence important to examine the moisture distribution in the African Monsoon region. Specific humidity (g/kg) distribution at 700-hPa is used as measure of moisture availability. The dry Sahara in the north and high-pressure gyres in the south squeeze the African monsoon region (Fig. 4.6). The highest specific humidity is consistent with the rainfall pattern (Fig. 4.2) and vertical velocity structure (Fig. 4.6) as expected.

d) Vertical motion

Vertical velocity (Pa s^{-1}) is given in Fig. 4.7 and ascending motion is depicted over tropical Africa. The rising motion in the Congo basin is thought to be the anchor-point for the Atlantic Walker Cell. To the east, descending motion is associated with the anticyclone circulation of the Southwest Monsoon and its diffluent flow. Over tropical Africa Monsoon region, ascending motion is depicted south of the ITCZ due the low-level convergence of monsoon and trade winds.

The east-west pattern of the vertical motion is examined across tropical North averaged over 5°N-20°N. Within African monsoon region (20°W to 40°E), rising motion is found. On either side of this structure, descending motion occurs.

The vertical motion is similarly examined meridionally and is shown in Fig. 4.8a. Two ascending cells are identified in West Africa. A secondary shallow cell is identified in the semi-arid region of Sahel. It extends to 600-hPa and is sustained by a heat low. Its vertical development is inhibited by the stable and dry Sahara airmass. The deep vertical motion within West Africa is balanced by subsidence associated with the St. Helena Anticyclone in the south.

The role the thermodynamics in the meridional circulation is identified in Webster et al. (1998) and shown in Fig. 4.8b. Their main findings are:

a) In deep convection region (OLR < 200 Wm^{-2}), latent heating is the dominant process play part. Regions that satisfy this OLR threshold are sources of latent heating (e.g., tropical North Africa during boreal summer). Where OLR > 280 Wm^{-2}, radiative and sensible heat are sources (e.g.: Sahara Desert and subtropical oceans).
b) Evaporation pays a minor role.
c) Sensible heat maintains the secondary circulation.

Over the tropical Pacific Ocean, easterly winds prevail within a broad latitudinal belt (15°S to 5°N). In the upper-level, westerly winds are depicted in southeast Pacific. Over the rest of the basin, easterly flows are prevalent and form a baroclinic tilt with Indian Ocean upper tropospheric circulation (Fig. 4.9(a to d)). The SST gradient between east and west Pacific is the source of the baroclinicity. The Indian-Pacific circulation linkage operates both at annual and ENSO timescale. The TEJ and east Pacific winds are significantly related. At annual timescale, r=0.862 to 0.935 and at interannual r =0.655 to 0.660. Superimposed on the monsoon flow, the Pacific Walker Circulation and the Hadley Cell play vital roles in the transmission of tropical signals (e.g.: angular momentum).

Using the NCEP/NCAR reanalysis data set (1950-1999), the Hadley circulation over the three major basins is studied in boreal summer. Over Pacific Ocean, ascending motion extends along the north-south direction from 12.5°S-25°N and vertically throughout. This huge cell is accompanied by descending motion from 35°S-15°S.

Across the Indian Ocean and the monsoon trough region, a large Hadley Circulation is present during boreal summer. The upward motion is not as intense as the west Pacific but the area coverage is very comparable. The

strongest ascending motion is located over the monsoon trough region in the lower layers of the atmosphere. Over the southern Indian Ocean subsiding motions are the largest.

Over the Atlantic sector, the ascending branch of Hadley Circulation is bounded within north equatorial latitudes and is controlled on both sides by the descending motion (Fig. 4.10). On these large-scale subsidence motions, the Azores High pressure in the north and the St. Helena in the south dominate the basin's circulation. The Hadley Circulation over the Atlantic and east Pacific has similar structure, likewise the ocean thermal structure as outlined in Chapter 7.

e) Velocity potential

Velocity potential depicts large-scale features in the tropical Circulation. The boreal summer mean divergent flow in the upper level depicts convective polarity between west Pacific and tropical South Atlantic (Fig. 4.11). In between, a strong gradient ($-\nabla\chi=\mathbf{V}(u,v)$ is shown over the tropical Indian Ocean. The tighter the isopleths of velocity potential, the divergent stronger the divergent wind in that region. It is here that TEJ core is located.

Deep convection is associated in the region of negative velocity potential (outflow). West Pacific, Bay of Bengal and India experience high rainfall as result during boreal summer. In the tropical South Atlantic, a quasi-permanent high resides and the upper-level inflow anchors this anticyclone to generate the low-level kinematics to sustain its dry climate.

4.4 Summary

The mean boreal summer circulations that control the climate over tropical North Africa are discussed. West Africa monsoon flows at lower level, the mid-tropospheric Africa Jet and upper tropospheric tropical easterly jet drive the annual cycle of climate over tropical North Africa.

Warm SST over the equatorial regions of Atlantic and cold over the south generates thermal low and high-pressure system in the respective region. As a result, a pressure-gradient force is directed towards the equator generating a curved monsoon flow: West Africa Monsoon: the West Africa Monsoon that 'pumps' moisture into tropical Africa. The Africa monsoon (moist and cool) and northeast trade winds (dry and warm) converge to produce the tropical convergence zone across tropical Africa along 15°N. The compound effect of ITCZ and Tropical Easterly Jet establish a deep convection zone across tropical North Africa. TEJ is an extension of Pacific Circulation through baroclinic process due to SST temperature between west and east Pacific. This concept opens a new avenue in the understanding of the link between Indian Ocean and Pacific circulation.

Near-mid-level feature important in West Africa climate is the African Easterly Jet. It demarcates the moist and cool Guinea coast from dry and warm Sahalian climate. The horizontal temperature between this zone maintains the AEJ through the thermal wind relationship ($\frac{\partial T}{\partial y} \Rightarrow \frac{\partial u}{\partial z}$).

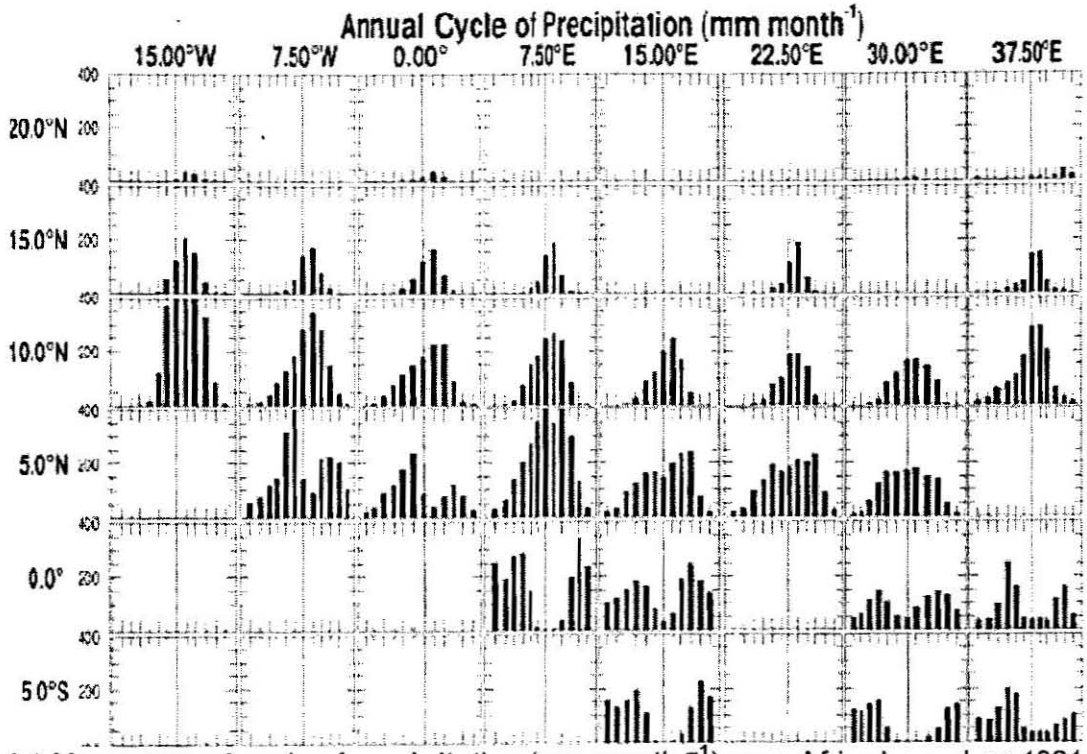

4.1 Mean annual cycle of precipitation (mm month $^{-1}$) over Africa based on 1901-1997 (Warren White, personal communication) showing the single and double rainfall regions.

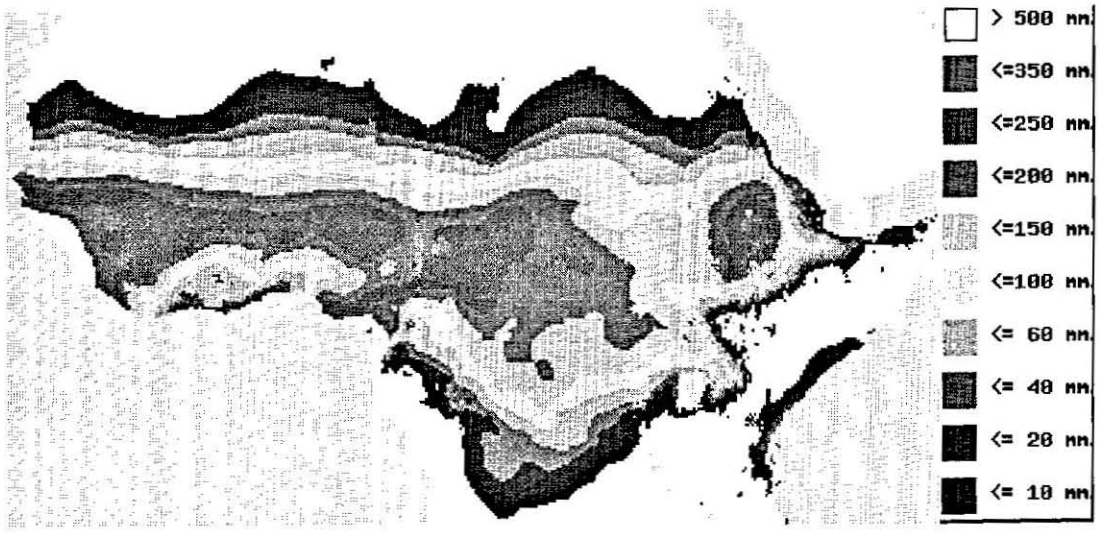

Fig. 4.2 Mean August rainfall (mm) of tropical North Africa based 1920-1980 raingauge data (Obtained from http://www.geog.ucsb.edu/~chris/africa/africa.html).

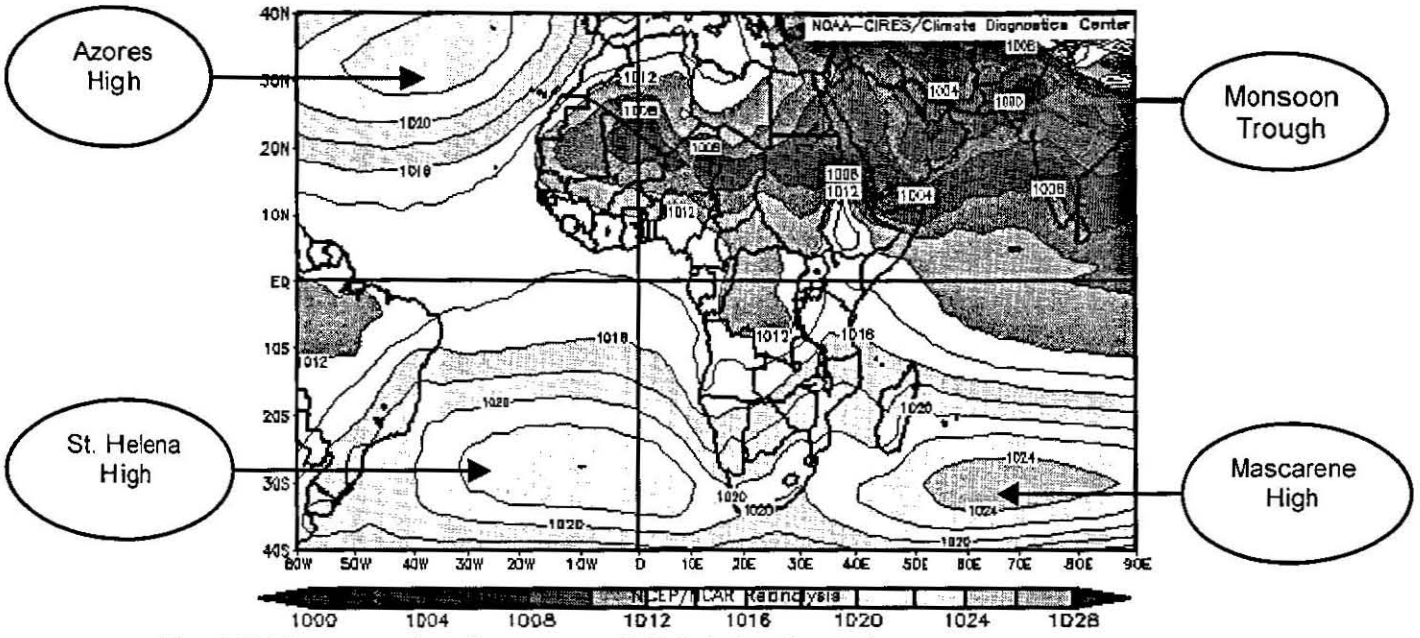

Fig. 4.3 Mean sea level pressure (hPa) during boreal summer.

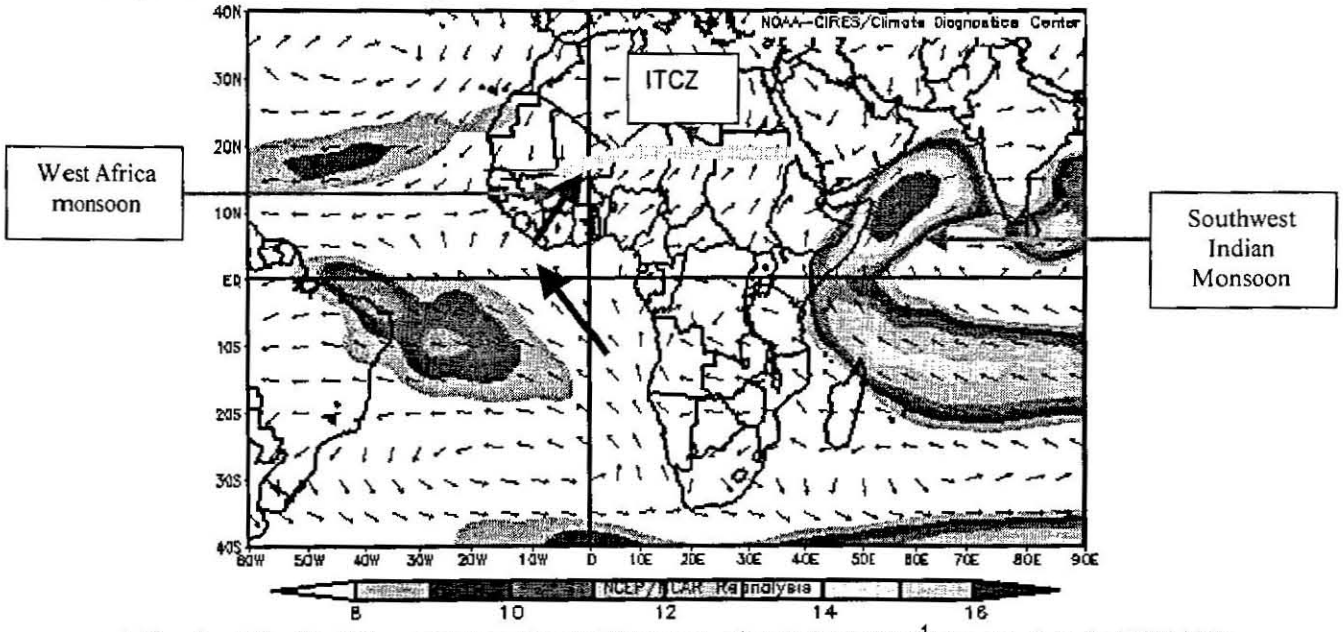

a) Tropical North Africa and Southwest Monsoon circulation (ms^{-1}) as depicted at 925-hPa.

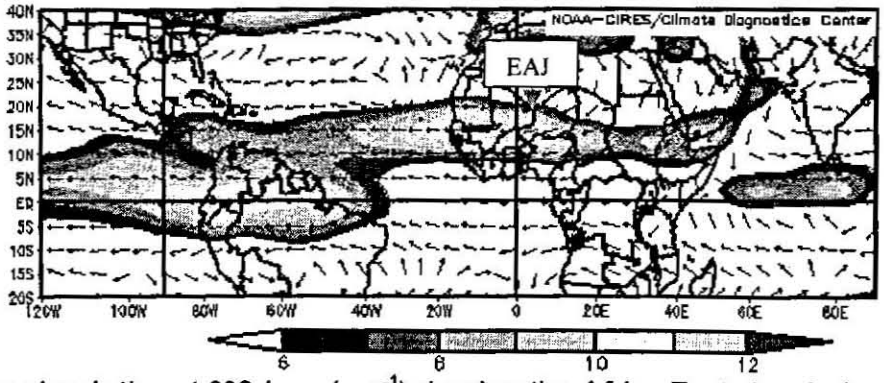

b) Mean circulation at 600-hpa (ms^{-1}) showing the Africa Easterly wind and the jet strength equatorial South America winds.

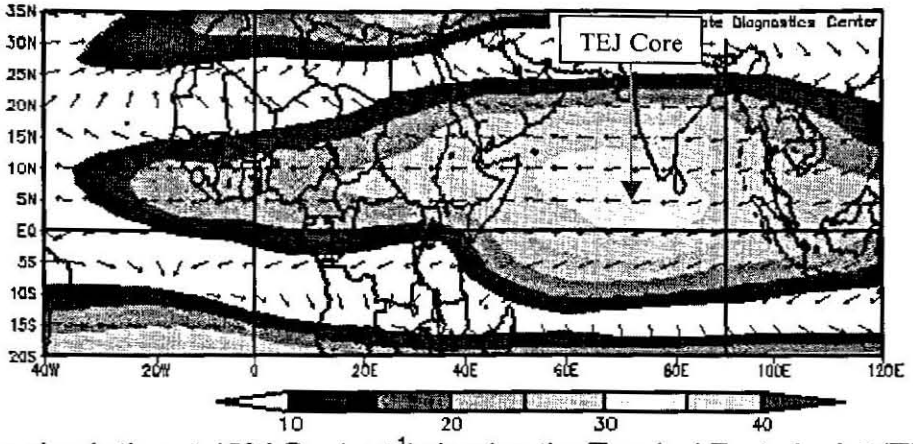

c) Mean circulation at 150-hPa (ms^{-1}) showing the Tropical Easterly Jet (TEJ). The core of TEJ is located over north equatorial Indian Ocean ([0, 10°N], [60°E, 80°E]).

Fig. 4.4 Salient features of boreal summer mean circulation (the monsoon flow, AEJ and the TEJ).

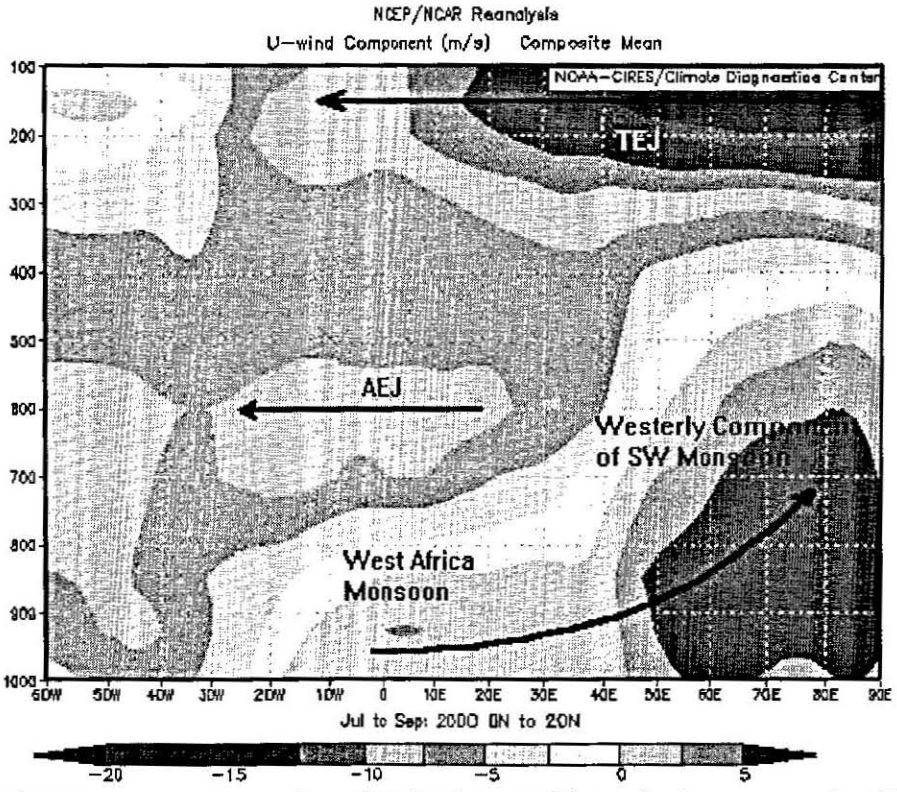

a) Longitude-pressure cross-section showing the most important components of tropical North Africa climate system.

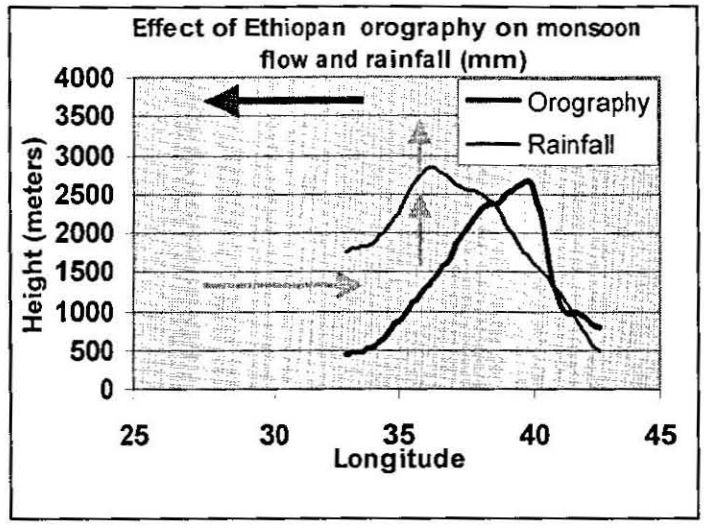

b) Interaction of monsoon flow and orography over Ethiopia. Note that the rainfall in this figure is multiplied by 10 and is based on 1987-1990 rainfall.

Fig. 4.5 The vertical structure of the boreal summer monsoon over tropical North Africa

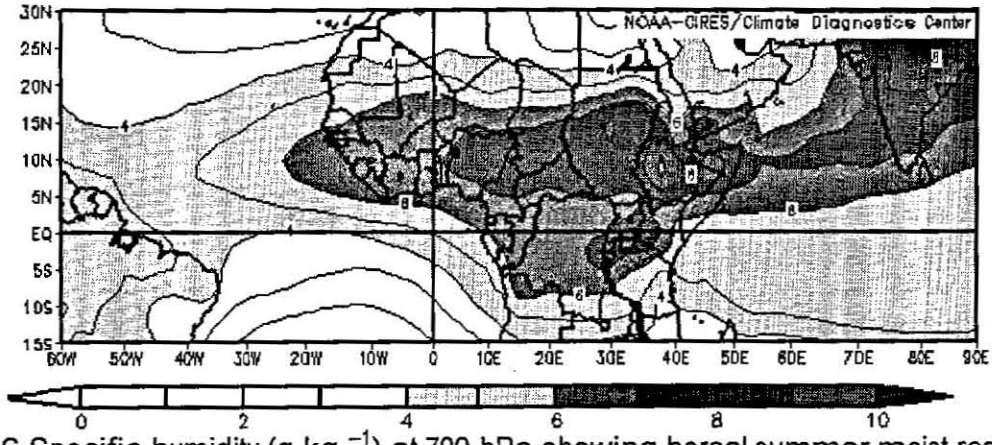

Fig. 4.6 Specific humidity (g kg $^{-1}$) at 700-hPa showing boreal summer moist region of tropical North Africa.

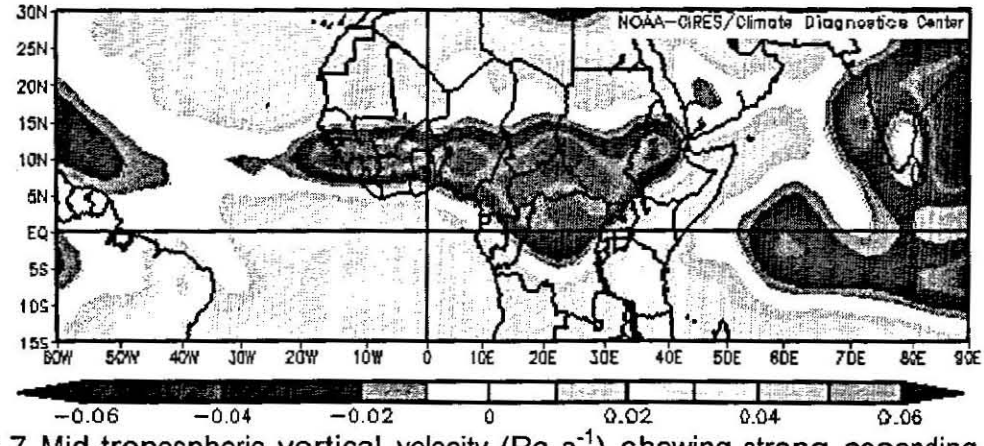

Fig. 4.7 Mid-tropospheric vertical velocity (Pa s^{-1}) showing strong ascending motion over tropical North Africa, India, Bay Bengal and southwest monsoon buffer zone.

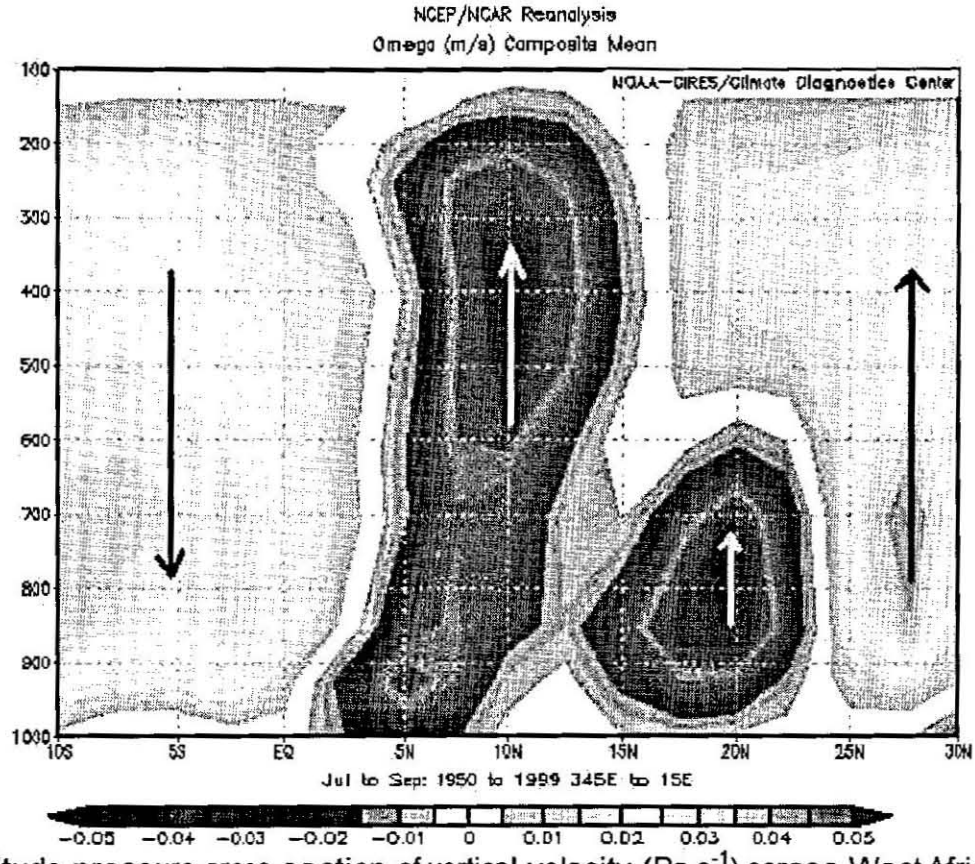

a) Latitude-pressure cross-section of vertical velocity (Pa s^{-1}) across West Africa.

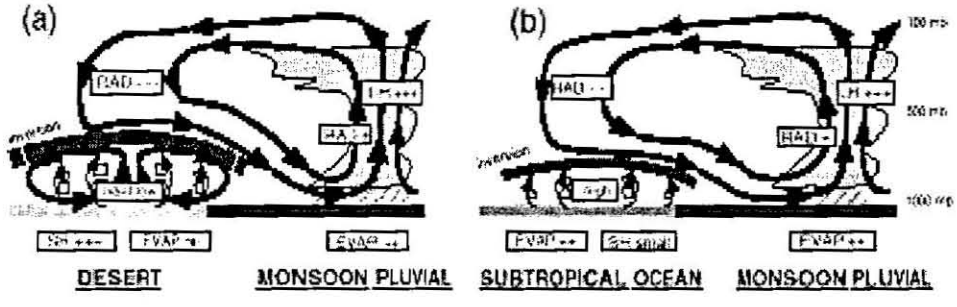

b) Meridional circulation over (a) the desert regions of North Africa and Near East and (b) the subtropical ocean regions and the precipitating (pluvial) part of the monsoon circulation respectively (after Webster et al., 1998). These are the components of monsoon that match the transverse and lateral monsoon components. The tropical North Africa secondary vertical motion has stronger cap and vertical extent to its counter part over southwest monsoon.

Fig. 4.8 Meridional vertical circulations showing Atlantic Hadley Circulation and a two-cell circulation over tropical Africa and over southwest Indian monsoon region.

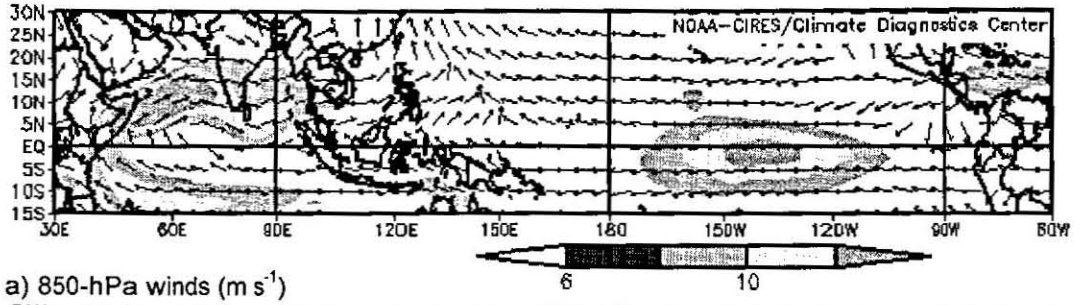

a) 850-hPa winds (m s^{-1})

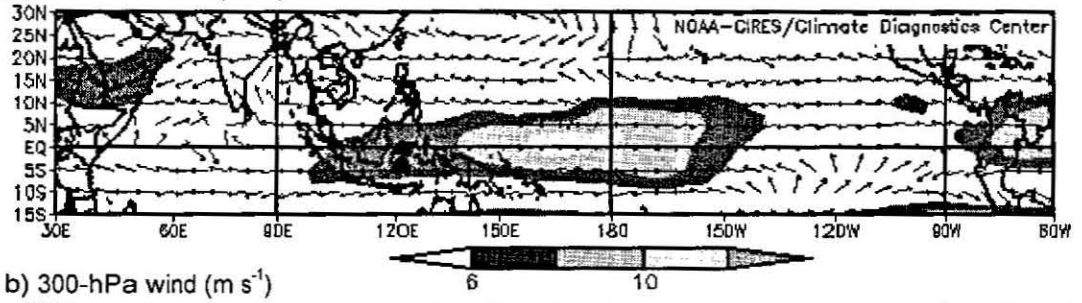

b) 300-hPa wind (m s^{-1})

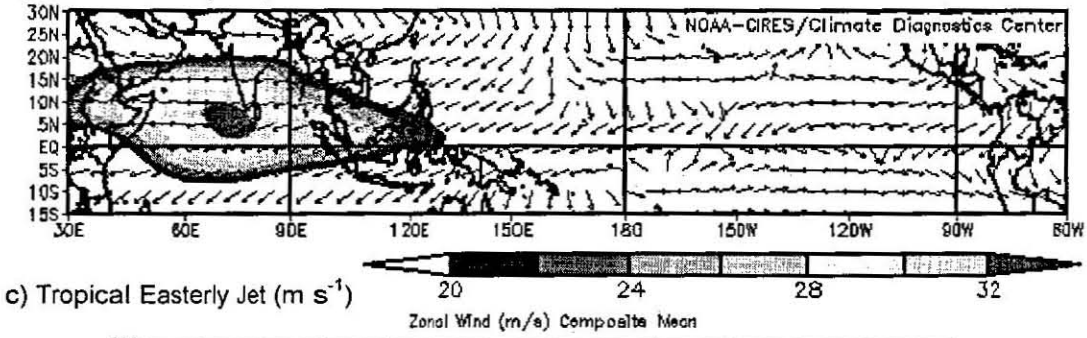

c) Tropical Easterly Jet (m s^{-1})

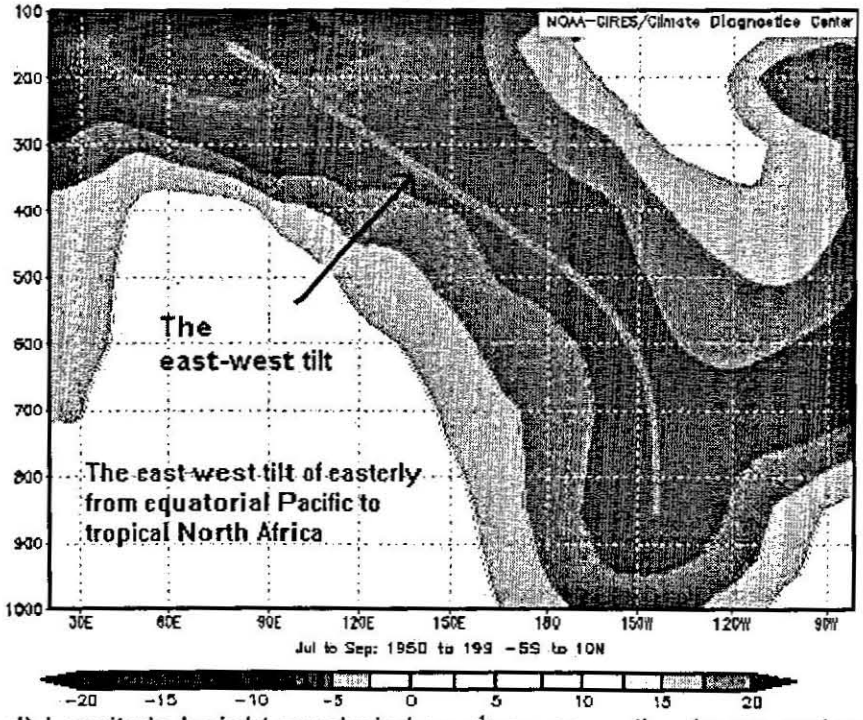

d) Longitude-height zonal wind (m s^{-1}) cross-section (averaged over 5°S-10°N).

Fig. 4.9 Link between equatorial Pacific and Indian winds.

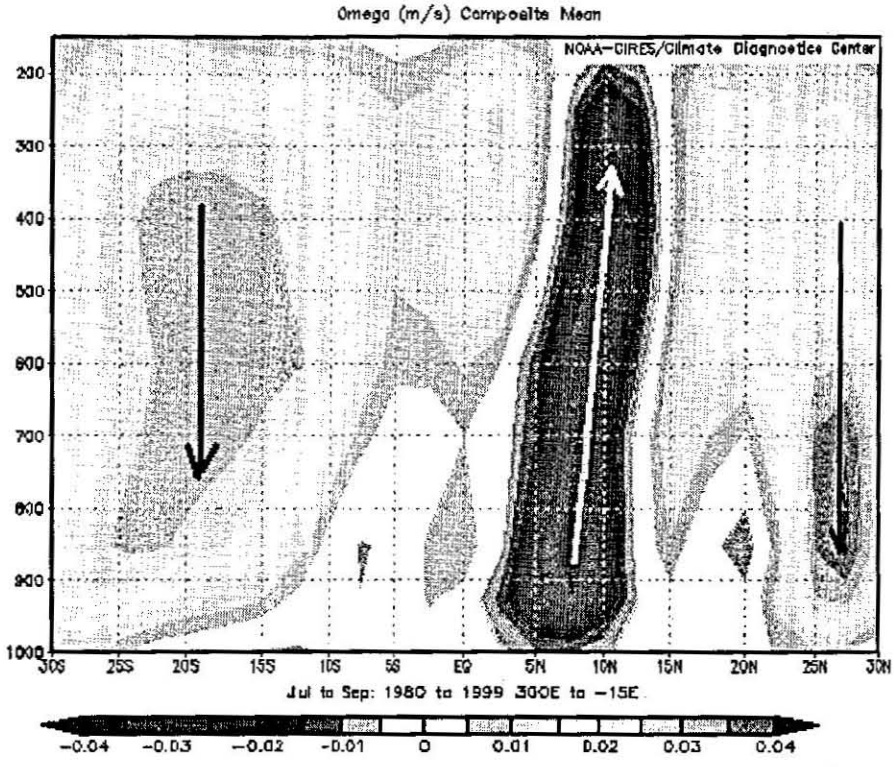

Fig. 4.10 The Hadley circulation in Atlantic depicted by vertical motion (m s^{-1}).

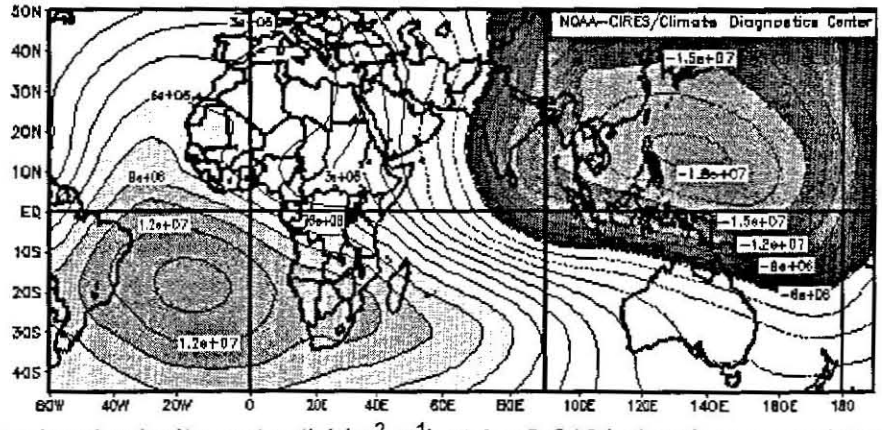

Fig. 4.11 Upper-level velocity potential (m^2 s^{-1}) at δ =0.2101 showing opposing centers of action between South Atlantic Ocean and West Pacific/ South East Asia.

CHAPTER 5

MODE OF ATMOPSHERIC CIRCULATION VARIABILITY WITH RESPECT TO NORTH AFRICA RAINFALL AND RIVER FLOW

5.1 Introduction

The temporal characteristics of the Northeast Africa hydroclimate are revealed in this Chapter using wavelet filtering in Section 5.2.

In Section 5.3, a composite analysis is used to describe the state of the ocean and atmosphere during the extreme phases of hydro-climate variability over tropical North Africa. Coherent structures that follow the continuity equations are revealed. These structures are shown to influence large areas of the tropics other than North Africa. In Section 5.4, correlation analysis is employed to determine the degree of association and teleconnections within the tropical belt and to corroborate the composite analysis. Section 5.5 covers the link between tropical circulations and hydroclimate/SST indices.

The last section covers the spectral links between hydroclimate variables and kinematic variable. This opens an avenue for statistical prediction discussed in Chapter 8.

5.2 Dominant mode of hydroclimate variability

In this Section, the principal mode of hydroclimate variability across Africa is studied using continuous wavelet transform (CWT to decompose the raw standardized timeseries into different time-scales and compute the modulus or evolving spectral characteristics). Additionally, the phase relationship between two timeseries is evaluated in Section 5.6.

a) Timeseries of hydroclimate

The standardised continuous monthly timeseries of the hydroclimate indices of Northeast Africa are plotted in Fig. 5.1. The timeseries entails 574 months of data set for Nile River flow and 588 months for East Sahel. High amplitudes of high-frequency signals are depicted during the 1950s and 1960s. Annual cycle patterns embedded the low-frequency swing known to characterise the Sahelian climate. The decline trend structure is exhibited within standardised timeseries. The Nile flow shares the same characteristics, particularly from 1950-1990 and then a general increase is observed within the variability.

In mono-modal rainfall/stream flow regime, a continuous timeseries plot of rainfall or river flow shows a 'critical line' beyond which no fluctuation is depicted (Fig. 5.1). A horizontal line can be drawn to show that the 'threshold-line'. The threshold-line for East Sahel is -1 and for Nile River flow is -0.5. On the positive side, the top range is 3.5 times the standard deviation revealing high variability. The variability shown in the Sahel rainfall is due to the swing of the boreal rainfall. During the rest of the year, it is a dry period. The Nile River hydrological events normally span from July to October. It is during this period that Nile flow is recharged. During other months, evaporation dominates and the stream flow becomes very low.

The time evolution of the standardised monthly rainfall of East Sahel shows high and low frequency variability (Fig. 5.1). A general increase in the first two decades is followed by a decline thereafter.

b) CWT decomposition of the hydroclimate timeseries

CWT is used to decompose the standardised hydroclimate timeseries into annual cycles to identify the high frequency characteristics and interannual variability.

Annual cycles

The annual cycle of the hydroclimate across Northeast Africa shows consistent high energy in Nile stream flow. The rainfall pattern shows pulsating rhythm in the annual cycle.

The Nile flow has accentuated amplitudes in the annual cycle. The envelope of the annual cycle amplitude modulations has a long cycle in the first half of the records (Fig. 5.2). On the second half it shows a varying amplitude modulations with relatively high values in the second half of 1970s and in the 1990s. In between, the annual cycle has local minimum in the neighbourhood of 1985.

The annual cycle of East Sahel rainfall is not as energetic as the Nile flow (Fig.5.2). It has varying amplitudes. In the first 20 years of the timeseries, horizontally oriented cone-shaped pattern is observed with high annual cycle in the first five years and a decreasing trend up to the late 1960s. From the 1970s to the first three years 1980s, the amplitude vacillates within -0.2 to 0.2. Amplitude increment is seen again from 1983 to 1987. For the rest of the time, the annual cycle oscillates with low pulsation.

Biennial to decadal signals of hydroclimate

Biennial to decadal signals is integrated into a single timeseries to see the holistic picture by excluding very high frequencies. Year-to-year variability embedded with low frequency signals is evident in the rainfall timeseries (Fig. 5.3). The strong biennial to decadal signal observed in the Northeast Africa rainfall, is not apparent in the Nile flow timeseries. At this time-scale, Nile flow signal lucks consistency.

c) Wavelet transform of hydroclimate

A wavelet transform is an important technique to identify the periods of localised maximum spectral energy in the 1.5-16-year filtered hydroclimate timeseries discussed above. The localised spectral energy is displayed in two-dimensional with ordinate showing the period (years) and abscissa representing temporal scale. With these two axes, spectral energy is displayed locally as opposed to Fourier Transform, which provides the overall spectral peak.

The modulus of wavelet transform of the annual cycle provides further insights on the mode of variability on Northeast Africa hydroclimate variability at high frequency timescale. Nile flow at Aswan possesses very consistent annual cycle throughout the record. Though, it is not as remarkable as the annual cycle, the semi-annual cycle has also its contribution. The modulus of the semi-annual to annual of Northeast Africa rainfall does not have the consistence and coherency as the river flow over the region. It meanders from one period to another. The lower range of the spectrum has annual cycle signals and dominates in the first 10 years of the record.

The wavelet transform for the longer time-scales is provided in Fig 5.4. The modulus of the interannual to decadal for Nile flow reveals high spectral energy within 1.5 to 4.0 years. Decadal component has a feeble signal. The East Sahel rainfall depicts strong interannual and decadal signal.

5.3 Ocean-atmosphere composite structures

In this section, the composite of atmospheric circulation and ocean structure is investigated. To achieve this, identification of the extreme modes of climate variability is conducted using a non-parametric approach. The identified extreme years are used to describe the causes of climatic extremes over tropical North Africa.

5.3.1 Hydroclimate composites

Nature of boreal summer rainfall and river flow in Northeast Africa

To unravel the physical mechanisms of the major mode of hydroclimate variability across Northeast Africa, a composite analysis is used. The major mode of variability of Northeast Africa climate in boreal summer is characterised by flood and drought (Fig. 5.5). The time evolution of the hydroclimate variables shows a distinct pattern of high flow /wet spells and low flow/ dry spells. Wet and high flow years occurred in the 1950s and 1960s. While, the 1980s and the first half of 1990s are characterised by dry spells/ low flow. Of these, the 1988 event was exceptional. It is one of the wettest/high flow years in recent times, not only in tropical North Africa, but also throughout the continent.

Selection procedures of composite years

In this study, the timeseries data of Fig. 5.5 is used to select the opposing extreme years for ocean-atmospheric composite analysis. The degree of association between the Nile flow at Aswan and Northeast Africa rainfall is high. The correlation values between July-October Nile flow at Aswan and June-September rainfall over East Sahel is 0.684 based on 1950-1997 data set, and 0.716 in the 1958-1997 period.

A subset of the above timeseries, 1958-1997 during boreal summer (rainfall over Northeast Africa) and July to October (Nile flow), is considered to select the contrasting years to be used in composite analysis on National Centre for Environmental Prediction web site http://www.cdc.noaa.gov/cgi-bin/composites. This period (1958-1997) was chosen, as certain variables like the NCEP reanalysis data for velocity potential and stream functions were available within this period during the write-up of this research.

Once the period is determined, the next stage is preparing contingency table of Nile flow verses East Sahel rainfall to choose the common extreme years for composite analysis.

These contingency tables show the covariability of the hydroclimate variables in Northeast Africa, in non-parametric mode. The number of occurrence in each category is also given in the contingency tables. Most of variability lies within wet/high flow, normal/ normal and dry/low conditions in both contingency tables. The common extreme years of Nile flow versus East Sahel rainfall are selected. The first five wettest and high flow years are 1958, 1961, 1964, 1975, and1988. The contrasting dry years are 1982, 1984, 1987, 1990 and 1991.

Ocean-atmosphere composite structures

Using the NCEP web site, sea surface temperature, sea level pressure, geopotential height, air temperature, wind vectors, divergent and rotational circulation, vertical velocity, and outgoing long wave radiation (OLR), are generated. These composite fields are mapped out in a Cartesian Co-ordinate system. Cross-sections are used to view the vertical structures of geopotential heights, air temperature, zonal wind, specific humidity and omega (ω = dp/dt, rate of pressure change along the parcel's motion).

a) Sea surface temperature composite anomalies

Sea surface temperature (SST) composite anomalies for wet minus dry years are discussed. Below normal SST are observed over the equatorial Atlantic Ocean, South Atlantic Ocean and Indian Ocean and may be attributed to upwelling and evaporation cooling, respectively (Servain, et al., 1998).

The composite SST structure of Pacific Basin exhibits cold tongue of SST anomaly in the east Pacific identical to a strong La Nina episode (Meyers et

al., 1986). This cold tongue is accompanied by warm SST on northwestern and cold in southwestern sectors of the Basin. These oceanic structures are required for the enhancement of convection over Northeast Africa and hence high flow of the Nile at Aswan.

b) Air temperature and geopotential height composite anomalies

To ascertain the thermodynamic structure and potential energy air temperature and geopotential composites are considered respectively. To understand vertical structure of the atmospheric thermodynamic, the air temperature is examined. In the low-level, east-west oriented negative temperature anomaly is shown in tropical North Africa. At 200-hPa a warm temperature straddles the cold equator. A positive temperature anomaly is found in sub-tropical regions of Africa.

In subtropical oceans of Atlantic and Indian Oceans, a wave of cold air temperature anomaly prevails. Vertical structure of air temperature in the tropical North Africa shows negative anomaly in the low-levels associated to precipitating hydrometeors and positive at mid and upper troposphere related to latent heat release of convective clouds.

c) Wind vector composite anomalies

Composite wind vectors are viewed to find out the dynamics responsible for extreme modes of climate variability in North Africa. A westerly anomaly wind extends from northern South America to western Ethiopia (Fig. 5.6a). Anomalous easterlies are strong at 200-hPa (Fig. 5.6b). The wind circulation over the equatorial Atlantic shows a vertical shear with a strong westerly flow in the low levels and strong easterlies at upper levels. This zonal overturning is a unique feature related both African rainfall and ENSO as indicated in the vertical height cross-section of the zonal wind (Fig. 5.6c). This will be further corroborated in the coming sections with other variables. The location of

upper level winds is the mirror image of the low-level wind vectors. This is a typical barotropic configuration of a Walker Cell, such as found in the Pacific.

The degree of association between hydroclimate variables and equatorial Atlantic zonal wind from 1000 to 150-hPa is examined in virtue of finding the connection between the dynamics of equatorial Atlantic and the climate hydroclimate variability across Northeast Africa during boreal summer. To this end, a correlation analysis is used. In this table the East Sahel rainfall relationship is considered as similar results are obtained with other hydroclimate variables. The correlation coefficients (CCs) values are significant and the sign of the relationship reverse in the upper levels. This depicts how the hydroclimate over Northeast Africa is related to the vertical structure of equatorial Atlantic zonal wind. Low- level westerlies coupled with upper-level easterlies result in rainfall augmentation and hence high flow across all Africa (Jury, 1999).

Over the equatorial Indian Ocean, a feeble circulation is depicted at 700-hPa. Increased southerlies pump moisture towards India. At upper level, easterlies extend to Africa.

Over the tropical Pacific Walker Circulation is formed with low-level easterlies enhancing upwelling there. The zonal wind height cross-section shows this cell vividly (5.6c).

The links between the Atlantic Zonal circulation and the Pacific Cell are considered. A strong degree of association between these circulations comes out clearly from the correlation analysis. It is evident that the two circulations are highly linked at lower levels. Pacific Ocean zonal winds are negatively associated with equatorial Atlantic at various levels. The upper level wind of Pacific is as well not coupled as much as the lower level with the Atlantic circulation. The lower limbs of the Pacific Walker Circulation explain 50-70% of the variance of the lower branch of the Atlantic circulation. Its link to the

velocity potential dipole of Atlantic Circulation is equally impressive and the associated average variance in Northeast Africa is 63% and it is by 14% more in South America.

d) Specific humidity composite anomalies

Rainfall production is possible if abundant moisture and rising motion are present at the required moment. Instability, large-scale dynamics and orographic lifting (local) generate the rising motion. The large-scale dynamics produces widespread rainfall. The importance of the latter was discussed above. Here, the availability of moisture and its spatial extents will be considered.

Specific humidity at 500-hPa over Africa is given in Fig. 5.7. Similar distribution is also depicted in the lower level. The moisture composite shows high positive values within 10°N - 22.5°N over Africa. To the east, high specific humidity extends to central Indian sub-continent and equatorial Indian Ocean. The rainfall enhancement over Africa during the boreal summer is possible due the strong rising motion and moisture availability.

A moisture dipole is also revealed in specific humidity field on both side of Atlantic, where tropical North Africa is moisture sink and tropical South America and Atlantic are the moisture source. The moisture field supports existence of opposing centres of action between Africa and South America as in the upper-level velocity potential.

e) Vertical Velocity composite anomalies

To identify the areas of ascent and descent over tropical North Africa and its environs, the ω-field is considered. The vertical motion at 500-hPa shows a dipole of ascending and descending motion in either side of Atlantic emerges consistent with velocity potential discussed above. The rising motion extends

across tropical North Africa. Its opposite structure centred in Brazil extends from tropical South America to St. Helena Anticyclone region of the South Atlantic.

A subsidence in equatorial region of tropical North Africa establishes a Guinea-Sahel dipole that is known to exist in rainfall (Rowell et al., 1995) and poses a problem in Guinea rainfall prediction during boreal summer. The causes of this dipole configuration are investigated in the coming section.

The omega at the mid-level also picks up the links between the tropical North Africa links and Indian Sub-continent. This will be clearer in the specific humidity and OLR composites.

f) Convection composite anomalies

Rainfall over the tropics is not a frontal type (stratified cloud). It is dominantly convective. This can be shown in the outgoing long-wave radiation, the proxy for convection. OLR is used here to identify regions of convection with respect to wet minus dry summers. The OLR shows deep convection over tropical North Africa and is reversed in South America as part of convection polarity between the two regions (Fig. 5.8). The convection also covers West Indian Ocean and Indian Subcontinent.

As discussed throughout this section and consistently shown in the climate system over tropical Africa and tropical South America, there is a physically teleconnection. ENSO plays a significant part in developing the two centres of action via east-west Atlantic Overturning.

g) Velocity potential composite anomalies

Areas of negative velocity potential anomalies are interpreted as regions of strong convection (upper divergence) and positive anomalies depict areas of

subsidence. The closer the isopleths of the velocity potential, the stronger the horizontal wind is.

The upper level velocity potential is studied and consideration is given to identify the centre of actions. The upper level velocity potential in Fig. 5.9 displays two distinct centres of action on either side of the tropical Atlantic. The upper divergent flow reveals a wave number one structure with opposing centres of action side by side. These opposing convective polarities are centred over Northeast Africa and South America (r=0.787 at 200-hPa and -0.871 at 700-hPa). This dipole is observed in vertical motion, specific humidity and OLR fields. These are discussed in the following sections. The implication of this convective polarity is that when widespread convection (rainfall) and high river flow occurs in tropical Africa and India, South America experiences drought and low river flows.

To further establish the physical connections between the two opposing convective regions, a correlation analysis is performed over the core regions of the velocity potential based on 1958-1998 data. The degree of association is studied over the whole vertical structure of the atmosphere. The core regions, where the velocity potential data are extracted, are Northeast Africa ((15°E, 60°E), (15°S, 30°E)) and tropical South America ((105° W, 30° W), (30 °S, 20°N)).

The correlation coefficient establishes a linkage between the two core regions. Correlation values as large as 0.90, in magnitude are obtained. The CCs of the vertical profiles bifurcated symmetrically. The low and the middle levels of the core region of Africa divergent flow are correlated negatively but significantly with South American core region velocity potential. This out of phase relationship becomes in phase when the higher-level irrotational flow of South American core region is correlated with low and middle level velocity potential. Here too the correlation values are very high. The converse holds when upper level χ over tropical North Africa is correlated to the divergent

flow of South America core regions. Hence, the two opposing centres of action are physical linked and are integral parts of Atlantic Circulation variability which govern the hydroclimate variability across tropical North Africa and tropical South America.

Velocity potential of these key regions and the equatorial Atlantic zonal circulation are related at 700 and 200-hPa. In phase relationship is found between Northeast Africa velocity potential and equatorial winds and 81% and 88% variances are involved in this association in low and upper-levels, respectively. A converse link is established over America with an average variance of 76%.

The tie between the East Sahel rainfall and the components of Atlantic Circulation is examined. Atlantic zonal winds accounts for 52% (at 700-hPa) and 57% (at 200-hPa) and its velocity potential at Northeast Africa contributes 60% (Fig. 5.10).

One of the objectives of this research is determine the role of Pacific Walker Circulation and its connection to tropical North Africa climate systems. In the above discussion, it is found that the Walker Circulation is related to the Atlantic Zonal Circulation. How the Walker Circulation is associated to the two centres of convective polarity is perused. The standardised timeseries of Pacific Ocean zonal wind at 850-hPa is correlated with the standardised timeseries of divergent flows over Northeast Africa and tropical South America (Fig. 5.11). The high positive correlation coefficients show the strong relationship between the Atlantic and Pacific overturning and suggest that it is an integral part of ENSO response. During La Nina, tropical South America will be under subsidence while the west Pacific and maritime continent experience substantial rainfall. Tropical North Africa convection is phased locked with the west Pacific but anti-phase with the east Pacific and tropical South America. These linkages have important implication for tropical Africa hydroclimate. The stronger the Atlantic low-level westerlies and upper level

easterlies, the more convection and higher river stream flow are in tropical Africa. Strong low level easterly over east and central Pacific leads to similar situation over Africa.

In summary, the Pacific Walker Circulation and cold episode over the east Pacific coupled with Atlantic zonal over-turning provides the necessary dynamics for widespread convection across Africa Monsoon region. These physical connections are discussed in detail in proceeding sections and in Chapter 6.

5.3.2 Role of regional and local circulation in tropical North Africa climate

a) Atlantic Zonal Circulation

To determine the robustness of the result obtained in hydroclimate composites, the vertical shear of Atlantic between 700 and 200-hPa is generated (u700-u200). From the boreal summer timeseries of this index, the strong positive/negative years are identified and the ocean-atmosphere composites are produced based on positive minus negative or westerly minus easterly flow regimes.

The tropical SST anomalies show La Nina mode of variability. Horizontal wind at 700-hPa reveals strong westerly anomaly from equatorial Atlantic to the highlands of East Sahel as expected. Associated to this low-level flow a cyclonic vorticity is generated north of Gulf of Guinea and anticyclonic circulation in central South America. At 200-hPa, anomalous easterly flow prevails in tropical Africa and Atlantic. Associated to the deformation field, anticyclonic flow is residing over South America; deriving descending motion. Other kinematic (vertical motion and velocity potential) and thermodynamic variables (specific humidity and convection) strongly confirm the existence dipole structures and convection polarity in favour of tropical North Africa at

the expense of South America during La Nina episodes that coincide with stronger Atlantic Overturning Circulation. In El Nino episodes, South America experiences deep convection at the expense of tropical North Africa. This aspect will be further investigated in Chapter 6. The same result is found when a Pacific Walker Circulation index is used in the composite analysis (as defined in Table 5.1).

It is corroborated that the hydroclimate composite structures can be reproducible using kinematic of east-west divergent circulations (Atlantic Zonal Circulation, Pacific Walker Circulation and Indian Transverse Monsoon Circulation) or using their upper or lower limbs. It is therefore concluded that the tropical Atlantic Circulation is a robust system that drives the tropical North Africa and South America convection through ENSO-Walker link. This physical link is further studied using observed data with wavelet analysis in the section to follow.

The same pattern can also be replicated using the TEJ, one of the most important planetary scale features strongly linked to ENSO. All the strongest TEJ occurs during La Nina years and all the weakest TEJ takes places in El Nino years (Fig. 5.22). A continuous data from 1950-1998 show that TEJ is notably coupled to Indo-Pacific SST, filtered data at 1-5 to 16 year bandwidth ($r = 0.747$ with Nino 3 SST). Strong TEJ generates enhanced convection in tropical North Africa and dry condition in tropical South America.

b) AEJ composites

Strong minus weak years of AEJ are used to determine the role of AEJ in the tropical North Africa climate system. Towards this end, composites of ocean-atmospheric structures are produced.

The mid-level specific humidity field reveals a strong north-south contrast between equatorial regions (moist) and Sahel (dry). This type of spatial dipole between Sahel and Guinea Coast has been recognised (Nicholson and Grist, 2001) but the mechanism has not been identified. The middle and upper troposphere vertical velocity also reflects the same patterns with ascending motion in the Guinea Coast and descending motion over West / Northeast Africa (Fig. 5.12). The latitude-height cross-section portrays the co-existence of ascending and descending motion within tropical North Africa (Fig. 5.13). The bean shaped omega fields reveal ascending motion throughout the atmosphere in the equatorial region and subsiding motion over West Africa around 15°N. The opposing circulation establishes the Hadley Circulation within tropical North Africa. Strong AEJ determines the north-south orientation of tropical North Africa rainfall. In OLR composite, intense convection over Guinea Coast and suppressed convection over West Africa is shown confirming the Nicholson and Grist (2001) result.

The upper-level divergent flow shows east-west centres of action between Northeast Africa and western Atlantic (Fig. 5.14) revealing upper-level divergent (deep convection) over West Atlantic and east Pacific and convergence (suppressed convection) over Blue Nile source region.

Strong AEJ produces north-south moisture, vertical velocity, and convection dipole. In the background the east-west centres of action occur between west Atlantic/ east Pacific (intensive convection) and Northeast Africa (suppress convection). The result demonstrates that AEJ has far-reaching dynamic implication in the making of tropical North Africa climate variability particularly in determining the meridional rainfall dipole configuration between Sahel and Guinea Coast. Whilst ENSO may drive the zonal overturning and convective polarity, the AEJ may respond to the north-south SST gradient and merdional overturning.

c) Angular momentum

Angular momentum of a unit mass of air at latitude φ and height z above the earth's surface is:

$$\underbrace{\{u + \Omega(a+z)\cos\varphi\}}_{\text{Momentum Per unit mass}} \underbrace{(a+z)\cos\varphi}_{\text{Displacement}}$$

Where u is the zonal wind and Ω is angular speed of earth rotation. In this equation, the height z (~10 km) compared to earth radius (a ~6371) is very small and negligible. Thus the angular momentum (M) can be reduce to:

$$M=(u + \Omega a \cos\varphi)\, a\cos\varphi$$

The angular momentum of a unit mass of air consists of two parts: the angular momentum due to earth's solid earth ($u + \Omega a^2 \cos^2\varphi$) and the relative angular momentum due to the atmosphere's motion relative to the rotating earth ($ua\cos\varphi$).

Here, the total relative angular momentum of the earth's atmosphere is the focus. This is given by:

$$\frac{2\pi a^3}{g}\iint [u]\cos^2\varphi\, d\varphi dp \qquad (5.1)$$

Where the square brackets denotes the zonal average.

The total angular momentum of the earth's atmosphere (Eq. 5.1) is the integral of the relative angular momentum over all latitudes and through the depth of the atmosphere (integrated with respect to pressure (p)).

The tropics constitute the principal source of angular momentum for the atmosphere while the mid-latitudes constitute the principal sink of angular momentum for the atmosphere.

In this section, globally integrated angular momentum (shown in Eq. 5.1) is used to identify an influence on tropical North Africa climate variability. The data of globally integrated angular momentum is obtained from http://www.cdc.noaa.gov/ClimateIndices/#Glaam generated by Weickmann et al. (2000). Composites are produced from the global integrated angular momentum to find out its influence on tropical North Africa climate variability. Correlation analysis and cross-wavelet transform are also used to find the link between the Atlantic Zonal Circulation and global angular momentum.

Composite structures

Ocean-atmosphere composites are formed based on strongly positive (1979, 1980, 1982, 1987, 1990, 1993, and 1998) and notably negative (1958, 1960,1964,1967,1970, 1988,1987) angular momentum years. The composite structures reveal strong easterly wind in the equatorial Atlantic/ tropical North Africa and strong westerly winds in whole equatorial Pacific, from one end to the other at low-levels. The upper-level winds show strong westerly winds in the equatorial Atlantic, as part of a huge cyclonic circulation over the southeast Atlantic - southern African countries - southwest Indian Ocean and easterly winds over the Pacific, as a part of the twin anticyclones. Strong easterly winds are also shown in the tropical Atlantic and Africa at 30-hPa connected to the quasi-biennial oscillation.

The vertically integrated zonal circulation within the equatorial belt reveals the Atlantic Zonal Circulation and Walker Circulation. These two east-west divergent circulations work in anti-phase mode such that the convection is established over East Pacific and tropical South America and subsidence over West Pacific and tropical North Africa. In this model, West Pacific and tropical North Africa convection are phase locked. In the same way, East Pacific and tropical South America are in phase in terms of convection. This can be shown in the vertical velocity, specific humidity, upper-level velocity potential and OLR composites.

Global angular momentum is teleconnected to Atlantic Zonal Circulation and Pacific Walker circulation in anti-phase mode. Therefore, the angular momentum exerts its influences on tropical North Africa through east-west divergent circulation. This teleconnection establishes upper-level velocity potential dipole between tropical North Africa and South America via the Atlantic Zonal Circulation. This is seen in the height - longitude correlation of angular momentum and zonal wind across the equatorial latitude belts (Fig. 5.15)

Globally integrated angular momentum is related to Pacific SST find out its degree of association with Indo-Pacific SST using 1958-2002 monthly data (n = 520 months). The correlation coefficient between these timeseries is 0.61. A correlation analysis is also performed after filtering the annual and seasonal cycle but maintaining the interannual components. The correlation coefficient after removing the high frequency signals is 0.71 (df=26). This convincingly shows that the global integrated angular momentum and Indo-Pacific Ocean thermal fields are strongly coupled. The cross-wavelet analysis result also supports this result and shows that the angular momentum and Pacific SST temperatures are strongly related at interannual timescale (between 2-6 years). Their co-spectral energy also resides within this period, SST leading the global angular momentum by 2.5 months. This is precisely the additional lead-time that users of climate predictions require.

The variance explained by the interannual timescale of these ocean-atmosphere variables to the total variance is also calculated. The result reveals that the interannual component of angular momentum explains 68% of the total variance. Nino 3 sea surface temperature accounts for 84% of the total variability. The ocean thermal fields therefore contain additional memory and a higher signal to noise ratio. It is through this ocean-atmosphere coupling that the angular momentum modulates the tropical North African climate variability. This is demonstrated in the following schematic illustration.

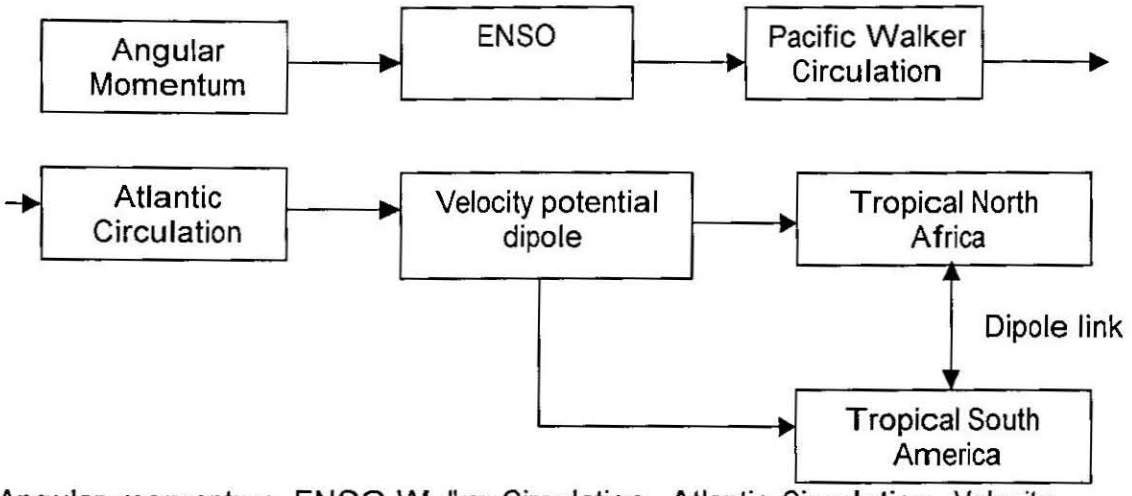

Angular momentum -ENSO-Walker Circulation -Atlantic Circulation -Velocity potential link

5.4 Sahelian climate and tropical circulation teleconnection

In Section 5.3, the composite structures during extreme years were discussed and the controlling dynamics for extreme mode of variability over tropical North Africa were described. In this section, ocean-atmosphere coupling in relation to tropical North Africa and tropical circulation is investigated based on July-August 1958-1997 data for East Sahel rainfall and 1950-1998 for tropical circulations. Indices are developed for tropical circulation based on the result found in the composite results and the study done by Webster (1998). The following temporal analysis is accomplished through wavelet transform technique.

5.4.1 Sahelian climate teleconnection

Sea surface temperatures

The degree of association between sea surface temperature and East Sahel rainfall shows a north-south oriented dipole over Atlantic Basin (the Atlantic SST dipole). This structure sustains itself at 6-month lead-time. This attribute

makes it one of the candidate predictors considered later in Chapter 8. In the equatorial Indian Ocean, a coherent connection is found between SST and East Africa rainfall at 3-month lead-time. A significant negative correlation is obtained in the Pacific cold tongue region east of the Dateline.

East Sahel rainfall is connected to the dominant modes of SST variability in Pacific: the ENSO mode. A new Pacific SST dipole (pSSTd) is found between Northwest and Southeast tropical Pacific at 6, 9 and 12-month lead-time. The same pattern is produced for West Sahel rainfall (Fig. 8.1). The Atlantic and Pacific SST dipoles are co-spectrally analysed using cross-wavelet. The result reveals a band of association in the interannual and decadal timescale. The time-varying modulus shows a shift of spectrum from interannual to decadal from 1950-1980. Since then, the co-spectral energy is anchored within the quasi-biennial timescale. The phase diagram shows a clear coherent signal from 1960-1985 where the Pacific SST dipole leads the Atlantic.

The key SST indices coherently (in time) associated to Sahelian climate are further studied in Chapter 6 to determine their role in tropical North Africa climate variability and will be used in developing prediction models in Chapter 8. The domains of these key areas are given in Table 6.1. The covariability of key thermodynamic indices, hydroclimate and kinematic variables are investigated in Section 5.6.

Zonal winds

The linkage between East Sahel rainfall and equatorial Atlantic zonal winds at 200-hPa is investigated using correlation analysis to determine the influence of the Atlantic Circulation. The result is mapped out in Fig. 5.16. At 700-hPa, a north-south wave pattern is depicted across the tropical Atlantic, Africa and Indian Ocean ($r > 0.6$). The relation is reversed in the Azore High and Sahara Desert implying a horizontal wind shear. The result confirms the composite

result that westerly anomalies lead to augmentation of rainfall over in tropical North Africa given other conditions.

The East Sahel rainfall teleconnection to upper-level Atlantic circulation is as impressive (Fig. 5.16a) but negative. This vertical shear flow is showing the existence of east-west divergent circulation in equatorial Atlantic equivalent to the Pacific Walker Circulation. Hereafter, this circulation is referred as the Atlantic Zonal Circulation.

In equatorial latitudes (10°S -10°N), East Sahel rainfall is related to the zonal wind. Atlantic and Pacific east-west divergent circulations appear to be the dominant preferred modes of variability that determine the Sahel climate swing (Fig. 5.16b). These preferred modes are means of transmission of ENSO signal to Sahel in particular and to tropical Africa in general. This aspect is further investigated in coming sections and Chapter 6.

Specific Humidity and OLR

The moisture field gives additional dimension to Sahel climate links with tropical circulation thermodynamically. Its contribution comes from the existence of a moisture sink in tropical Africa (except Coast of Guinea) and sources in South America and South Atlantic (Fig. 5.17). Of these, the link between Sahel rainfall and South Atlantic moisture is the stronger. A reversed pattern is obtained when convection (OLR) is considered in the same domain. A negative relation is shown in tropical North Africa and in-phase relationship in the moisture source regions (South Atlantic and South America) revealing that Sahelian climate is teleconnected to South Atlantic in out-phase mode. This link is through a Hadley overturning and monsoon circulation as discussed in Chapter 4 (Fig. 4.11).

Velocity Potential

In identification of centres of action in connection to East Sahel climate, the upper velocity potential is related. A wave number one dipole pattern is found between tropical Africa (negative) and Americas (positive). Pillars of the dipole in tropical North Africa and South America replicate, with longer timeseries data, the relation found in the composite analysis in 5.18. The result signifies that Atlantic Zonal Circulation influence on tropical Africa and South America is through the establishment of divergent flow (velocity potential dipole).

Vertical motion

The east-west pattern vertical motion across the equatorial latitude (10°S, 10°N) in a longitude-height plot shows within 140°W-30°W and from the surface to 100-hPa an in-phase relationship between East Sahel rainfall and East Pacific/Atlantic. Outside this region that includes west Pacific and western Indian Ocean, the relation is reversed (Fig. 5.19). It can be concluded that ascent in these regions is related to convection over tropical Africa and hence convection. It is further developed in the section to follow and in Chapter 6 that convection in West Pacific (excluding the Maritime Continent) and tropical North Africa is in phase. It will be pursued that South America and east Pacific convection operates in unison and it is "tuned" to the El Nino signal.

The main result of East Sahel rainfall and tropical atmosphere teleconnection is that Atlantic Over-turning is an integral part ocean-atmosphere coupling that influences the tropical North Africa climate.

5.4.2 Tropical circulation teleconnection

In this section, teleconnections are established within the tropical circulations and links to tropical North Africa climate variability. To find these connections, the interannual timescale of key atmospheric circulation (Table 5.1) is spatially mapped with ocean-atmosphere parameters. To identify ENSO and non-ENSO modes of teleconnection, ENSO signals are determined using the same procedure.

The Atlantic Zonal Circulation and Pacific Walker Circulation are co-involved in the tropical circulation teleconnection. The other preferred mode of variability is the Transverse Monsoon Circulation entailed in the works of Webster et al (1998) and shown in Fig. 5.20. Indices that represent these east-west circulations are shown in Table 5.1 and are used in telconnection analysis.

Southern Oscillation

The Southern Oscillation Index (SOI) is associated with SST and the result reveals cold tongue in east Pacific, opposite pattern in equatorial Atlantic and a phase lock in East Indian Ocean. With the 200-hPa zonal wind, an anti-phase relationship is found between equatorial Pacific and tropical Africa. Particularly, the strong anti-phase pattern between southern equatorial region/tropical North Africa and equatorial Pacific shows the opposed response of Atlantic and Pacific circulations to ENSO mode of variability. The upper-level velocity potential and SOI further reveal the polarity between the tropical Pacific and tropical Africa. The amplitude of the relationship ($|r| > 0.6$) is enhanced between Congo, East Africa, Indian and East Indian Ocean, and east Pacific. The main result is that the upper limbs of Atlantic Zonal Circulation and Pacific Walker Circulation operate in anti-phase mode associated to ENSO variability and generates an 'Atmospheric Bridge'. Tseng (1999) described the "atmospheric bridge" as the mean of transmitting ENSO

signal to Atlantic through global Walker Circulation adjustment. A stronger atmospheric bridge is identified in SOI and sea level pressure field in the Southeast Pacific ($r > 0.7$) and East Indian Ocean ($r < -0.7$). The spatial patterns and magnitudes of SOI links are replicated when Indo-Pacific SST is related to these fields and the teleconnection identified are therefore ENSO connections.

Equatorial Atlantic preferred mode of variability

The equatorial Atlantic is a preferred region of Atlantic Zonal Circulation that influences the tropical North Africa and tropical South America oppositely. The interannual component of equatorial Atlantic zonal wind at 200-hPa is related to the SST, 700 and 200-hPa zonal wind and upper-level divergent flow. Indo-Pacific SST variability signal is depicted in tropical Pacific (Fig. 5.21a). It reveals the same structure and amplitude as SOI in all tropical oceans. The same pattern is found in low and upper-level zonal wind. At 700-hPa, the pattern further suggests that the equatorial low-level circulation of Atlantic and Pacific Oceans operate in a dipole mode (Fig. 5.21b). The same result reported in SOI and velocity potential is reproduced within the Atlantic Zonal Circulation that leads to the conclusion that the interannual variability of Atlantic Zonal Circulation is operating under the influence of ENSO. The same teleconnection patterns are produced using Pacific Walker Circulation and the Indian Transverse Monsoon Circulation Indices. One of the principal points that can be drawn in the tropical circulation teleconnection is that the link between the Pacific Walker Circulation and Atlantic Zonal Circulation is determined by ENSO mode (5.21c). In this low-frequency teleconnection, Africa and South America climate variability swings oppositely (Fig. 5.21d).

5.5 Interplay between tropical circulation, tropical North Africa hydroclimate and SST indices

The relationship of the tropical divergent circulations to tropical North Africa and tropical sea surface temperature is further examined in the temporal domain.

5.5.1 Links between tropical circulation and hydroclimate

To examine the strength of the physical connection between tropical Circulation and key convection regions are related using standardised raw timeseries data of tropical North Africa rainfall, Nile River flow, Brazil and Indian rainfall. The east-west divergent circulations (Atlantic, Walker and transverse Monsoon) and key tropical jets identified important in African Monsoon (African Easterly Jet and Tropical Easterly Jet) are considered.

These circulations are linked to tropical ocean SST indices at interannual timescale. The correlation coefficients are evaluated with df = (n-1)/18.

Tropical circulation and tropical easterly jets

A correlation analysis is performed on the tropical east-west circulation and the tropical easterly jets (the AEJ and TEJ). These jets are significantly related to all the tropical east-west circulation indices at 95% confidence level. The AEJ is strongly but negative associated to the transverse monsoon circulation (r= -0.941). The second highest correlation value (r) is found with the Walker Circulation (r =0.593). Its relation with Atlantic Zonal Circulation is the lowest but significant (r=-0.348). It is recalled that AEJ is a regional wind flow over West Africa. But, it is connected to remote tropical circulations that are global in nature. Compared to AEJ, the TEJ is a large-scale feature in the tropical circulation during boreal summer. The TEJ also is linked to Atlantic

Circulation and the Walker Circulation. The strength of the connection to the east-west circulation is comparable.

Tropical Circulation and rainfall / stream flow

A similar analysis is also performed on rainfall/ river flow and tropical region circulation indices. The result shows the strong connection between these areas and the tropical divergent flows. The degree of association is notably high with the transverse Monsoon Circulation with Sahel and Brazil (r^2= 81% for each region based on n=588 from 1950-1998). The polarity between tropical North Africa and Brazil convection is reflected in these relationships. The Monsoon Circulation is coherent and phase-locked with the tropical North Africa and Indian rainfall. The sign of connection is maintained to the connection to Atlantic Circulation but the amplitude of the relation is generally lower than the Monsoon Circulation. The same can be said with the Walker Circulation index with the sign of the correlation reversed.

Linear regression is applied to the principal east-west divergent circulation indices key hydroclimate regions (entailing Nile River flow at Aswan) to determine the contribution of each circulation to variability of hydroclimate in these regions. The linear regression models are developed based on continuous monthly data from 1950 to 1998 (n= 588 months). For Nile River flow, the regression is based on n= 574 months. Very vital results are obtained from this analysis and the developed models and the adjusted variance ($r_{adj.}^2$) are shown below. In this analysis, the dipole relationship between the Atlantic Zonal Circulation and the Walker Circulation is amply shown with respect to tropical North Africa and South America rainfall. The response of Walker and Atlantic / Indian Transverse Monsoon Circulation on Brazil rainfall is opposite to that of tropical North African rainfall. The Indian Transverse Monsoon Circulation contributes the largest variances in explaining the rainfall variability over these regions. The amplitude of the variance accounted owing to Transverse Monsoon on Brazil and Sahel

rainfall is the same. Walker Circulation accounts for the larger variances of Guinea and Brazil rainfall than Atlantic Zonal Circulation. Tropical North Africa rainfall is however more closely related to the Atlantic Zonal Circulation. The other point that comes from this regression analysis is that the polarity between Brazil and tropical North Africa observed in dynamical, moisture and convection is reflected in the regression models. The out-of-phase relationship between the Pacific Walker and Atlantic Circulation is also illustrated in the relationship between east-west circulations and tropical North Africa-Brazil rainfall.

Atlantic and Walker Circulations

Ethiopian-rainfall	= 0.547(aCIR)-0.410(wCIR), $r_{adj.}^2$ = 50%,
East-Sahel-rainfall	= 0.611(aCIR)-0.439(wCIR), $r_{adj.}^2$ = 75%.
West-Sahel-rainfall	= 0.606(aCIR)-0.484(wCIR), $r_{adj.}^2$ = 65%.
Guinea-Coast-rainfall	= 0.351(aCIR)-0.565(wCIR), $r_{adj.}^2$ = 48%.
Nile-River-flow	= 0.547(aCIR)-0.410(wCIR), $r_{adj.}^2$ = 50%.
Brazil-rainfall	=-0.323(aCIR)+0.526 (wCIR), $r_{adj.}^2$ = 41%.

Note: Atlantic (+) and Pacific (-) overturning.

Transverse Monsoon Circulation

Ethiopian-rainfall	= 0.866(mCIR), $r_{adj.}^2$ = 75%.
East-Sahel-rainfall	= 0.908(mCIR), $r_{adj.}^2$ = 83%.
West-Sahel-rainfall	= 0.906(mCIR), $r_{adj.}^2$ = 82%.
Guinea-Coast-rainfall	= 0.799(mCIR), $r_{adj.}^2$ = 48%.
Nile-River-flow	= 0.570(mCIR), $r_{adj.}^2$ = 32%.
Brazil-rainfall	=-0.909(mCIR), $r_{adj.}^2$ = 83%.

Note: Indian Transverse (+) overturning.

5.5.2 Tropical Circulation and SST indices

The connection between the tropical circulation and thermodynamic variables (domains shown in Table 6.1) are performed with the standardised raw data and at interannual timescale. Equatorial Atlantic and Gulf of Guinea SSTs are connected significantly to the easterly jets, Walker Circulation and the transverse Monsoon Circulation (negatively). Opposite relation but with low r is found with the Atlantic Circulation. The link with tropical Atlantic SST dipole (TASI) is stronger and the sign is reversed. Most of the variance of the association with TASI comes from the tropical South Atlantic SST suggesting it is more sensitive to ocean-atmosphere coupling (with the AEJ and TEJ) than its northern counterpart. North Tropical Atlantic SST is oppositely but strongly related to the Pacific Walker Circulation.

The equatorial Indian Ocean east-west SST dipole is poorly linked to tropical Circulation. But the southern Indian Ocean is interactive and its relation with the tropical easterly jets principally to transverse Monsoon Circulation (r= -0.81), Tropical Easterly Jet and the Africa Easterly Jet (positive and r^2= 70 and 76, respectively) is high.

The same analysis is repeated but for the interannual signals. Generally the amplitude of the relationship is low except for Indo-Pacific SST. The Atlantic Zonal Circulation shows better association in Atlantic. The AEJ is negatively related to TASI, and show that warm south-cold north tropical Atlantic strengthens AEJ. The IOD is poorly connected to the tropical Atlantic Circulation. The Walker Circulation is associated with the southern Indian Ocean SST but not with Atlantic SST. Of all these thermodynamic indices, the strongest atmosphere circulation and SST links comes from Indo-Pacific Ocean. In this connection, Indo-Pacific SST is notably but negatively associated with the transverse Monsoon Circulation, the Tropical Easterly Jet (r = -0.70). Its link with Atlantic and Pacific Walker Circulations is moderate. The link between tropical circulation and SST confirms that ENSO is a key

mode for ocean-atmosphere coupling and atmospheric teleconnection within the tropics. The amplitude of ENSO - Northern Indian Ocean atmospheric circulation connection is exceptionally strong. The TEJ leads the ENSO signal consistently (Fig. 5.27).

5.6 Co-spectral character of tropical circulation: hydro-climate and SST indices

To understand the time evolution of the co-spectral power of tropical circulation indices, hydro-climate and environmental indices, a cross-spectral analysis is applied. To determine the phase relation, a time delay that evolves with time is computed. In all these computations, interannual signals are isolated with a 1.5-16-year wavelet filter.

Atlantic Zonal Circulation

The temporal evolution of the Atlantic Zonal Circulation and the Pacific Walker Circulation circulations covary with time (Table 5.1). The common spectral power reveals a central peak at 4-year period. The amplitude of the power at this frequency is strong from 1965-1990 (Fig. 5.22). During this period, there is no common spectral power > 6-year period, the energy at lower frequency is weak. At quasi-biennial frequency, the wavelet shows a wave structure. The dynamical feature that operates on the ± 4-year timescale is the ocean Rossby wave (White, 2001).

The temporal evolution of the phase relationship shows a variation, where Pacific Walker Circulation leads Atlantic (with a maximum of 10-month) from 1950-1965. The coupling was weak from 1965-1980. The Atlantic-Pacific circulation coupling is stronger from 1980 with the Atlantic leading. This is important finding in ocean-atmosphere interaction and Sahelian climate. The wet epochs of Sahel rainfall occurs when Pacific leads. The dry period of Sahel corresponds to the Atlantic leading. During the decoupling period of

interaction (1965-1980), the Atlantic Zonal Circulation coupled to equatorial Atlantic SST mode. It is during this period that Atlantic Circulation and equatorial Atlantic Ocean shows interaction (Fig. 5.23). The co-spectral energy between Sahel (east and West) rainfall and the Atlantic circulation depicts spectral power in the interannual to decadal timescales. The low frequency signal shows stronger cross-spectral energy. In the phase diagram, the Atlantic Circulation leads throughout the record beyond the annual cycle from 1950-1980. The delay time shows coherent signals during the period when Atlantic Circulation was leading Pacific Walker Circulation (10-month lead). Similar spectral energy and delay-time are obtained between Pacific Walker Circulation and Sahel rainfall.

The temporal evolution of Atlantic and the Indian Transverse Monsoon Circulation indices vary smoothly, particularly during the period 1950-1965. In this period, the two timeseries are in anti-phase. The relationship is very coherent in time principally since the 1980s. Some of these changes could be the result of more data in-filling in the reanalysis model gridded products. The cross-spectral modulus shows co-spectral signal in ENSO timescale (Fig. 5.24). In the phase relation, the Indian Transverse Monsoon Circulation leads the Atlantic Circulation in all years considered. The same phase relationship is found between the Atlantic Zonal Circulation and the Tropical Easterly Jet (leading).

The Atlantic Circulation is co-spectrally analysed with the Nile River flow. The wavelet analysis reveals that Atlantic Circulation and Nile flow have strong common spectral power in the second half of the 1980s. This spectral power is centred at 3-year. A secondary co-spectral energy is present in the second half of the 1960s and the first half of the 1970s in the neighbourhood of 4-year period. The phase relationship depicts a curve that lies above the zero line in most of the years except the first ten years signifying the lead of Atlantic Overturning with respect to the Nile flow.

The equatorial Atlantic and Gulf of Guinea SST displays a similar spectral power and lead-lag relationship when co-analysed with the Atlantic Zonal Circulation. The cross-wavelet spectral modulus reveals a broad spectral power within 1.5 to 6 year period with a 'hole' in the 1970s and the beginning of the 1980s (Fig. 5.23). The amplitude of the spectral power is high in the late 1980s between 3 to 4-year period. A common spectral power is also present at the decadal time scale. The phase curve wobbles in the neighbourhood of the zero line in all years but the 1970s. Then the Gulf of Guinea SST leads the Atlantic Zonal Circulation.

A different pattern is obtained where the tropical Atlantic SST dipole and the Atlantic Zonal Circulation are co-analysed in a spectral wavelet domain. The two indices have decadal signals in their timeseries. This is well reflected in time evolution of their cross-wavelet spectral modulus (not shown). Besides a decadal wavelet spectral signal, a spectral power exists at the interannual timescale. A strong spectral power is portrayed in the 1960s, the beginning of the 1970s, and the 1980s at 4-year period. A quasi-biennial signal is also found in the 1950s and the 1990s. In the phase relationship, the tropical Atlantic SST dipole leads the Atlantic Zonal Circulation in the 1950s and most of the 1970s. The reverse happens during the 1960s, most of the 1980s and the beginning of the 1990s.

The Indo-Pacific SST and the Atlantic Zonal Circulation displays a coherent evolution with time. Their spectral power in the wavelet domain is full of interannual variability from 1965 to 1990 (Fig. 5.25). The overall spectral power is at four-year period with an extension toward the higher frequency. In this cross-spectral modulus, there is no decadal signal. In the phase-relationship, the Indo-Pacific SST generally leads the Atlantic from the beginning of the 1950s to the second half of the 1980s. Commencing from the second half of the 1980s, the Atlantic Circulation takes the lead.

Walker Circulation

The Pacific Walker Circulation spectral relation with tropical circulation, hydro-climate over tropical North Africa and tropical SST indices was examined.

Its cross-spectral modulus with Indo-Pacific SST shows high spectral amplitude at 1.5 to 6-year period from 1970-1990. The phase relation diagram signifies that Indo-Pacific SST drives the Pacific Walker Circulation with a maximum lead of five-month (not shown).

The Walker Circulation and tropical North Africa hydroclimate is analysed in cross-spectral domain. The result reveals a strong link between the two.

Transverse Monsoon Circulation

The transverse Monsoon Circulation and Indo-pacific are analysed in wavelet domain. The Monsoon Circulation and Pacific SST are twined at the heart of the interannual timescale. In this relationship, the monsoon circulation leads the east Pacific SST. The same result is found between the Tropical Easterly Jet and Indo-Pacific SST.

The transverse Monsoon is connected to Nile River flow at ENSO timescale. The phase relationship reveals that the Monsoon Circulation leads the Nile River flow in almost all years considered (Fig. 5.26).

The upper limb of the transverse Monsoon, the TEJ, shows a spectral and time delay association to Nino 3 SST (Fig. 5.27). These covary harmoniously with time and spectrally in ENSO frequency band (within 1.5-8-year period). The amplitude of spectral energy is strong in the 1970s and 1980s. In the phase relationship, the TEJ leads Nino 3 coherently throughout the period (1950-1998) with half of the annual cycle vital for prediction purpose.

5.7 Conclusion

Understanding the physical mechanism of hydroclimate across tropical North Africa has been a challenge for researchers for quite some time (Servain et at, 1998). This challenge is a driving force for this study. Various methods are employed to shed light on it. Wavelet transform proffers better insight on the nature of the temporal evolution of hydroclimate variables. Spectral decomposition reveals that the Nile River flow possesses a high frequency signal. But, the Sahel rainfall has dominantly biennial to decadal components. The understanding of the time evolution of the hydroclimate leads to answering the question: what is the driving mechanism for these modes of variability? Composite and correlation analyses are used to describe the problem. The composite analysis, underpinned by longer time correlation analysis, revealed a dipole SST structure over the Atlantic (cold anomaly in the south, warm anomaly in the north) and a cold tongue over east and central Pacific. Simultaneously, the Atlantic zonal circulation and Walker Circulation are established. These east-west circulations influence the regional climate in turn. As a result, two opposing centers of action are established on either side of the tropical Atlantic (via upper level divergent flow) to generate convection polarity between tropical North Africa and South America. The transmission of these opposite responses is executed through the Atlantic Zonal Circulation. The Walker circulation provides additional impetus for widespread subsidence over tropical South America. The link between the ocean-atmosphere coupling and Africa climate is the equatorial Atlantic zonal shear ($\partial u/\partial z$) that transmits the ENSO signal kinematically.

The modulus of co-spectral energy between the Atlantic Zonal Cirulation and the Sahelian rainfall shows a common energy at ENSO and low frequency, particularly during the period when Atlantic Zonal Circulation leads the Pacific Walker Circulation. The time-delay in the phase diagram three turning periods: Walker Circulation leading (1950-1970, wet epochs of Sahel), passive ENSO-coupling (1970-1980, dry periods of Sahel), and Atlantic

leading (after 1980). During the equilibrium period, the Atlantic Zonal Circulation being a thermally driven circulation has to interact with the underlying equatorial Atlantic SST. Though the Atlantic SST is a "slave" to ENSO during weak or inactive ocean-atmospheric in Pacific, the Atlantic SST mode plays a significant role in driving the Atlantic Zonal Circulation. The other important finding is the strong coupling between the Indian Transverse Monsoon Circulation and ENSO signal and the coherent lead of northern Indian Ocean circulation over Indo-Pacific SST that provides an avenue for climate prediction.

Regionally east-west divergent circulations determine the convection polarity between tropical North Africa and South America. Locally, the AEJ delineates the north-south configuration of thermodynamics and kinematics across Sahel-Guinea Coast through meridional Overturning. A strong AEJ generates deep convection in the Guinea Coast and subsidence over the West Sahel, thereby producing the Sahel-Guinea Coast rainfall dipole.

The other pivotal issue that is addressed in this Chapter is global tropical teleconnection. The key tropical circulations at interannual timescale reveal the ENSO mode and large-scale configuration: SST dipole, a pressure sea-saw, and opposing upper-level divergent flow and convection polarity between Pacific, Atlantic and Indian Ocean operating through three principal divergent circulation (Walker Circulation, Atlantic Zonal circulation and transverse Monsoon Circulation). The main finding of the correlation analysis is that Atlantic Circulation and Walker Circulation operate in opposite mode where ENSO signal explain most of the variability of this anti-phase relationship (Fig. 5.28). The east-west circulations are more sensitive to the Indo-Pacific SST than to other equatorial SST signals in the Atlantic and Indian Ocean except during weak atmosphere-ocean coupling in Indo-Pacific (e.g.: when the ocean Rossby Wave forcing conflicts). This is clear in the teleconnection between ENSO and east-west divergent circulations.

Increased global angular momentum suppresses convection over tropical North Africa. Some of the dynamical features of these interactions are further examined and explained in the coming sections.

A phenomenon that comes closest to exhibiting periodic characteristics in the mean zonal winds of the equatorial stratosphere is the quasi-biennial oscillation (QBO). This oscillation has zonally symmetric easterly and westerly wind regimes (easterly and westerly phases) that alternate regularly with a period varying from 24 to 30 months. It is depicted at 50-30-hPa levels. QBO derives its energy and momentum from the tropical troposphere through mixed-Rossby-gravity waves and Kelvin waves. The energy of these gravity waves leaks through the tropopause.

The west phase of QBO appears to be in-phase with the Pacific SST and Atlantic SST dipole. This QBO-ocean coupling results in suppressed convection over tropical North Africa (Fig. 5.29).

When the Pacific SST signal is weak and a reversal of tropical Atlantic dipole mode occurs, then the Atlantic dipole modulates the surrounding regions through the meridional Overturning shifting the centres of convection (the ITCZ) to equatorial regions of tropical North Africa. As a result, dipole configuration is established between Sahel-Guinea regions.

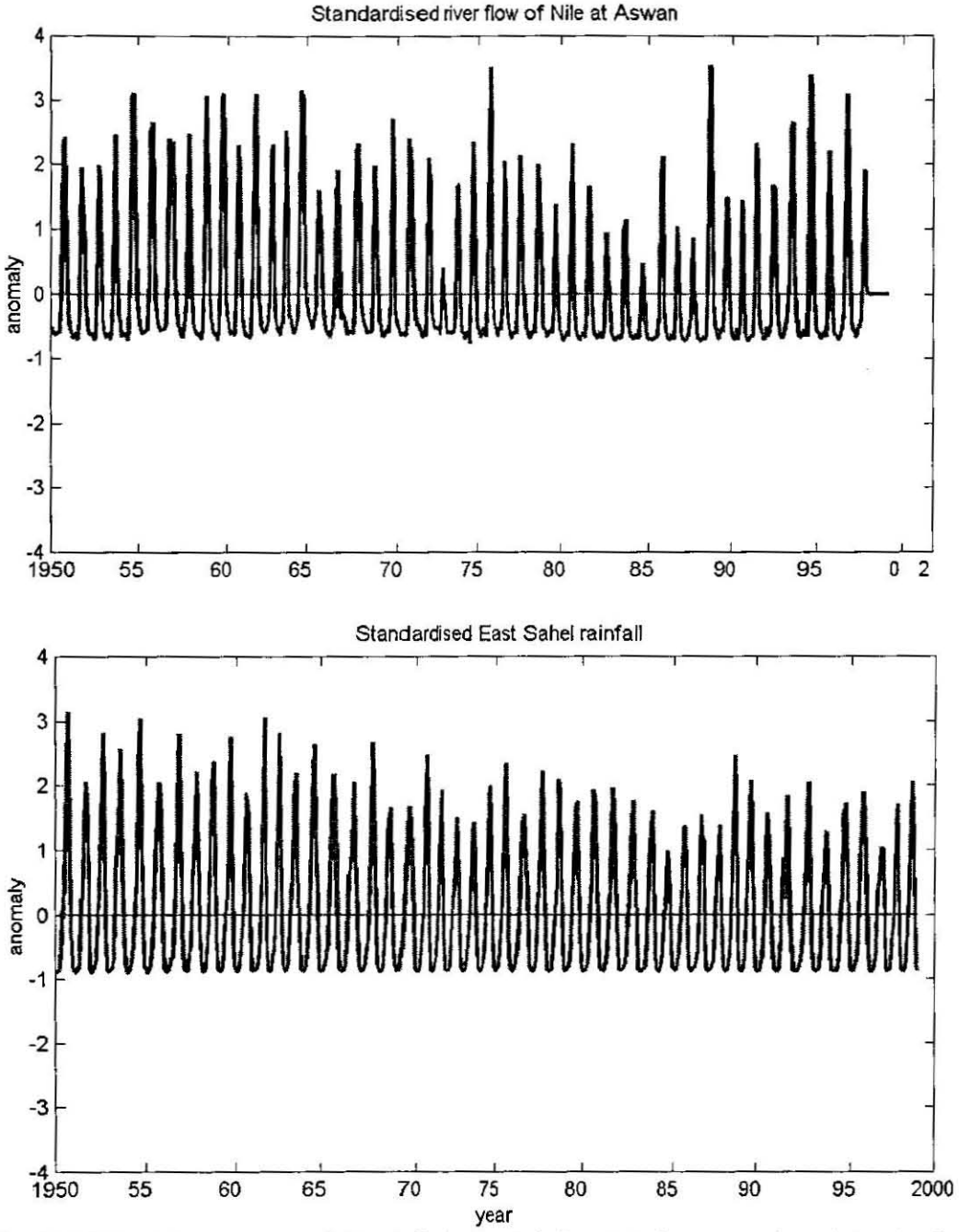

Fig. 5.1 Nile River flow and East Sahel rainfall monthly timeseries (standardised) where the annual and interannual timeseries are derived from (refer Fig. 5.2 and Fig. 5.3).

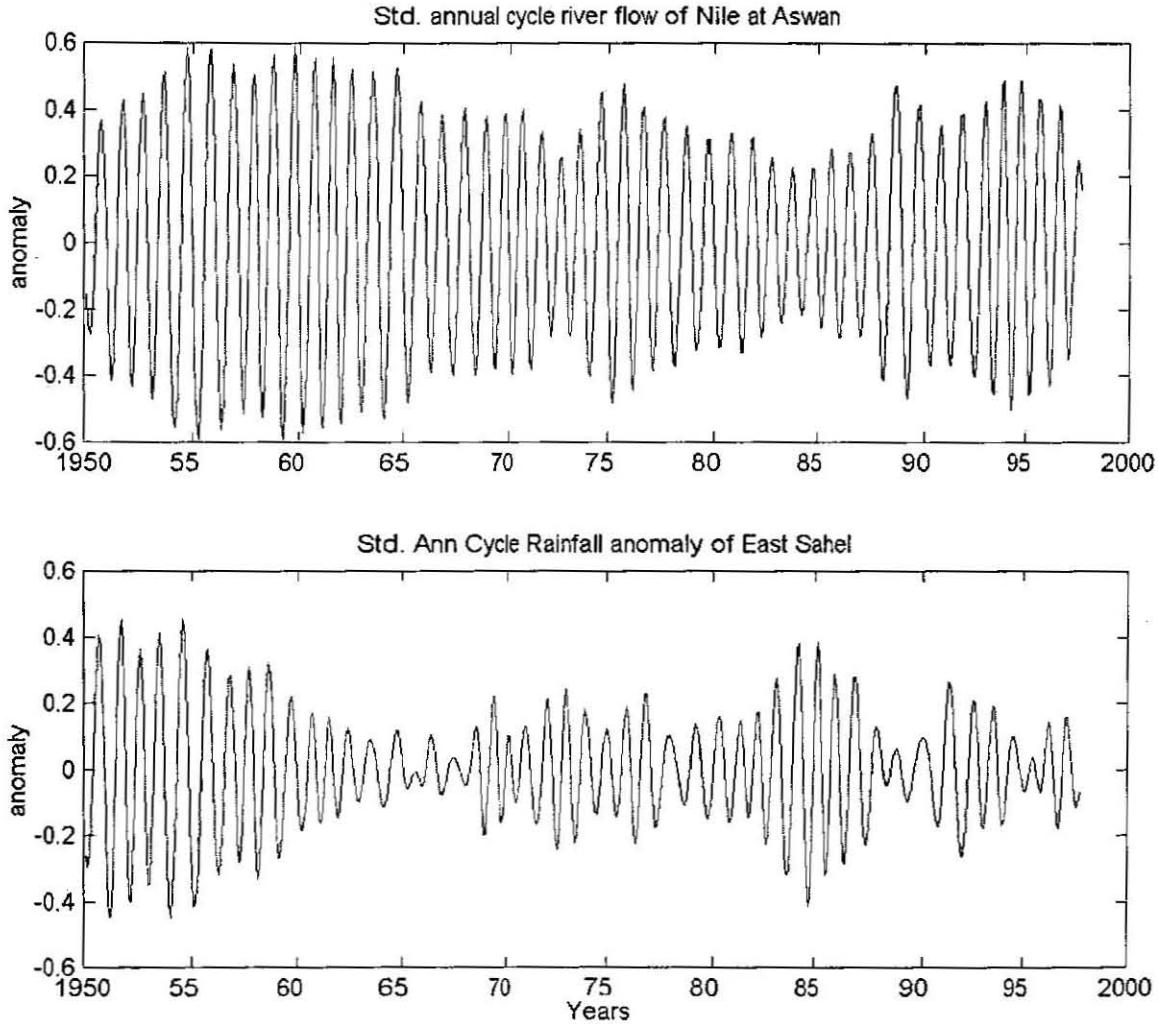

Fig. 5.2 Annual cycle of Nile flow at Aswan and East Sahel rainfall (standardised).

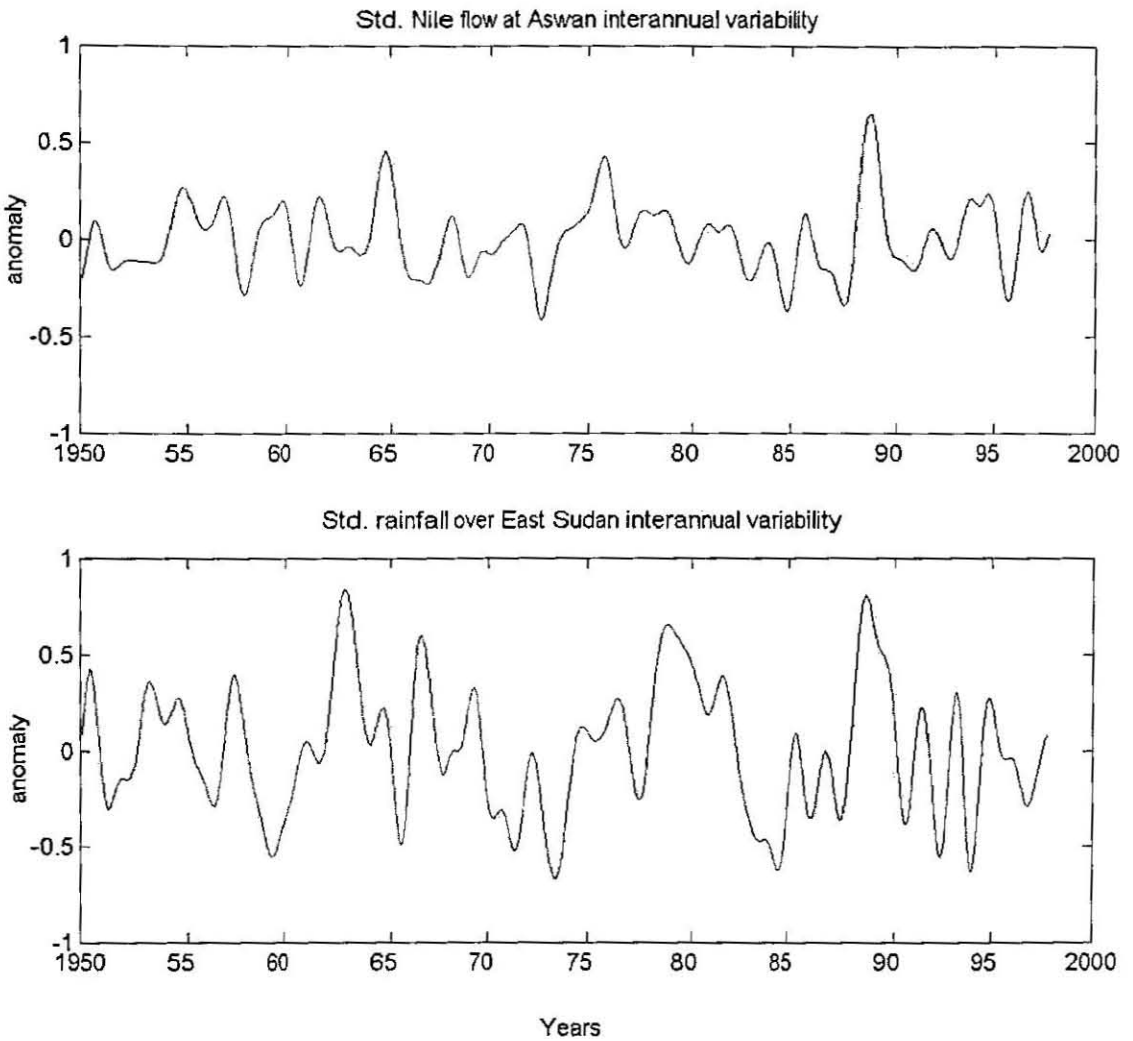

Fig. 5.3 Interannual variability (filtered in the range 1.5-16 years) of Nile flow at Aswan and East Sahel rainfall (standardised).

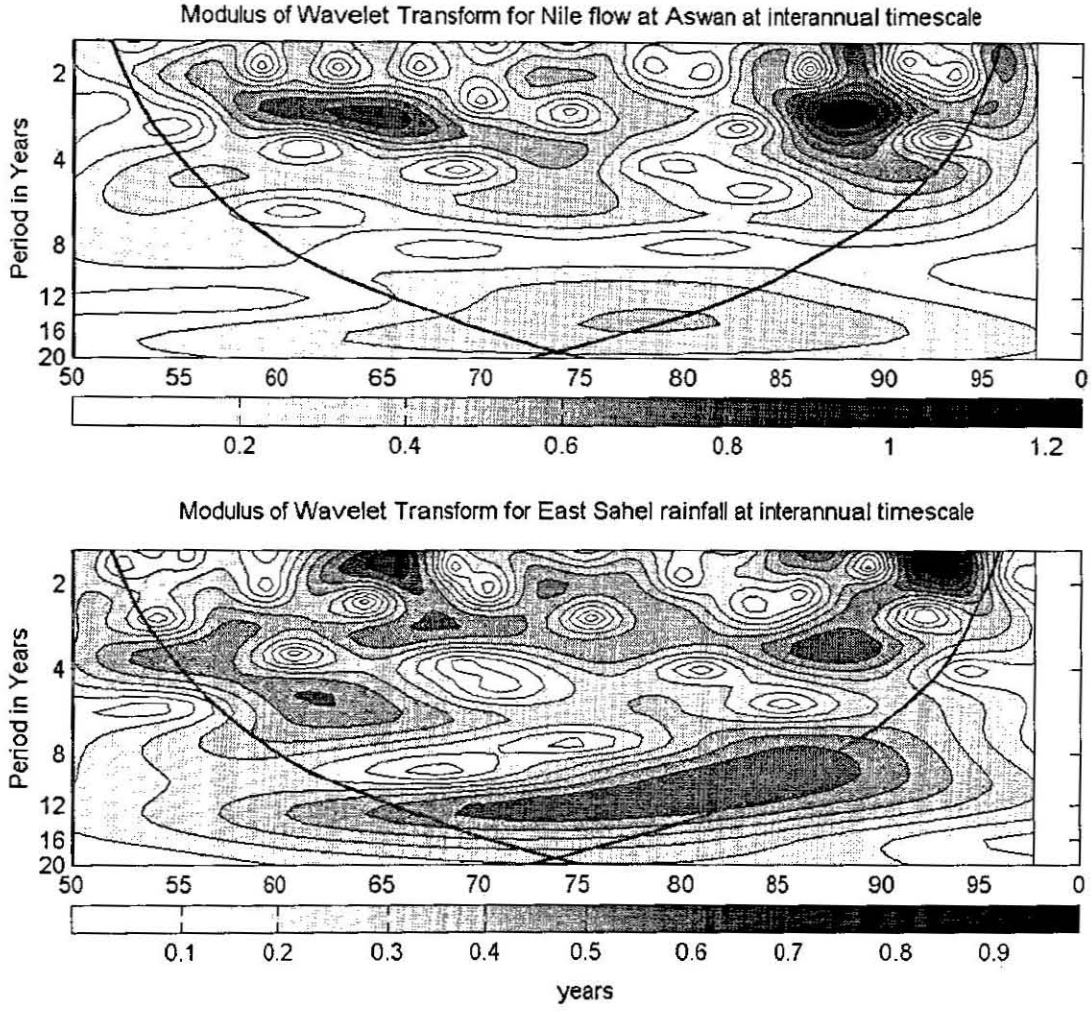

Fig. 5.4 Modulus of wavelet transform for Nile flow at Aswan and East Sahel rainfall.

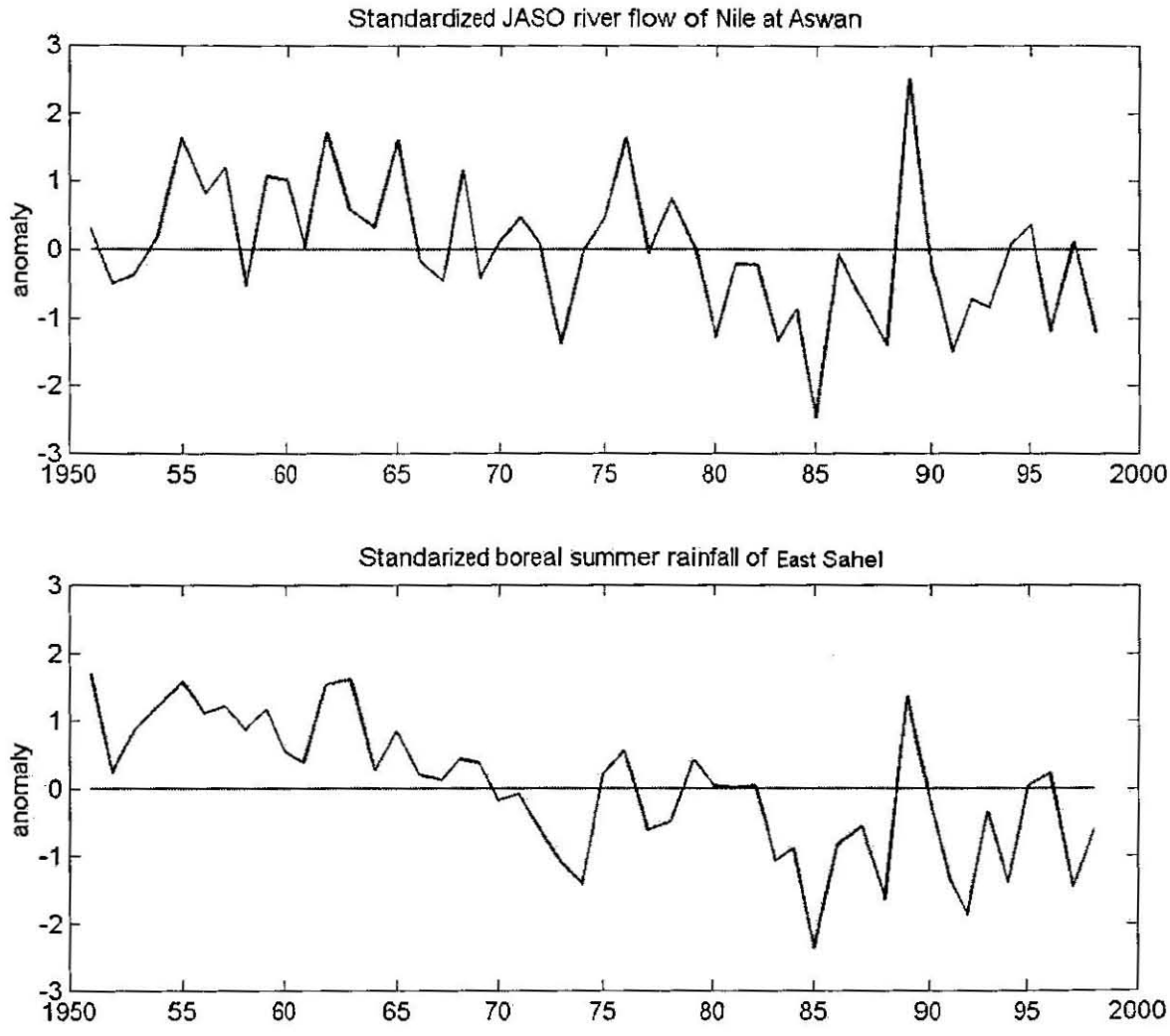

Fig. 5.5 Standardised temporal evolution of boreal summer Nile flow at Aswan and Northeast Africa rainfall where the wet/high flow and dry/low flow years are selected.

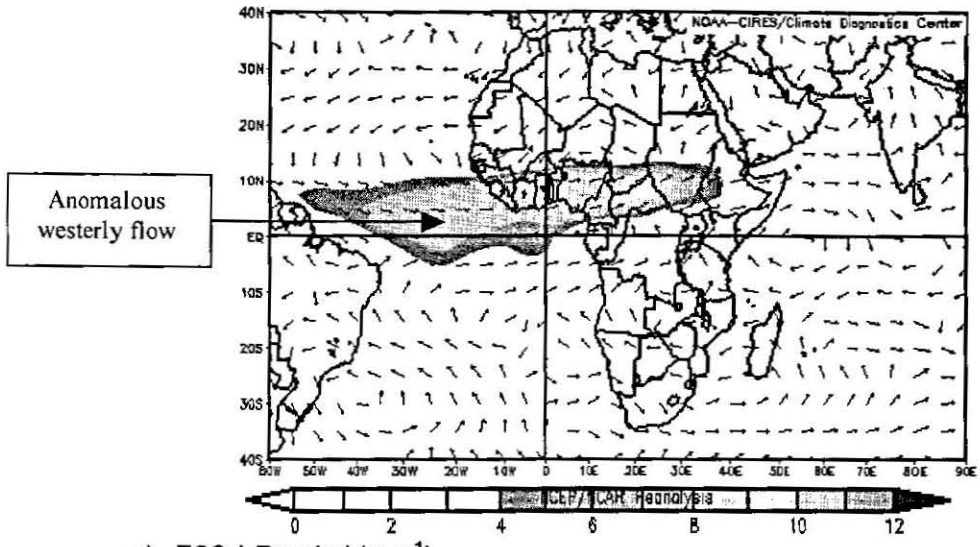

a) 700-hPa wind (ms^{-1})

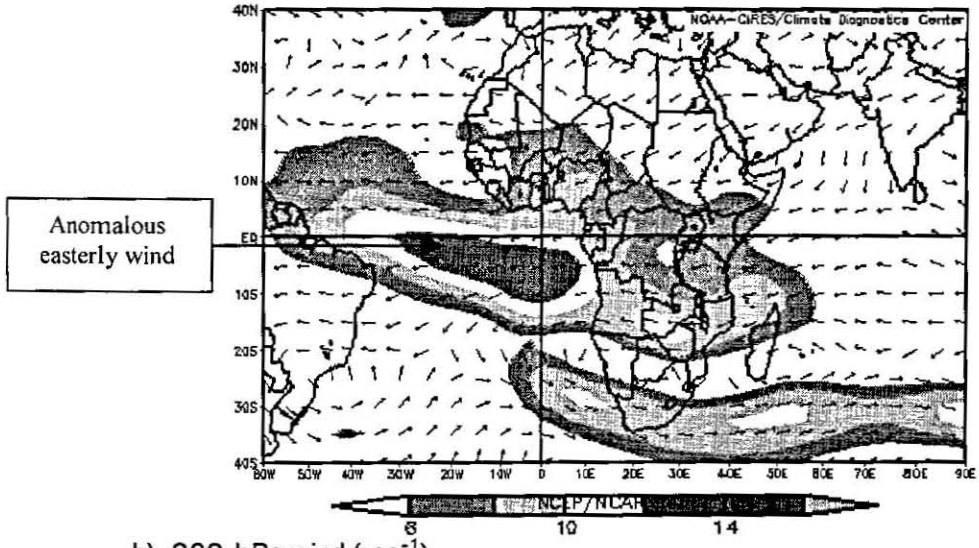

b) 200-hPa wind (ms^{-1}).

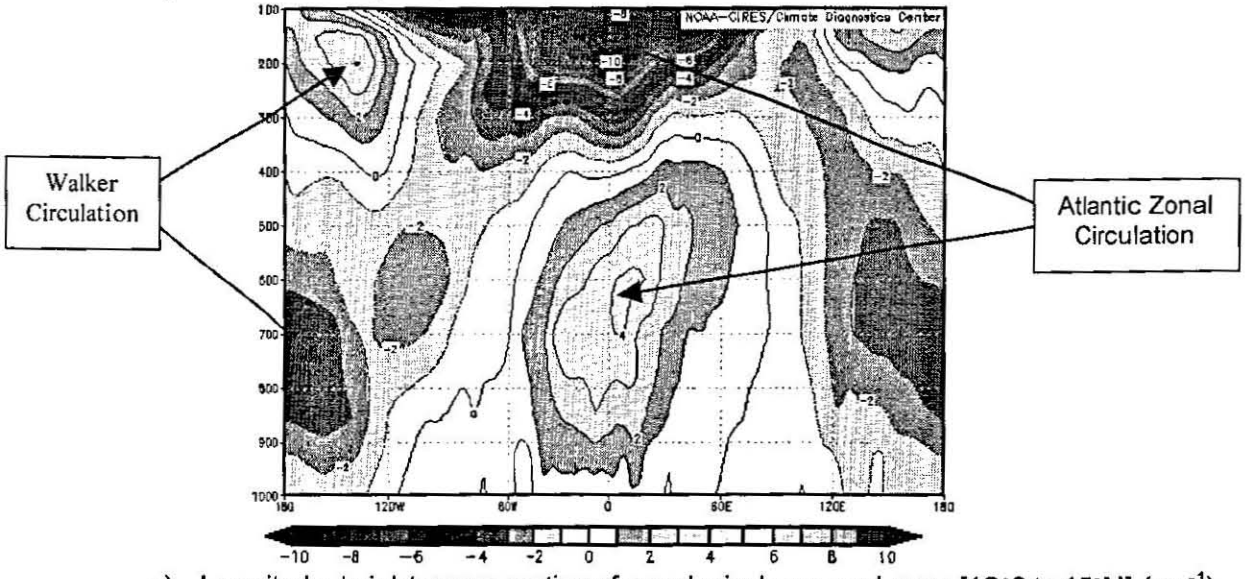

c) Longitude -height cross-section of zonal wind averaged over [10°S to 15°N] (ms^{-1}).

Fig. 5.6 Circulation patterns during wet and high flow years over Northeast Africa based on JJAS rain and JASO river indices.

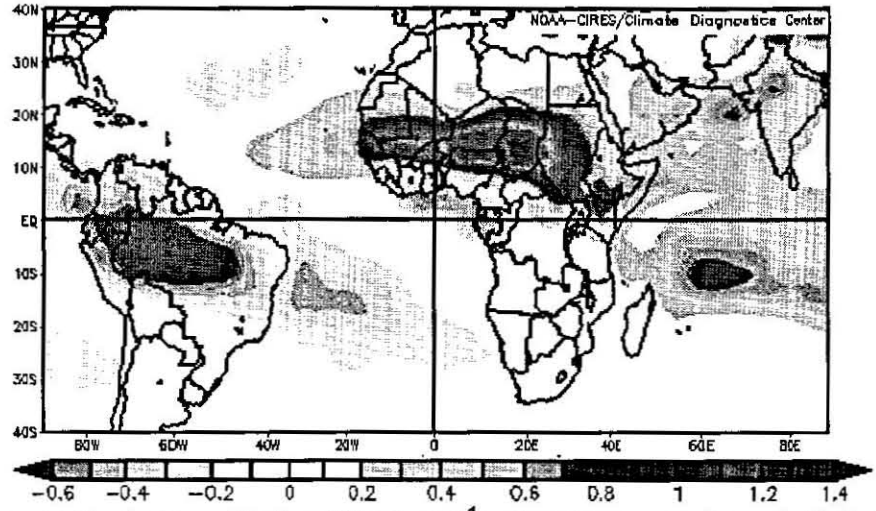

Fig, 5.7 Mid-tropospheric specific humidity (g kg^{-1}) showing opposite polarity between tropical North Africa and South America.

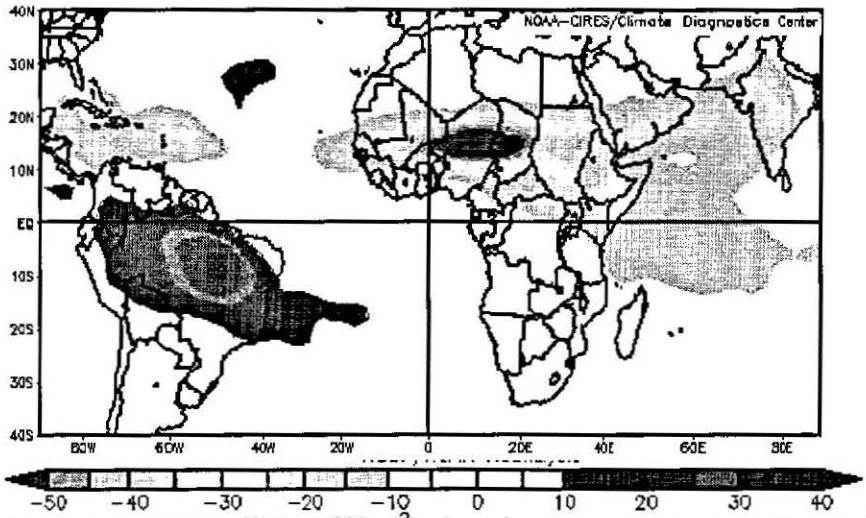

Fig. 5.8 Outgoing long-wave radiation (Wm^{-2}) showing opposing convection polarity between tropical North Africa and South America.

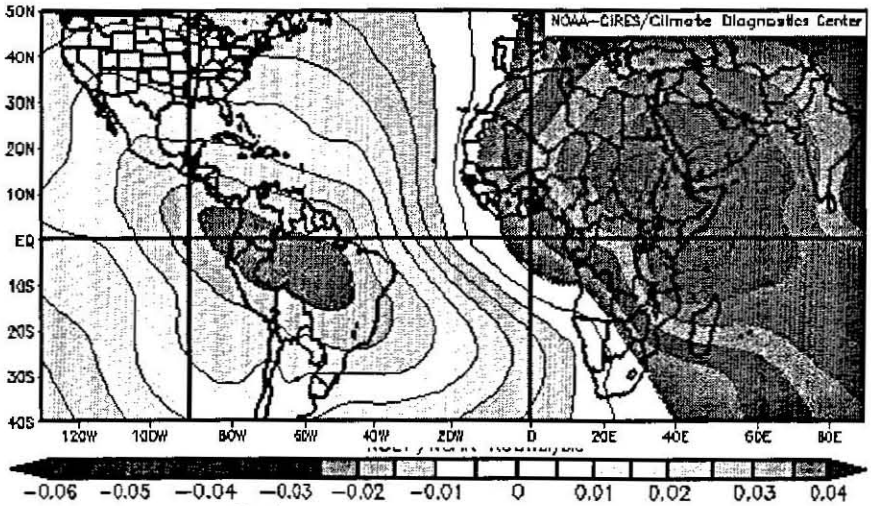

Fig. 5.9 Velocity potential (m^2s^{-1}) at δ = 0.2101 showing upper level outflow over tropical North Africa and inflow over tropical South America with respect to wet/high-dry/low years.

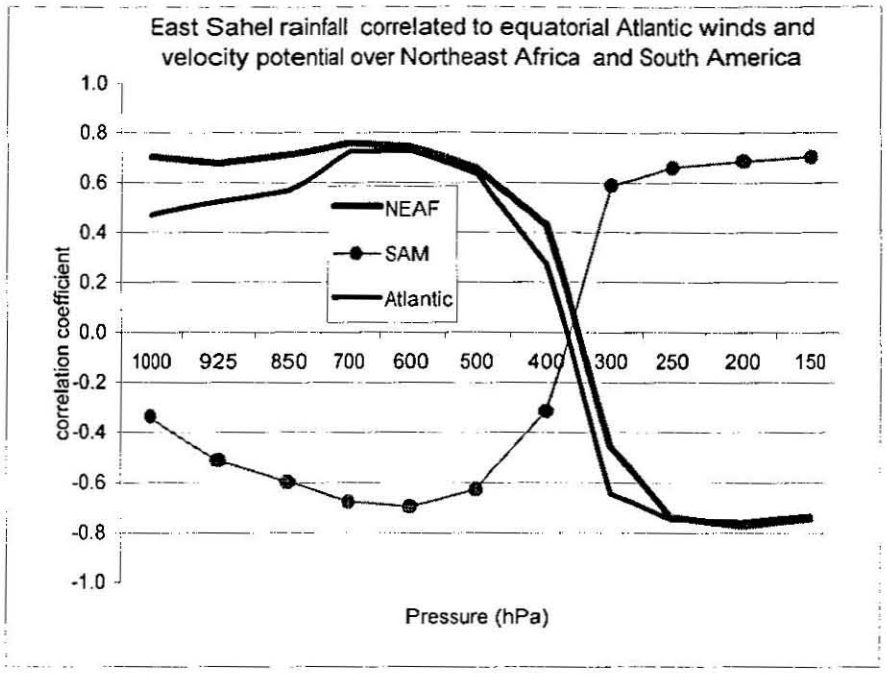

Fig. 5.10 Correlation between East Sahel rainfall and the velocity potential over Northeast Africa (NEAF) and tropical South America (SAM) showing the coupling of rainfall activity over East Sahel with Atlantic Zonal wind (Atlantic) and opposite velocity potential polarity over tropical North Africa and tropical South America.

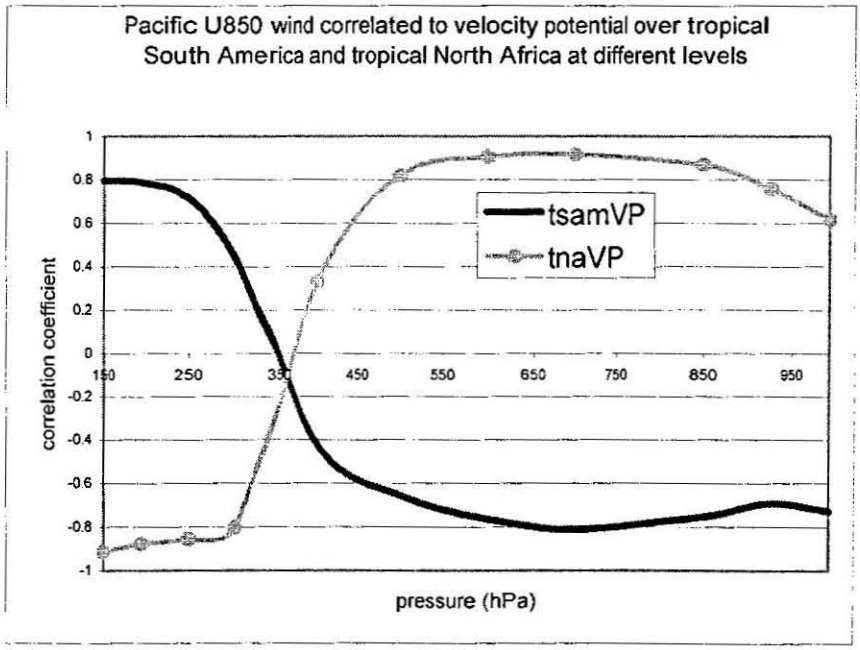

Fig. 5.11 Links between Pacific 850-hPa zonal wind and 200-hPa velocity potential over tropical North Africa (tnaVP) and tropical South America (tsamVP).

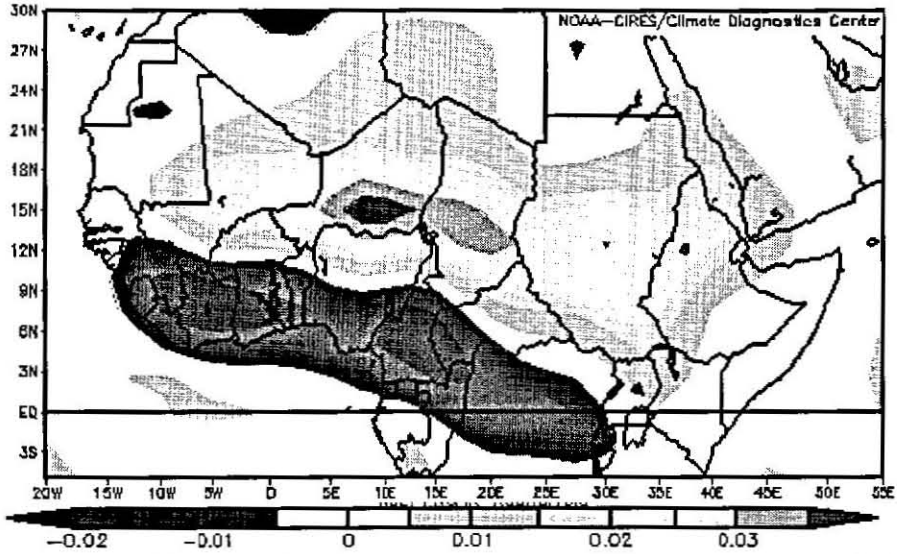

Fig. 5.12 Strong minus weak AEJ composite of 500-hPa vertical velocity (Pa s^{-1})

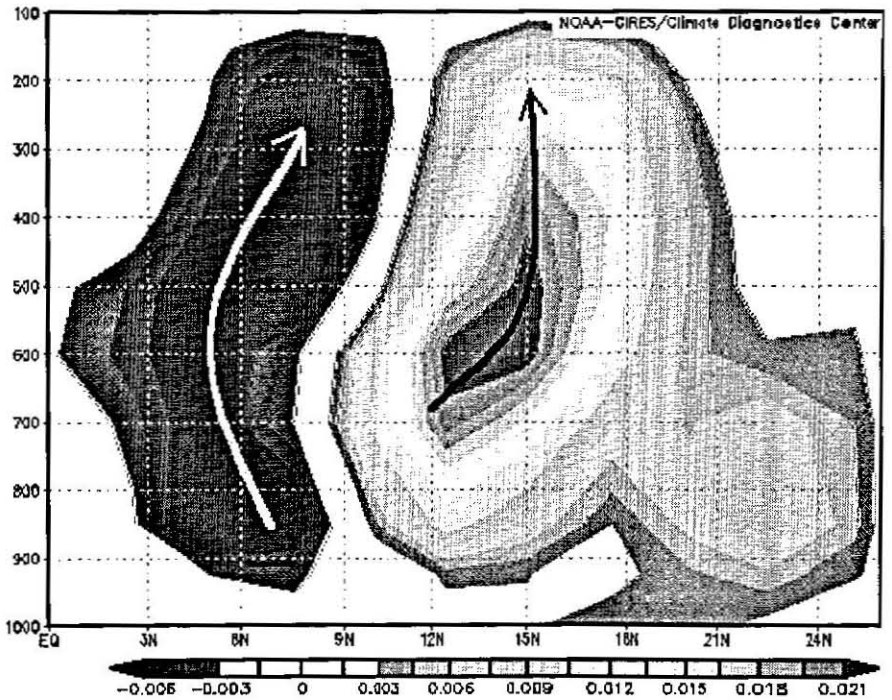

Fig. 5.13 Strong minus weak AEJ composite of vertical velocity (Pa s^{-1}) averaged across [20°W, 20°E] within tropical North Africa.

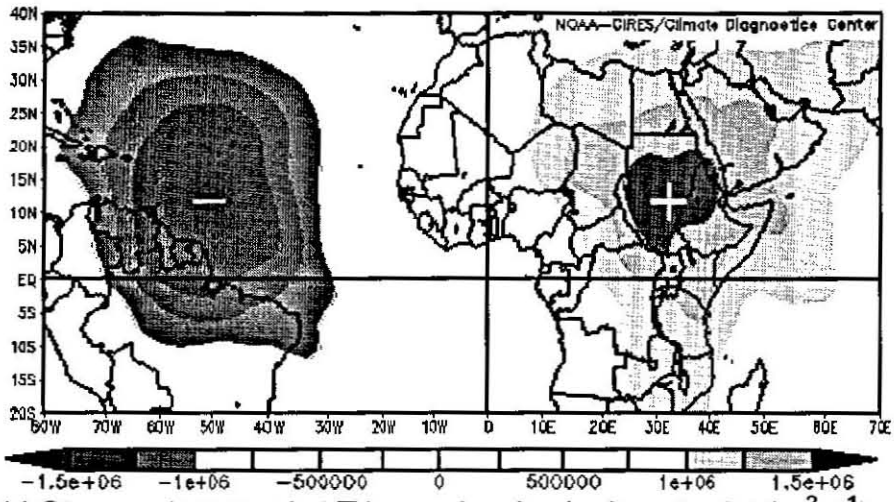

Fig. 5.14 Strong minus weak AEJ upper-level velocity potential ($m^2 s^{-1}$).

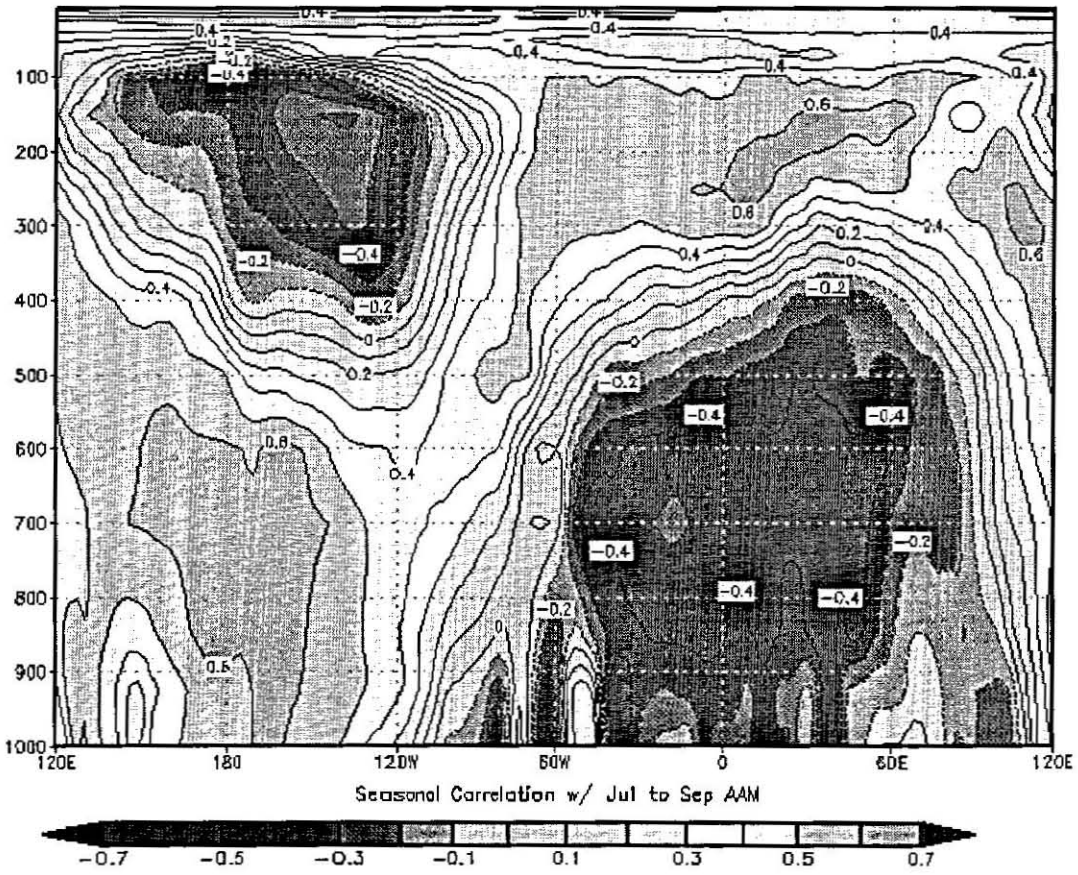

Fig. 5.15 Height -longitude cross-section correlation of angular momentum and zonal winds averaged over [10°S, 10°N] showing its relation to the divergent Atlantic Zonal Circulation and Pacific Walker Circulation.

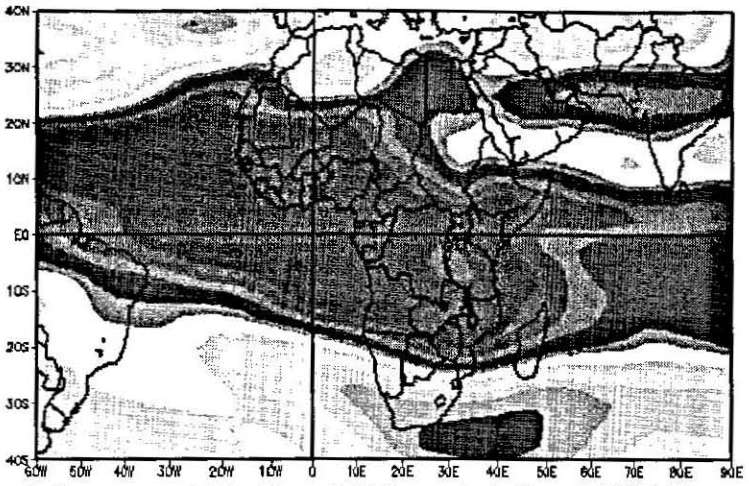

a) Correlation map of Northeast Africa rainfall and 200-hPa zonal wind.

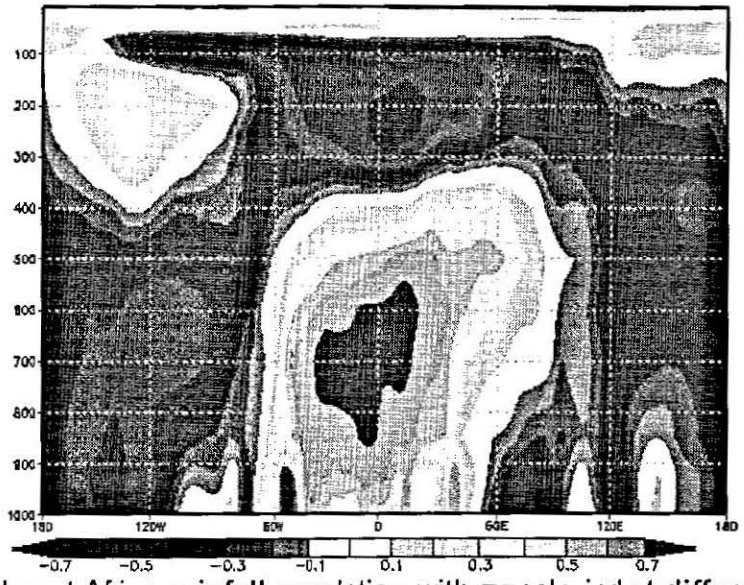

b) Northeast Africa rainfall correlation with zonal wind at different height.

Fig. 5.16 Correlation map of East Sahel rainfall and zonal winds.

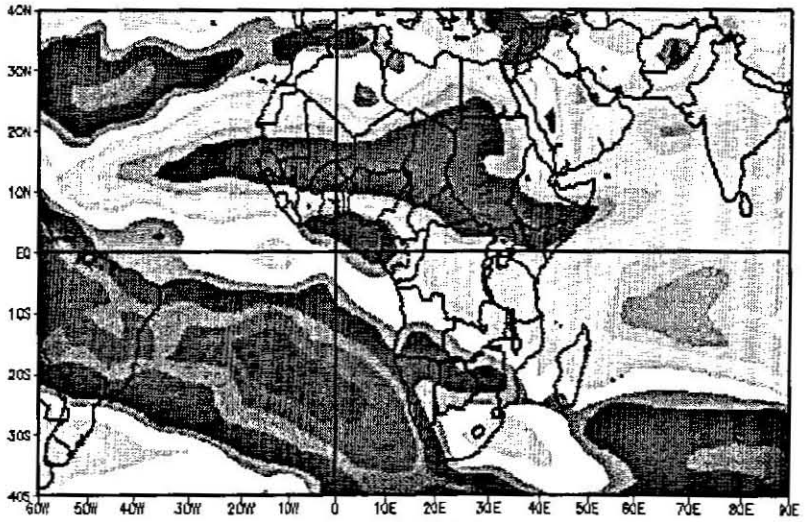

Fig. 5.17 Correlation map of East Sahel and mid-tropospheric specific humidity.

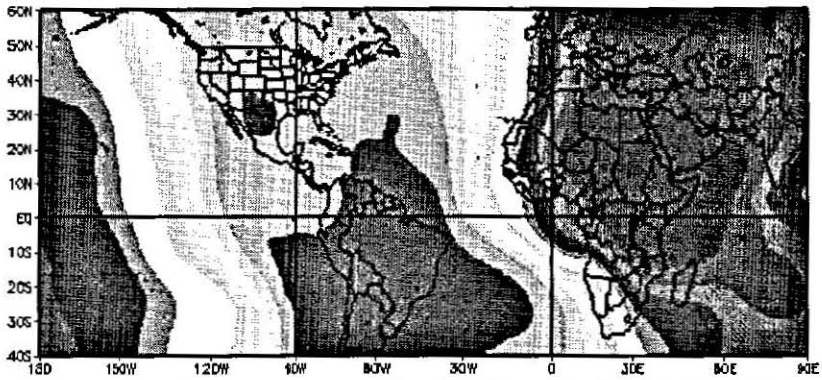

Fig. 5.18 Correlation map of East Sahel and velocity potential at δ =0.2101.

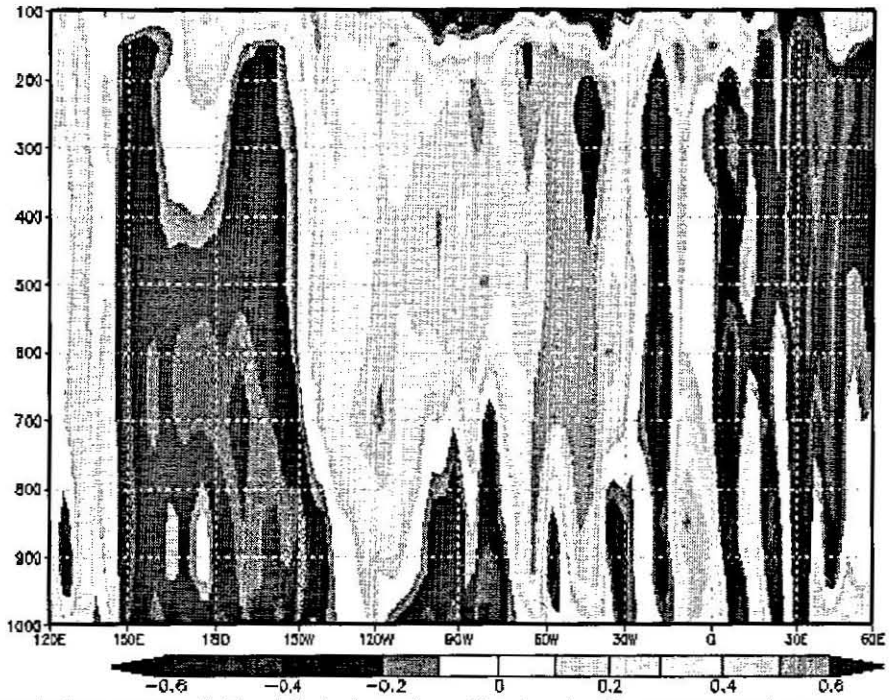

Fig. 5.19 Correlation map of East Sahel and vertical velocity averaged over (10°S, 10°N) latitudinal belt.

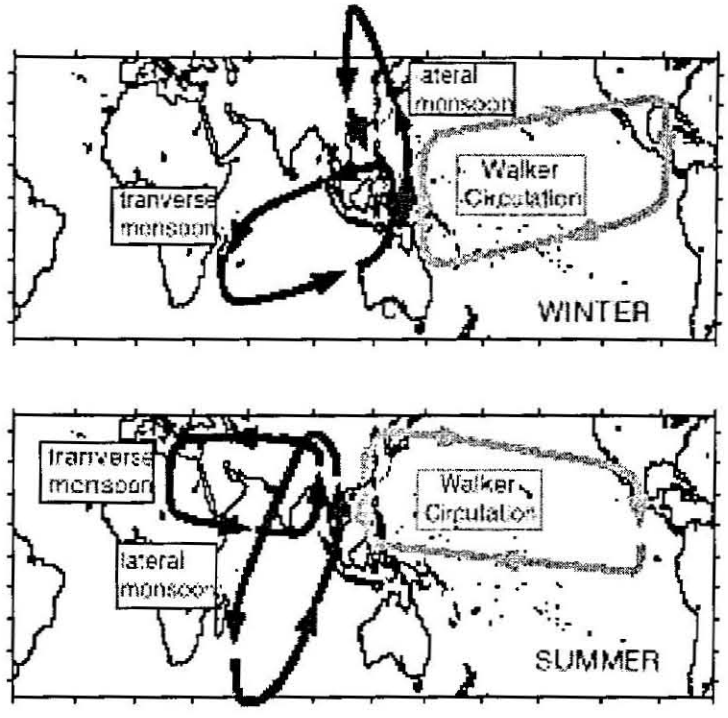

	TM	LM	WC
Mass	12	18	15
LH	49	61	17
Rad	20	21	8

	TM	LM	WC
Mass	25	25	18
LH	72	56	20
Rad	36	20	9

Fig. 5.20 Monsoon-ENSO connection showing the three major circulations associated with the boreal and austral summer monsoon (After Webster et al., 1998).

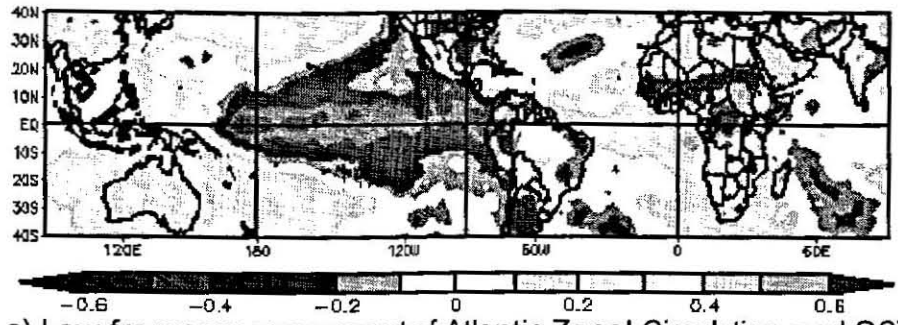

a) Low frequency component of Atlantic Zonal Circulation and SST correlation mapping showing in opposite relationship in equatorial east Pacific Ocean.

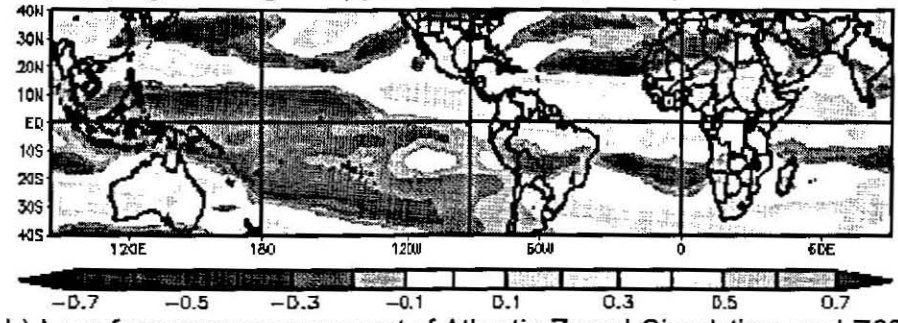

b) Low frequency component of Atlantic Zonal Circulation and 700-hPa wind correlation mapping showing polarity in equatorial Pacific Ocean and Atlantic.

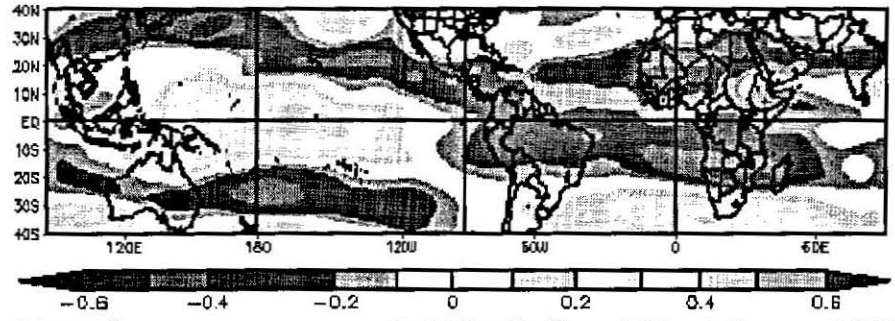

c) Low frequency component of Atlantic Zonal Circulation and 200-hPa wind correlation mapping showing polarity in equatorial Pacific Ocean and Atlantic.

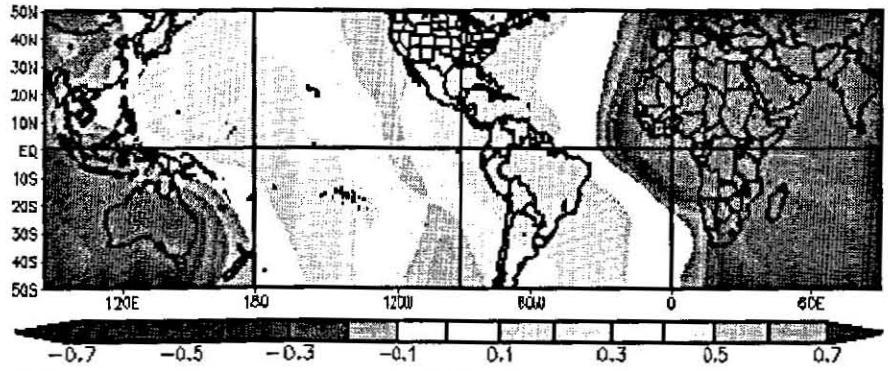

d) Low frequency component of Atlantic Zonal Circulation and upper-level divergent flow correlation mapping showing polarity between Pacific Ocean and Africa.

Fig. 5.21 Atlantic Zonal Circulation teleconnection using interannual filtered data.

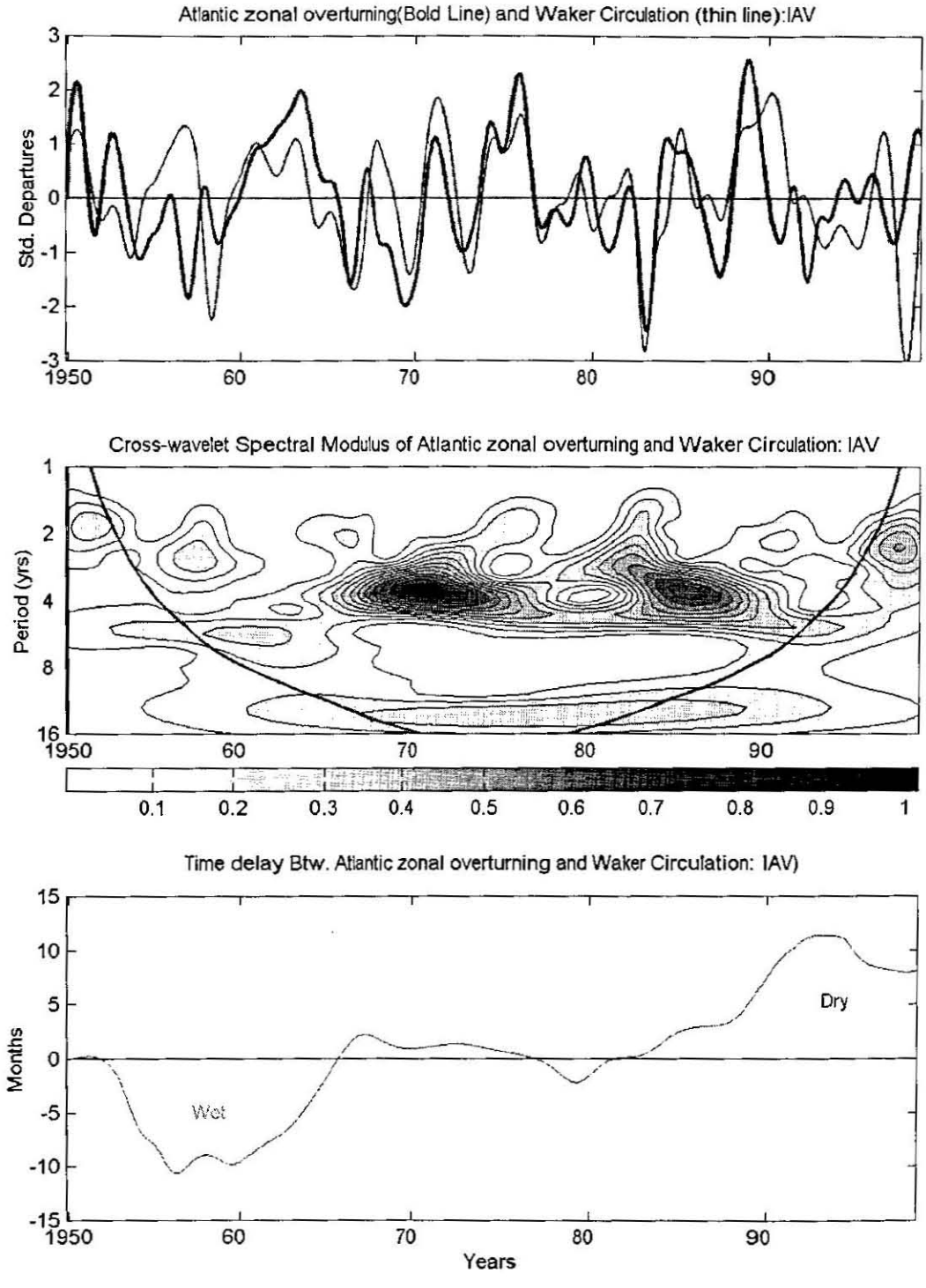

Fig. 5.22 Co-spectral wavelet transform between Atlantic Zonal Circulation and Walker Circulation. The wet (Wet) and dry (Dry) periods of tropical North Africa rainfall are labeled.

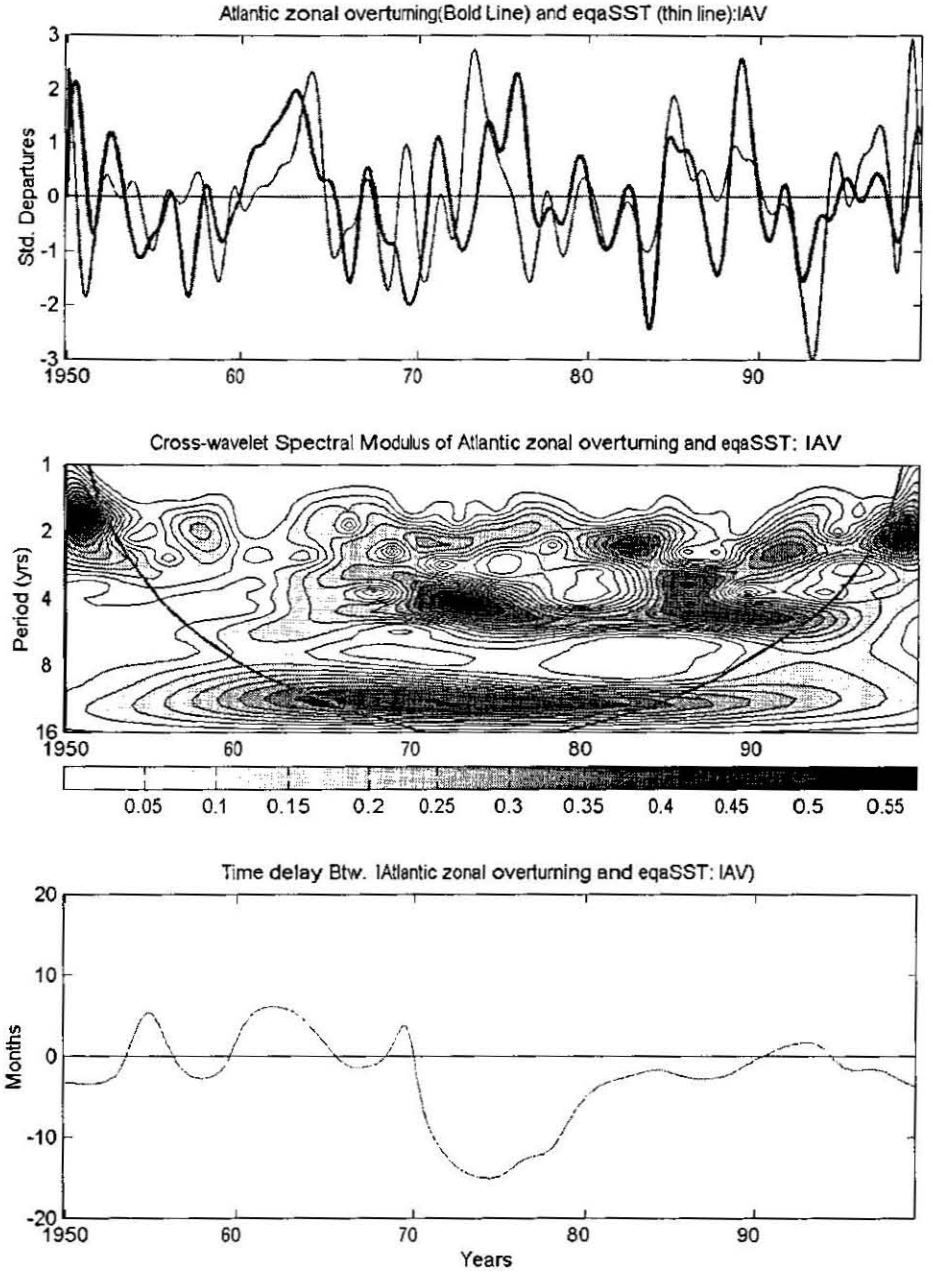

Fig. 5.23 Co-spectral wavelet transform between Atlantic Zonal Circulation and equatorial Atlantic sea surface temperature.

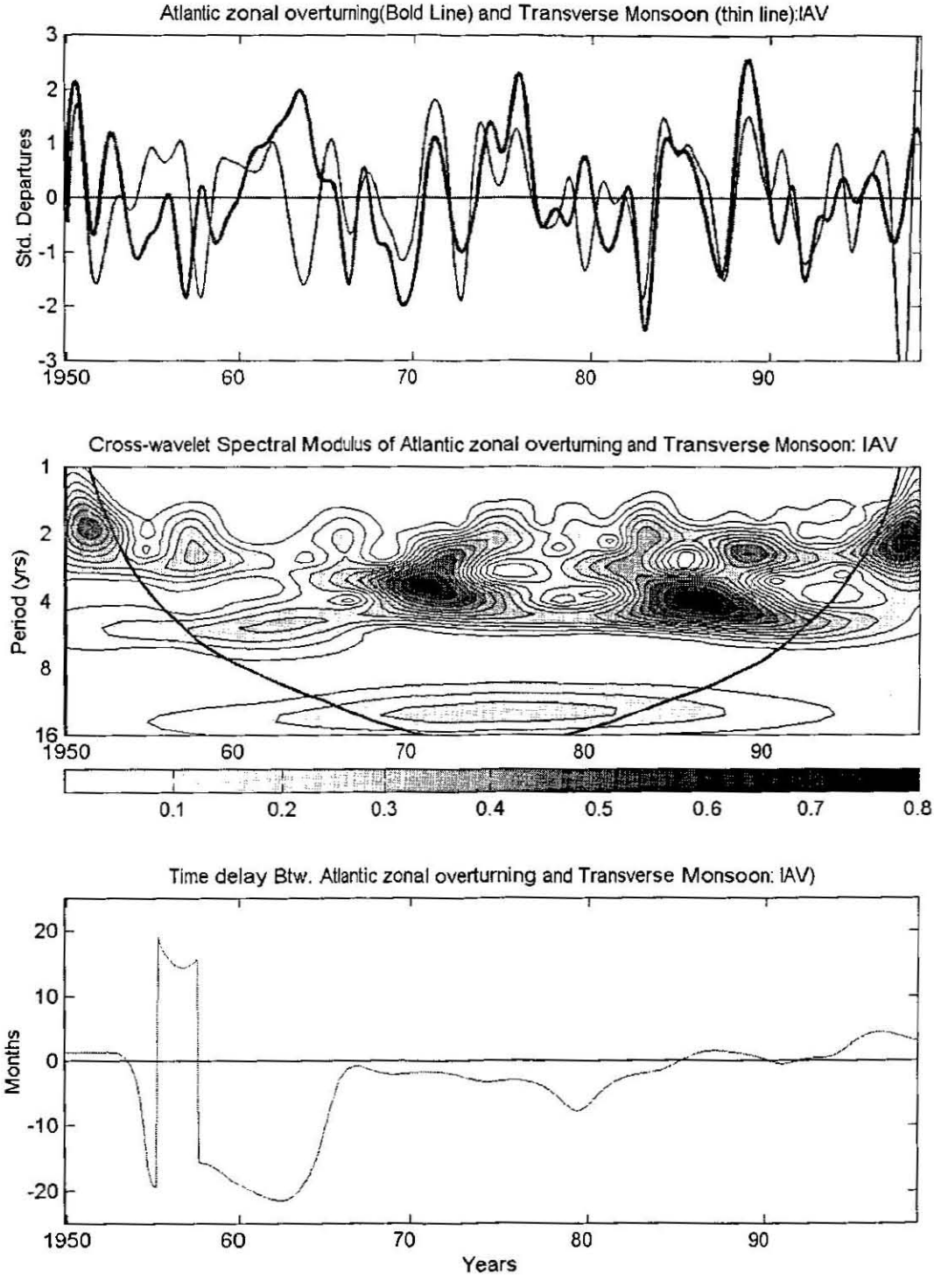

Fig. 5.24 Co-spectral wavelet transform between Atlantic Zonal Circulation and transverse monsoon circulation.

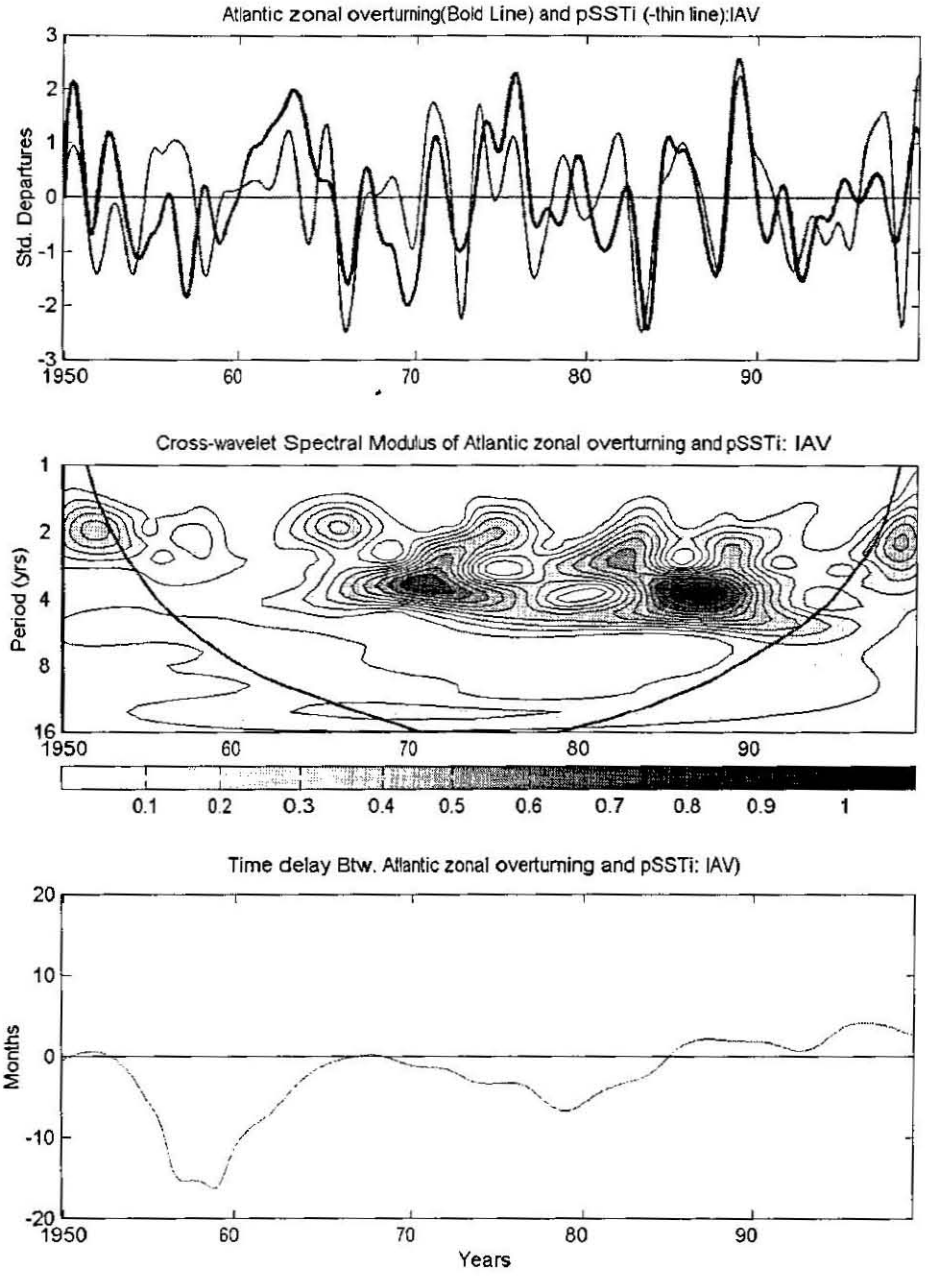

Fig. 5.25 Co-spectral wavelet transform between Atlantic Zonal Circulation and Indo-Pacific sea surface temperature.

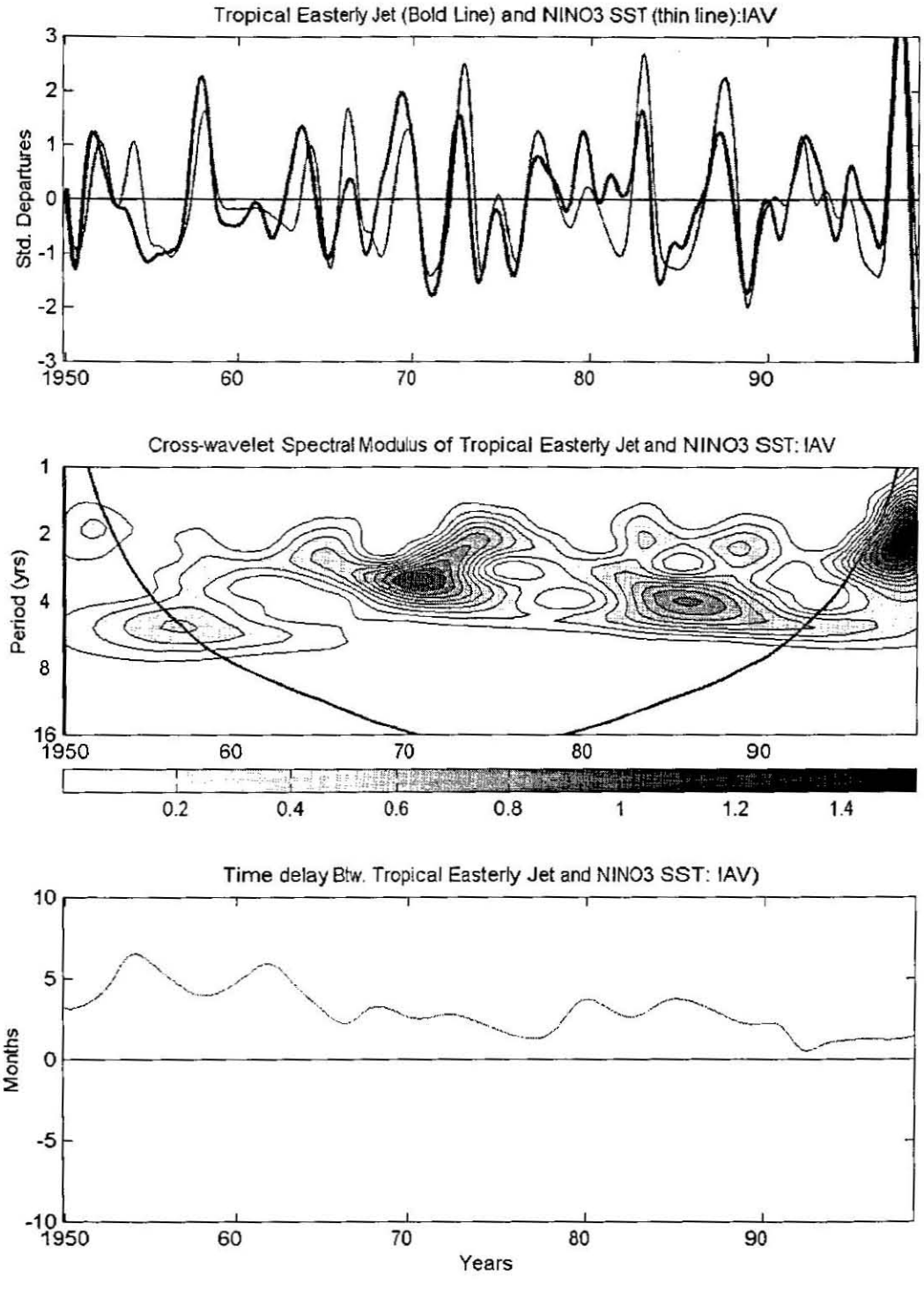

Fig. 5.27 Co-spectral wavelet transform between Tropical Easterly Jet and Nino 3 SST.

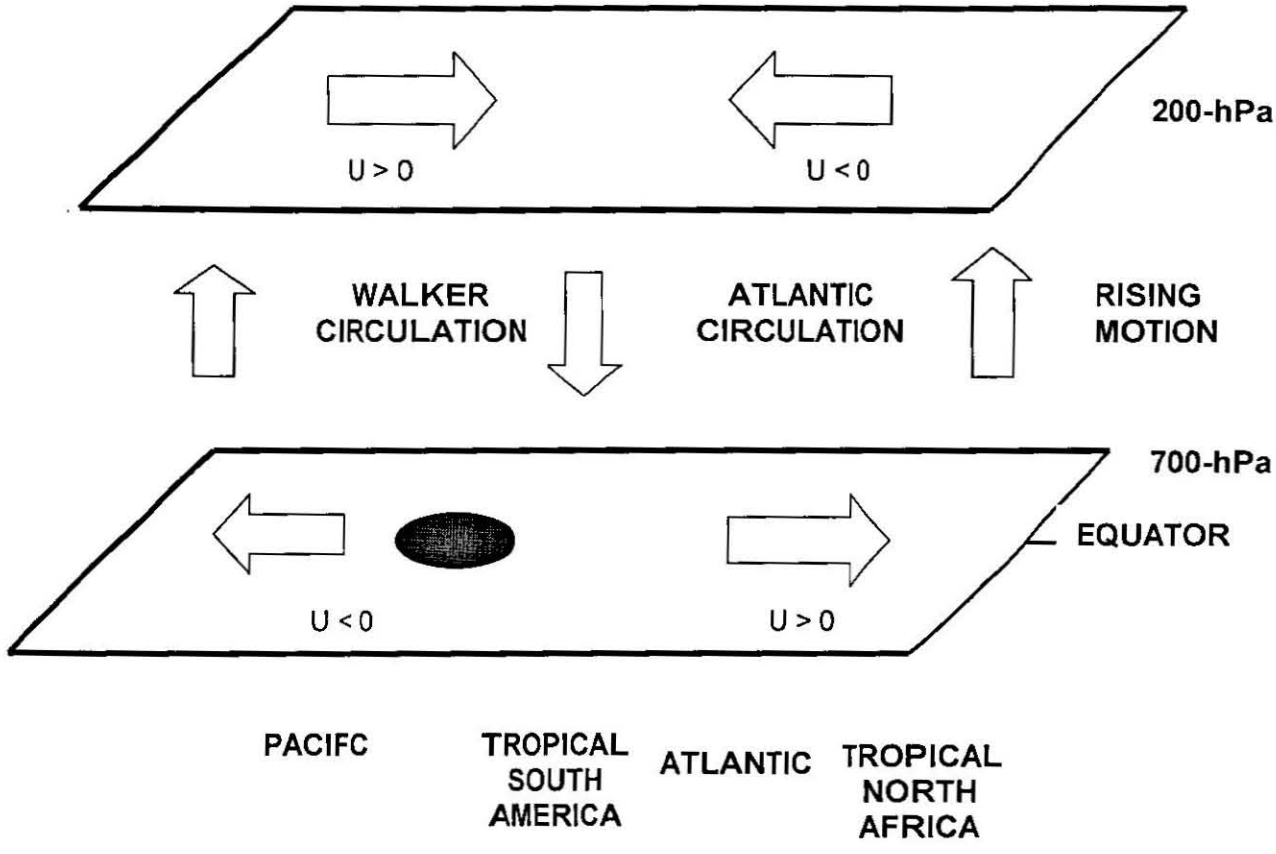

Fig. 5.28 La Nina (shown in shaded oval shape) driven east-west divergent Circulations resulting into enhanced convection over tropical North Africa and subsidence over tropical South America through the anti-phase mode between Walker and Atlantic Circulation. During El Nino, the circulation reverses and hence the centres of convection flip.

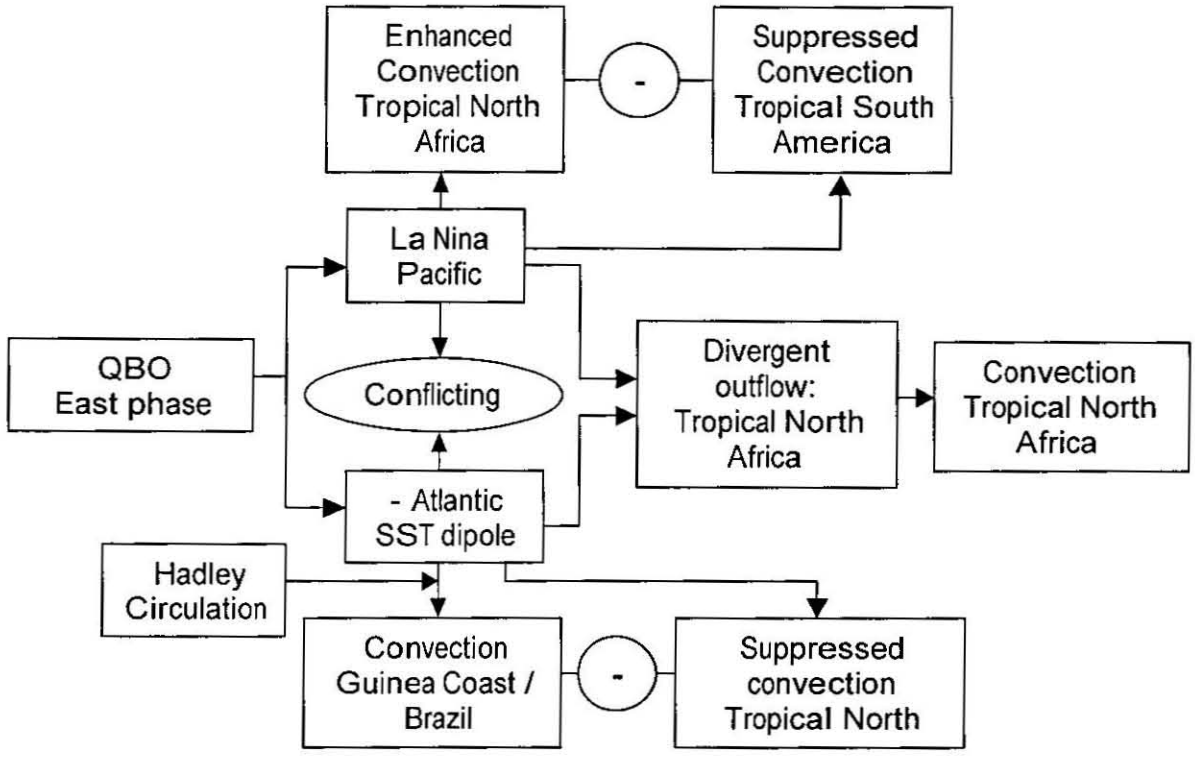

Fig. 5.29 Influence of QBO during east phase through Indo-Pacific-Atlantic connection.

Table 5.1 Key kinematic indices.

NO.	Parameter and key area	KEY AREA NAME	Key area location
1	Equatorial Atlantic 700-hPa zonal wind	eqaU700	(40°W, 15°E), (10°S, 10°N)
2	Equatorial Atlantic 200-hPa zonal wind	eqa200	(40°W, 15°E), (10°S, 10°N)
3	Atlantic Zonal Circulation	aCIR= eqaU700-eqU200	(40°W, 15°E), (10°S, 10°N)
4	Indian Ocean zonal Circulation	mCIR=niU850-TEJ150	niU850: (50°E,75°E), (5°N,20°N) TEJ150: (50E, 90E), (5°N, 20°N)
5	Tropical Pacific zonal wind	tpU1000	(180°W, 75°W), (20°S, 20°N)
6	Tropical Pacific zonal wind	tpU300	(180°W, 75°W), (20°S,20°N)
7	Walker Circulation	WCIR= tpU300-tp1000	(180°W, 75°W), (20°S,20°N)

CHAPTER 6

MODULATION OF REGIONAL AND GLOBAL SST WITH RESPECT TO HYDROCLIMATE VARIABILITY

6.1 Introduction

Sea surface temperature (SST) is an important factor in the physical processes underlying the surface energy balance, the sensible and latent heat exchanges at the air-sea interface, and the circulation of the atmosphere and oceans. The SST drives the global or regional climate through coupling mechanisms mainly involving responses of ITCZ convection to small changes in equatorial SST.

In this Chapter, the influence of tropical SST on tropical North Africa climate system is dwelt. To this end, composite SST patterns for the tropical Pacific, Atlantic and Indian Oceans are studied. A correlation mapping is performed to further understand the strength of teleconnection in Section 6.2.2. Atmospheric responses to tropical SST anomaly over Atlantic, Indian and Pacific oceans are ensemble using the NCAR Community Climate Model (CCM3). The model is forced by observed tropical SST and ensembles of the model output variables for the boreal summer are examined and compared with the composite structure.

The co-spectral characteristics of the tropical SST indices and the tropical key hydroclimate areas are considered in Section 6.3.2 to identify the common spectral energy and phase differences between the thermodynamic and hydro-climatic indices.

6.2 Modulation of tropical SST on tropical North Africa atmospheric circulation

In this section, two principal issues are addressed. The first is tropical SST variability over Atlantic, Indian and Pacific Oceans. The second is degree of association between tropical SST key areas and tropical North Africa climate.

6.2.1 Mode of tropical SST variability and their influence on tropical North Africa climate

Influences of Pacific ENSO, the equatorial Atlantic SST and the Atlantic on tropical North Africa climate are examined.

Composite analysis

a) Indo-Pacific

In Pacific the mode of variability at interannual is the El Nino- Southern Oscillation. Its modulation on tropical climate is documented but its transmission to West Africa Monsoon in boreal summer is not well understood.

To produce the ocean-atmosphere composite structures, ENSO years are identified from Nino 3 SST for boreal summer. These are 1965, 1972, 1982, 1987, and 1991 (El Nino) and 1956, 1964, 1971, 1974, 1988, and 1999 (La Nina) using a one standard deviation threshold as defined in Chapter 3. Ocean-atmosphere composite structures are formed from El Nino minus La Nino years. As these composites are using similar to the pattern presented in Chapter 5 (except of opposite sign) they are not shown and only briefly discussed.

The SST composite over the equatorial Pacific reveals a warm anomaly east of 170°E. The Atlantic Zonal Circulation responds with low-level easterly and upper-level westerly. In the equatorial Pacific, westerly winds prevail in the low-level and the reverse in the upper level. The Pacific Walker Circulation and Atlantic Zonal Circulation are tuned to the ENSO oscillation. This atmospheric adjustment to Pacific warming results in the formation of the velocity potential dipole that favours deep convection over South America and East Pacific and suppressed convection over Tropical North Africa and West Pacific. ENSO therefore transmits its influence on tropical North Africa through the zonal divergent circulation.

b) Equatorial Atlantic

The tropical Atlantic Ocean exhibits two primary modes of variability in spatial domain (Servain et al., 1998). These are the equatorial mode and the tropical Atlantic dipole. Warm and cold events of the equatorial mode are identified from boreal summer SST. Warm events of equatorial Atlantic are 1963, 1968, 1973, 1984, 1985, 1987, 1988,1989, 1993, 1995 and cold years 1958, 1959, 1964, 1965, 1967, 1979, 1970, 1976, 1982 and 1992. The difference between the warm and the cold years are manifested in the:

i) wind circulation over tropical Africa and equatorial Atlantic.
ii) source and sink of moisture perturbation,
iii) velocity potential polarity and convective between tropical North Africa and tropical South America.
iv) vertical velocity ascending and descending motion between tropical regions on either side of the Atlantic.

The SST composite depicts the Atlantic El Nino in the equatorial band and Gulf of Guinea (Fig. 6.1). In response to this positive SST anomaly, the pressure declines locally. This attracts wind from the surrounding. So, the westerly component of the West Africa monsoon becomes feeble and the penetration of moist equatorial Atlantic westerly winds to the interior part of tropical North Africa is limited (Fig. 6.2). The trough over the highest positive SST anomaly region confines the moisture flux to be the Guinea Coast and coastal regions of West Africa.

In response to the equatorial Atlantic El Nino a vertical shear in zonal wind is formed over Atlantic and Tropical North Africa. The shear structure shows easterlies within 1000-400-hPa layer and westerlies from 300-100-hPa revealing the Atlantic Zonal Circulation in a "dry" phase.

Descending motion dominates over tropical North Africa and ascent occurs within 70°W-20°W (Fig. 6.3). These motions are dynamically underpinned by divergent

flow at upper and lower-levels. As a result, Tropical North Africa experiences widespread subsidence while rainfall is enhanced over tropical South America.

These centres of action are an integral part of the Walker Circulation and Atlantic east-west overturning (Fig. 6.4). It is demonstrated that SST changes over the equatorial Atlantic and Guinea Coast play a vital part in shaping the tropical North Africa. This modulation is related to the co-occurrence of El Nino or La Nina events in Atlantic and Pacific.

c) Equatorial east Pacific-equatorial Atlantic SST dipole

The impact of opposing SST polarity between equatorial east Pacific and equatorial east Atlantic on tropical North Africa climate variability is addressed. Standardised SST index is developed for SST dipole between equatorial east Pacific ([120°W, 80°W], [5°S, 5°N]) and equatorial Atlantic ([15°W, 10°E], [5°S, 5°N]). Years of positive SST over equatorial east Pacific and negative SST over equatorial Atlantic are selected concurrently for boreal summer. The years are selected in such a way that opposing SST polarity between Pacific (warm) and Atlantic (cold) co-occurred. The years that satisfy these conditions are 1983, 1982, 1976 and 1965. To form the composite opposite conditions in both oceans are considered. These are 1960, 1974, 1980 and 1990. The ocean-atmosphere composite structures are then produced for the east Atlantic/Pacific opposing SST pattern.

The SST composite pattern portrays the opposing SST anomaly over Pacific and Atlantic. Warm SST pool over equatorial east Pacific and cold pool over equatorial Atlantic comes out from the composite analysis (Fig. 6.5). A height-longitude cross-section of air temperature displays a cold air temperature throughout the troposphere in cold equatorial Atlantic from the surface to 800-hPa. Over the warm waters of the equatorial east Pacific, warm air is depicted in

the lower layers of the atmosphere. The sign of the anomaly changes in the middle and upper-levels as expected.

The wind vector composite shows low-level easterly and upper level westerly anomalies in equatorial Atlantic revealing anomalous Atlantic Zonal Circulation, a replica of the El Nino pattern (Fig. 6.6). In the upper levels, the westerly wind of Atlantic Zonal Circulation and the easterly winds of the Pacific Walker Circulation form a divergence that facilitates the ascending motion in accordance to continuity equation. In the regions of easterly winds in the lower-levels, positive geopotential height anomalies are seen to build up a high potential energy hence anticyclonic circulation. The velocity potential pattern in the Atlantic extends outward to the West Pacific revealing the influence of SST polarity to tropical North Africa that leads to suppressed convection.

The most important result that is elicited from the SST polarity between the east Pacific and east Atlantic composite analysis is that the opposing anomalous east-west divergent circulations transmit the ENSO to tropical North Africa through the Zonal Circulation. As a result, the region in point falls under the influence subsidence and suppressed convection. The other vital find is that the equatorial Atlantic SST is a "slave" (passive) to ENSO and its influence on tropical North Africa climate is masked by ENSO signal. However, during inactive ENSO period, the Atlantic mode is important to ocean-atmosphere coupling within the basin and its modulation on tropical North Africa is noticeable. Hence the system is non-linear.

An index was developed that depicts the Pacific-Atlantic SST polarity during boreal summer 1950-1998 to identify its teleconnection pattern. Its interplay with Pacific and Atlantic SST shows the dipole structure (Fig. 6.15). Its link to other thermodynamic and kinematic fields shows a pattern identical to that found for the SOI teleconnection in Chapter 5. It is therefore understood that ENSO has an overriding influence on the equatorial Atlantic SST and tropical North African climate variability.

d) Tropical Atlantic SST dipole

Tropical Atlantic SST dipole is one of the modes of variability of tropical Atlantic SST. The modulation of this mode of variability on tropical North Africa climate is examined. This mode of variability, as identified by Chang (1997), is the difference between tropical North Atlantic ([40°W, 20°W], [5°N, 20°N]) and Gulf of Guinea SST ([15°W, 5°E]), ([5°S, 5°N]). This index is called Tropical Atlantic SST dipole Index (TASI) (Table 6.1).

Ocean-atmosphere composites are produced based on the mode of variability of tropical Atlantic SST dipole as defined by Chang (1997). The composites are formed based on warm events in the tropical North Atlantic SST and cold events in the Gulf of Guinea during boreal summer. These are 1958, 19967, 1976, 1980 and 1983 (warm) and 1963, 1972, 1973, 1974, and 1984 (cold).

The SST composite shows cold pool in equatorial Atlantic and warm in tropical North Atlantic (Fig. 6.7) similar to (Chang 1997) as expected. The response of atmospheric circulation to this anomalous Atlantic SST dipole reveals salient circulation patterns that establish the link between Atlantic SST dipole and tropical North Africa climate.

The height-latitude cross-section of zonal wind anomaly over equatorial Atlantic shows two opposing east-west divergent flows in a meridional direction (Fig. 6.8). Within 9°S-6°N, easterly flows are present below 600-hPa. Aloft anomalous westerly flow is shown from 600-300-hPa. This east-west circulation induces subsidence over the Gulf of Guinea. The circulation north of 6°N is a westerly anomaly from surface to 400-hPa. Above this level, an easterly wind anomaly prevails from the equator to 15°N within 500-100-hPa. It is conducive to rainfall production over tropical North Africa regions.

The upper velocity potential reveals opposing centres in the central Atlantic and Indian Ocean. The $-\nabla\chi$ (upper-level easterly wind) dominates the tropical North Africa. Northeast Africa falls in negative side of the velocity potential from Indian Ocean side and western half under positive (influence from Atlantic side). As a result dry condition prevails in Gulf of Guinea and wet in West Sahel and Northeast Africa (Fig. 6.9). The same rainfall dipole configuration is produced during strong AEJ associated to ENSO in Chapter 5. Hence, tropical Atlantic SST dipole and AEJ delineate the locally contrasting Sahel-Guinea climate through meridional overturning (Fig. 6.10).

6.2.2 Modelling of the responses of tropical SST forcing

The National Centre for Atmospheric Research (NCAR) Community Model (CCM3) is used to generate ensembles for key tropical SST patterns discussed in Section 6.2.1 and Section 6.1.2 and their responses. The CCM3 is the fourth generation in the series of NCAR's Community Climate Model. The historical development and detail attributes of the model can be referred at http://www.cgd.ucar.edu /cms/ccm3/.

The standard version of the NCAR CCM3 is a three-dimensional global spectral general circulation model with T42 horizontal resolution (roughly 2.8° x 2.5° Gaussian grid) and 18 vertical levels in the vertical. Deep convection is ensemble by mass-flux scheme of Zhang and McFarlane (1995) and the triplet convection of Hack (1994) simulates shallow convection. The complete description of the physical and numerical methods can be referred in the works of Kiehl et al. (1996).

The CCM3 generates ensembles of 12 runs each forced using observed tropical SST fields and observed global SST fields. The inputs for generating the ensembles are the episodic years for warm or cold events of ocean basins. The forcing and the outputs are defined (chosen) from the menu based CCM3 model.

The CCM3 is used to produce the ENSO ocean-atmosphere patterns, the equatorial Atlantic warm event and the SST polarity between equatorial east Pacific and equatorial Atlantic. The tropical Atlantic SST dipole is also considered in this endeavour. The responses of the CCM3 SST ensemble on tropical North Africa climate are considered below.

In the run of the SST and the atmospheric patterns, the tropical SST drives the CCM3. The input for the model is the observed SST for composite years that are to be investigated. The output is ensembles of the runs generated by different boundary conditions. The model is executed http://www.cdc.noaa.gov/ Composites/CCM/ web site. The integration of the ensembles is generated from 12 runs. The variables available from the CCM3 as outputs are surface air temperature (as a proxy for sea surface temperature), sea level pressure, geopotential height, zonal wind, meridional wind, and precipitation. These variables are available at the surface, 850-hPa, 700-hPa, 500-hPa, 300-hPa and 200-hPa.

a) Generation of cold tongue of ENSO using CCM3 Ensembles

The years that represent ENSO episodes are considered to generate ensembles of the cold tongue over east and central Pacific along the equatorial plane in forcing CCM3 Model by observed tropical SST.

Selected variables and levels that depict important patterns are displayed. The surface temperature as a 'proxy' for SST, the upper-level and vertical structures of zonal wind is portrayed as responses of the ensemble SST structure and amplitude. The ensemble 'SST' produces the cold pool over equatorial regions of central and east Pacific Ocean. Weak cold SST is obtained over western Indian Ocean. The southern part of the horseshoe shaped SST structure is well represented in CCM3 integration. The northern component of the horseshoe SST pattern is however underestimated by CCM3 ensemble. The amplitude of cold

tongue in the CCM3 ensemble on the other hand is amplified in particular on the positive SST anomaly. The observed SST is less by 0.5°C in positive side. In the negative side, the ensemble is half of the observed.

The upper-level zonal wind shows an easterly wind anomaly from southern tropical Indian Ocean across the central regions of southern Africa countries and then bifurcates on either side of the equatorial Atlantic Ocean. The zonal wind North of the equator has higher amplitude than south. Over equatorial east Pacific, the bifurcated wind anomalies merge and form a broad zonal wind anomaly. A weak westerly wind anomaly over western equatorial Atlantic is surrounded on either side of the tropics by the bifurcated easterly wind anomaly. Positive zonal wind anomaly is also observed over the northern and southern regions of tropical Atlantic. The maximum regional zonal wind anomaly is sitting in the southern edge of Africa and the Indian Ocean. The contrast between the ensemble upper zonal wind and the composite zonal wind (considered as the observed) lies over equatorial and north tropical Atlantic where the westerly winds prevails. In the observed wind structure, these patterns are not there. The ensemble vertical structure of the zonal wind averaged over from 10°S-10°N depicts a feeble westerly wind in the low- and mid-troposphere and easterly wind anomaly over the top of the Atmosphere. The Atlantic zonal circulation is therefore weakly represented in the CCM3 ensemble. The difference lies in the amplitude and the depth of upper easterly wind. The model underestimates the strength of the Atlantic zonal circulation. Yet the circulation is maintained at a level about half of the observed.

b) Producing the equatorial Atlantic warm pool using CCM3 ensemble

The warm equatorial Atlantic SST is generated from CCM3 atmosphere general circulation model integration tropical SST as forcing. Ensembles of the model output variables for boreal summer are evaluated using the composites produced under warm minus cold SST over the equatorial east Atlantic. The warm and cold

SST years are used as inputs in the model. The composites are formed through subtracting the cold years from the warm ones. Then, with same forcing the CCM3 model produces the observed field (Fig. 6.11). The low-level flow shows anomalous westerly wind flow over the equatorial warm pool (Fig. 6.12a). The westerly wind anomaly extends to equatorial regions of Africa and over Indian Ocean south of the equator with weaker amplitude. Over north tropical Atlantic and most parts of Africa, easterly wind anomaly dominates. The easterly wind anomaly extends to Arabian Sea and equatorial Indian Ocean.

Features that are similar to the ENSO circulation influence from the Indo-Pacific regions are produced under warm SST over equatorial Atlantic. The CCMS integration produced the upper-level twin anticyclones over tropical Atlantic (Fig. 6.12b). Identical patterns are observed over Pacific Ocean during the warm phase of ENSO. Within the north tropical Atlantic latitudinal belt (10°N, 25°N), anomalous westerly flow is found. South of this westerly wind anomaly, easterly wind dominates in the upper-level. South of this easterly anomaly, westerly flow is present to form an anticyclone in the south tropical Atlantic.

Jury et al. (2000) found similar results using the Australian atmospheric general circulation (CSIR09). The numerical model is run with perpetual warm event embedded within annual cycle. Their run produced westerly winds in the equatorial Atlantic similar to Fig. 6.12a. The upper level wind forms a twin anticyclonic gyre symmetric to the equator, as a response to the warm Atlantic SST. This structure is in unison with the empirical result.

c) Equatorial east Pacific and equatorial Atlantic SST dipole depiction in CCM3 ensemble

CCM3 is used to produce the equatorial east Pacific-Atlantic SST dipole and its influence in relation to tropical North Africa climate. As response to the prescribed SST forcing (tropical SST), various ensembles are produced.

The CCM3 output of the "SST" shows negative "SST" over Guinea Coast and most parts of equatorial Atlantic. The opposite pattern is produced in east equatorial Pacific. The cold SST over equatorial Atlantic is elongated towards the equatorial West Atlantic as compared to the observed. Over the equatorial Pacific, the opposite situation is reflected where warm pool is confined to the very east of Pacific (e.g. El Nino). While, the observed SST pattern over Pacific is extended beyond 120°W. In short, the CCM3 "SST" integration has a large spatial extent over equatorial Atlantic and smaller in the equatorial east Pacific. A difference in the amplitude is also observed. The CCM3 underestimates the SST over both equatorial basins.

The tropical SST forcing with prescribed composite years generate zonal wind anomalies in tropical Africa and surrounding oceans. The 700-hPa zonal wind shows anomalous easterly flows over equatorial Atlantic and feeble westerly winds over tropical North Africa. Most parts of South Atlantic are dominated by easterly wind anomaly. In the composites of warm equatorial east Pacific minus cold equatorial Atlantic, the easterly wind anomalies are the most dominant structures over north tropical Atlantic. Thus, the ensemble and observed low-level zonal wind disagree over tropical North Africa but are the same in the equatorial Atlantic Ocean. Further differences are found over the western Indian Ocean. In the upper troposphere, the ensemble shows anomalous westerly winds in the equatorial Atlantic and easterly anomaly in southern tropical Atlantic.

The vertical-longitude structure of the zonal wind averaged over 10°S to 10°N is modelled with tropical SST forcing to find out if the Atlantic zonal circulation is sensitive to this forcing. The ensemble circulation reveals that a westerly wind anomaly in the lower and troposphere east of 0° (longitude). Aloft an easterly wind anomaly dominates. Opposite pattern is replicated west of 0° longitude with low-level easterly and upper level westerly anomaly. In the observed case, the equatorial Atlantic is a region of singular zonal overturning.

d) Generating the tropical Atlantic SST dipole using CCM3 ensemble

The ensemble for Atlantic dipole is consistent with the observed structure (Fig. 6.7). A difference exists in the amplitude of SST where the cold SST pattern is underestimated and the warm is overestimated. However, the ensemble atmospheric structures are out of phase with the observed pattern. In tropical Africa and its environs, the ensemble feature is an upper-level easterly anomaly over the equatorial regions (Fig. 6.14) whereas the observed structure is easterly. The westerly wind anomaly is accompanied in the north by easterly wind anomaly that extends from West Atlantic to Ethiopia. The same pattern prevails in Southern Hemisphere that includes Atlantic and Indian Ocean.

Tropical SST forcing produces the appropriate thermal structure. However, the modulation of the Atlantic and the Africa circulations are not properly produced, particularly the Atlantic Zonal Circulation.

6.3 SST teleconnection and interplay with hydroclimate

The ocean-atmospheric connection is establishing at ENSO timescale using key SST indices. The contribution of each SST index to the variability of hydroclimate in tropical North Africa is examined in this section.

a) Teleconnection

East Pacific minus equatorial Atlantic SST mode low frequency mode is subjected to correlation analysis with SST and zonal wind within tropics. The SST teleconnection reveals a dipole between ENSO signal and equatorial Atlantic SST mode (Fig. 6.15). The connection with tropical zonal flow in the upper troposphere of the tropics portrays the preferred mode of low-frequency signal where a twin anticyclone fingerprint in a zonal wind is found in tropical Pacific with negative correlation in equatorial central Pacific. This equatorial Pacific pattern is anti-phase to tropical Atlantic, Africa and Indian zonal wind. The

pattern is found in east-west divergent circulations and SOI at ENSO timescale discussed in Chapter 5 and in subsurface thermal field dwelt in Chapter 7.

The SST dipole in Indian Ocean teleconnection reveals ENSO pattern in SST in tropical Pacific with positive correlation east of the International Dateline and negative in horseshoed region, west Pacific (entailing Maritime continent) and Southeast Indian Ocean (Fig. 6.17). Weak positive correlation is found western Indian Ocean. IOD connection to tropical zonal wind depicts the same teleconnection pattern as the preferred mode of low-frequency teleconnection (Fig. 6.18) with strong association with core of TEJ.

6.4 Co-spectral energy characteristics between tropical North Africa hydroclimate and tropical SST

In this section, the timeseries of the tropical North Africa and the tropical SST (refer Table 6.1) are co-analysed using cross-wavelet modulus. The spectral analysis is performed at seasonal/annual cycle and interannual timescale to understand time-varying co-spectral energy between tropical SST and tropical North Africa hydroclimate. Cross-wavelet modulus and phase relationship between the tropical SST and the tropical North Africa hydroclimate are presented.

6.4.1 Seasonal and annual mode of tropical SST variability

The seasonal cycle is the largest atmospheric-ocean signal in the tropical Atlantic (Hurrell, 2000). The interannual and long-term variations may be partly interpretable as modulations of the mean annual cycle. As opposed to the tropical Pacific, anomalies in tropical Atlantic SST are primarily driven by changes in the surface winds, which can be forced locally or remotely. Local forcing arises from changes in the position and intensity of the ITCZ and subtropical. Remote forcing comes, for instance, from variability of the ENSO.

Other variability besides the seasonal cycle is present in the tropical Atlantic. Superimposed on the mean seasonal cycle, two modes of coupled atmosphere-ocean variability are observed in the tropical Atlantic Ocean. The first one is characterised by a north-south inter-hemispheric gradient in SST, with associated changes in trade winds that exert considerable influence on the regional climate. Chang et al. (1997) developed a SST index that represents this meridional SST gradient in the tropical Ocean. The temporal fluctuations of Atlantic meridional SST dipole mode display markedly large power on timescale of 8-16 years. The second is an equatorial mode of variability similar to ENSO, although weak relative to the Pacific Ocean variability.

Temporal variability of Atlantic SST annual cycles

The temporal evolution of the equatorial Atlantic SST depicts the annual cycle of equatorial Atlantic SST. It exhibits high amplitude of annual cycle. The same pattern is found in the tropical Atlantic SST dipole. A different pattern is identified in the Indian Ocean SST dipole. It evolves with as envelope (packet of energy) and depicts a pulsation with time. High amplitude is found in the beginning of the 1960s and second half of the 1980s.

6.4.2 Interannual variability of co-spectral energy characteristics between tropical North Africa hydroclimate and tropical SST

Spectral energy in a wavelet domain of tropical North Africa hydroclimate and tropical SST indices is studied to understand the time-evolution of the cross-wavelet spectral modulus and the phase relationship.

The wavelet analysis is applied on standardised filtered tropical North Africa rainfall, Nile River flow and tropical SST timeseries. The filtered data preserve the interannual timescale (1.5 to 16-year) signals. A cross-wavelet analysis proffers the co-variation between the timeseries. The temporal evolution of the

co-spectral energy in the wavelet domain depicts the common energy. The phase difference gives the lead-lag relationship vital for prediction.

Equatorial Atlantic SST and Nile flow

The Nile River flow and the equatorial Atlantic SST is co-analysed using cross-wavelet spectral analysis. The modulus of common energy between Nile and equatorial Atlantic is given in Fig. 6.19. Three spectral regimes are revealed. Within 2 to 4-year period, a band of spectral energy is notable. Within these periods, high amplitudes of the spectral energy are concentrated in most of the 1960s and 1990s. In the middle of the interannual time-scale, two packets of spectral energy are present in the 1960s and in the 1990s. A feeble low frequency signal is notable at 10-year period. The decadal signal is weaker than the interannual timescale. It can be inferred from the cross-wavelet spectral modulus that the Nile flow and the equatorial Atlantic SST share common spectral energy at interannual timescale in the 1950s and the beginning of the 1980s. The decadal co-spectral energy is feeble.

The phase relationship between the filtered timeseries of Nile stream flow and equatorial Atlantic SST is also computed to determine the lead-lag relationship. The Nile stream flow leads the equatorial Atlantic SST from 1960-1990. In the 1950s and the first half of the 1990s, the equatorial Atlantic SST leads the Nile flow. This predictor is unstable.

Tropical Atlantic SST dipole and Nile flow

Temporal evolution of Nile flow and the SST dipole are used in the cross-wavelet analysis to find out the common spectral energy between Nile flow and tropical Atlantic SST index timeseries. It shows a strong co-spectral energy at quasi-biennial timescale. The amplitude of the co-spectral is very high in all but the 1970s. In the later case the decadal timescale has a strong signal.

Indo-Pacific SST and East Sahel rainfall

The standardised filtered East Sahel rainfall and Pacific Nino3 SST are subjected to cross-wavelet analysis. The two timeseries share common spectral energy modulus within in high and low frequency bands. Co-spectral energy shows strong amplitude from biennial to interannual timescale starting from 1960. A feeble signal is found in the decadal timescale.

The time-delay shows unstable time-varying phase with lead-time steadily decreasing with time. An in-coherent pattern is observed from 1950-1970.

6.5 Conclusion

The modulation of regional and global sea surface temperature on tropical North Africa climate variability was studied. Of these, the ENSO influence is greatest. The El Nino influences the tropical North Africa climate variability through the Atlantic Zonal Circulation and large-scale velocity potential dipole strengthening the low-level easterly flow and the upper-level westerly winds. In response, a strong AEJ is established. As a result, sinking motion and suppressed convection prevails in tropical North Africa during El Nino. South America on the other hand experiences enhanced convection. A local meridional circulation creates enhanced convection over the Guinea Coast at the expense of West Sahel through sinking motion and hence suppressed convection. As a result, Sahel-Guinea rainfall dipole configuration is generated (Fig. 6.20).

The equatorial Atlantic and Guinea Basin SST influences on tropical North Africa were also considered. Warming pool over these regions modulates the convection of tropical North Africa in same way as El Nino through low-level easterly/upper-level westerly flow of the Atlantic Zonal Circulation. This provides the necessary dynamics for suppressed convection. On the other side of the Atlantic, an opposing centre of upper divergent outflow and rising motion is set up for deep convection over tropical regions of South America. As in the El Nino

case, the warm SST in equatorial Atlantic accelerates the AEJ. A strong thermal gradient ($\partial T/\partial y$ produces a southward shift of convection over the equatorial region and dryness in Sahel through establishment of meridional cell with rising motion in the equatorial region and sinking in the north (Fig. 6.20)

The dipole configuration between equatorial east Pacific (warm pool) and equatorial Atlantic (cold pool) is also studied with a view to its modulating effect on tropical North Africa climate variability. As a result of this opposing SST configuration, anticyclonic circulation is formed over Gulf Guinea with easterly flow over equatorial Atlantic. In the upper level, a huge cyclonic circulation is formed across the tropical southern latitudes. The Atlantic SST dipole influence is that of a 'slave' to equatorial east Pacific SST. That means any episodic event in the east Pacific Ocean dominates the tropical North Africa climate variability regardless of Atlantic SST dipole variability, despite its proximity to tropical North Africa. The combination of the two can alter the vertical structure and orientation of the Atlantic Zonal Circulation through tilting it to south with height. The influence of equatorial Atlantic mode is significant in the tropical North Africa climate variability during weak periods of ENSO modulation.

In conclusion, the tropical North Africa climate variability is modulated by ENSO, equatorial Atlantic and meridional SST mode and Indian Ocean SST dipole through the Atlantic Zonal Circulation connection. Locally ENSO modulates tropical North Africa through strengthen the AEJ. Strong AEJ produces a meridional cell within the tropics that generates Sahel - Guinea rainfall dipole. The other main result is that tropical North Africa climate variability is more sensitive to ENSO than equatorial Atlantic SST. The integrated view of the tropical SST influence on tropical North Africa is schematically presented in Fig. 6.20 and 6.21.

The contribution of key SST indices to the variability of tropical North Africa climate is examined using continuous monthly rainfall data from 1950-1997 and SST with standardised raw data and at interannual. The SST contribution at

ENSO timescale is very low and maximum variance does not exceed 17%. The variances with raw data are much better for Atlantic SST. The Indo-Pacific SST has a low signal. But, ENSO influence on this part of Africa is established through regional and local circulations. This could signify that ENSO modulation on tropical Africa is "indirect".

The equatorial Atlantic SST mode accounts for 16-50% variance in the tropical North Africa hydroclimate variability. The maximum variance comes with association to Nile River flow variability. Atlantic SST dipole (as defined by Chang (1997)) explains by 13-15% more than Atlantic Nino mode. Most of the contribution of the dipole comes from South Atlantic SST (40% variance). Camberlin et al. (2001) found similar results in the teleconnection between Atlantic SST and rainfall in the tropical North Africa.

A comparison is made on the variance explained by the kinematic and thermodynamic variables and the cumulative average difference shows that the east-west divergent circulations, discussed in Chapter 5, accounts for 36% more variance than the SST with respect to tropical North Africa rainfall. These indices will be considered in Chapter 8 in developing prediction scheme.

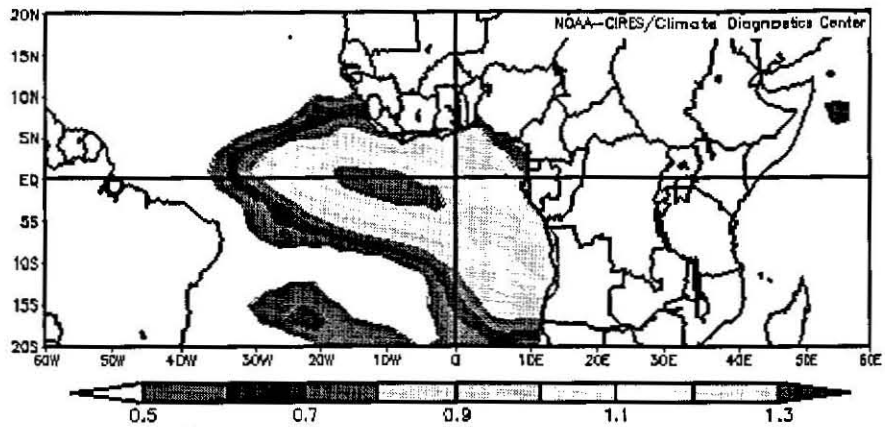

Fig. 6.1 SST Anomaly (^{0}C) depicting the warm phase of the equatorial Atlantic SST (positive SST minus negative SST over [40°W-10°E] and [15°S-5°S] box).

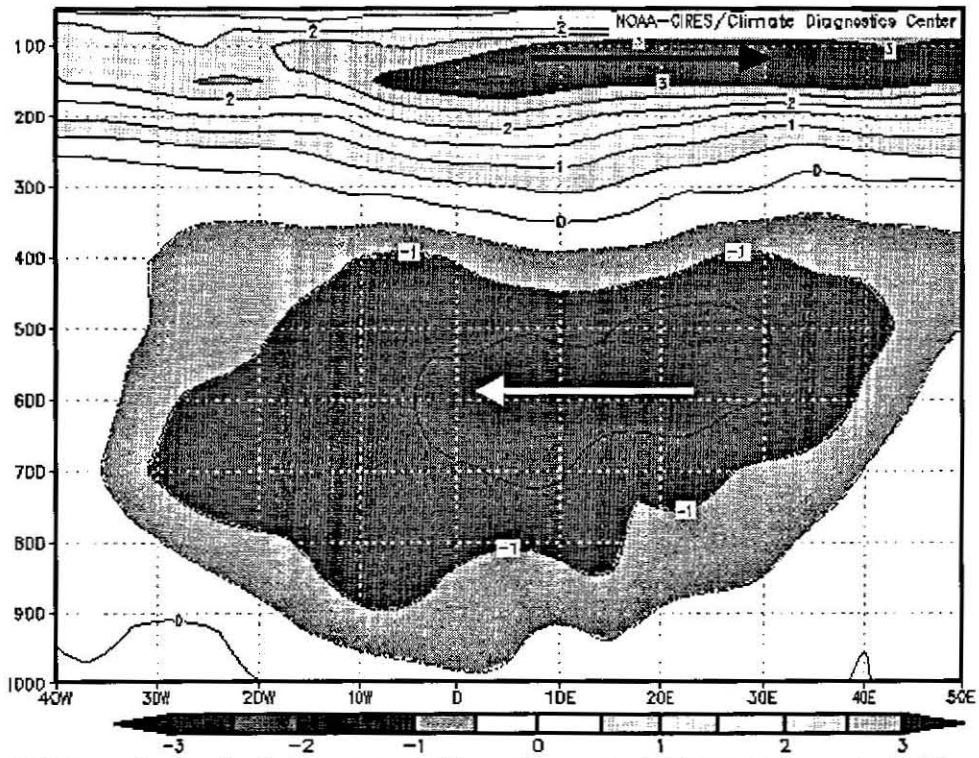

Fig. 6.2 Longitude - height cross-section of equatorial Atlantic zonal wind (m s^{-1}) averaged over [10°S, 20°N] latitudes depicting equatorial Atlantic circulations during equatorial Atlantic warm episodes.

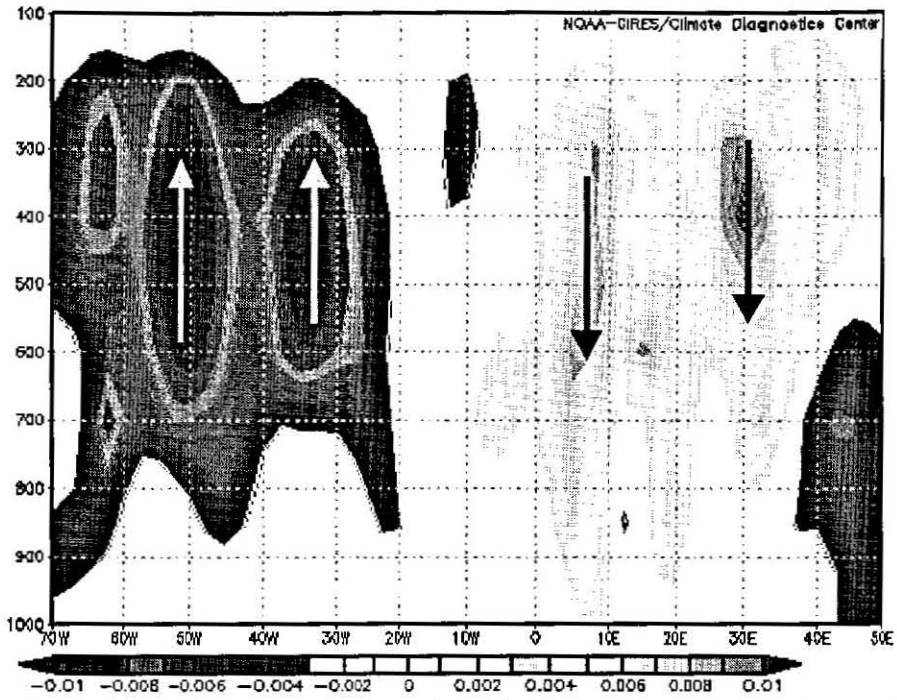

Fig. 6.3 Longitude-height cross-section Vertical velocity anomaly (pa s^{-1}) averaged over [10°S, 20°N] latitudes showing descending motion in tropical Africa and ascending in Atlantic Ocean associated to Equatorial Atlantic warming.

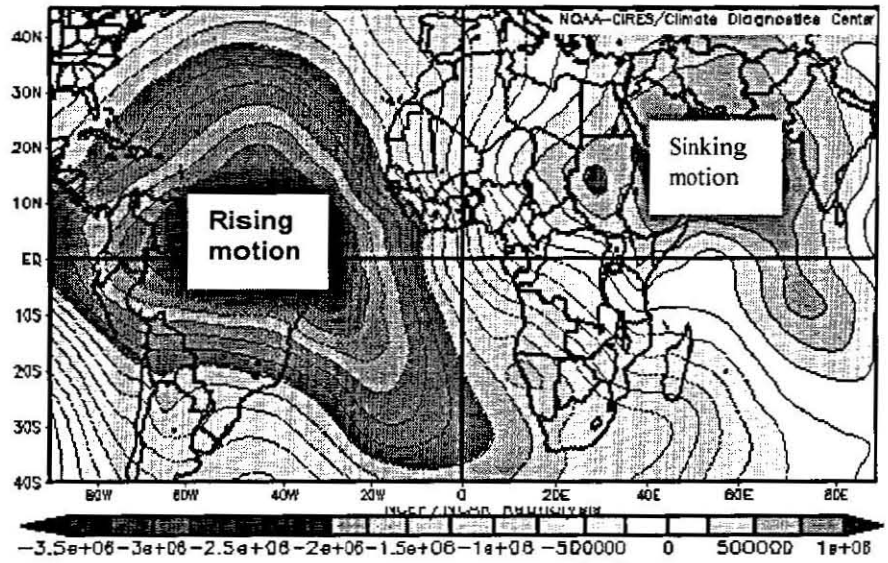

Fig. 6.4 Upper-level Velocity potential polarity (m^2 s^{-1}) between Northeast Africa and tropical South America / Atlantic revealing the outflow over the latter regions and inflow in the former.

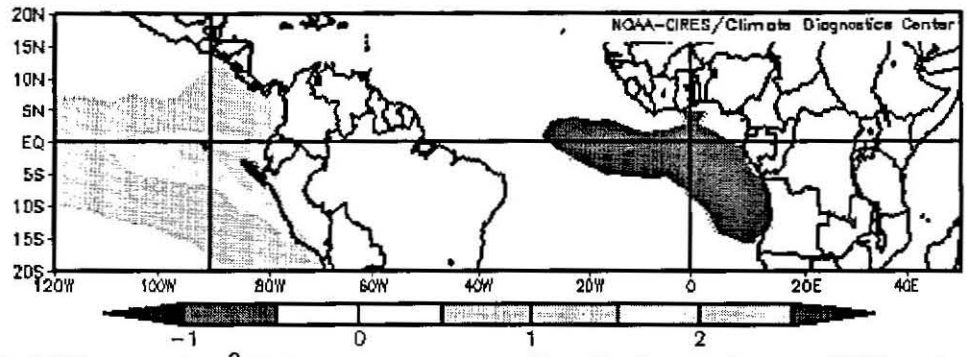

Fig. 6.5 SST anomaly (^{0}C) for equatorial east Pacific Ocean (warm SST) and equatorial Atlantic (cold SST).

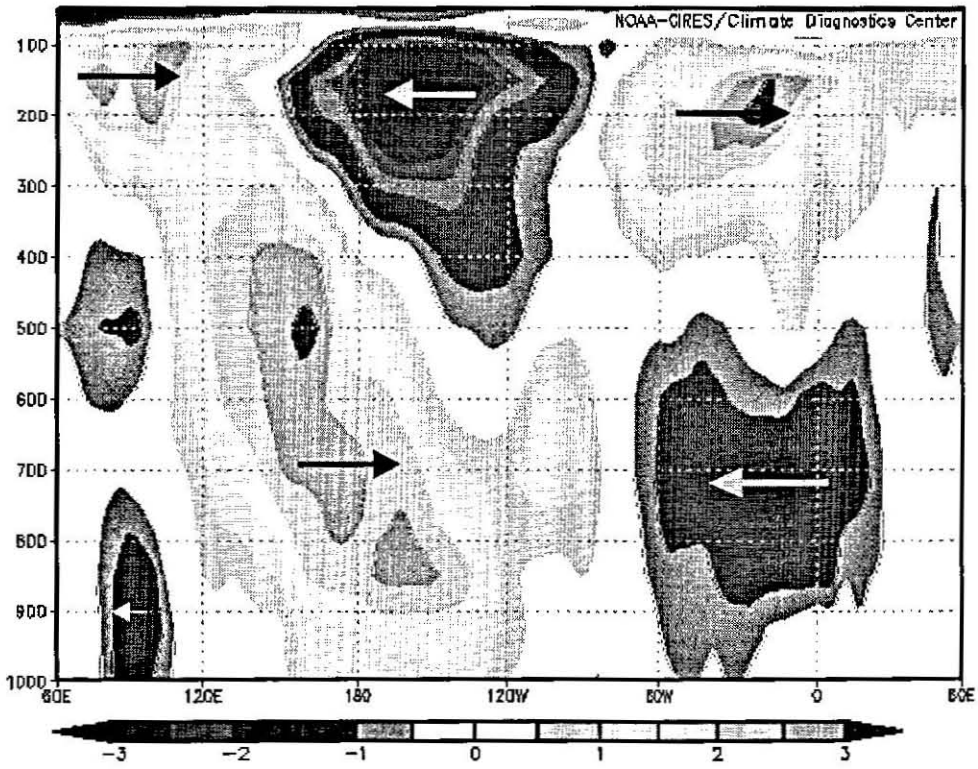

Fig. 6.6 Longitude-height cross-section of zonal wind (m s^{-1}), averaged from 10°S to10°N, showing Atlantic Zonal Circulation, Pacific Walker Circulation and Indian Ocean Circulation as a response to equatorial east Pacific warming and equatorial Atlantic cooling. The interaction of equatorial Pacific and Indian Ocean wind can be seen in the zonal wind field.

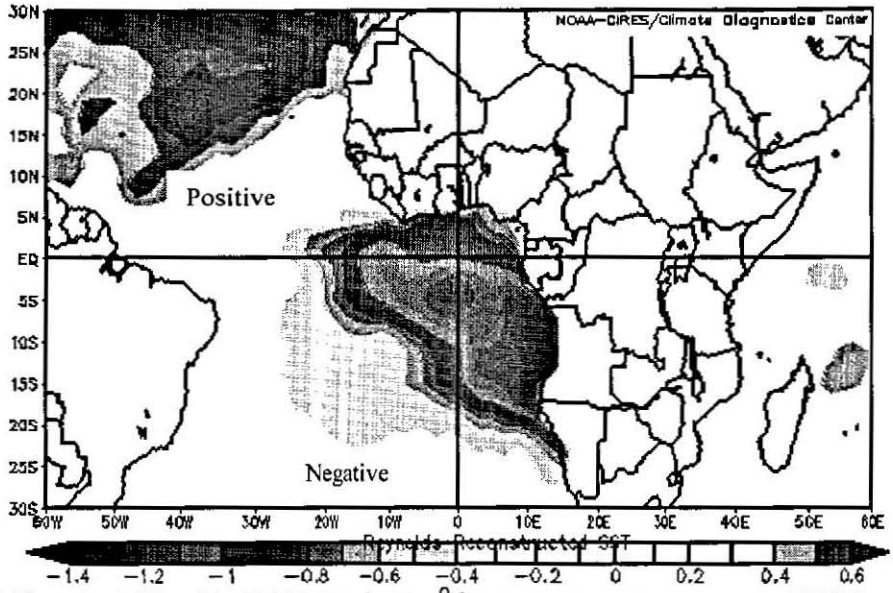

Fig. 6.7 Tropical Atlantic SST dipole (in ^{0}C) as defined by Chang (1997) produced using TASI composite analysis.

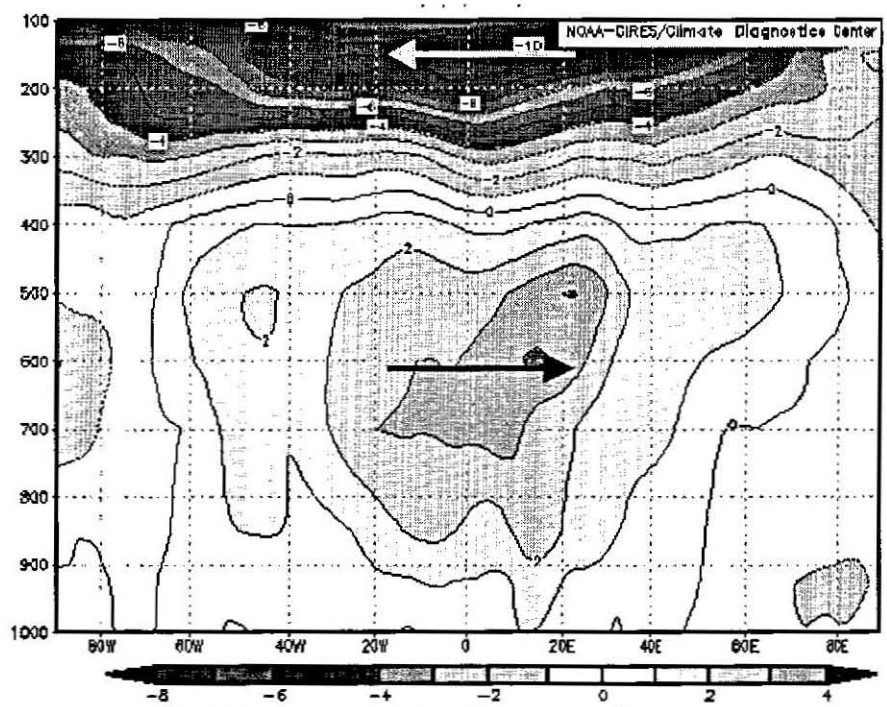

Fig. 6.8 Response of Atlantic Zonal Circulation (m s^{-1}) to Atlantic SST dipole as defined by the relationship between Sahel rainfall and Atlantic SST (averaged from 10°S-10°N).

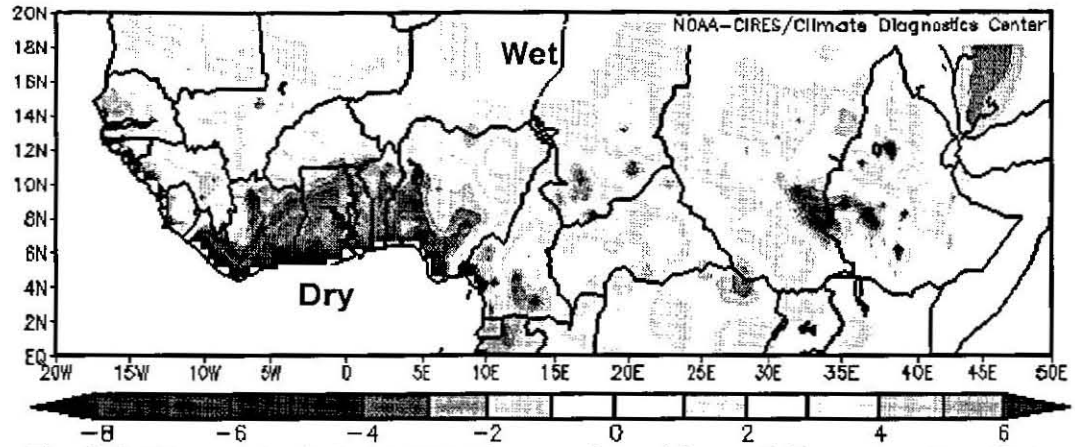

Fig. 6.9 Observed rainfall composites produced from TASI composites: Guinea (Dry) and other tropical North Africa areas (Wet).

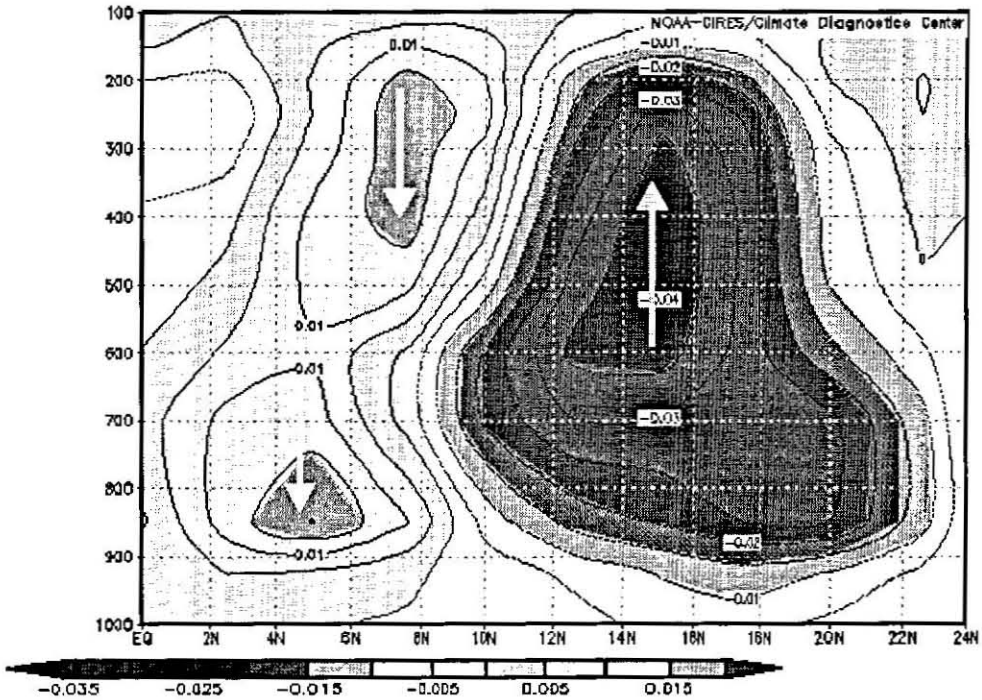

Fig. 6.10 Meridional anomalous vertical velocity (Pa s^{-1}) averaged within 18°W to15°E showing the rising motion in Sahel and sinking in Guinea Coast as part of the meridional overturning.

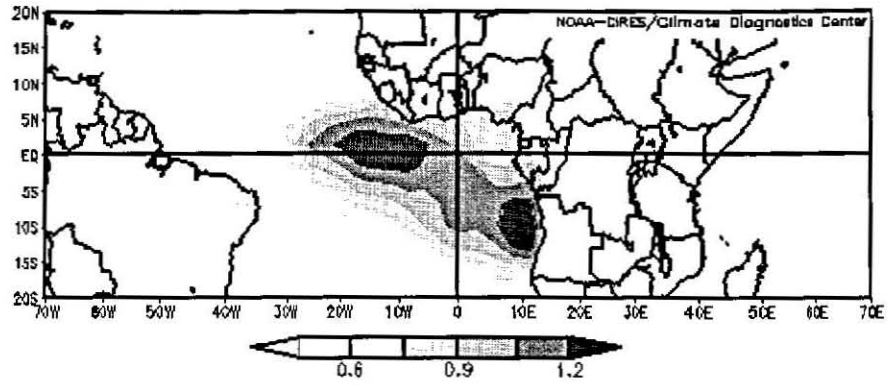

Fig. 6.11 CCM3 ensemble of surface air temperature (°C) showing the equatorial Atlantic warm pool.

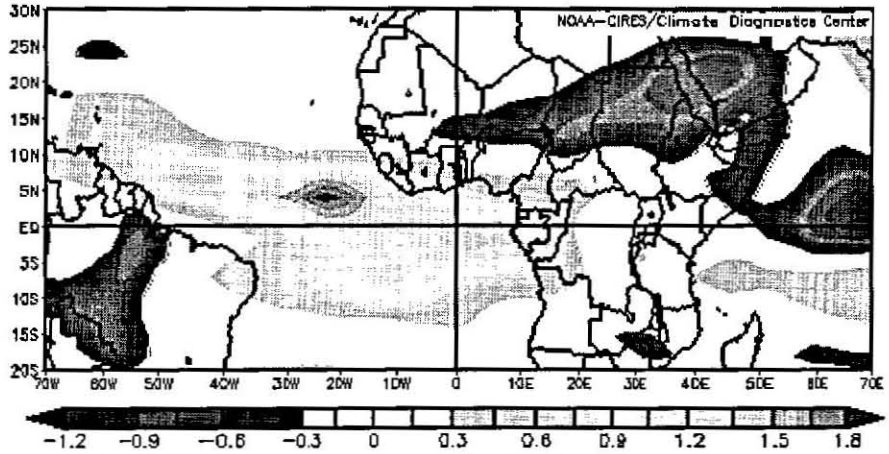

a) CCM3 ensemble of 700-hPa zonal wind (ms^{-1}) showing anomalous westerly over the equatorial Atlantic Ocean as a response to equatorial Atlantic warm pool.

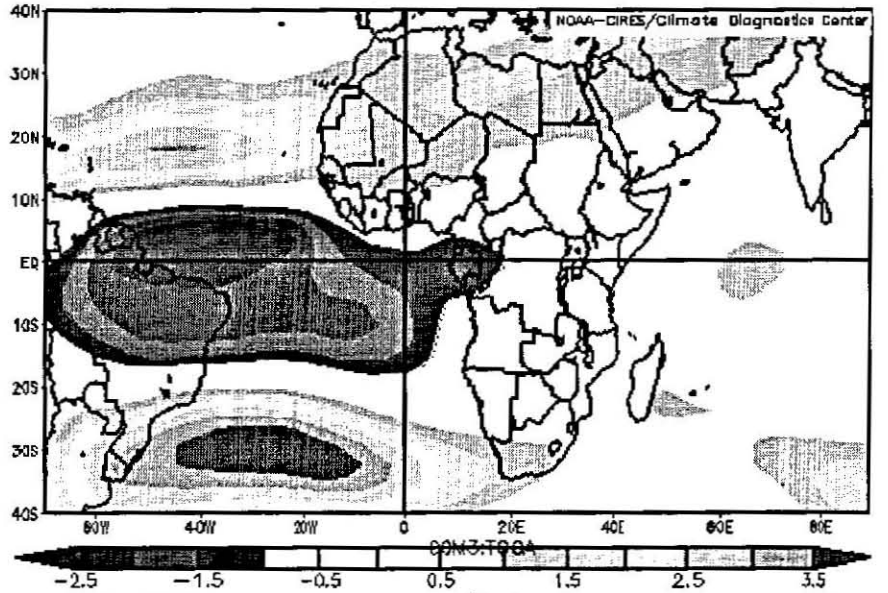

b) CCM3 ensemble of 200-hPa zonal wind (ms^{-1}) showing anomalous easterly over the equatorial Atlantic Ocean as a part of the twin anticyclone as a response to equatorial warming.

Fig. 6.12 CCM3 ensemble of equatorial Atlantic circulation as a response to equatorial Atlantic warm SST.

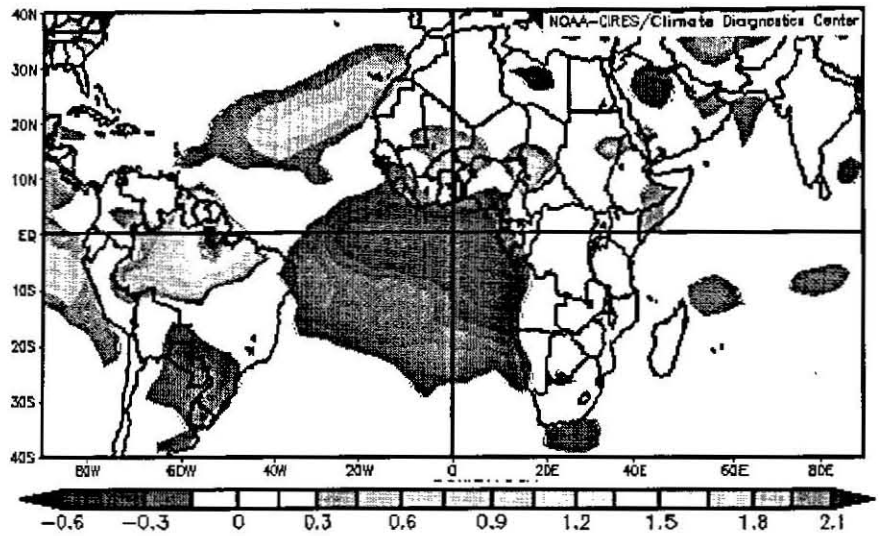

Fig. 6.13 Tropical SST forced CCM3 simulation of Atlantic SST dipole in surface air temperature (°C).

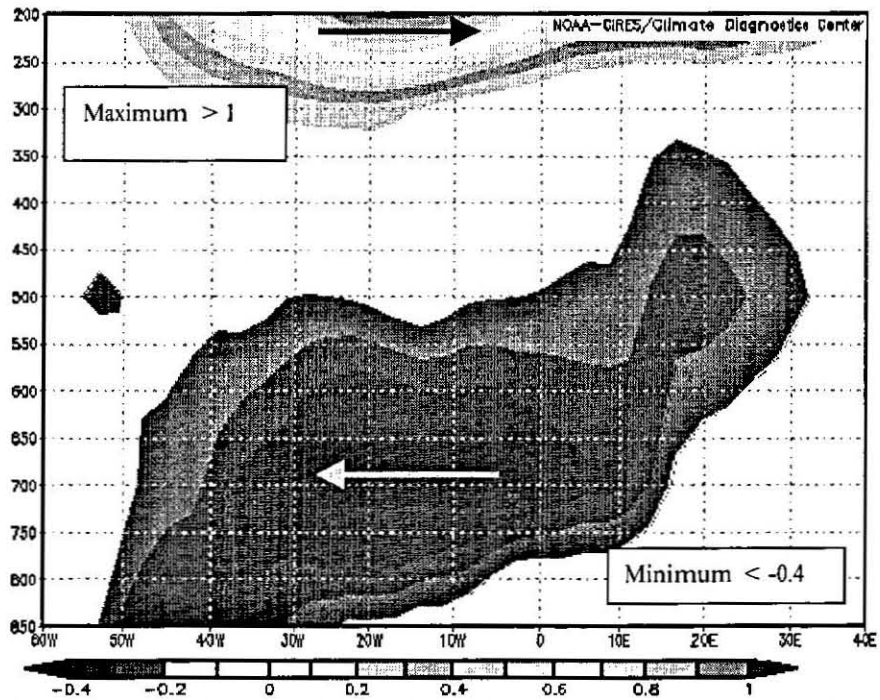

Fig. 6.14 CCM3 ensemble of longitude - height cross-section of zonal wind (ms^{-1}) averaged over [-10°S, 10°N] latitudes as a response to Atlantic SST dipole.

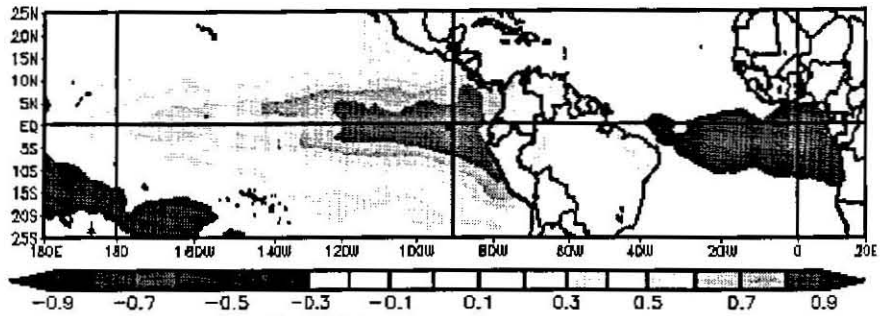

Fig. 6.15 Equatorial east Pacific SST minus equatorial Atlantic SST index interplay to SST tropical Pacific and Atlantic Oceans (anti-phase phase).

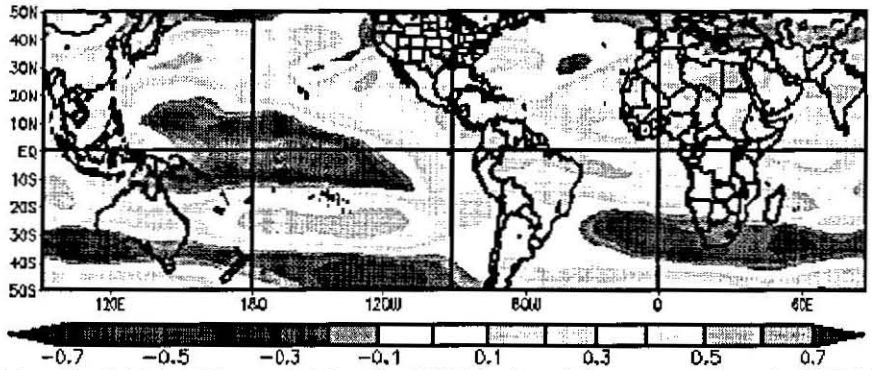

Fig. 6.16 Equatorial Pacific and Atlantic SST index teleconnection to 250-hPa zonal wind.

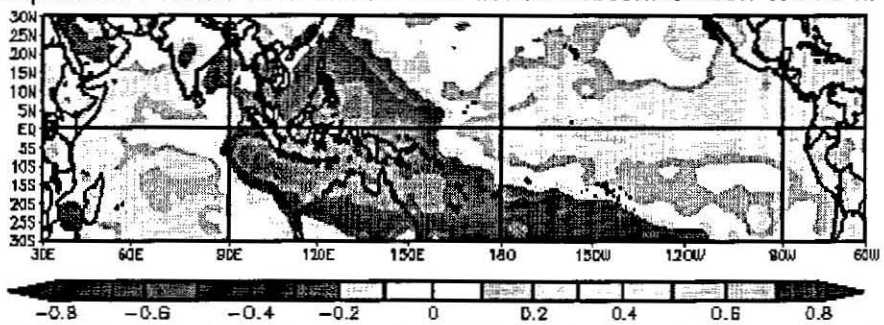

Fig. 6.17 IOD and tropical SST connection showing ENSO teleconnection signal.

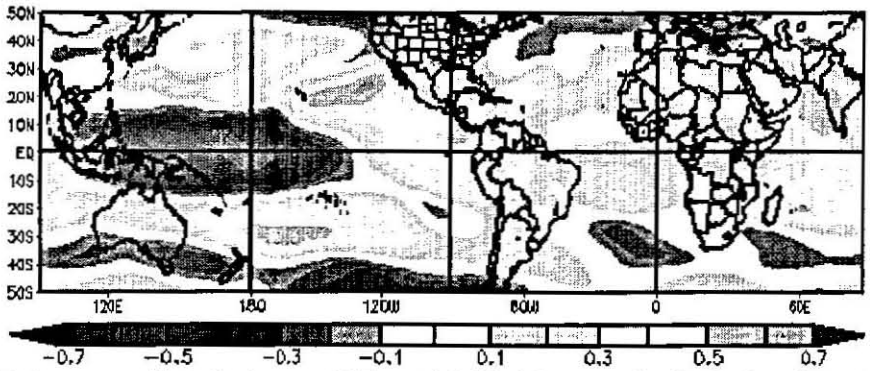

Fig. 6.18 Teleconnection between IOD and 200-hPa zonal wind showing strong connection to core of TEJ.

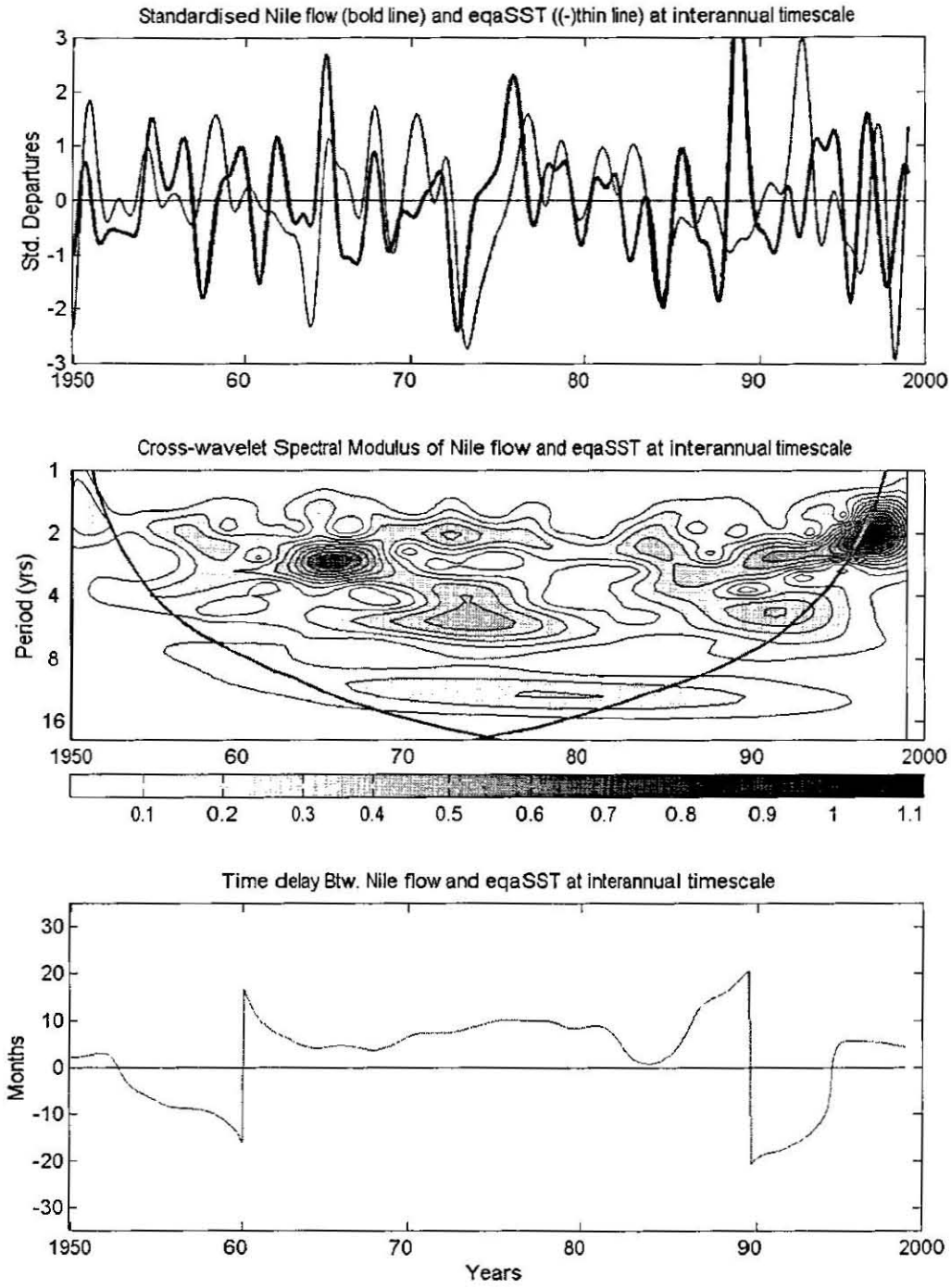

Fig. 6.19 Temporal evolution of cross-wavelet variants as applied to Nile flow and equatorial Atlantic SST (eqaSST) revealing common spectral energy in interannual and decadal timeseries. This delay depicts the Nile flow leading the equatorial Atlantic SST from 1960-1990 at interannual timescale.

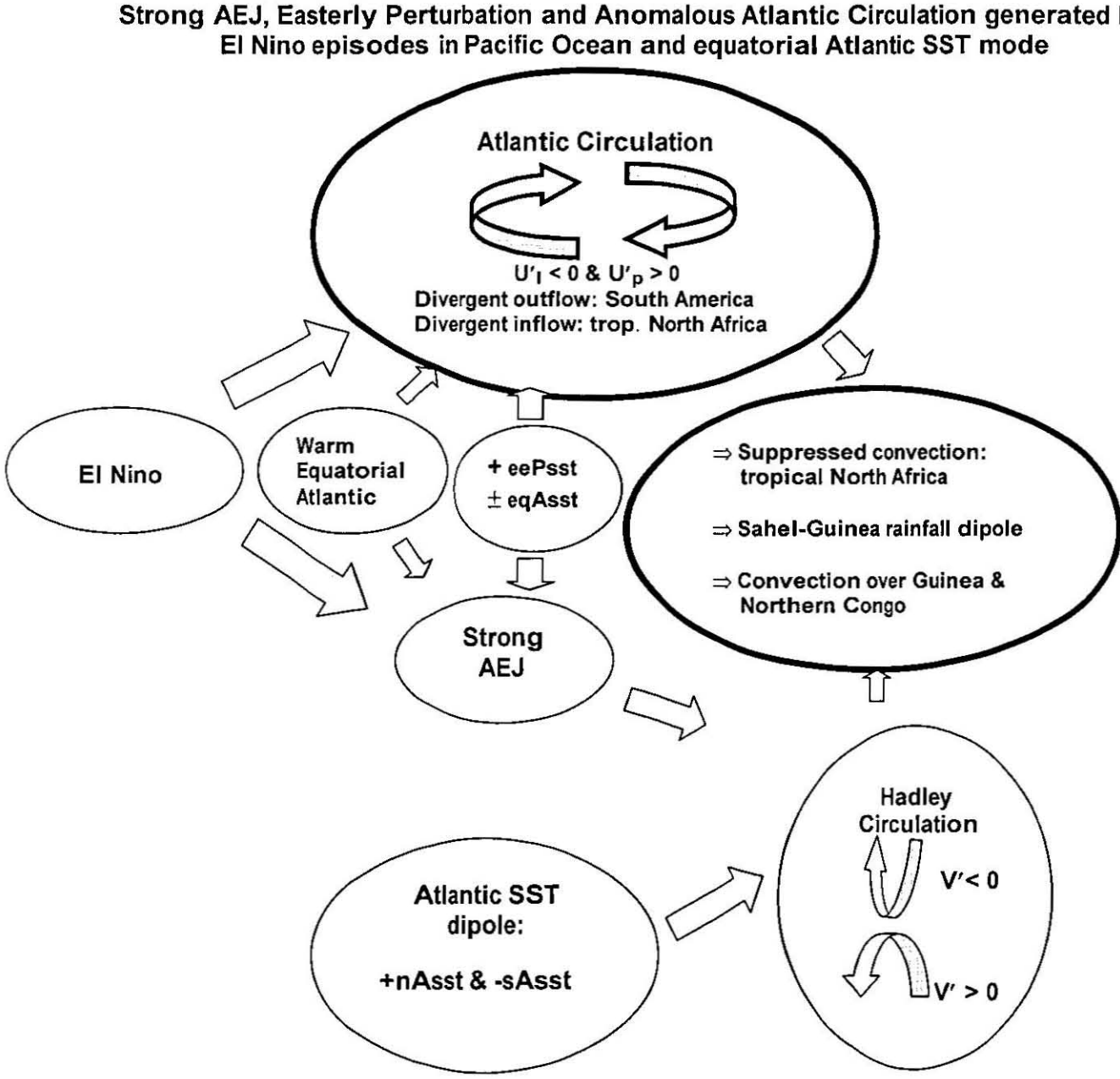

Fig. 6.20 Influences of tropical SST modes on tropical North Africa climate variability through Atlantic Zonal Circulation and Hadley Overturning.

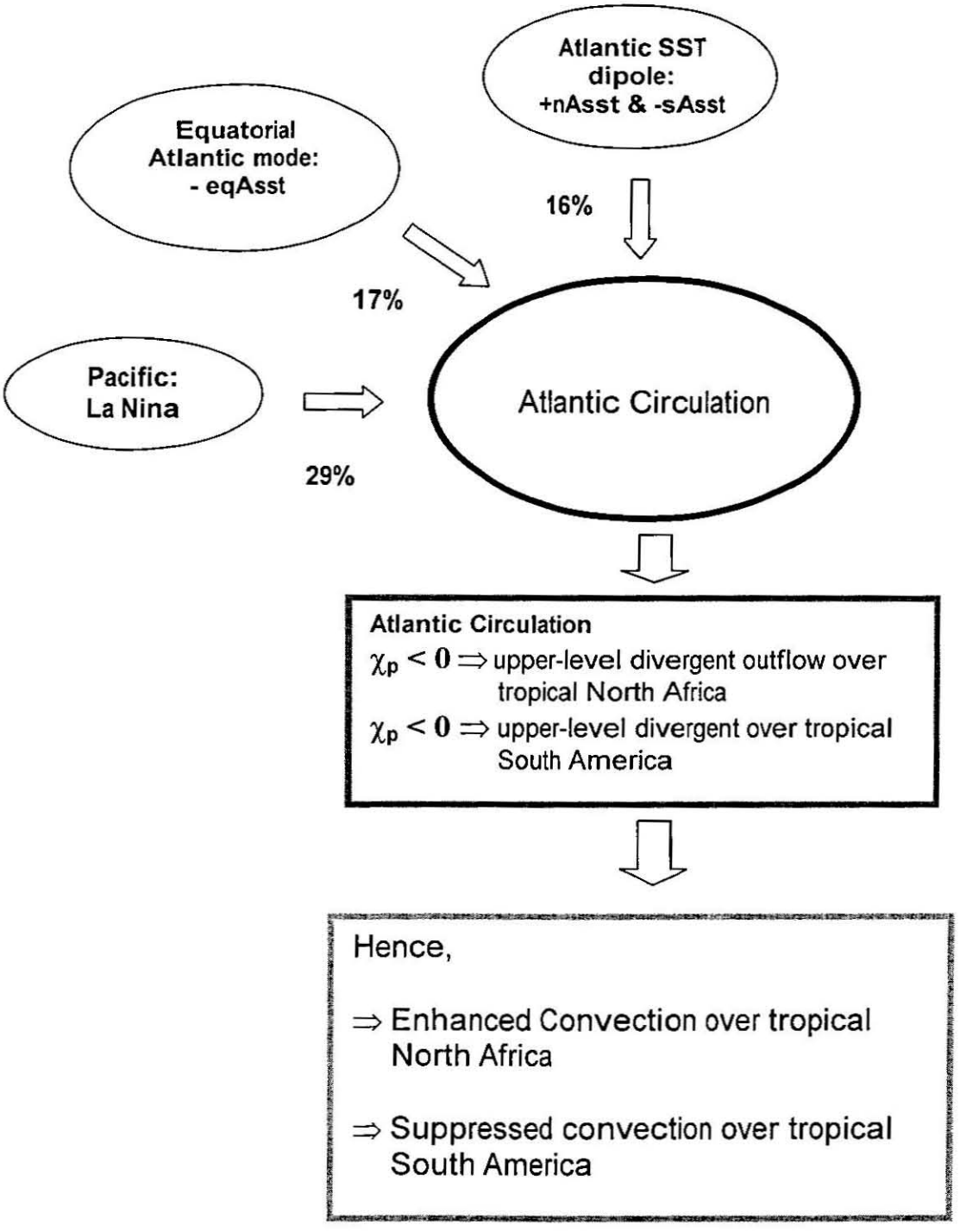

Fig. 6.21 Conceptual diagram depicting the modulation of Pacific, equatorial Atlantic, and Atlantic SST dipole on tropical North Africa and South America climate swing through Atlantic Zonal Circulation. The number shows the contribution of individual SST index to low-frequency Atlantic Zonal Circulation. Collectively, they contribute 43% of variance. Computation is based on 1950-1998 continuous filtered data (1.5-16-year).

Table 6.1 Environmental and field indices key areas.

	Parameter	Key parameters representation	Key area location
1	Tropical Atlantic SST dipole index	TASI	(40W,20W), (5N,20N)$^{\alpha}$ (15W,5E),(5S,5N)$^{\beta}$
2	Equatorial Atlantic	eqaSST	(40W,10E), (15S,5S)
3	Gulf of Guinea	GoG	(20W,10E),(10S,5S)
4	Pacific SST index	pSSTi	(160E,90W), (10S,10N)δ (90E,150E), (10S,10N)$^{\varepsilon}$
5	Equatorial east Pacific-equatorial Atlantic SST	eepaSST	(15W,10E), (5S,5N)$^{\phi}$ (120W,80W),(5S,5N)$^{\gamma}$
6	Pacific SST dipole	pSSTd	(140E,155W), (10N,35N)$^{\eta}$ (140W,75W), (35S,10S)$^{\iota}$
7	Indian Ocean SST dipole	IOD	(50E,70E), (10S,10N)$^{\varphi}$ (90E,110E), (10S-0)$^{\kappa}$
8	NINO 3	Nino3	(150°W,5°N) (90°W, 5°S)

Note that SST stands for sea surface temperature. TASI is the SST difference between south ($^{\alpha}$) and north ($^{\beta}$) Atlantic (as defined by Chang et al. (1997)). The pSSTi is the SST difference between equatorial Pacific Ocean cold tongue region$^{\delta}$ and the Maritime Continent$^{\varepsilon}$. The difference in SST between the equatorial east Pacific$^{\phi}$ and equatorial Atlantic$^{\gamma}$ is denoted as eepaSST. The pSSTd is the SST dipole between Northwest Pacific$^{\eta}$ and Southeast Pacific$^{\iota}$. The IOD is SST difference between the western tropical Indian Ocean$^{\varphi}$ and eastern tropical Indian Ocean$^{\kappa}$.

CHAPTER 7

MODE OF VARIABILITY OF TROPICAL OCEAN SUBSURFACE TEMPERATURE AND HEAT CONTENT: IMPORTANCE TO AFRICA CLIMATE

7.1 Introduction

Though several studies in the last decades discuss the variability of the sea surface temperature there are very few studies that describe the subsurface variability (Suryachandra et al., 2002) and these are Tourre and White (1995), Meyers (1996), Murtugudde and Busalachu (1999), and Schiller et al. (2000).

In this Chapter the equatorial subsurface variability is studied using various techniques to identify oceanic mechanism for the velocity potential dipole signature of Atlantic Zonal Circulation established between tropical North Africa and tropical South America. The climatology of the equatorial oceans is considered, to begin our paramount for understanding the equatorial subsurface variability.

Various techniques are used to unravel the interplay between subsurface ocean temperature and tropical North Africa climate variability. The availability of expanded satellite database and improved Ocean-General Circulation simulation, provide the opportunity to conduct studies on space-time variability of subsurface thermal structure and atmospheric coupling in the tropics. The tropical ocean heat content is investigated using singular value decomposition and correlation analysis. The space-time modes of variability are identified. The leading modes are considered and variability is linked to ENSO mode. The modes of zonal wind stress are compared with subsurface thermal modes and key circulation indices identified in earlier chapters.

7.2 Climatology of subsurface temperature and circulation

The upper-ocean thermal field plays an important role in ocean-atmosphere coupling. Ocean-atmosphere interaction in turn determines the climate teleconnection regionally or globally. A thermocline is a distinct interface between surface waters and cooler, deeper waters. It is an interface where temperature declines rapidly with increasing depth. On the top of this layer, a relative thin layer at the air-sea interface is present. This layer is called the wind mixed layer. In equatorial thermocline, wind circulations are important in the vertical advection of water from sub-surface to top or vice versa through upwelling and downwelling. Upwelling is equivalent to rising motion in the atmosphere. Upwelling is a process by which cooler water rises from may hundreds of metres depth and results in a shallow thermocline and a cooling of coastal waters. Upwelling causes a colder water to be found near the surface of the ocean. Downwelling on the other hand causes the water to sink and results to deepening of the subsurface thermocline. Because these processes are driven by wind forced Rossby and free Kelvin Waves they are very vital in shaping the temperature variability of the equatorial upper ocean. Interaction with ITCZ is then important especially at non-linear threshold of SST > 27°C.

In this Section, the climatology of the subsurface temperature and wind of the equatorial oceans is discussed. The boreal summer climatology is computed based on model assimilated ocean data of http://iridl.ldeo.columbia.edu/expert /SOURCES /.UMD /.Carton/ .goa/.beta7/ averaged over the period 1950 to 2000.

Equatorial Atlantic Ocean

The mean subsurface thermocline of equatorial Atlantic is examined for July. East-west vertical structures of subsurface temperature and zonal velocity of the equatorial oceans are analysed (averaged over [5°S, 5°N]) except Atlantic Ocean where the north-south structure is also considered. It is the first 200-m of the

upper ocean temperature and circulation that is considered as the thermocline variability greatest near 100 m depth.

The equatorial Atlantic east-west structure shows a sloping thermocline, shoaling and colder in the east (10°W to 10°E) and depressed and warmer in the west (50°W to 30°W). The temperature in the east does not exceed 24°C near the surface; in the west it is > 26°C in the upper 80-m. Underneath the surface, the isotherms are packed together within 80-180-m depth. In this region, the temperature falls at the rate of 0.075 $°Cm^{-1}$. In the east, the temperature gradient is within 20 to 40-m depth from 10°W -10°E. The temperature lapse rate is 0.05 Cm^{-1}. The 20°C isotherm has a slope of –3 m deg^{-1}.

To unravel the maintenance of the oceans' thermal structure, currents are examined. The mean zonal velocity shows easterly flows. Below 60 m depth, a reversal of circulation is observed revealing the vertical current shear $(\frac{\partial u}{\partial z})$ relation to the thermal structure. In the east Atlantic, upwelling elevates cold near the surface.

A north-south view of the subsurface temperature tropical Atlantic (averaged over 30°W to 15°W) is considered in understanding the mean upper ocean thermal field of Atlantic. The meridional shows a warm pool on either side of the equator. In the south (18°S-4°S), the thermocline is deeper. Cold water is found over the equator (4°S to 2°N) and the isotherms are steep.

Meridional currents are analysed to explain the north-south subsurface temperature structure of Atlantic. A flow from South is found in the upper 40-m from 10°S - 6°N, except with 0-20 m from 0° to 5°N. South of the equator and below 40-m, the circulation is reversed (from the north) to establish $\partial V/\partial y$ current divergent and uplift over the equator.

Equatorial Indian Ocean

The subsurface temperature structure in the equatorial Indian is different from Atlantic and Pacific. Its thermocline is of constant depth. East of 60°E, the lapse rate is nearly constant and the slope of the isotherms is horizontal to a great extent. In the Southwest monsoon current, the wind mixed layer is deep and cold waters affect the surface. The east-west slope of the 20°C isotherm (0.5 m deg^{-1} of longitude) is small. This is one-sixth of the slope of 20°C isotherm of the equatorial Atlantic and two-fifth of equatorial Pacific. The lapse rate in east is 0.1 $°Cm^{-1}$ and in the west 0.08 $°Cm^{-1}$ in the west. Xie et al (2002) associated the flatness and deepness of the equatorial Indian Ocean with weak westerly (downwelling) winds there. The shallowest area of the thermocline (40 m) is the zonal ridge along 8°S from 50-80°E.

Similar mechanism, discussed above, operates in modulating the subsurface temperature other oceans. The difference is that a strong eastward current drives the Indian Ocean; where as in tropical Atlantic and Pacific Oceans trade winds spin westward currents (Philander, 1990).

Equatorial Pacific Ocean

The mean subsurface thermal structure of the Pacific shoals in east and deepens in the west. The 20°C isotherm has a -1.2 $°Cdeg^{-1}$ longitude slope. In the east, the lapse rate is 0.625 $°Cm^{-1}$; in the west it is 0.7 $°Cm^{-1}$.

A westerly current with a speed of 0.25-ms^{-1} propagates to the east below 20 m within 180-90°W. Shallow easterly winds are shown in upper 60-m. This shear generates an east-west circulation that determines the temperature structure as discussed above and results in upwelling in the east (hence cooling) and downwelling (hence warming) in the west.

In the off-equatorial belt of all Oceans, anticyclonic (cyclonic) wind stress curl anomaly drives anomalous downwelling (upwelling) Ekman pumping of thermocline depth (White, 2000). Hence atmospheric Walker cells may induce standing ocean Rossby Waves that tilt the tropical thermocline additionally contributes to east-west shifts in convection.

Processes involved in redistribution of temperature in the thermocline

The spatial variations in the depth of the thermocline are associated to large horizontal density gradients that reflect the dynamical response of the ocean to the surface winds. The pressure gradient associated with the slope of the thermocline in the equatorial plane balances the wind stress (Philander, 1990).

The sea surface temperature and thermocline structures are influenced through the Ekman transport and heat flux across the ocean surface through the processes of advection, upwelling and mixing. These processes in turn determine the stability of low frequency basin-scale waves. Sea surface temperature in the western equatorial Pacific falls during El Nino when the thermocline in that region shoals with easterly wind-driven equatorial upwelling and increased heat flux (Meyers, et al., 1986). During El Nino, the warming of eastern Pacific is caused by eastward advection of warm surface waters associated with the elevation of the thermocline in the west and deepening in the east (Philander, 1990). According to numerical results (Hirst, 1986), when sea surface temperature is a function of thermocline depth, the high frequency Kelvin amplifies while low frequency basin-scale Rossby wave is damped. If the sea surface temperature depends on horizontal advection, then the low frequency basin-scale Rossby Wave becomes unstable and disturbances propagate westward. Under this scenario, the Kelvin Wave is damped. If the air-sea processes specified here are absent then the wave modes are equatorially trapped.

The principal causes of changes in the depth of the tropical thermocline are a horizontal redistribution of warm waters in response to changes in the large-scale winds (Wyrtki, 1975; Merle, 1980 (a and b); Duing and Leetmaa, 1980; Stevenson and Niller, 1983; Molinari et al, 1985). This can be by wave-induced sea-saws in the thermocline depth.

7.3 Space-time modes of tropical oceans vertically integrated heat content

To assess the interannual variability of tropical ocean heat content monthly data from 1950 to 1999 are subjected to singular value decomposition discussed in Section 3.3.5. This computation results in the identification of spatial-temporal modes of vertically integrated heat content to 125-m depth. The leading spatial and temporal modes are discussed here. The variance explained by each component is given in Table 7.1.

Tropical Atlantic heat content

The heat content of the tropical Atlantic Ocean is passed through an eigen-based Empirical Orthogonal Function that gives as outputs the eigenvalue and the most dominant spatial and temporal characteristics of heat content isolating the most important signals, filtering the noise from the variability matrix.

The dominant spatial structure of EOF1 reveals a coherent pattern in the east equatorial Atlantic (Fig. 7.2a) and explains 19% of the variability. Half of the variability of PC1 is explained by the interannual timescale signal (Fig. 7.2). The equatorial Atlantic and Gulf of Guinea SST are weakly related to this leading mode ($r = 0.44$ and $r=0.40$ in that order).

The second EOF depicts a dipole structure between the southern Gulf of Guinea and tropical North Atlantic with negative loading mainly within 0° to 15°N (Fig. 7.1b). This structure explains 10% of the HCA variance and shows a year-to-year fluctuation (60% of the variance). This component is more closely related to

equatorial Atlantic and Gulf of Guinea SST with r=0.59 and r=0.56, respectively. All the leading principal components of tropical Atlantic heat content (Fig. 7.2) are poorly related to the principal east-west circulations identified as key indicators of North Africa climate. It is significant that the second mode reflects the north-south dipole structure commonly found in surface analysis, but with a narrow north-south extent.

Tropical Indian Ocean heat content

The singular value decomposition is performed on the spatio-temporal variability of tropical Indian Ocean heat content. The dominant EOF shows a distinct dipole between the western and eastern Indian Ocean (Fig. 7.3a). This structure accounts for 32% of the HCA variance, with 73% coming from the interannual frequency. The first leading principal component of tropical Indian heat content (Fig. 7.4) is tied to equatorial East Indian wind and Pacific SST variability as shown later. It reflects the Indian Ocean SST dipole and a variance of 23% is involved in this relationship.

The spatial structure of the second EOF of tropical Indian heat content represents a coherent interannual variability embedded in a trend (Fig. 7.3b). Its spatial structure is an equatorial mode in the eastern basin. Its temporal evolution shows a trend signal (Fig. 7.4).

To examine the robustness of the identified EOF using SVD, a comparison is made with the study done by Suryachandra et al. (2002) on the heat content (using Complex EOF analysis) and TOPEX /POSEIDON sea level data (EOF analysis) in Indian Ocean. The dipole structure identified in the heat content in this study resembles that of dominant modes of the spatial structures of the SST and sea surface height despite the short data set used in their analysis (1983 – 1989 as compared to 1950-1999 data used in this study).

The subsurface space-time variability of the heat content anomaly influences the surface property (example sea surface temperature in general and the tropical Indian Ocean SST dipole (IOD). This is evidenced by Suryachandra et al. (2002) using a correlation analysis between sea level in the eastern Indian ocean and SST (in key regions of IOD) anomalies, it is found that the subsurface dipole influences the IOD through the propagation of Rossby Wave (Suryachandra et al. 2002).

Tropical Pacific heat content

The first two leading spatial EOFs are shown in Fig. 7.5. These EOF patterns explain in that order 36% and 12% of the total variance of the tropical Pacific Ocean heat content. These structures and the vertically integrated thermocline temperature of tropical Pacific match conspicuously. The first mode of tropical Pacific Ocean heat content reveals a dipole structure that corresponds to ENSO signal (Fig. 7.5a). The temporal variability of this structure exhibits interannual timescale variability with embedded high frequency signals. 85% of the variability of the leading principal component is within the internannual timescale variability. The spectral decomposition of the PC1 reveals that the interannual variability has the largest signal of both seasonal and annual cycles (Fig. 7.6).

PC1 is closely tied to Pacific Nino 3 SST (r = -0.871). It is also markedly related to the zonal wind in the equatorial Pacific (r=-0.834) as expected. Its interannual component is linked to the east-west divergent circulation, particularly with transverse monsoon circulation (r = 0.849). The correlation at annual cycle is also impressive.

The second EOF shows a strong loading within equatorial Pacific accompanied by opposite pattern in either side of east Pacific (Fig. 7.5b). The temporal component has weak amplitudes from 1950 to 1965 possibly due to sparse or poor observation. Year-to-year fluctuation is then depicted until it shows a declining trend commencing from 1985. 55% of the variability of PC2 is

attributable to interannual timescale swing (Fig. 7.6). But, this temporal component is not part of the ENSO signal.

The third leading temporal pattern of heat content in the tropical Pacific Ocean has importance in ocean-atmospheric coupling but not as much as the leading mode.

7.4 Eigen-mode of east-west sections of subsurface temperature variability within equatorial oceans

Eigenfunction analysis using singular value decomposition is applied to east-west sections of equatorial oceans subsurface temperatures. The most important spatial structure and temporal variability that signal the mode of variability of equatorial subsurface temperature are identified. The associated eigenvalue (variance) is shown in Table 7.1. These space-time structures are discussed in relationship to the interplay of the coupled ocean-atmosphere system.

7.4.1 East-west subsurface temperature within the equatorial belt

Atlantic subsurface temperature

The spatial structure of the first EOF displays a singular pattern in the east Atlantic (Fig. 7.7a) with maximum loading within 20 to 60-m depth from 2°W to 10°E, near Africa. The leading temporal component of the equatorial Atlantic upper-ocean temperature shows a slowly increasing trend (Fig. 7.8) and explains 30% of the total variance. The interannual frequency (1.5-16-year) of PC1 accounts for 46% of the signal. The leading temporal pattern is weakly related to equatorial Atlantic and Gulf of Guinea SST and its relationship with east-west divergent circulation is feeble too. This is true for most other modes of variability of equatorial Atlantic subsurface temperature. The EOF2 exhibits equatorial Atlantic subsurface thermal dipole with positive loading west of 10°W (Fig. 7.7b).

The associated temporal component reveals a decadal signal from 1975-1999 (Fig. 7.8).

Indian Ocean subsurface temperature

The equatorial Indian Ocean east-west subsurface temperature is also investigated in the same line. The first EOF shows a negative loading in the western equatorial zone again near Africa at 100-m depth (Fig. 7.9a). This structure explains 44% of variance (Table 7.1) and the interannual frequency is 61% of variance. PC1, shown in Fig.7.10, is poorly related to the equatorial Atlantic, Indo-Pacific SST and east-west circulations.

The EOF3 of the zonal wind stress shows a dipole structure south of the equator and negative loading north of the equator. In the South, the pattern reveals a wave number structure with centres of positive loading at (62.5°E, 22.5°S) and negative at (85°E, 17.5°S). The third EOF of HCA over the same basin reveals the same structure with maximum loading located within 12-6°S latitudes.

To determine interaction between the surface zonal wind stress and subsurface thermal field, SVD is performed on east-west vertical slice at 10°S from surface to 250-m depth. The first mode reveals mono-pattern with maximum amplitude located 40-140-m depth from 50-65°E (not shown). The second mode shows east-west dipole (negative in the west), a separating line at 60°E. The temporal variability of the leading PC reveals mainly year-to-year fluctuation and the second component too shows yearly fluctuation from 1950-1970. But, the period from 1978-1991 in PC2 is characterised by high frequency signals.

The main point here is that the main action is in the western Indian Ocean near Africa. The ocean-atmosphere coupling is a large-scale pattern. Murtugudde and Busalacchi (1999) suggested that the southwest tropical Indian Ocean obtains a large SST anomaly because of a shallow thermocline and entrainment effects

associated with the winds stress curl and ocean Rossby Waves propagating in the region.

East-west pacific subsurface temperature

The most dominant signals of the equatorial Pacific Ocean east-west subsurface temperature are investigated. The leading EOF portrays a polarity in the subsurface with negative loading in the first 160-metre depth (Fig. 7.11a). This structure broadens with decreasing height (towards surface) in the central and east Pacific. The opposite loading widens up with increasing depth. The variance associated to this global dynamic wave structure is 36%. The first leading temporal component (Fig. 7.12) is closely tied to Indo-Pacific SST and the correlation coefficient is equal to -0.81. The PC1 is also strongly related to the atmospheric east-west circulations. The degree of association between the Walker Circulation and the leading principal component is notably strong both at annual cycle and interannual timescale. Its relationship to other east-west atmospheric circulations is also significant. The correlation coefficients (at interannual timescale) with Walker Circulation, Atlantic Zonal Circulation and transverse Monsoon Circulation are in that order 0.79, 0.56 and 0.69. The significance of this relation is that the leading spatio-temporal structure of the equatorial Pacific is within a coupled atmosphere-ocean system that is closely tied to the east-west divergent circulations.

The second EOF mode shows oval shaped singular structure with negative loading in the central Pacific (Fig. 7.11b). The variance associated to the second leading space-time variability is 31%. The PC2 reveals year-year variability with high frequency dominating in the first fifteen years of the record (Fig. 7.12). High amplitude is shown in the 1980s and at the end of the period. The interannual time-scale signal contributes 76% of the signal of PC2.

Kirtman (1996) found using coupled ocean-atmosphere simulation that the maximum variability of the Pacific thermocline is associated with off equatorial

Rossby waves. The simulation produced a regular five-year oscillation (ENSO signal) consistent with the delayed oscillator theory; the oscillatory behaviour produced by the reflection of the gravest Rossby wave off western boundary and the period of the oscillation determined by the off equatorial Rossby waves. The structure depicted in Fig. 7.11a is a global dynamic wave. This wave has 2-8 oscillations and 66% of its variability is associated to ENSO. This coupled Rossby wave determines the structure and oscillation of the east-west subsurface temperature in equatorial Pacific.

7.4.2 North-south mode of variation of subsurface temperature in tropical Atlantic and Indian Ocean

Modes of meridional variability of subsurface temperature within the tropical Atlantic and Indian Ocean are identified using EOF analysis. The most dominant meridional structures of the upper ocean temperature, averaged over 30°W to 15°W, are identified. Similar analysis is done over the tropical Indian Ocean averaged over 60°E to 90°E. Space-time structures of the thermal fields are identified using singular value decomposition as before and their variance is shown in Table 7.1. The first two modes are discussed here.

Atlantic Ocean

The EOF1 of the meridional structure of the upper ocean thermal field in the tropical Atlantic reveals a singular structure with negative loading across the basin in the north-south direction (not shown). The loading south of 8°S has a deeper vertical extent. The structure within 4°S to 4°N is limited within 20 to 120-m depth. North of 4°N, the surface and subsurface thermal fields are coupled. This mode explains 24% of the total variance and contains a trend. Variability at interannual timescale contributes 43% of signal. Yet this mode is uncoupled with North Africa climate and atmosphere circulation. This is also true for other modes of variability of tropical Atlantic meridional vertical structure. The leading amplitude of EOF1 varies in time with low frequency signal.

The second spatial mode of variability exhibits a dipole mode of variability in the subsurface temperature of tropical Atlantic Ocean (not shown). The configuration associated to EOF2 reveals a negative loading south of 10°S and positive north of 10°S. This is poorly correlated with the SST dipole however. Low frequency variability characterises the north-south thermal structure of Atlantic Ocean.

Indian Ocean

The principal space-time structures of the subsurface temperature in the tropical ocean are studied using the same techniques as above. The north-south variability is analysed averaged over 60°E to 90°E. The first mode unveils a coherent structure with strong signal from 6-12°S centred at 60-100-m depth (not shown). The negative loading is linked to the surface. The ENSO timescale variability accounts for 73% of the signal of PC1 (not shown). This mode holds 27% of the variance of the meridional structure of subsurface temperature in the tropical Indian Ocean and is focused on the thermocline "ridge" that is coupled to the atmosphere and modulated by Rossby Waves (Xie et al, 2002). The leading zonal wind stress is strongly tied to Indian Ocean dipole with r= -0.71 at ENSO timescale.

The second mode of variability in the subsurface temperature is focused in the equatorial band in the 40 to 160-m depth (not shown). EOF2 explains 19% of the variability and its loading spread to 16°N. The corresponding temporal pattern shows high frequency signal that may be an aliased MJO (Madden-Julian Oscillation) and year-to-year fluctuation. Nearly half of the variance of PC2 comes from the ENSO timescale.

The space-time structure of the tropical Indian Ocean shows ocean-atmosphere coupling structures. But, its modulation on tropical North Africa climate is not reflected in the east-west atmospheric circulation.

In all significant EOFs, the tropical Southern Indian Ocean reveals a strong loading. Xie et al. (2001) suggested that a unique open ocean upwelling exists in the tropical South Indian Ocean as a result of wind curl between the southeast trades and equatorial westerlies, raising the thermocline along 8°S. They showed ENSO to be the dominant forcing for this thermocline variability with SST variability off Sumatra, revealing the coupled Rossby wave potential in predicting SST and tropical cyclone activity in the southwestern Indian Ocean.

7.5 Space-time structure of tropical zonal wind stress

Variability in SST is affected by anomalous entrainment, variation of mixed layer depth, advection and diffusion processes and heat fluxes. Many of these processes are modulated by wind stress:

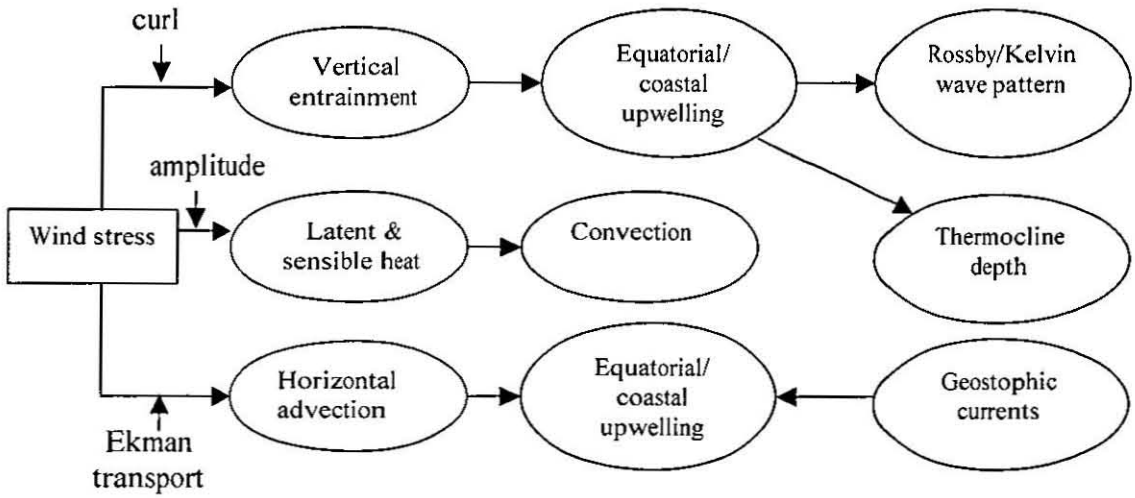

Influences of wind stress (adapted from Sutton et al, 2000).

Wind stress in ocean dynamics is vital in understanding in the processes shown above. Determination of the most dominant space-time structure of wind stress brings us quickly to understand ocean-climate linkage. Towards this goal the most dominant modes of space-time variability of zonal wind stress are identified using eigenvector analysis. The first two modes are discussed.

Tropical Atlantic Ocean zonal wind stress

The tropical Atlantic Ocean is dominated by trade winds as discussed in Chapter 4. The first mode of variability of zonal wind stress is loaded in both hemispheres sympathetically (Fig. 7.13a) and explains a quarter of variance. The score reveals high frequency signals (Fig. 7.14). The interannual variability embedded in the record accounts for 41% in the PC1, one-third in the PC2 (Fig. 7.20) and half of the variance in PC3 (Table 7.1). This mode is weakly connected with Atlantic HCA PC1 (r=0.403).

The EOF2 structure reveals zonal wind stress dipole known to exist in the tropical Atlantic SST as one of the most dominant modes of variability. The meridional subsurface temperature loading shows a dipole structure in the tropical Atlantic, negative in the south Atlantic (Fig. 7.13b). This dipole mode explains 17% of the variance of the zonal wind stress structure of the tropical Atlantic Ocean. The temporal component is not connected to any of the HCA principal components. But, the third temporal mode is tied to the second tropical Atlantic HCA (r=0.58) and equatorial Atlantic east-west subsurface temperature (PC2) with r=-0.61.

The EOF3 is a dipole structure between the equatorial Atlantic and tropical north Atlantic. This pattern is also shown in SST within the Atlantic Basin (Chang, 1997). The temporal variability of this structure reveals low-frequency variability. Despite that fact that modes of variability Atlantic SST and zonal wind stress share common structures in eigenvector domain, the temporal modes of both signals are unrelated to ENSO. The main modes of variability of tropical Atlantic zonal wind stress are unrelated to neither the east-west atmospheric circulation nor the Indo-Pacific ENSO mode at interannual timescale.

Tropical Indian Ocean zonal wind stress

The zonal wind stress of the tropical Indian Ocean passed through the singular value decomposition to unveil the principal mode of variability of zonal wind stress. Salient space-time modes of variability are identified from the first three modes. The EOF1 reveals a singular structure within equatorial region centred at the heart of the ocean (Fig. 7.15a). This mode explains 22% of the total variance (Table 7.1). Nearly half of the signal is interannual. The PC1 of tropical Indian Ocean (Fig. 7.16) is notably tied to Pacific SST at interannual variability (r =-0.69). This mode is also associated to east-west divergent circulations in Indian and Pacific Oceans. It is known that changes in zonal wind propagate slowly westward across the equatorial zone (Matitu, 2001) inducing Rossby waves and the IOD itself (Jury and Huang, 2002).

The leading mode of Indian Ocean zonal wind stress (Fig. 7.16) is sensitive to ocean coupling locally and remotely. It is coupled to the first leading time coefficient of the tropical Indian HCA EOF with 61% variance. It is related to north-south subsurface temperature of central Indian Ocean (r=0.56). It is also teleconnected to the leading temporal components of Pacific HCA and equatorial Pacific subsurface temperature with variance 49% and 40% in that order. Its interplay with Indo-Pacific SST is equally strong (r= -0.68). It is coupled to the local SST in the South Indian Ocean (r= -0.56) and northwest Indian Ocean SST (r= -0.49). But, the second and third temporal coefficients of Indian Ocean zonal wind stress are as active as the first component in the context of ocean-atmosphere coupling. All their scores reveal ENSO timescale from 2-4-year periods.

The annual mean winds (westerly), deep thermocline and the absence equatorial upwelling confine the effects of thermocline depth variability on SST (the Bjerknes feedback) to the area south of the equator.

The EOF2 of tropical Indian Ocean zonal wind stress picks the Southwest monsoon zonal circulation pattern with negative loading south of the equator and positive north of the equator (Fig. 7.15b). The leading spatial structure of the zonal wind stress in the Indian Ocean accounts for 13% of the total variance. The PC2 shows large swings and high frequency signals. Nearly one-third of the variance of the second leading temporal variability of the zonal wind stress is within the interannual band (Fig. 7.16).

Tropical Pacific Ocean zonal wind stress

The EOF analysis is applied to the zonal component of wind stress in the tropical Pacific Ocean to determine the space-time variability. 62% of the variance of PC1 comes from the interannual timescale variability (e.g. ENSO, Fig. 7.18). Its relation with Pacific SST is notably strong (r= -0.79) and with the east-west divergent circulation over the Atlantic (r= 0.51), Indian (r= 0.710) and Pacific Ocean (r=0.51). Locally, the temporal coefficient actively coupled to the ocean property and the amplitude of the coupling is the strongest of all oceans. Of this coupling, the first amplitudes of tropical Pacific HCA and zonal wind stress take the large variance (70%). ENSO mode is also associated to this zonal wind stress (r=-0.684). The interplay operates within the ENSO timescale in concurrent mode, without any delay response. The spatial loading shows a large loading but negative in central Pacific. A weak positive structure is shown in the east Pacific (Fig. 7.17a).

The second spatial mode shows positive loading over the central/west and negative loading on north and south tropical Pacific (Fig. 7.17b). Over east Pacific, a broad negative loading is shown, e.g. east-west dipole and north-south wave structure. This structure explains 7% of the variance and only 38% of the signal is interannual. PC2 is not linked locally or remotely to east-west circulations (Fig.7.18).

7. 6 Interplay between subsurface temperature and SST/circulation indices

To identify ocean-atmosphere coupling within the subsurface thermal variability of the equatorial oceans, a correlation analysis is used to relate the heat content, Indo-Pacific SST and convection over tropical North Africa.

Nino 3 SST is correlated to subsurface temperature in the equatorial oceans. The correlation structure shown in Fig. 7.19 reveals a dipole structure over Pacific and Indian Ocean (Fig. 7.19(b and c)). The Indo-Pacific SST and Atlantic temperature section do not show any common pattern that ties them together (Fig. 7.19a). Pacific SST is however related to equatorial Indian Ocean temperature, as a dipole mode (Fig. 7.19b).

Comparison with similar studies

Studies reveals that a considerable evidence of the relationship between negative phase of Southern Ocean Index and equatorial Atlantic warm events during 1980-2000 (Covey and Hastenrath, 1978; Hastenrath et al., 1987; Wolter, 1989; among others). Modelling experiments have established links between the intensity of the tropical Atlantic trades and the ENSO (Tourre et al., 1985; Carton and Huang, 1994; Delecluse et al., 1994). A significant coherence and phase relationship at 12-month lag for 3.5-year period is found between ENSO (Nino 3) and equatorial Atlantic SST mode suggesting that one-year after fully developed El Nino in the east Pacific, a warming of the equatorial Atlantic Ocean is identified (Tourre et al., 1999). The maximum SST anomalies occur in the Gulf of Guinea (Hisard, 1980). The event of 1982-1983 El Nino followed by Atlantic warm event of 1984 and 1987/88 are given as examples to support the 'delayed' link between ENSO and equatorial Atlantic SST mode. Works of Philander (1990), Tourre and White (1995), and Latif and Barnett (1995) confirm this result. The Atlantic response to Pacific ENSO signal is transmitted through the "Atmospheric bridge" (Lau and Nath, 1996). Tseng (1999) showed that the 1986-1987 ENSO event is transmitted to North America –North Atlantic sector in 1987-

1988 through a thermally induces Rossby wave train with a pattern resembling PNA (Pacific-North America) pattern. He further demonstrated that ENSO induced changes in the atmosphere circulation and altered the strength of the global Walker circulation.

The findings in chapter 5 and 6 amply demonstrate that ENSO is transmitted signal to tropical Africa through the Pacific Walker Circulation-Atlantic Zonal Circulation teleconnection. Sperber and Hameed (1993) identified a 3.6-year period in the northern tropical Atlantic SST and argued that it is one of the timescales the Pacific Walker Cell interacts with tropical Atlantic Zonal Circulation to modulate the track of Atlantic ITCZ. The results in Chapter 5 (Fig. 5.26) shows that Atlantic Zonal Circulation and equatorial Atlantic SST mode share a broader spectral energy from biennial-decadal and the SST leads the Atlantic Circulation during 1970-1980 when the Walker and Atlantic Circulation are in a state of equilibrium (ENSO mode is weak). During this period, the interaction between ocean-atmosphere in Atlantic attains its peak and equatorial Atlantic SST leads consistently Indo-Pacific SST by 10-month. And the kinematic modes of ENSO transmission are in a strong state during these periods.

7.7 Equatorial Pacific subsurface and Atlantic Zonal Circulation centres of convection polarity

The focus of this Section is thus on the interaction of upper-ocean temperature variability and the Atlantic Overturning (atmosphere) Circulation that determines the upper-level divergent flow dipole between tropical North Africa and South America.

The question is what is the structure of the equatorial ocean subsurface thermocline when the upper-level divergent dipole is strong, and how does this vary from season to season?

To find answers to these questions, a composite of thermocline structure is formed based on years when the velocity potential dipole on either side of the Atlantic is strong. Cross-spectral wavelet modulus is also employed to identify the connection between the Atlantic Zonal Circulation and the ocean thermocline variability in the equatorial latitudes.

The upper-layer temperature-depth composite over equatorial Pacific for boreal summer is given in Fig. 7.20a. This composite reveals a dipole in subsurface temperature between east and west equatorial Pacific Ocean. The positive core is > 2.0°C from 40 to 140-m depth between 130°W to 90°W. Over West Pacific, the negative core is from 160 to 80-m depth within 145°E -160°E.

In Section 6.2.1a, it is found that warming over the east Pacific generates anomalous Atlantic Circulation that results in subsidence over tropical North Africa and enhanced convection over South America. It is further confirmed here that the equatorial Pacific subsurface thermocline drives the centres of convection polarity between tropical North Africa and South America through the zonal overturning Circulation teleconnection between the Atlantic and Pacific regions. The structure shown in Fig. 7.20 is depicted at 6-month (January-March) signifying the stability of the dipole mode. Dipole modes of subsurface thermal fields are observed in equatorial basins of Atlantic dipole and Indian oceans revealing that the velocity potential variability of tropical North Africa- South America is determined by thermal polarity in the equatorial oceans (Fig. 7.20 (b and c)).

The equatorial east Pacific subsurface thermocline "see-saw" accounts for 53% (n =625 and degree of freedom ≈ 35) of variability of the upper-level component of Atlantic Zonal Circulation at interannual timescale. It is also true that the equatorial east Pacific Ocean subsurface thermocline signal is dominantly interannual, e.g. 76% of variance. Over equatorial Atlantic, on the other hand, the seasonal and annual cycle dominates the total variance.

7.8 Ocean teleconnection to SST and tropical Circulation

The first modes of HCA of tropical Oceans are used in establishing regional and global atmospheric connection in boreal summer. Global links of ocean-atmosphere coupled signals are found. These results are reported in this section.

Atlantic HCA leading principal component

The leading PC of HCA of Atlantic has a trend structure in tropics in association with global tropical SST. Strong phase-locked link is found in equatorial Indian Ocean and in Maritime Continent. Its teleconnection with 700-hPa zonal reveals an anti-phase structure in equatorial Atlantic/northern equatorial Africa and Pacific depicting the lower limbs of Atlantic Zonal Circulation and Walker Circulation (Fig. 7.21a). The link with these circulations is more evident in the longitude-height structure within the equator (10°S-10°N), where imprints of Atlantic Zonal Circulation and Pacific Walker Circulation are identified. The east-west tilt that connects Pacific-Indian Ocean winds in baroclinic mode suggests that these regions are tied to both surface Pacific and subsurface of Atlantic. The connection found offers signals that are coupled to upper atmospheric circulation (Fig. 7.21b). A similar pattern is depicted in angular momentum and east-west circulation teleconnection (Fig. 5.15).

Using the same approach, the PC1 of Indian Ocean HCA is teleconnected to global SST within tropics with the opposite sign shown in Fig. 6.17.

Pacific HCA leading principal component

A global spatial pattern of the association between Pacific HCA PC1 and SST shows the structure produced in the interplay between east-west divergent circulation and surface thermodynamics in Fig. 5.21. The correlation structure reveals ENSO signal in Pacific; opposite sign in the Atlantic Nino region and in phase with western Indian Ocean suggesting the principal HCA temporal

variability is a coupled mode that varies in ENSO timescale. Its link with 200-hPa zonal wind shows a twin cyclonic circulation signal in equatorial Pacific similar to Atlantic Zonal (Walker Circulation) preferred mode of teleconnection (Fig. 5.21c).

The principal notion that comes from subsurface HCA, SST and upper zonal circulation interplay is the east-west zonal circulation of Pacific Walker circulation and Atlantic Zonal Circulation are integral part of upper ocean teleconnection.

7.9 Cross-wavelet analysis of east-west circulations and leading modes of HCA / subsurface temperature anomaly

Atlantic HCA

Atlantic heat content anomaly (HCA) second leading mode and the Atlantic Zonal Circulation co-vary with time at interannual time scale (Fig. 7.22). The PC1 HCA leads the Atlantic Zonal Circulation in phase domain for the first thirty years of the record. They maintain near balance condition since the 1980s when observations were assimilated.

The PC1 of the tropical Pacific Ocean heat content is also co-analysed with Atlantic Zonal Circulation. The temporal evolution of the PC1 of Pacific HCA and east-west circulation in equatorial Atlantic vary in harmony (Fig. 7.23) particularly from 1970 to 1995. The cross-wavelet between Atlantic Zonal Circulation and Pacific PC1 HCA shows interannual timescale signal. The amplitude of the cross-spectrum is more pronounced from 1970 to 1990. In the 1950s and 1960s, the signal is very weak possibly due to reduced ocean observation then. The phase relationship between Atlantic PC1 HCA of Pacific Ocean shows almost a balanced state but lead incline towards the PC1 HCA.

Indian HCA

The first leading principal component of tropical Indian Ocean HCA that reveals a dipole structure in EOF space is co-plotted with the Walker Circulation from 1950 to 1999 (Fig. 7.24). The first twenty years show out-phase-relationship between the Walker Circulation and PC1 of HCA in tropical Indian Ocean. For the second two decades, the two timeseries are phase-locked. A cross-spectral reveals an ENSO as the timescale common spectral energy. The amplitude of the spectrum is strong from 1970 to 1990. The tropical Indian Ocean HCA leads the Walker Circulation in the first twenty years of the record. A near balanced state is attained since then.

The transverse Monsoon Circulation is co-spectrally linked to Indian Ocean HCA in ENSO timescale. The Indian transverse east-west circulation leads generally the leading amplitude of HCA of tropical Indian Ocean (Fig. 7.25).

Pacific HCA and subsurface temperature

The Walker Circulation and equatorial Pacific Ocean subsurface thermocline temperature are in a complete equilibrium as expected. The same result is obtained in the cross-spectral modulus between the leading PC of HCA of tropical Pacific Ocean and the Walker Circulation. But, due off-equatorial dynamics (Rossby wave), HCA leads the Walker Circulation in a coherent mode within the annual cycle range. The same co-spectral-time pattern is found in the relationship between this HCA and the Transverse Monsoon Circulation (Fig. 7.26). In the phase domain, transverse Monsoon Circulation leads. Identical energy-phase is found between this circulation and the main structure of the thermal field in equatorial Pacific.

7.10 Conclusion

Reasonable representation of tropical ocean data are used to characterise the space-time structures of heat content, east-west subsurface temperature and zonal wind stress anomalies in tropical oceans from 1950-1999 using SVD, correlation, composite and wavelet analyses.

Upper ocean heat content is a crucial indicator of the dynamic displacement of the thermocline and oceanic wave propagation (Huang and Shukla, 2002) and vital for ocean-atmospheric coupling. The principal modes of variability of the heat content anomaly, east-west/north-south subsurface temperature fluctuation and zonal wind stress in the tropical oceans are identified. Key connection between velocity potential dipole, Atlantic Zonal Circulation, and the east-west subsurface thermocline temperature sea-saw is found. The cross-wavelet analysis and phase relationship highlight the co-variations between the HCA (heat content anomaly) / east-west equatorial subsurface temperature/zonal wind stress and east-west divergent atmospheric circulations.

The upper-ocean thermal structure and zonal wind stress in the Pacific Ocean are the most important in revealing the ocean-atmosphere coupling operating in ENSO timescale. It is this connection that permits these modes to be teleconnected to east-west circulations over the Atlantic and North Africa climate. The interannual amplitudes of the first modes of HCA and zonal wind stress in Pacific and Indian Ocean oscillate with time in harmony (Fig. 7.27 and Fig. 7.28 lower panels). This in phase relationship is captured in time and wavelet domains. Coherent time varying phase differences are depicted between HCA and zonal wind stress in these basins. The HCA and zonal wind stress are in the neighbourhood of concurrent state. In the Indian Ocean, the zonal wind stress leads coherently the HCA (Fig. 7.28 in the lower panel). The temporal pattern and time delay curve for the leading coefficients of HCA and the zonal wind stress in tropical Atlantic are not as consistent (Fig. 7.28 upper panels).

The ENSO timescale accounts for 85% of temporal variability of HCA in the tropical Pacific Ocean. This mode is connected to the leading mode of zonal wind stress. The Pacific Walker Circulation is also notably coupled to this HCA mode. Nearly half of the variance of Walker Circulation comes from the leading mode of Pacific HCA. Atlantic Zonal Circulation is tied to the HCA of tropical Pacific Ocean. One-third of the variance of the Atlantic Circulation is associated with the leading temporal variation of tropical Pacific HCA. The sea-saw in subsurface temperature in the equatorial Pacific is notably associated to ENSO mode of variability and extends to the large-scale east-west circulation. More than 60% of the swing of the Pacific Walker Circulation and a quarter of the Atlantic Zonal Circulation fluctuation are due to the subsurface temperature dipole of equatorial Pacific. The velocity potential dipole between tropical North Africa and South America is associated with this subsurface thermocline oscillation. Perturbation in space and time induced by ocean Rossby waves (White, 2000) reflect onto the velocity potential dipole that influences the climate variability of tropical North Africa. It may be the slower interannual scales that operate around the lowlands of Africa in boreal summer, whereas the faster interannual scales of austral summer impact the highlands of Africa. The ocean-atmosphere coupling and its teleconnections to tropical North Africa are schematically presented in Fig. 7.29.

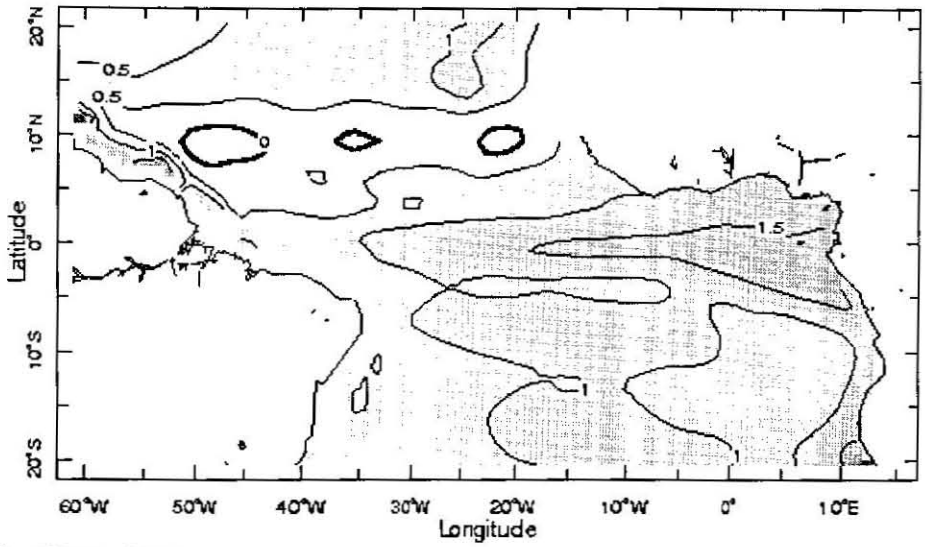

a) EOF1 of HCA

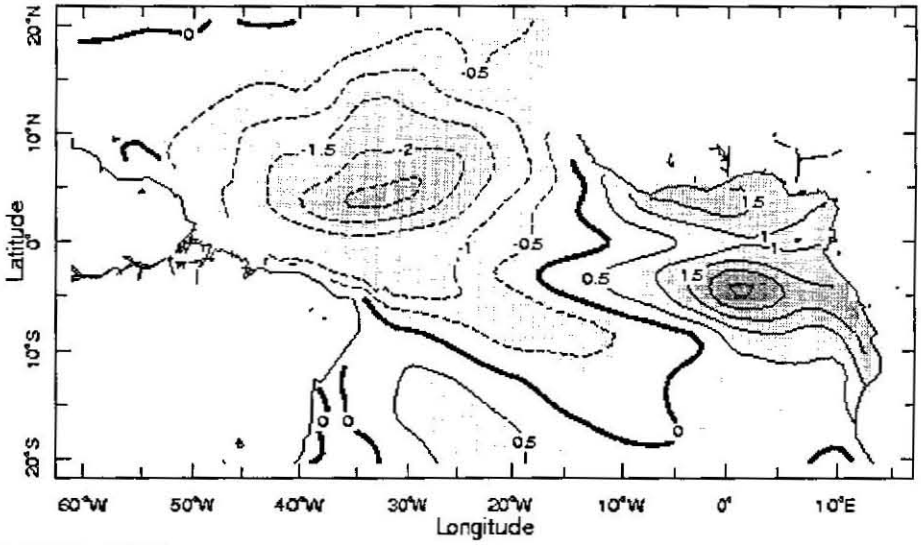

b) EOF2 of HCA

Fig. 7.1 The first two EOFs of Atlantic vertically integrated (for the first 125-m depth) HCA.

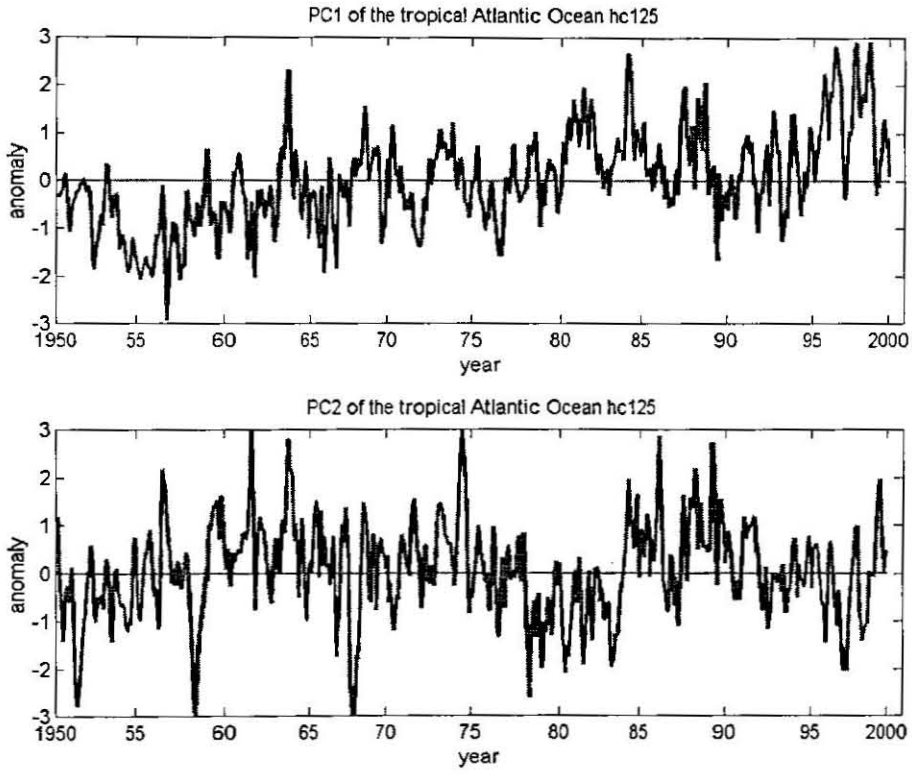

Fig. 7.2 Time coefficients of SVD of Atlantic vertically integrated (for the first 125-m depth) HCA.

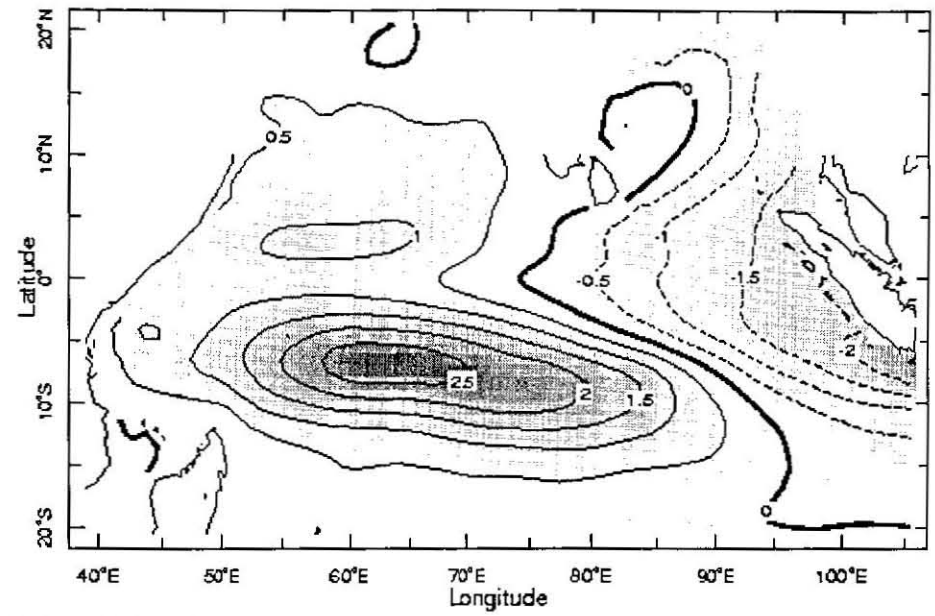

a) EOF1 of HCA

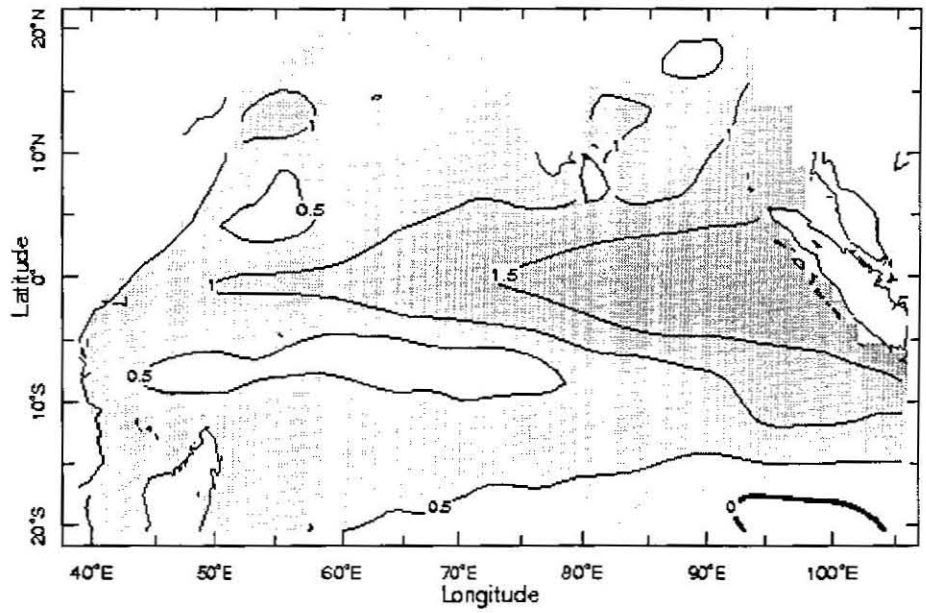

b) EOF2 of HCA

Fig. 7.3 The first two EOFs of Indian Ocean vertically integrated (for the first 125-m depth) HCA.

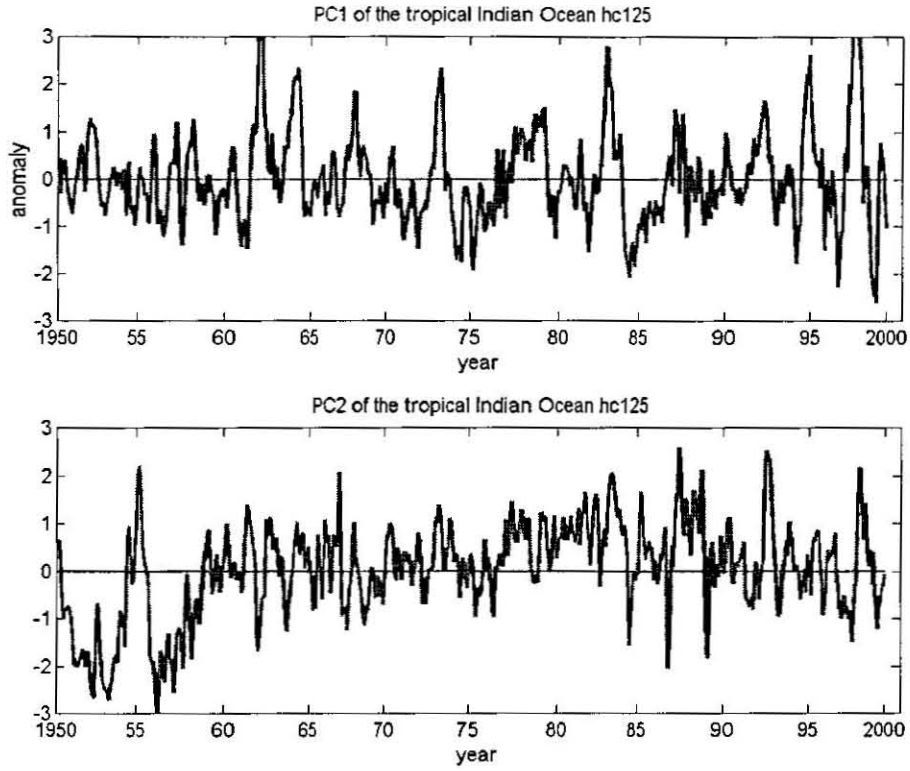

Fig. 7.4 Time coefficients of SVD of Indian Ocean vertically integrated (for the first 125-m depth) HCA.

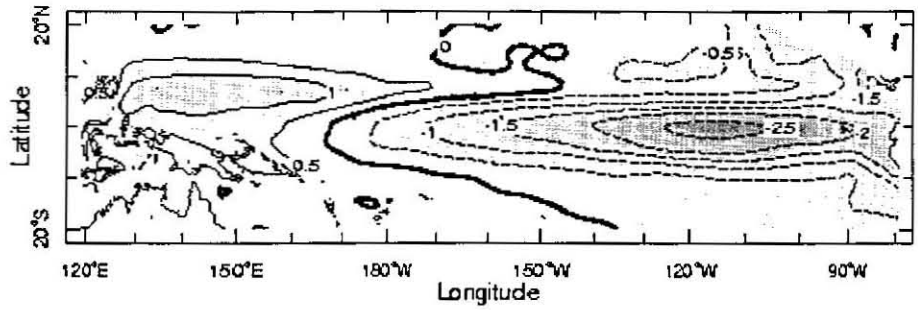

a) EOF1 of HCA

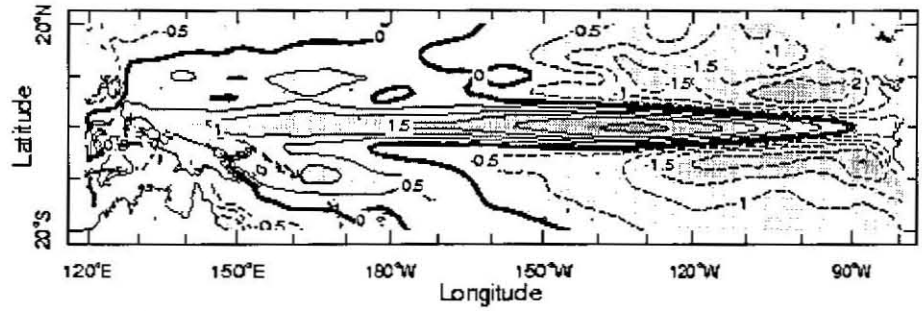

b) EOF2 of HCA

Fig. 7.5 The first two EOFs of Pacific Ocean vertically integrated (for the first 125-m depth) HCA.

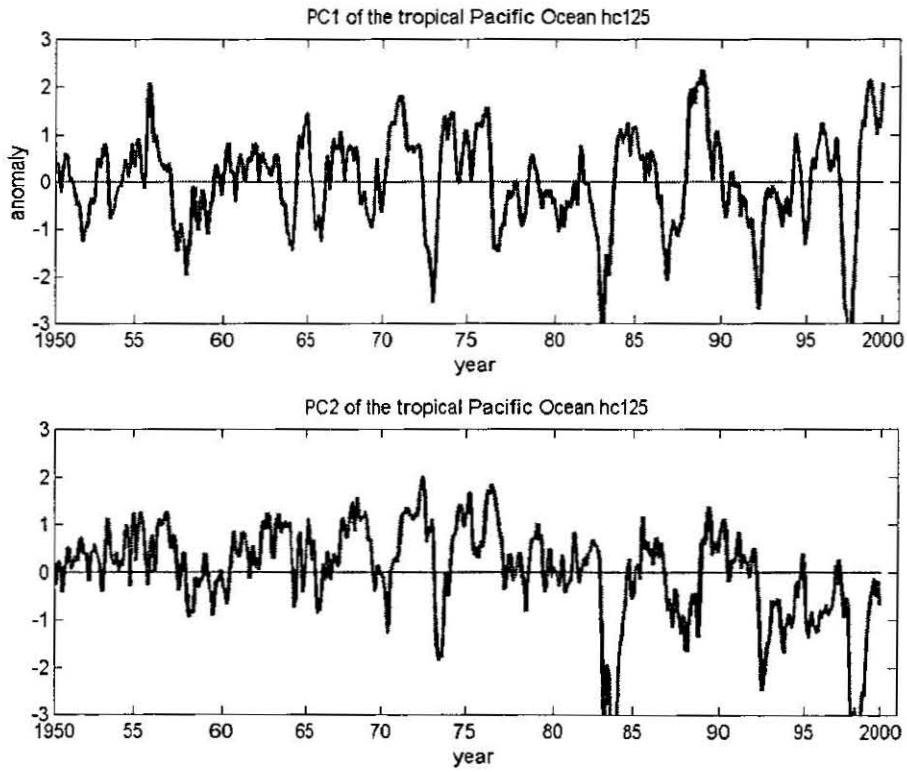

Fig. 7.6 Time coefficients of SVD of Pacific Ocean vertically integrated (for the first 125-m depth) HCA.

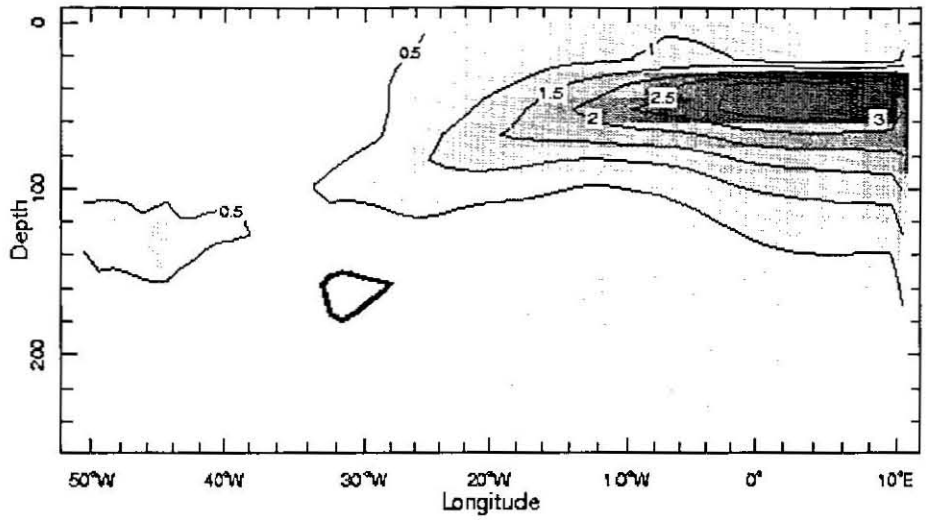

a) EOF1 of subsurface thermal field

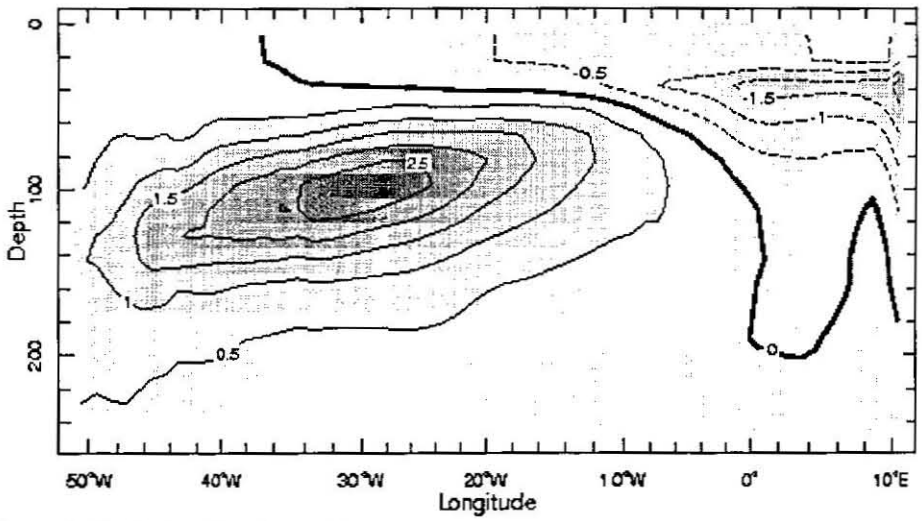

b) EOF2 of subsurface thermal field

Fig. 7.7 The first two EOFs of equatorial Atlantic east-west subsurface temperature.

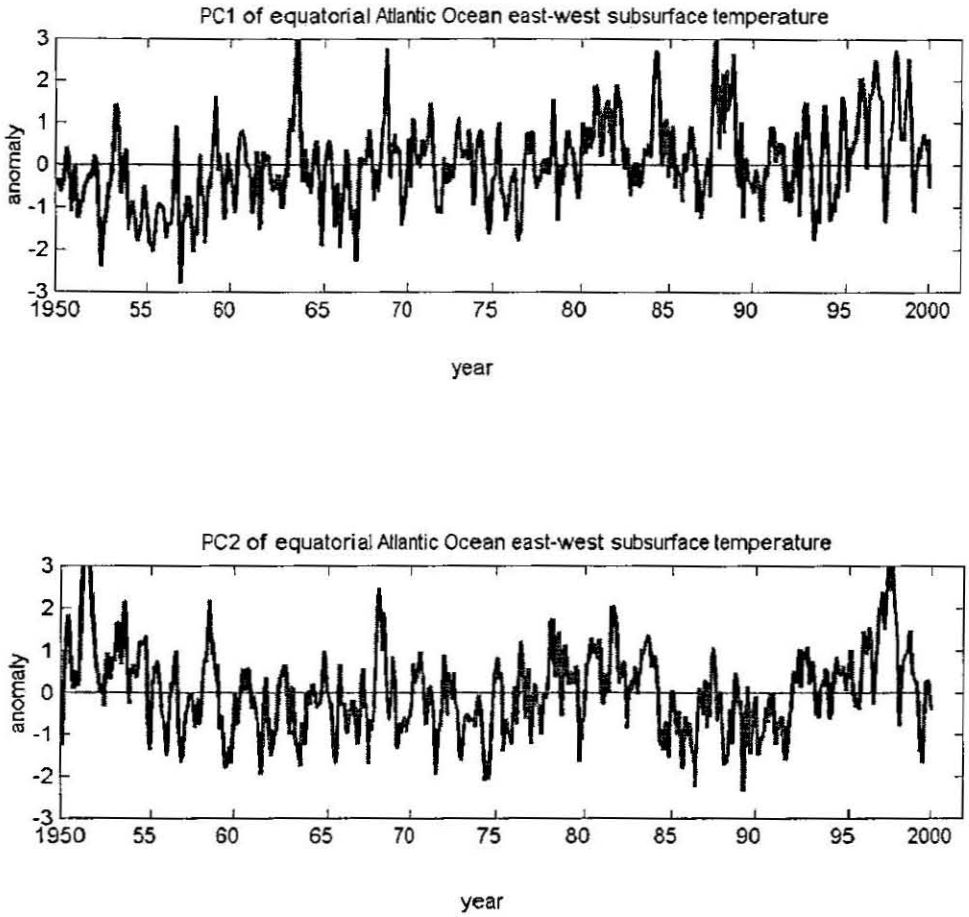

Fig. 7.8 Time coefficients of SVD of equatorial Atlantic subsurface temperature.

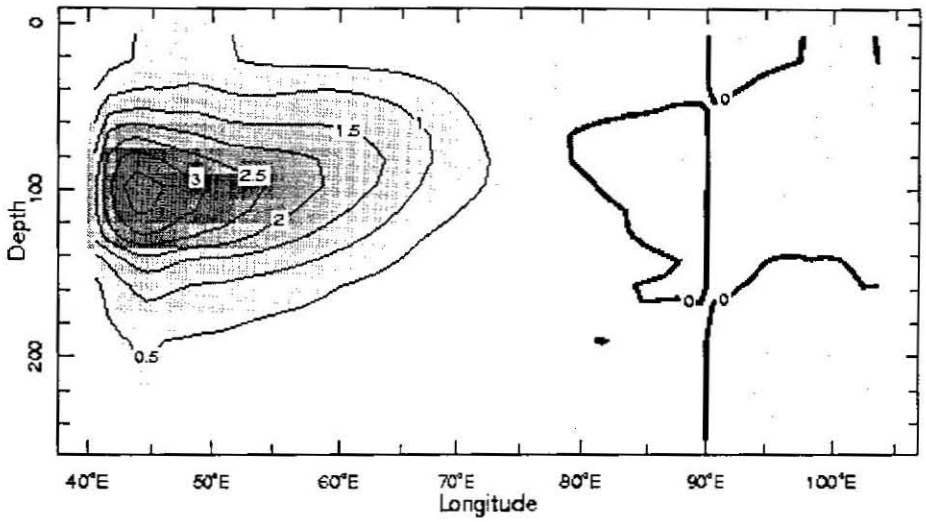

a) EOF1 of subsurface thermal field

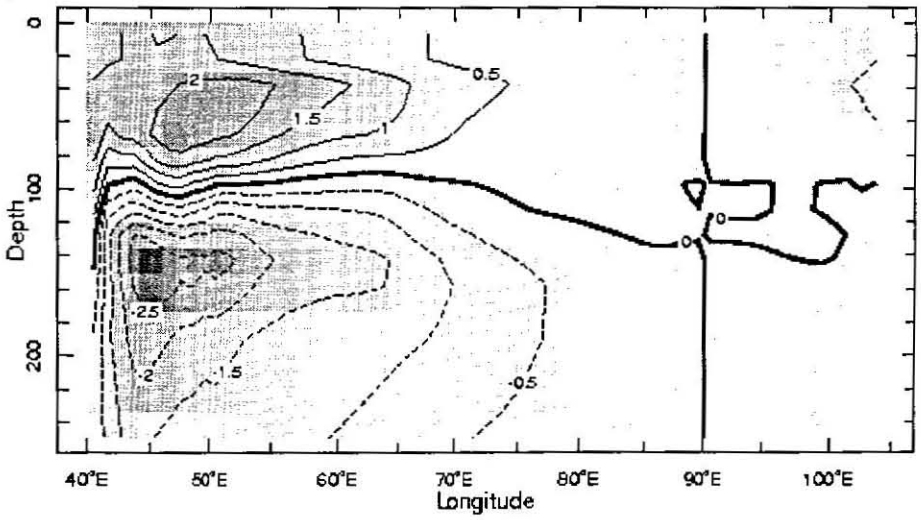

b) EOF2 of subsurface thermal field

Fig. 7.9 The first two EOFs of equatorial Indian east-west subsurface temperature.

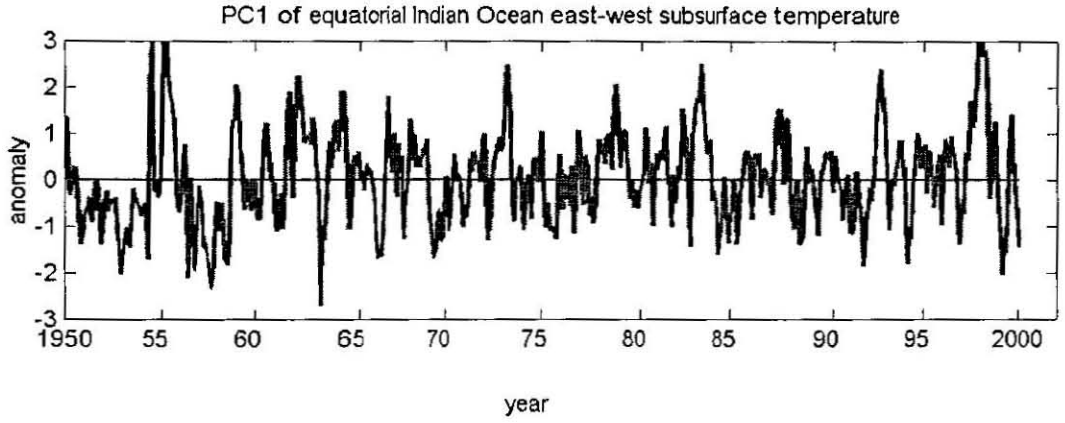

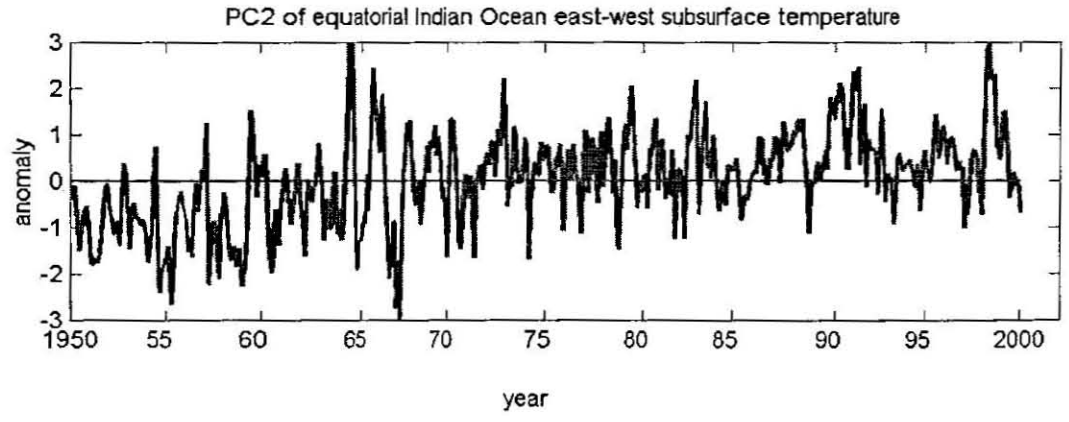

Fig. 7.10 Time coefficients of SVD of equatorial Indian subsurface temperature

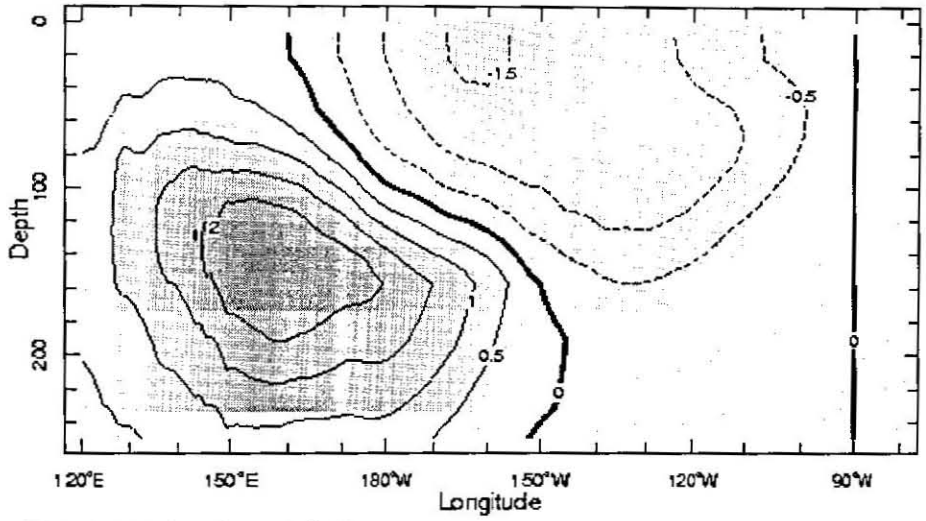

a) EOF1 of subsurface thermal field

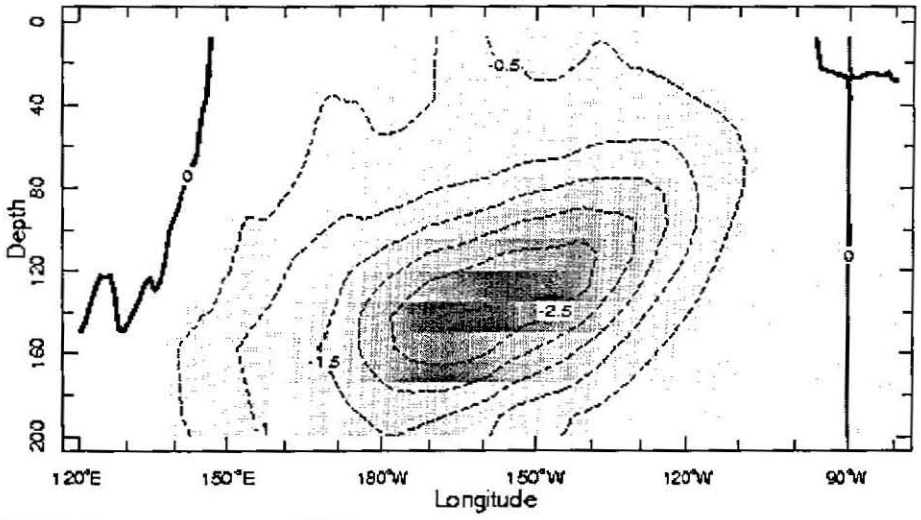

b) EOF2 of subsurface thermal field

Fig. 7.11 The first two EOFs of equatorial Pacific east-west subsurface temperature.

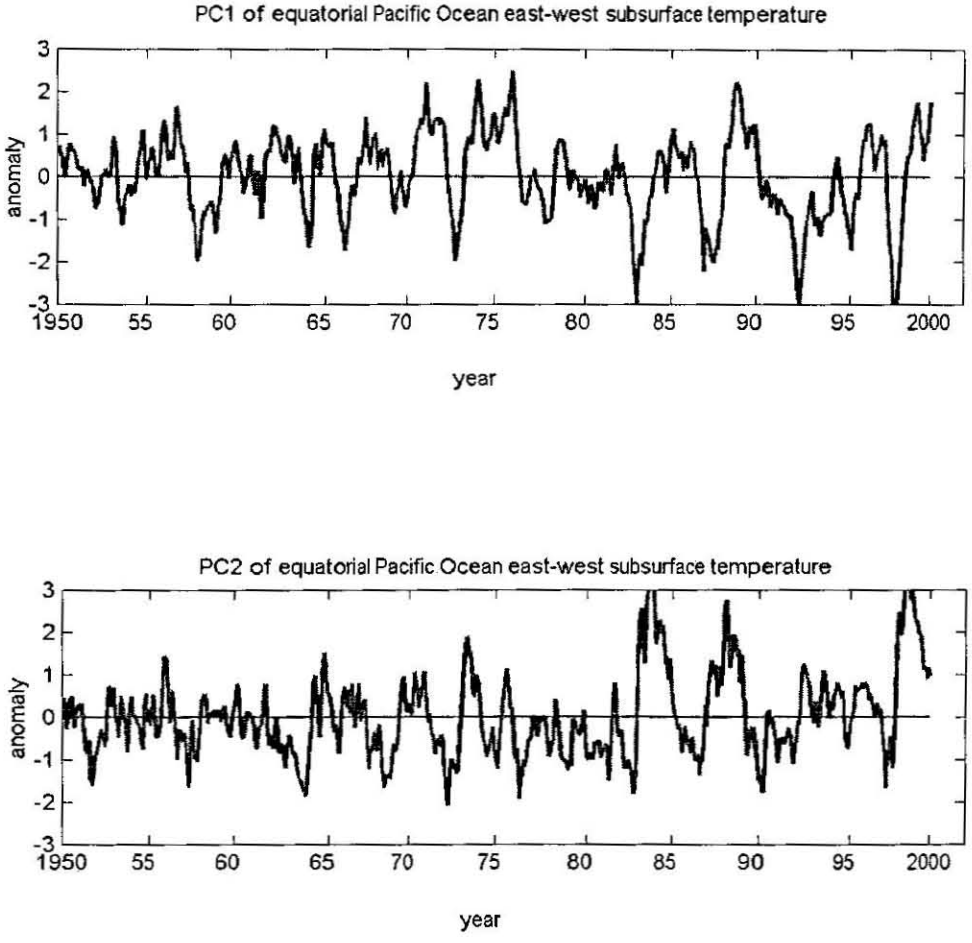

Fig. 7.12 Time coefficients of SVD of equatorial Pacific subsurface temperature

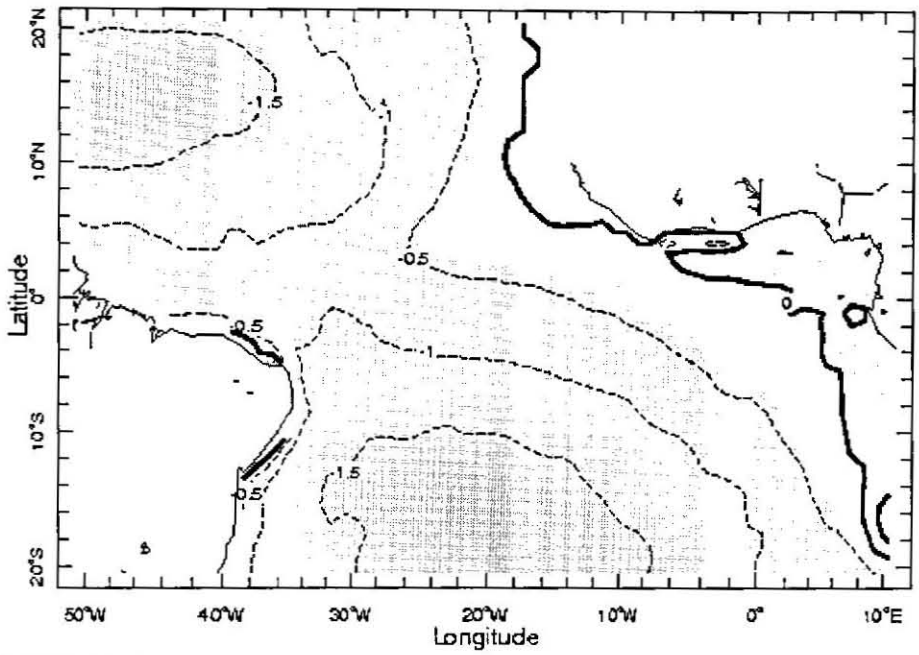

a) EOF1 Atlantic zonal wind stress.

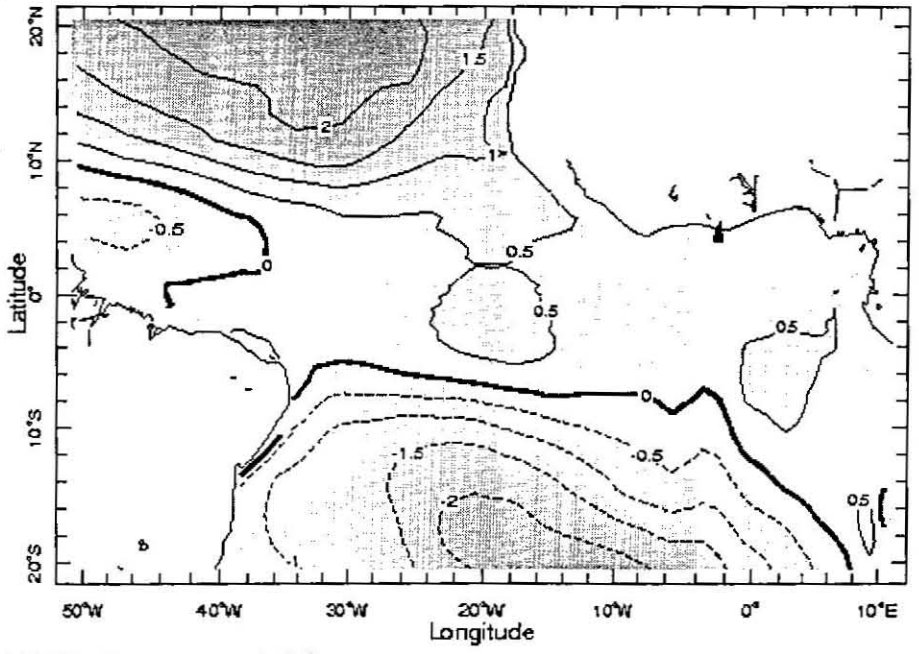

b) EOF2 of Atlantic zonal wind stress.

Fig. 7.13 The first two leading EOFs of zonal wind stress in tropical Atlantic Ocean.

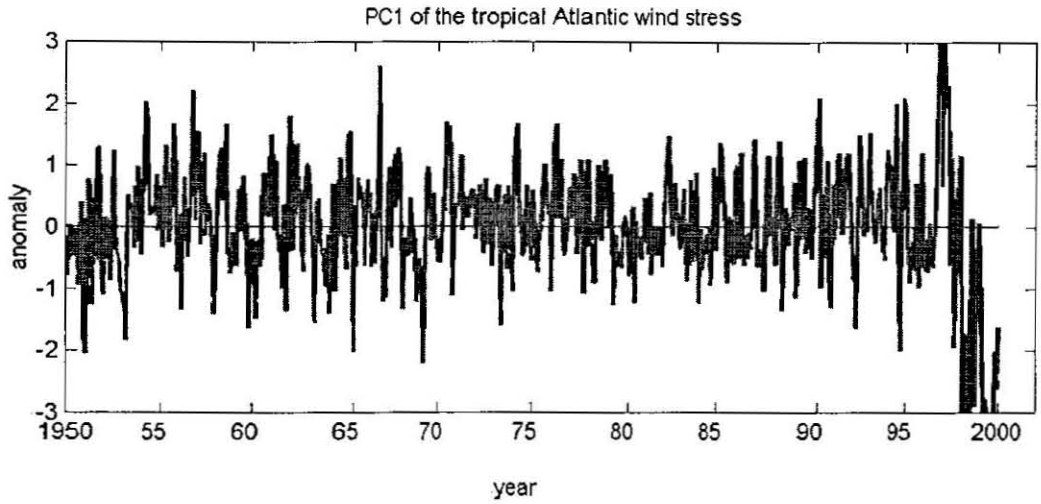

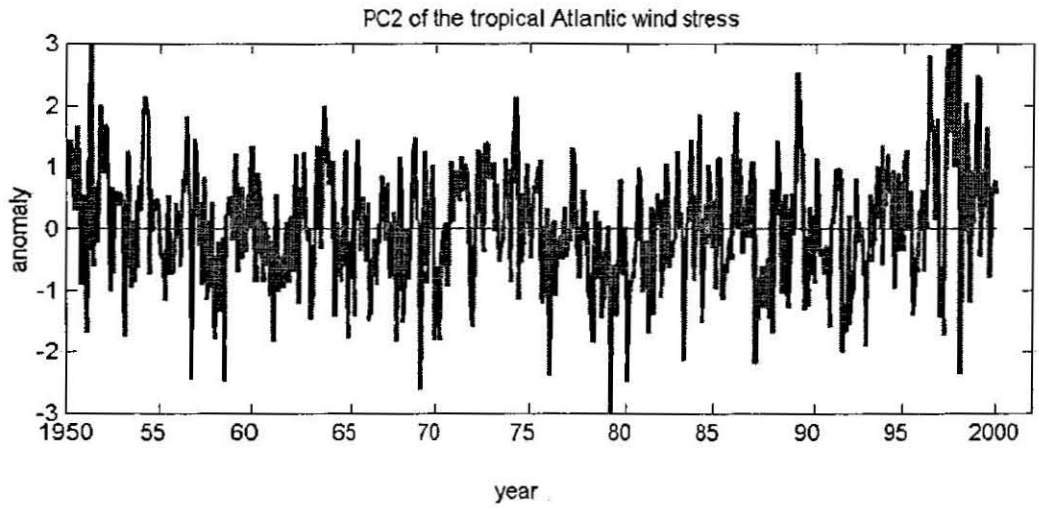

Fig. 7.14 The first two leading PCs of zonal wind stress in tropical Atlantic Ocean. The amplitude of abrupt decline trend shown in the leading mode of zonal wind stress seems doubtful.

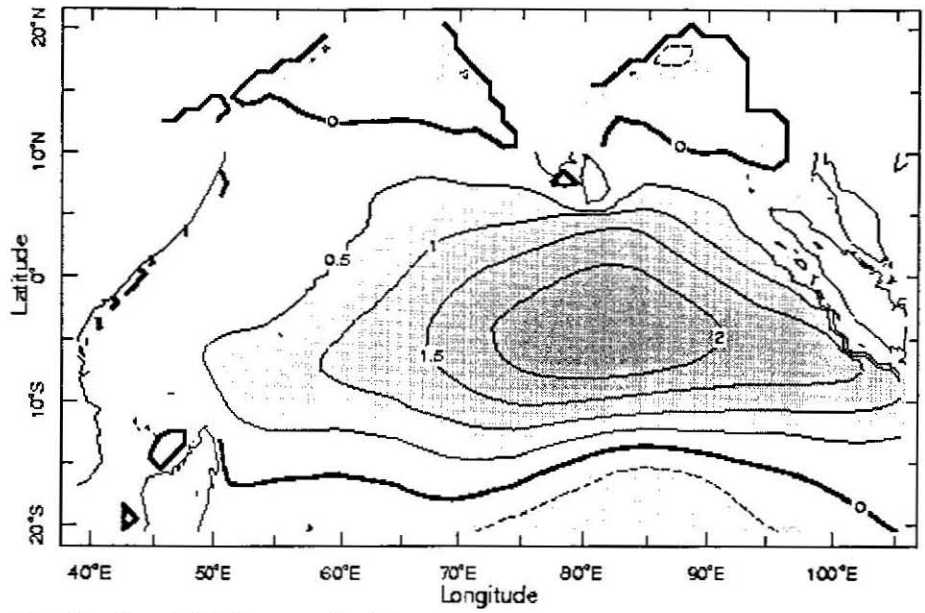

a) EOF1 of tropical Indian zonal wind stress.

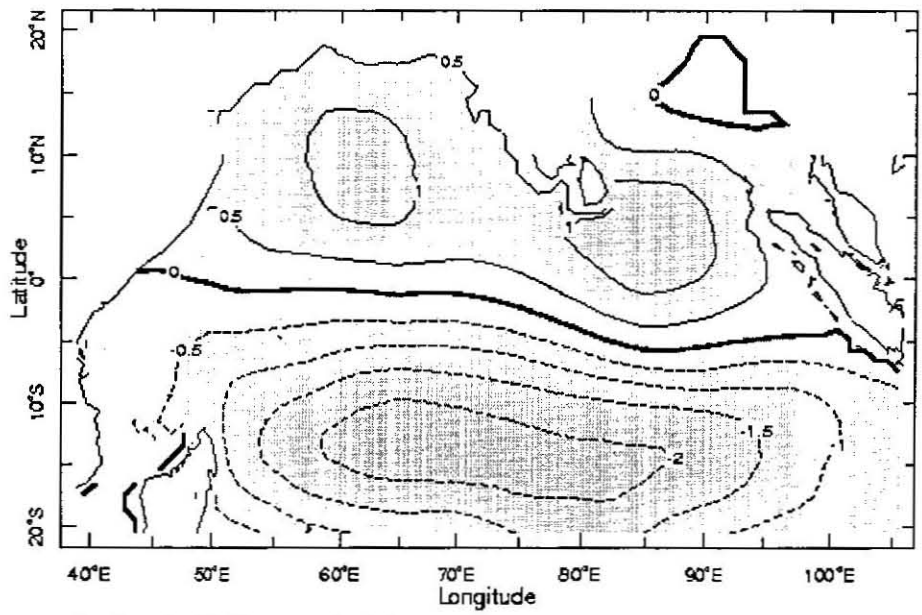

b) EOF2 of tropical Indian zonal wind stress.

Fig. 7.15 The first two leading EOFs of zonal wind stress in tropical Indian Ocean.

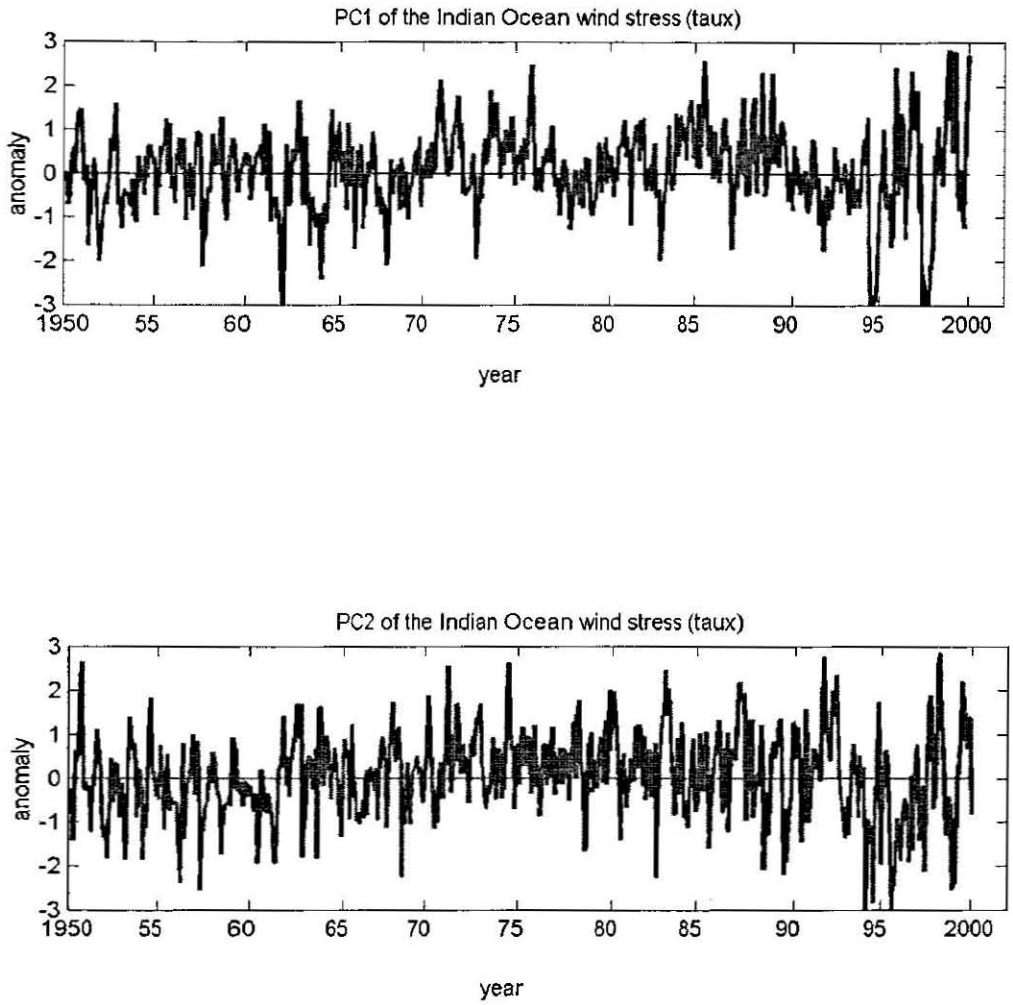

Fig. 7.16 The first two leading PCs of zonal wind stress in tropical Indian Ocean.

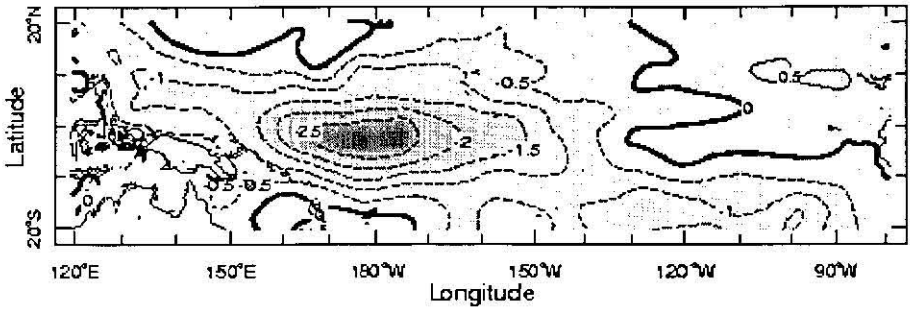

a) EOF1 of zonal wind stress in tropical Pacific.

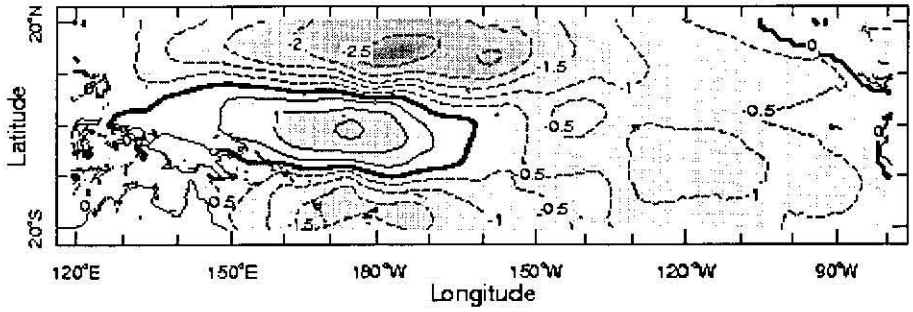

a) EOF2 of zonal wind stress in tropical Pacific.

Fig. 7.17 The first two leading EOFs of zonal wind stress in tropical Pacific Ocean.

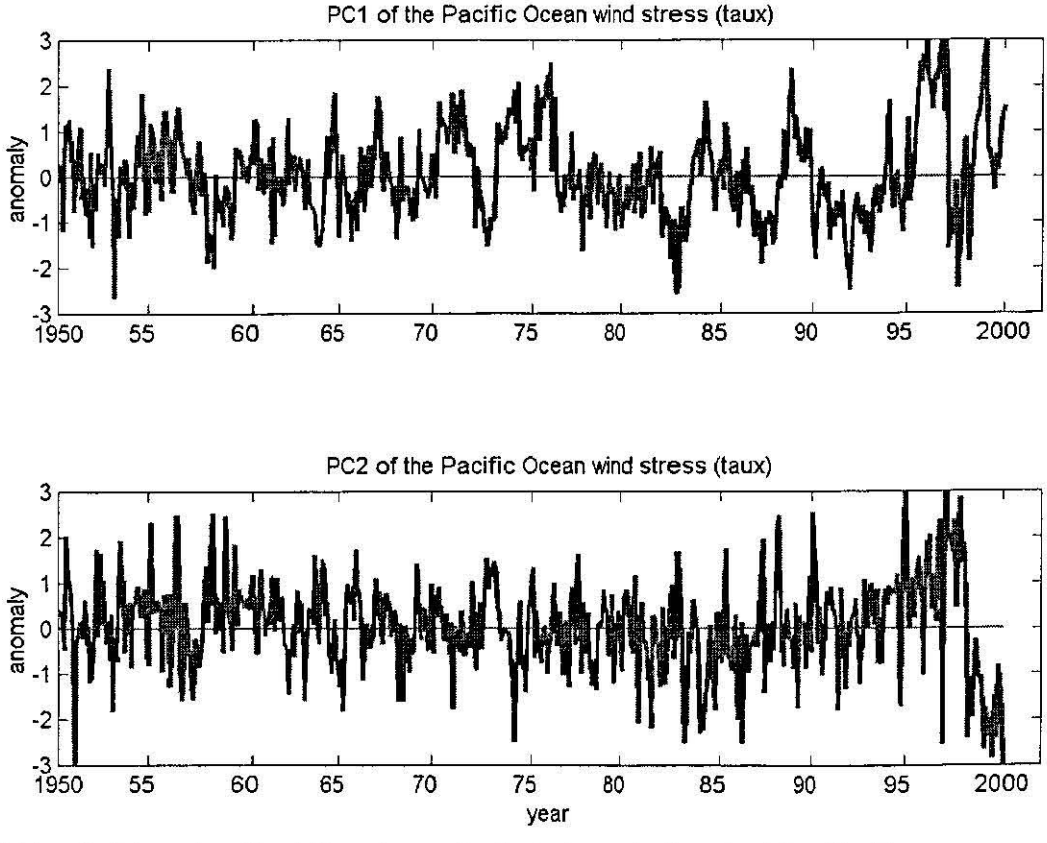

Fig. 7.18 The first two leading PCs of zonal wind stress in tropical Pacific Ocean.

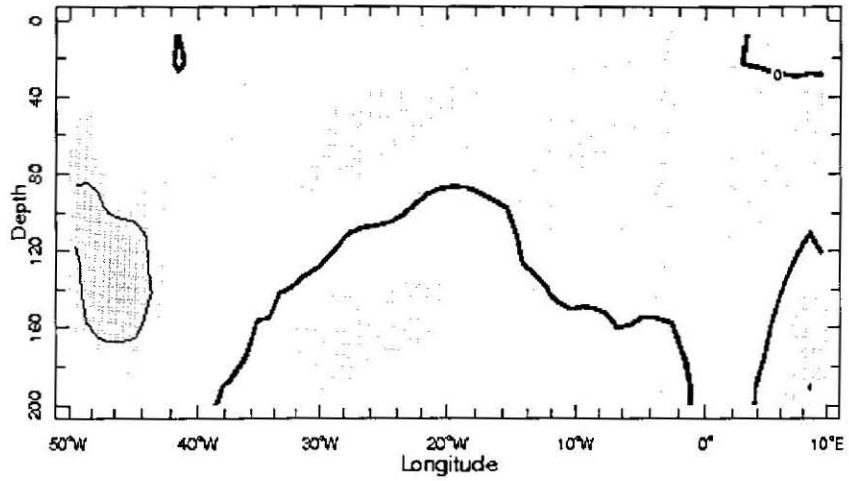

a) Equatorial Atlantic Ocean subsurface temperature ties with Nino 3 SST.

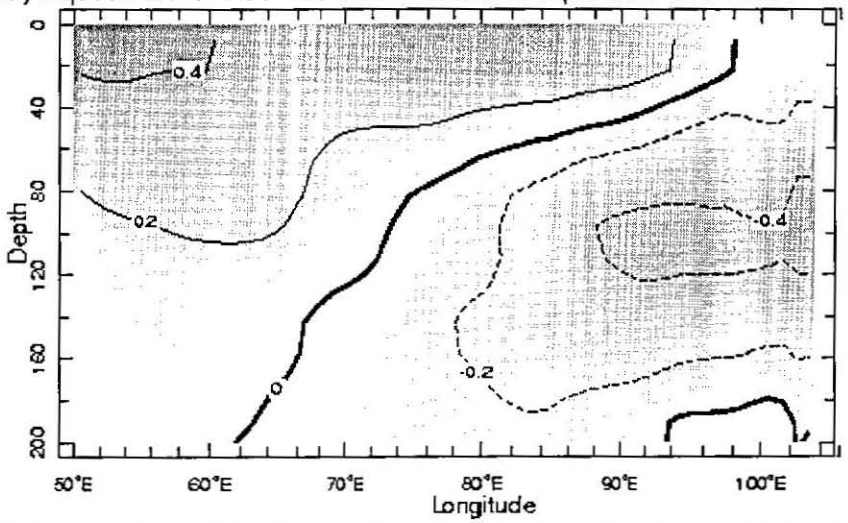

b) Equatorial Indian Ocean subsurface temperature ties with Nino 3 SST.

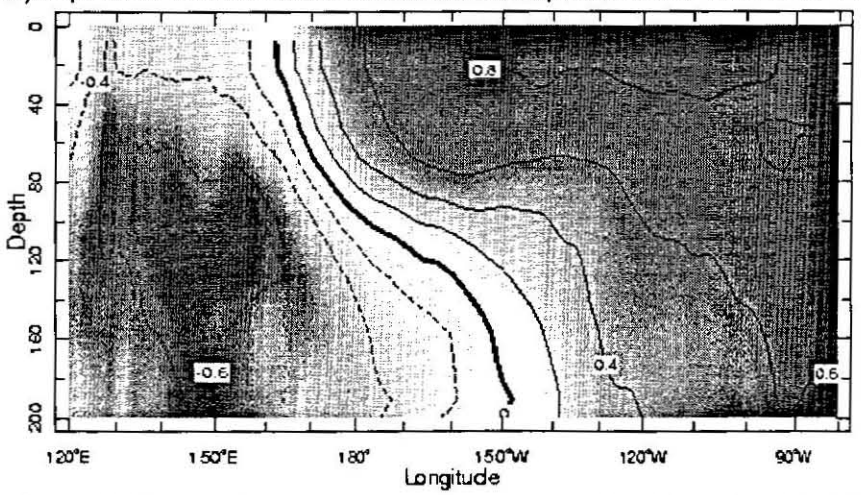

c) Equatorial Pacific Ocean subsurface temperature ties with Nino 3 SST.

Fig. 7.19 Links between Nino 3 SST and equatorial Ocean subsurface temperature.

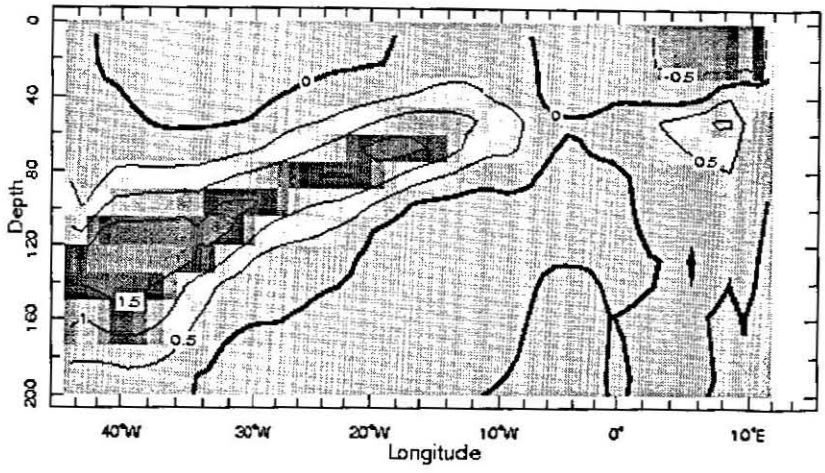

a) Equatorial Atlantic subsurface temperature composite.

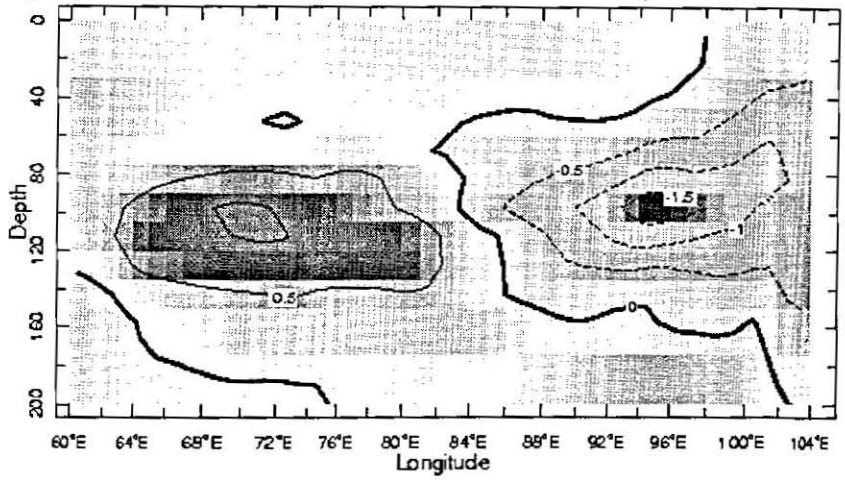

b) Indian Ocean subsurface temperature composite

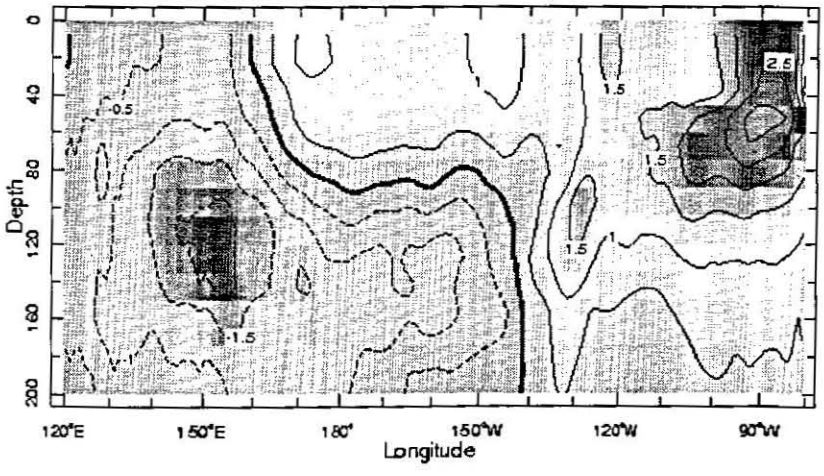

c) Equatorial Pacific subsurface temperature composites.

Fig. 7.20 Atlantic velocity potential velocity composites (Northeast Africa (+) minus South America (-)) show east-west equatorial oceans subsurface thermal oscillation.

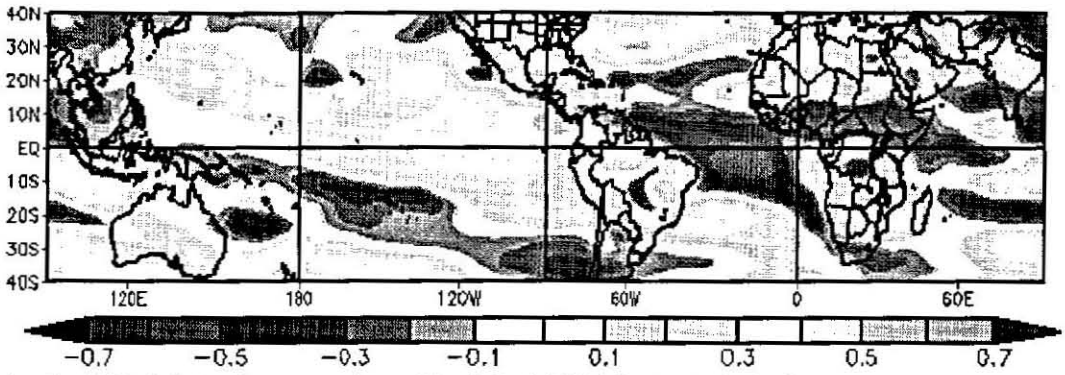

a) Atlantic HCA PC1 teleconnection with global 700-hPa zonal wind

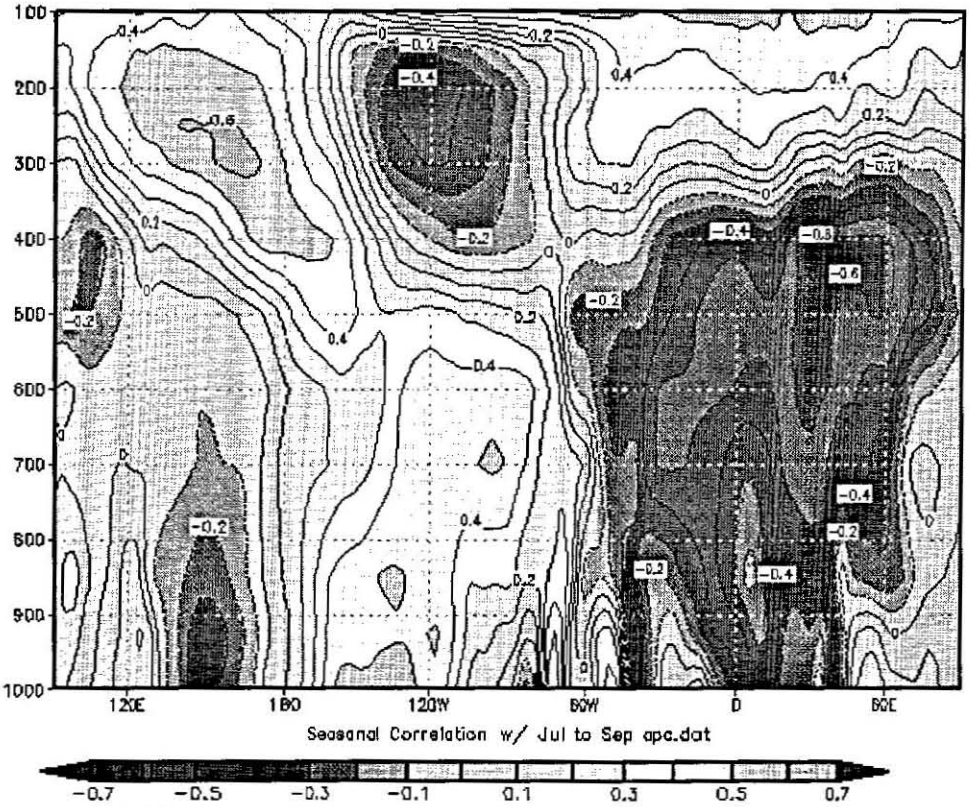

b) Atlantic HCA PC1 connection to longitude-height equatorial zonal wind cross-section (averaged from 10°S to 10°N).

Fig. 7.21 Tropical Atlantic HCA PC1 teleconnection east-west circulations.

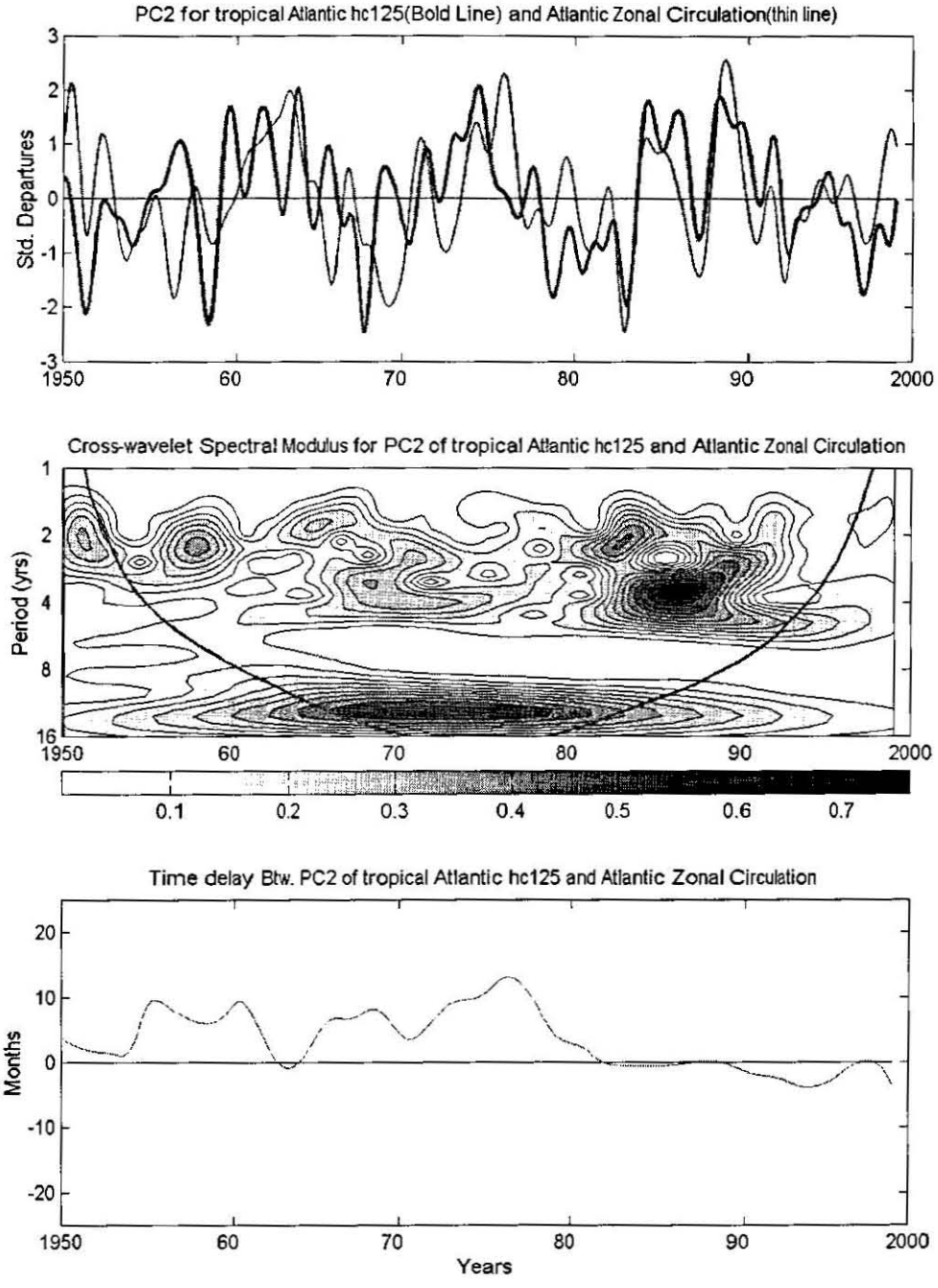

Fig. 7.22 Temporal evolution of co-spectral power and time delay between tropical Atlantic HCA PC2 and Atlantic Zonal Circulation.

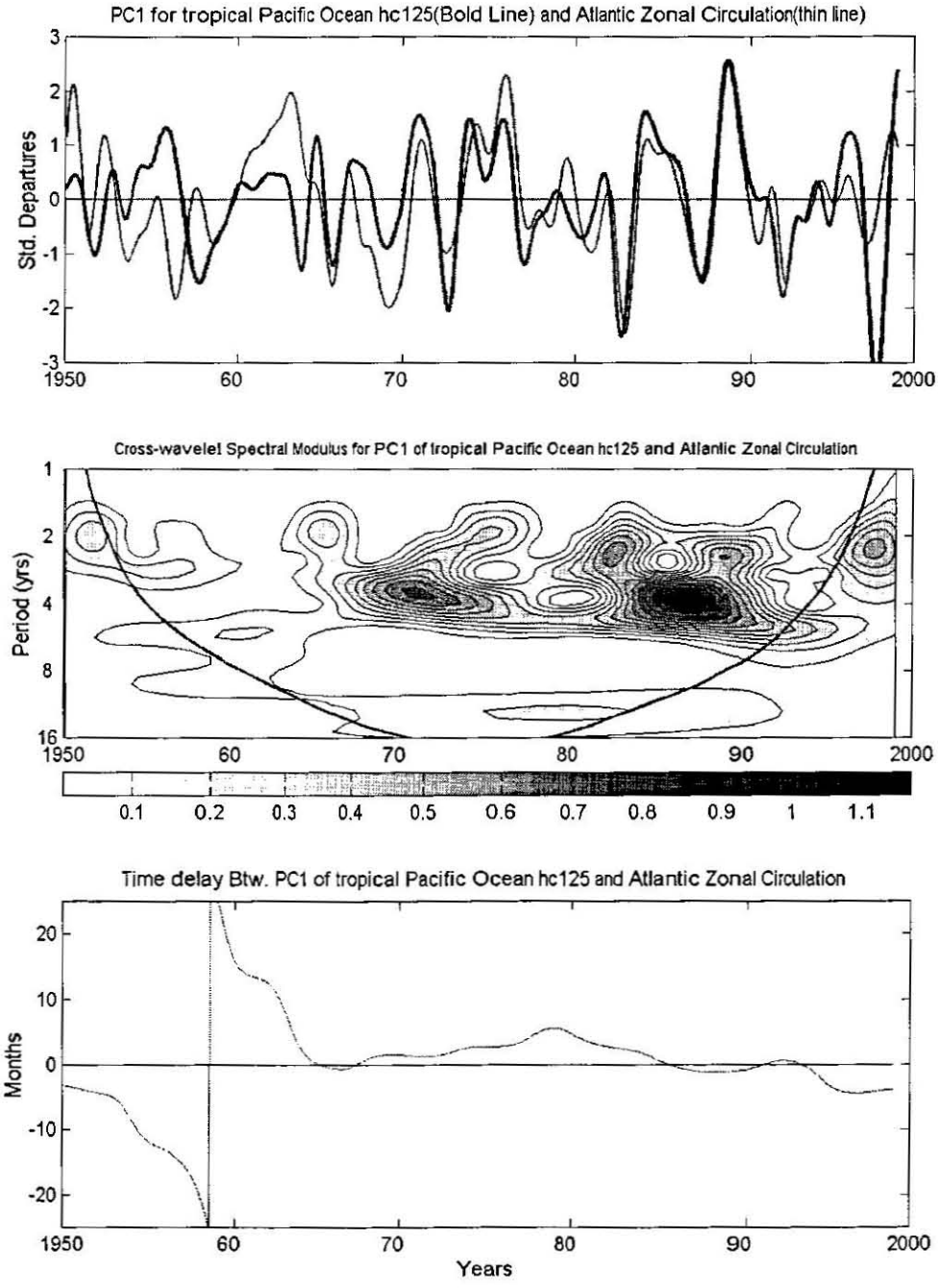

Fig. 7.23 Temporal evolution of co-spectral power and time delay between tropical Pacific Ocean PC1 HCA and Atlantic Zonal Circulation.

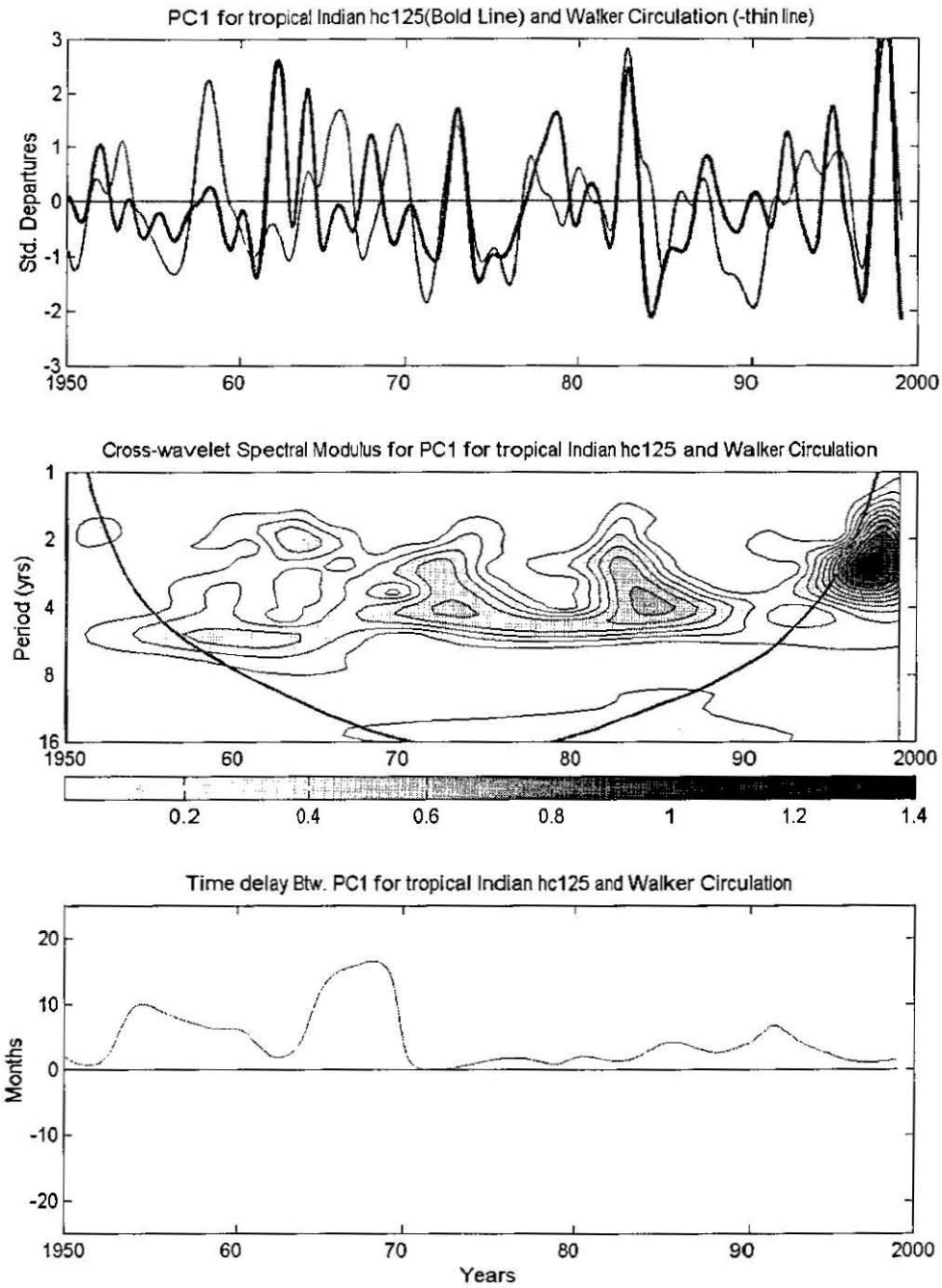

Fig. 7.24 Temporal evolution of co-spectral power and time delay between tropical Indian Ocean PC1 HCA and Pacific Walker Circulation.

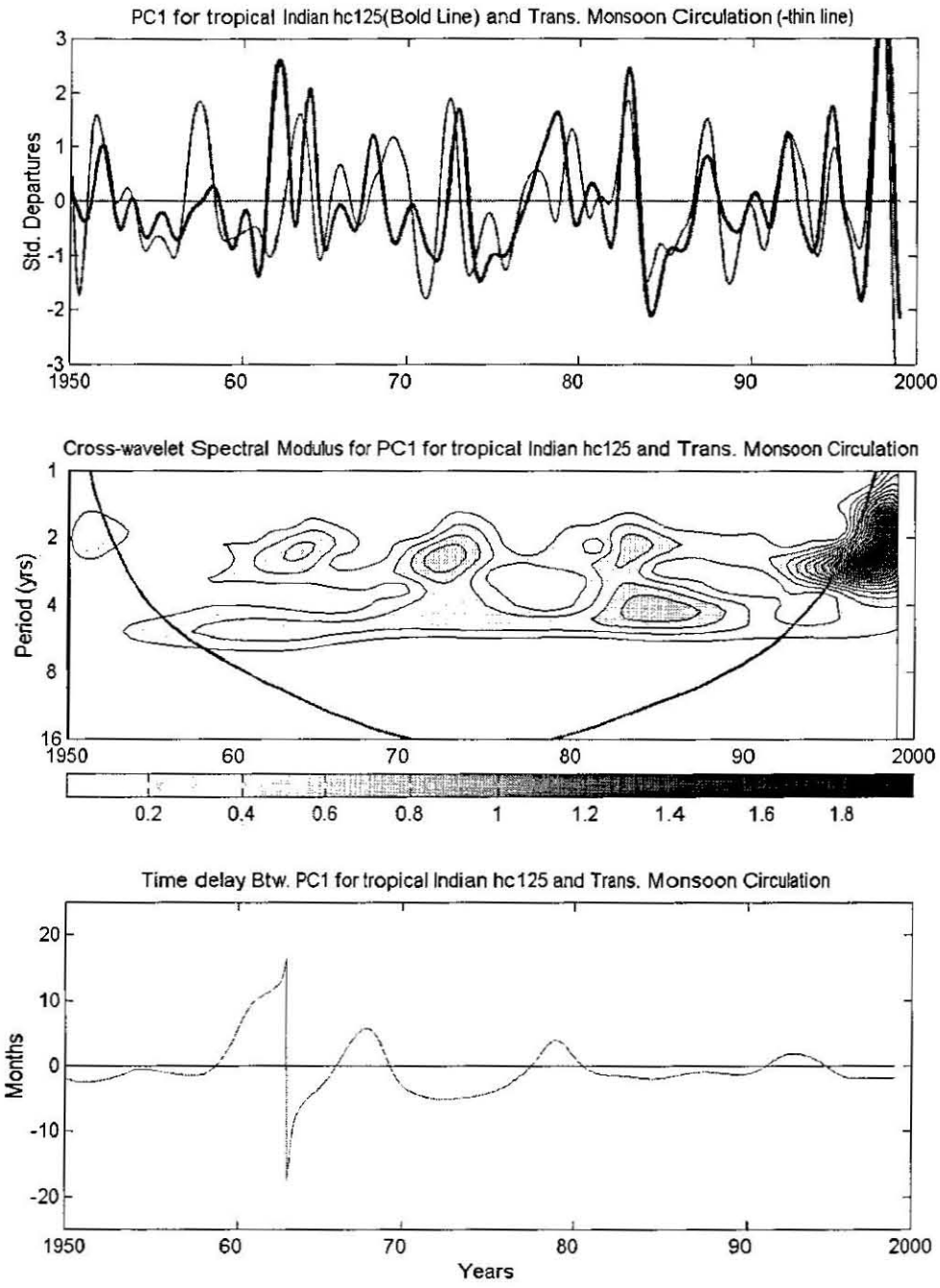

Fig. 7.25 Temporal evolution of co-spectral power and time delay between tropical Indian Ocean PC1 HCA and transverse Monsoon Circulation.

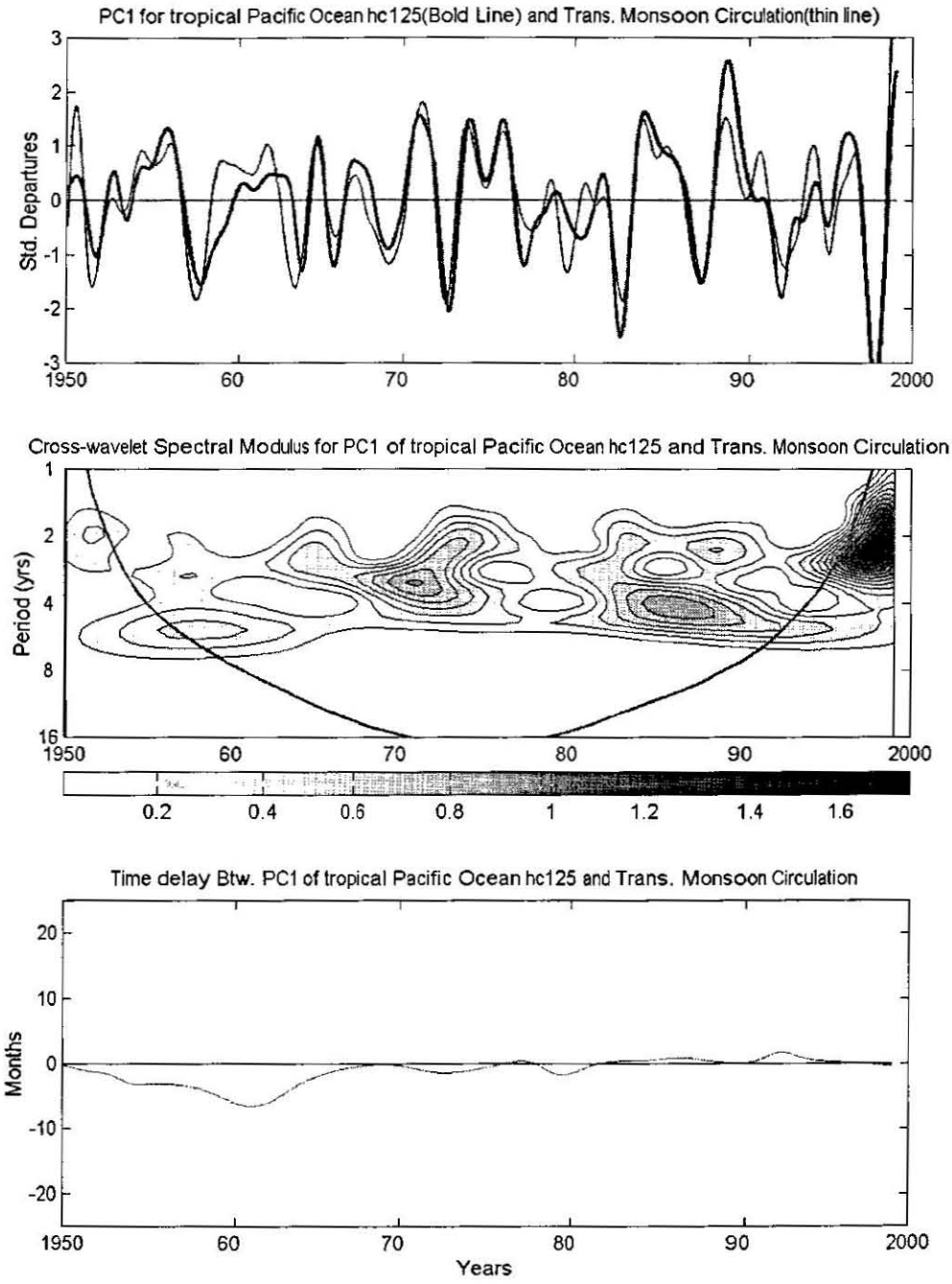

Fig. 7.26 Temporal evolution of co-spectral power and time delay between tropical Pacific Ocean PC1 HCA and transverse Monsoon Circulation.

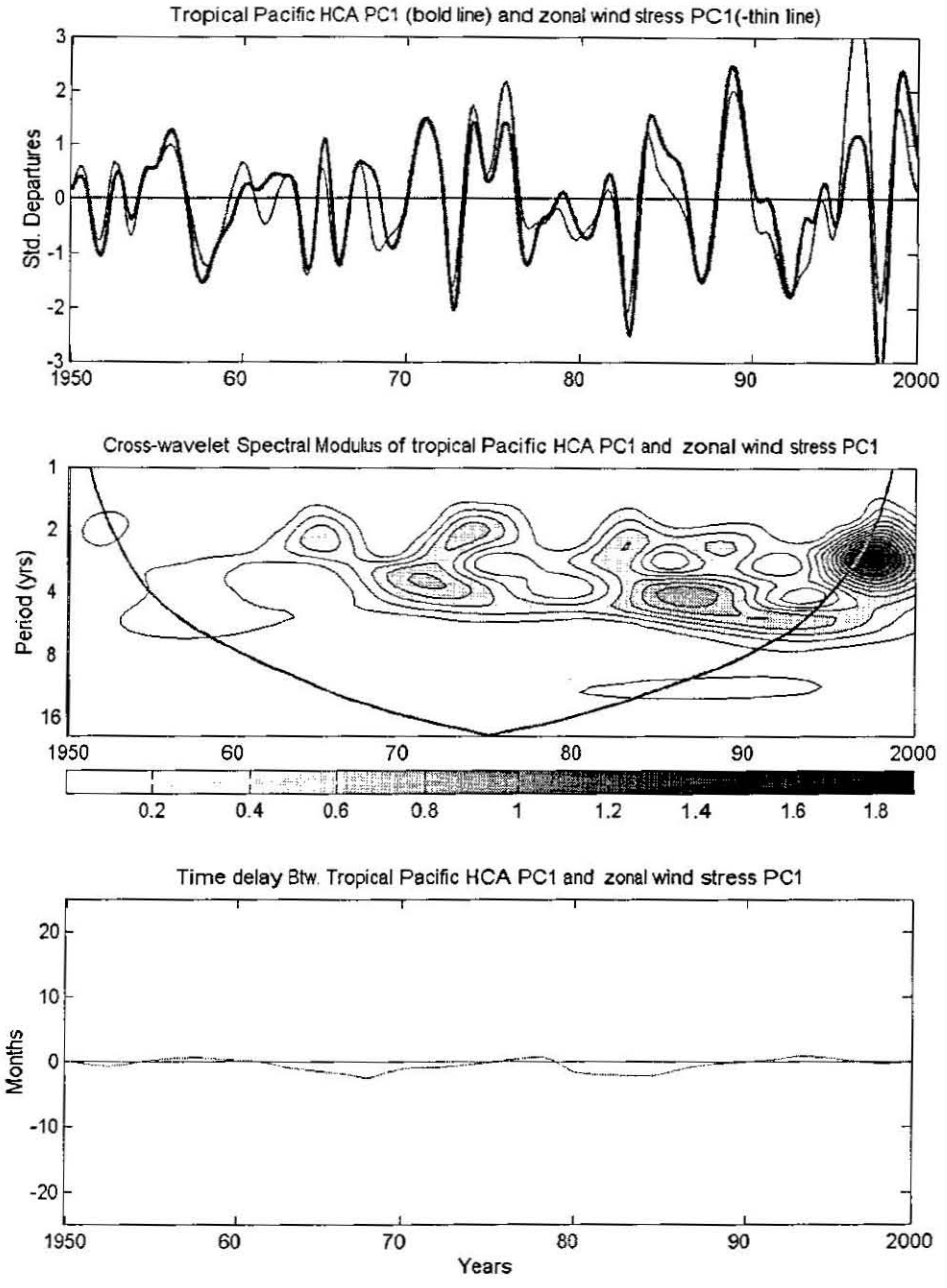

Fig. 7.27 Time varying cross-wavelet variants of leading HCA and zonal wind stress in tropical Pacific Ocean.

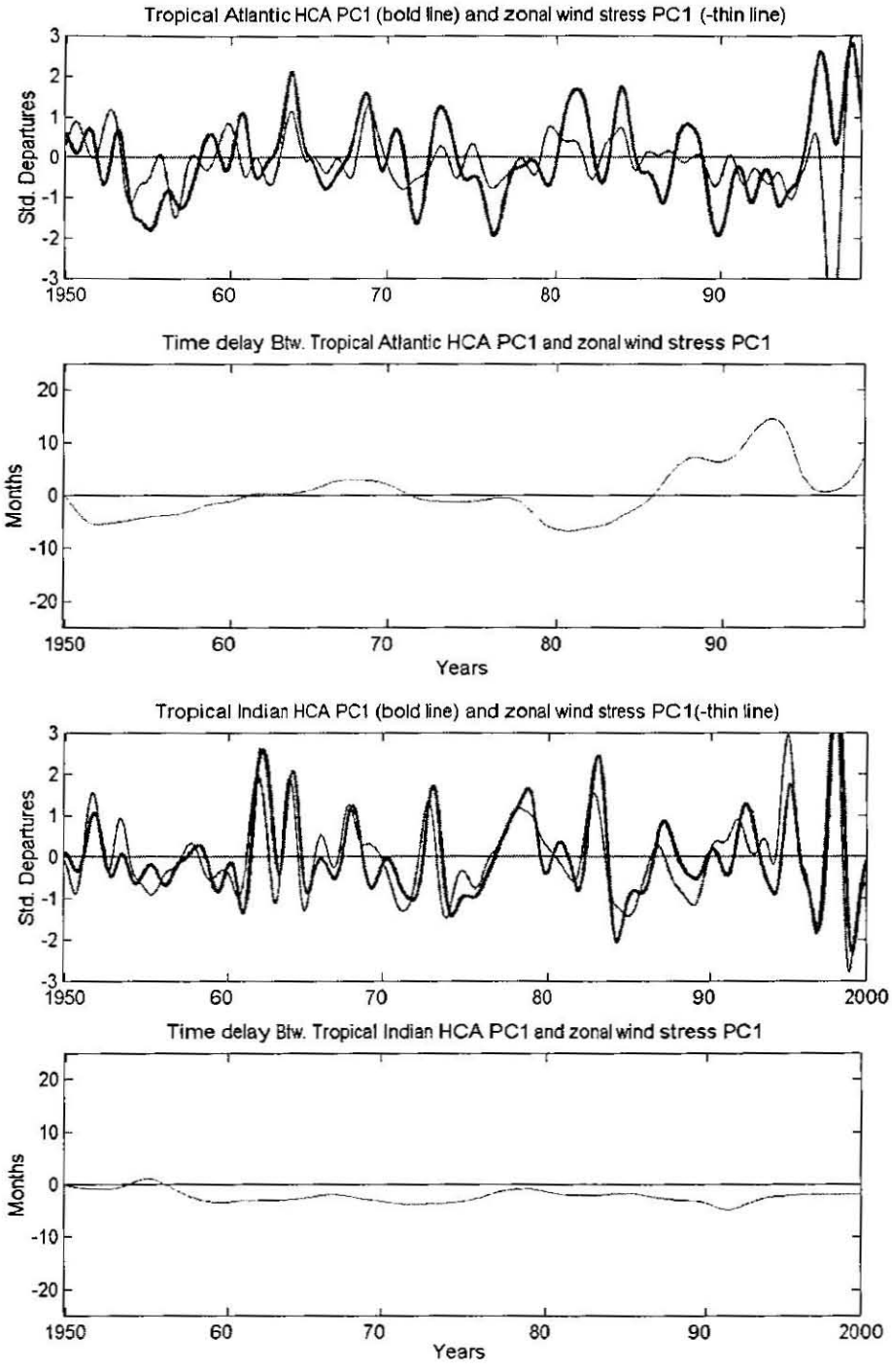

Fig. 7.28 Time varying cross-wavelet variants of leading HCA and zonal wind stress in tropical Atlantic and Indian Ocean.

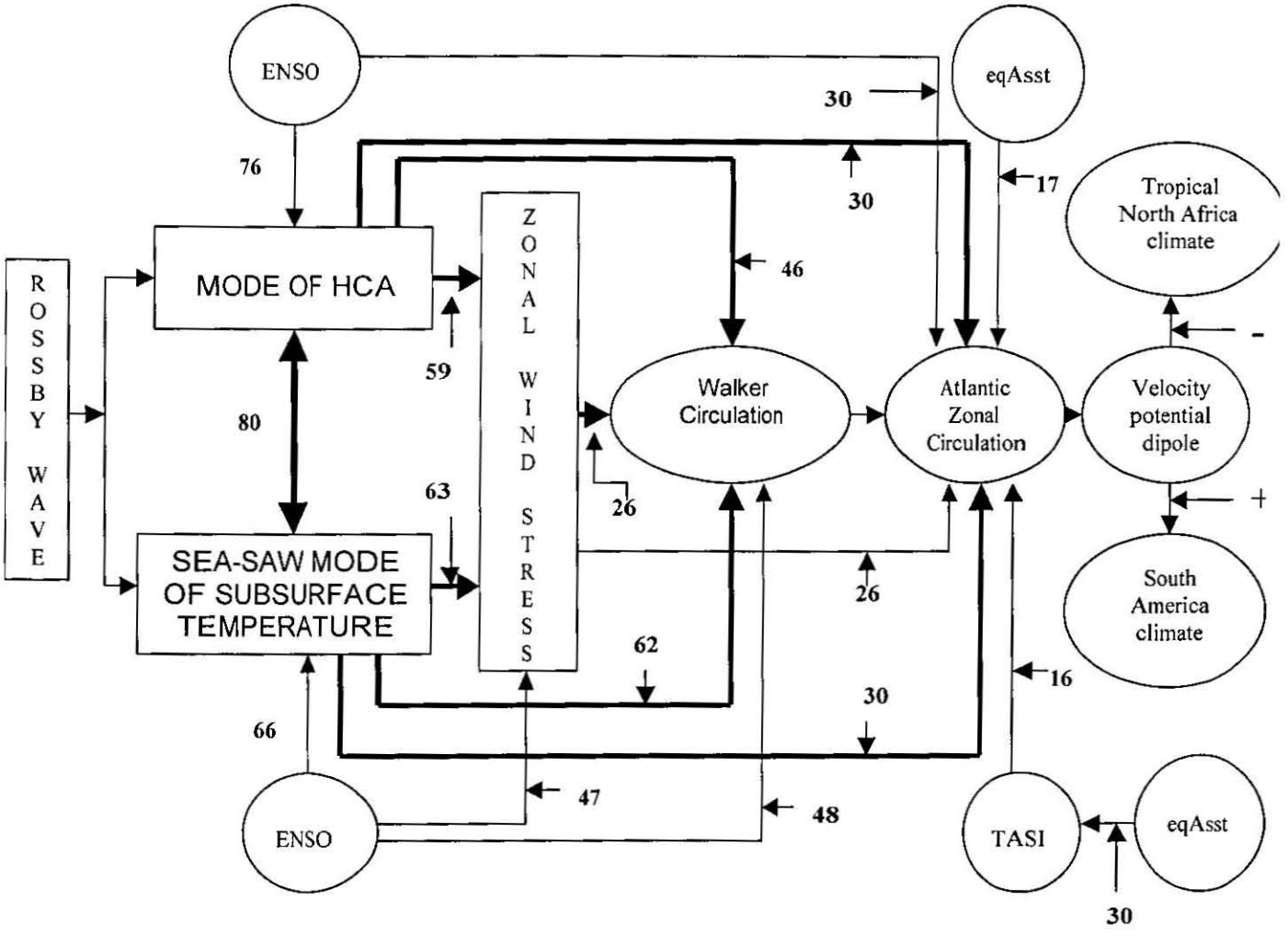

Fig. 7.29 Ocean-atmosphere interannual signal teleconnection of leading mode of tropical HCA and equatorial east-west subsurface thermal field of Pacific Ocean with Atlantic Zonal Circulation. Values show the variance (%) explained in the link. The ENSO and Atlantic SST modes are entailed to show the their contribution to the variability. ENSO mode and Atlantic SST are poorly related.

Table 7.1 Variances explain (%) by the first four leading EOFs of tropical HCA, subsurface temperature and zonal wind stress.

	Components			
Regions and parameter	1	2	3	4
Atlantic Ocean HCA	19	10	8	6
Indian Ocean HCA	23	14	8	6
Pacific Ocean HCA	36	12	7	4
Equatorial Atlantic east-west subsurface temperature	44	12	9	~9
Equatorial Indian east-west subsurface temperature	42	10	9	6
Equatorial Pacific east-west subsurface temperature	38	31	7	4
North-south Atlantic subsurface temperature	24	19	9	7
North-south Indian subsurface temperature	27	19	11	7
Tropical Atlantic wind stress	28	17	9	6
Tropical Indian wind stress	13	14	8	6
Tropical Pacific wind stress	11	7	6	5

CHAPTER 8

DEVELOPMENT OF OBJECTIVE STATISTICAL HYDROCLIMATE PREDICTION SYSTEMS

8.1 Introduction

In this study, the physical mechanisms that drive the climate and stream flow fluctuation over tropical North Africa and tropical South America were identified in Chapter 5. Links to tropical circulation and kinematic influences were investigated. The modulation by ENSO and regional SST on the tropical North Africa climate was examined in Chapter 6. In Chapter 7, the modes of subsurface thermal variability and their links to tropical circulations and the influences of Walker Circulation, Atlantic Circulation and the transverse Monsoon Circulation are investigated. In this Chapter, the predictability of climate, water resource and agriculture variations are studied. The FAO data are employed in this studied. To check the quality of data, the food and cash crops, agricultural export and import are related to rainfall for Ethiopia case. It is found that agricultural production and import and export are strongly correlated. In rain-fed agriculture system like Ethiopia, rainfall and agricultural production are closely tied.

Objective statistical prediction models useful in managing the climate sensitive socio-economic sectors are developed for tropical North Africa. Models are developed for climate fluctuations, water resources and food and cash crops. The prediction more than one season ahead benefits the people of tropical North Africa whose livelihood is impacted and contingent upon the water and agriculture sectors.

The prediction for climate, agriculture and water over tropical North Africa is possible due the underlying sea surface temperature influences on the climate over these regions and the kinematic link with the Atlantic Circulation. Despite the general fact that the atmosphere has less memory than the Ocean due low thermal inertial, the equatorial Atlantic and Pacific low-level winds are exceptions to this. They inherently posses longer 'memory' than the sea surface temperature in tropical oceans. This

inherent characteristic makes the equatorial Pacific and Atlantic surface winds useful and stable predictors.

It has been documented in the earlier Chapter that ENSO indirectly dictates the tropical North Africa climate variability. The Pacific El Nino leads to low-level westerly flow and upper-level easterly flow and mid-level rising motion over the warm pool region as a part the Pacific Walker Circulation. The Pacific and Atlantic Circulations are linked in anti-phase manner. Concomitant to this ENSO signal, the Atlantic Zonal Circulation responds through producing upper-level divergent inflow and sinking motion over tropical North Africa. Consequently, the tropical North Africa falls under the subsidence and hence suppressed convection during El Nino. It is through Walker - Atlantic Zonal Circulation that the ENSO modulations on the tropical North Africa climate variability are transmitted that lead to drought and less water resource and poor agriculture production during El Nino. La Nina episodes on the other hand bring enhanced convection over much of tropical Africa.

Embedded in remote teleconnections, regional ocean-atmosphere - coupling that surrounds tropical Africa also places a vital role in driving the climate over this part of Africa. The tropical Atlantic inter-hemisphere modulation imparts the tropical climate through the Hadley and Atlantic Zonal Circulations.

Any perturbation in the north - south SST dipole over this Basin perturbs the climate over the tropical North Africa and hence the water and the agriculture resources of the region. It also influences the tropical South American climate variability. A negative SST in the tropical north Atlantic and a positive in the southern counterpart results into a Hadley Circulation with ascending motion in the equatorial region of Africa and tropical South America and opposite circulation over tropical North Africa. In response to this SST gradient, a deficiency of water and reduction of agriculture is encountered over the later regions while benefiting the equatorial regions and Brazil. On the other side of Africa, the Indian Ocean is located. A positive SST over western Indian Ocean and a negative in the east favour good rainfall over most regions of tropical North Africa. Any

reversals of the sign of the SST over this basin can lead to drought over the region and hence pressure on water and agricultural sector.

The key issues addressed above are the kernels of predictability for tropical North Africa climate, stream flow and agriculture production. To give a regional flavour to the prediction models, kinematic indices of monsoon circulations on either side of Africa are also considered.

8.2 Targets and Predictors

The first task in developing prediction models is identifying the predictors and targets. These are tropical North Africa rainfall and resources. The target variables are chosen based on the importance of the variables in point on climate studies and socio-economic significance (Table 8.1). Rainfall and temperature are considered as the climate target variables for tropical North Africa and also for tropical South America. The temperature data for these regions are extracted over Sahel, Guinea Coast and Central Africa.

Stream flows over Nile, Niger and Senegal (tropical North Africa) and Parana (Brazil) are also deemed as hydrological target variables. Food (Maize and wheat) and cash crops (coffee and cotton) are also selected considered as agricultural production targets. The cash crops are selected from tropical North Africa and South America countries. To give economical dimension on application of climate studies on socio-economic sphere, agricultural import and export values from tropical North Africa countries are included in the target pool. The complete lists of the targets are given in Table 8.1.

Next it is necessary to determine the predictors that proffer multivariate models with high skill and with less co-linearity problem. There are various ways to accomplish this task. In this study, candidate predictors are selected from pair-wise lagged correlation (Fig. 8.1 and Fig. 8.2) and from results obtained from Chapter 4 to Chapter 7 that are

recognised as important in the modulation of tropical North Africa climate variability. The pair-wise correlation is performed between global sea surface temperature, sea-level pressure, zonal and meridional surface winds. However, the correlation result between sea-level pressure and Nile flow was poor and hence not considered for further discussion. The use of surface winds is preferred due to the availability of data routinely in the global telecommunication system of Word Meteorological Organisation. In identifying the potential predictors, one of the criteria is that the key area be large enough to the uptake of teleconnection and influence remotely the tropical North Africa climate variability. In addition, the surface winds are preferred to be over tropical oceans than the land surface to obtain the necessary 'memory' statistical prediction. These factors are taken into account to assure a sufficient time for mitigation strategies for. Predictors that can give 12-month, 9-month, 6-month and 3-month lead-time are identified. The predictors are listed in Table 8.2.

Temporal Evolution of lagged correlation

The global tropics SST and zonal wind are considered with respect West Sahel. Similar work was performed for other parts of tropical North Africa, but for brevity will be not be shown or further discussed – as the patterns are quite similar. Contrasting results are given in some cases for Brazil.

a) Sea surface temperature

Lagged correlation structures

The concurrent correlation in boreal summer between the global tropical SST and the West Africa show an inter-hemispheric dipole in the tropical Atlantic and Pacific Oceans (Fig. 8.1). In the Atlantic, the axis is oriented north-south direction (negative - south), over Pacific; the orientation of the dipole is southeast - northwest (positive – northwest). The West Africa rainfall is associated negatively to SST over the central and east Pacific SST. Over Indian Ocean, a singular negative correlation pattern dominates as

an indication of an enhanced northward flow in the Indian Monsoon. The West Africa rainfall is oppositely correlated to the equatorial and tropical south Oceans. In contrast, the Brazil rainfall - SST pattern is confined within the Atlantic Ocean. It shows dipole structure with negative SST in the north and positive in the south. The West Sahel and Brazil rainfall respond oppositely to the tropical Atlantic SST.

The 3-month pattern is similar, with reduced negative area in the central Pacific. The Brazil correlation at 6-month evolves with a change in the configuration of the tropical north Atlantic SST and additional feature over Pacific Ocean. The southwest - northeast axis in the tropical North Atlantic assumes a more zonal pattern.

At 9-month lag, the degree of association between West Sahel and SST over all Oceans becomes weak and the gradient in SST dipole also is feeble (Fig. 8.1). Negative SST regions too reduced. The Indian Ocean shows a horse-shaped negative sea surface temperature symmetric to 20°S latitude line. A positive SST is along western of Africa and within the equatorial Atlantic. A similar weakening is confirmed for Brazil.

At 12-month lag, the disintegration of the dipole pattern in respect of West Sahel rainfall continues. The Brazil rainfall finds a strengthening pattern of association in the tropical North Atlantic.

Covariance eigenvectors

A global sea surface temperature for all-seasons for 1901-1980 is analysed using covariance eigenvector (Folland et al., 1991). The second unrotated spatial pattern of the eigenvector matrix reveals a strong ENSO signal over central and east Pacific Ocean with opposite patterns over north and south Pacific. High positive loading is also depicted west and southwest Atlantic Ocean. The tropical region of Indian Ocean shows a coherent pattern throughout the basin. The third EOF (spatial pattern of the eigenvector analysis) reveals the tropical Atlantic SST dipole with negative loading in

the tropical North Atlantic (centred to West Atlantic) and positive tropical south Atlantic (with the highest loading over southwest Atlantic Ocean). A dipole in SST between equatorial regions of Pacific and North Pacific also comes out from the unrotated eigenvector analysis. In the Indian Ocean, the consistent and coherent pattern with higher loading to southern regions characterised the SST pattern in the EOF domain. In Atlantic and Indian Ocean, the loading is very high in southern regions. In Pacific, the high loading is in the equatorial plane. Varimax rotated version of the second EOF shows a singular pattern and maximum loading over the equatorial Atlantic, Gulf of Guinea and Angola Basin and spatially coherent loading in Indian Ocean. In southern rim of tropical Atlantic and Indian Ocean, a negative loading is also present.

The covariance eigenvector analysis of global SST reveals the principal modes of variability in the EOF domain. The principal modes are the ENSO signal over Pacific, the north - south Atlantic SST dipole, the equatorial Atlantic mode and the coherent and consistent Indian mode.

From the lagged correlation and EOF patterns, the equatorial regions of central and east Pacific, the northwest and northeast Pacific, the tropical Atlantic SST inter-hemispheric dipole and the equatorial Atlantic SST are the most important potential areas in prediction for tropical North Africa climate (Table 8.2). In Chapter 6, it is found that the east-west SST dipole Indian Ocean controls the climate variability of tropical North Africa. The index quantifying this pattern (extracted for the appropriate season) is also considered.

b) Surface zonal wind

Global tropical zonal wind has found to be related at different lags to indices of Sahel climate. Here, the lagged correlations of surface zonal wind and West Sahel rainfall are mapped at 3-month interval to one year. These lagged correlation maps are shown in Fig. 8.2. Positive correlation concurrently dominates over the equatorial Atlantic and negative over Indian Ocean and the northern and southern region of tropical Atlantic.

The only significant positive correlation is found in the northern equatorial region of Atlantic. It is very interesting to see the equatorial Pacific and Atlantic zonal winds are opposed with respect to tropical North Africa rainfall. At 3-month lag, similar patterns are shown. But, the amplitude of the correlation weakens over oceans. At 6-month lag, the main patterns are maintained over the Indian Ocean. Over Atlantic, the positive correlation expands to tropical North Atlantic. In Pacific, the oval and organised pattern of three-month lag is now widespread maintaining the sign. After three month later, the pattern reorganised over equatorial Pacific. Over Atlantic, the negative regions nearly vanish but in the equatorial regions, the positive correlation is persistently dominating. In the Indian Ocean, weak patterns are seen in the west. At 12-month, more coherent and strong pattern of alternative signs dominating the equatorial belt similar to the concurrent pattern: with negative (equatorial Pacific), positive (equatorial Atlantic) and negative (equatorial Indian Ocean). The Atlantic "opposition" has very important implication for understanding and prediction of climate over tropical North Africa.

The most stable and coherent surface zonal winds useful for key areas are the equatorial Atlantic and Pacific regions (Fig. 8.3, Fig. 8.6 and Table 8.10). The zonal wind over equatorial Indian Ocean is not coherent in time to be a stable predictor. Other wind predictors considered from Chapter 4 are key areas of West Africa and Southwest Monsoon. The meridional component of West Africa is drawn into the potential predictor list (Table 8.2). From the Indian Monsoon circulation, off-equatorial zonal components are part of the potential predictor list. Its meridional component over western Indian Ocean is also considered as a potential predictor. The complete list of predictors is given in Table 8.2 and Table 8.3.

8.3 Model development

Multivariate linear regression models are developed using a forward stepwise regression. Historical area rainfall, stream flow and agricultural yields are optimal fitted. To prevent artificial skill and over-fitting, the number of predictors in a particular model is limited to three. Models are formulated to optimise hindcast-adjusted variance. Co-

linearity is screened to r^2 < 10% when it is popped up in the construction of the multivariate models. Different models for different targets (refer Table 8.3) are developed based on the predictors listed in Table 8.2. The prediction models are constructed at seasonal lead times to 12 month.

a) Multivariate linear prediction models

The constructed multivariate linear models for climate, stream flow, cash and food crops and import and export are given from Table 8.4 to Table 8.9. The "deflated" degree of freedom is listed for assessment. The hindcast fit r^2 is also deflated for persistence of target variables and pool size of predictor that leads to randomness. The persistence is evaluated from autocorrelation. West and east Sahel rainfall show strong persistence to year +3. So, the degree of freedom declines to 15 (from 46). Persistent is not a problem for Ethiopia, Guinea Coast and Northern Congo rainfall as the autocorrelation function decrease rapidly with time and hence the degree of freedom is n -1. Multivariate models for other target variables are also assessed accordingly and the adjusted variances are r^2 deflated as necessary.

To find the randomness generated by the pool size of the predictors, a Monte Carlo Test was conducted. The simulation was done based on the number of predictors involved in the construction of the model and the number of years involved in building the models. The results obtained shows very interesting implication to predictability of tropical Africa rainfall. The rainfall over equatorial regions of Africa (Gulf of Guinea and Congo) is stochastic in nature and hence a problem to predict rainfall over this region at least a season ahead. Over East Sahel, West Sahel, and Ethiopia, the rainfall is more deterministic and hence prediction at longer lead-time is possible. As a result, the Guinea Coast and North Congo rainfall prediction models show rapid decline in r^2 fit at lead time > 3 months.

Analysis is also done on stability and key predictors of rainfall over tropical North Africa. The equatorial Atlantic and east Pacific zonal winds are the best the predictors of

tropical North Africa Climate (Fig. 8.10 and Fig. 8.11). In climate prediction, it is considered that long-range forecast is possible using tropical sea surface temperature due the high thermal inertia of the Ocean. On the contrary this study shows that atmospheric zonal winds obtain a higher prediction potential than the sea surface temperature. The tropical winds over the ocean have longer 'memory' to predict not only climate but also resources such as stream flow and agricultural outputs. Predictors are also associated with detrended agriculture and coffee yields (from 1961 to 1998) as shown in Table 8.2. The result is shown in Table 8.7 and Table 8.8. For instance, the largest coffee exporter in the world is Columbia. The coffee yield there is closely related to southeast Pacific SST (r = 0.74), to equatorial Atlantic zonal wind (r = -0.55), and equatorial Pacific zonal wind (r = 0.59) at 12-month lag. Ethiopian Coffee (Arabica) is highly correlated. Indonesia is the other coffee growing tropical country where coffee production is highly related to tropical North Atlantic SST (r= 0.578), southeast Pacific SST (r =0.750), and equatorial east Pacific zonal wind (r=0.679). Coffee yields over tropical Southern America negatively correlated to equatorial Atlantic zonal wind. Many of these relationships are persistent at leads of 6 to 12 months.

Cotton production in tropical North Africa is associated with key kinematic predictors to 12-month lead-time (Fig. 8.5). High prediction potential of cotton production is found at 9 to 12 lead-times, more contribution coming from equatorial Atlantic zonal wind. Again, it is demonstrated that the key predictors determined for climate prediction are showing their importance for resource prediction. The same diagram is produced for Sahel rainfall (Fig. 8.4) to show the contribution the leading kinematic predictors to Sahel rainfall prediction. It is revealed that these kinematic variables explain and predict the swing of Sahel climate.

b) Cross-validation (Skill Test)

Validation tests are done by blanking out, alternatively, the first and last quarter of years (12 years each). Target variables are then predicted based on the hindcast model

variables. The performance of the model is assessed by tercile categories hit, correlation analysis and scatter plots.

The tercile hit rates and the correlation coefficients are displayed in Table 8.12 for rainfall stream flow and temperature for boreal summer. The cross-validation for certain targets are given. The hit rates during the independent test period for East Sahel rainfall predictor models are 76% for 12-month, 88% for 9-month, 77% for 6-month, and 70% for 3-month leads. Similarly, the hit rates for West Sahel rainfall prediction model are 85% at 12-month, 71% at 9-month, 77% at 6-month and 70% at 3-month leads. The hit rates for temperature models for tropical North Africa boreal summer temperature is very coherent throughout the region. For instance the hit rates for Sahel region temperature are 80% at 9-month and 70% at 6-month.

The stream flow models for Niger at Mali and Parana in Brazil also show high rates. The rates for Niger stream flow at different lead-time are 67% at 12-month and 55% at 9-month. Parana stream flow prediction model has a hit rate of 57% at 12-month and 55% at 9-month.

The cross-correlation between observed and predicted rainfall (detrended), temperature and stream flow over tropical North Africa also reveals high skill of the prediction models developed and the depiction of the patterns of the observed timeseries. The correlation between the observed and predicted rainfall over Sahel region ranges from 0.64 to 0.80. For temperature, it general ranges from 0.65 to 0.77 except Guinea regions where the correlation values range from 0.33 (at 12-month) to 0.71 (at 3-month). The stream flow over Niger and Parana also show high correlation values between the observed and predicted that range, at different lead-time, from 0.45 (12-month) to 0.70 (9-month) for Niger and 0.75 (at 12-month) to 0.85 (at 9-month).

The scatter diagram between the observed and predicted timeseries for boreal summer rainfall and temperature are also presented to see in which quadrants in the x-y plots the predicted values fall with respect to the observed. This can assists to identify the

strength of the model in picking up the extreme mode of variability such as drought, flood, hot and cold cases. To this end, the scatter plots for rainfall and temperature for boreal summers are shown in Fig. 8.7. The predicted and the observed values are in most case fall in the proper quadrants that depict alarm for drought or flood. This is particularly true for West Africa. Similar patterns are shown in boreal summer temperature over Sahel Region except at 3-month lead where cold events are not picked. Except the spread, the scatter plots for Guinea Coast temperature resemble to the Sahel temperature scatter plots.

The temporal evolution of the observed and predicted rainfall and temperature are also examined to find out the pattern. The wet and dry period of Sahel rainfall is identified (Fig. 8.12 (a and b). This is a multi-decadal oscillation that causes the Sahel region to undergo different rainfall and temperature regimes before the late 1970s and after 1970s. Wet events (and hence cold) dominate during the former period and the opposite after the late 1970s. The validation data incorporate both periods. The prediction models for rainfall and temperature produce the observed rainfall and temperature pattern of the region. Next, the trend was removed (e.g.: linear de-trending). Then models are developed on the new de-trended data for rainfall and temperature. The adjusted variances for the models significantly dropped for tropical North Africa region. In some cases, no model fit is found. For instance, models could not be developed for West Sahel at 6-month, for East Sahel rainfall at 6- and 3-month and for Nile flow at 6 and 3-month lead. Still, reasonable high hit rates are obtained for boreal winter for the South America region. The multivariate models for the de-trended data are given in Table 8.9. The signs of the models for de-trended data and predictor influence on the target are not in harmony. The detrending nullifies the multi-decadal oscillation that ties the ENSO-related predictors and the African targets. It also shows that only one degree of freedom may be embedded in the data.

The result obtained in this study is useful in climate, stream flow and food and cash crops prediction for tropical North Africa. In Operational mode, seasonal outlook is given for tropical North Africa countries in June for boreal summer using the equatorial

Atlantic, Nino 3 and Northwest Atlantic sea surface temperatures. Predicting the rainfall in June is too late for early warning systems and for decision making to ameliorate the adverse impact of climate over the region. But, the result here, may enable mitigation of socio-economic impacts.

8.4 Predictors stability and physical cause of predictability

To determine the influence of predictors in the statistical models discussed above, the cumulative score and frequency of appearance of the predictors are given in Fig. 8.10. The result reveals that the equatorial Atlantic and Pacific Oceans zonal winds have longer "memory" than the tropical sea surface temperature (Fig. 8.10 and Fig. 8.11). Second these winds are very stable and coherent at different lead. Third, the importance of tropical SSTs emerges at 0 and 3-month lags for Central Africa import. Of all cases, the tropical SSTs have greatest influence within season in JAS (0 lag, not shown). As discussed above, the current practice (2002) is to provide a forecast for boreal summer climate outlook at 3-month lead when the tropical SST appears to be important. But, the tropical zonal wind is the way to break this predictive barrier at decadal timescale. This is evident in the autocorrelation patterns on both raw and fitted data (Table 8.10 and Table 8.11).

New predictors for the future

The upper-level zonal wind at 200-hPa is also correlated to West Sahel rainfall and shown in Fig. 8.8. The lagged correlation depicts a coherent and stable negative correlation pattern from the equatorial Atlantic to Indian Ocean, in between tropical Africa. At 6-month and 9-month lag, the pattern is confined within equatorial Atlantic and tropical North Africa. In the lagged correlation between West Sahel and low-level zonal, it is found that a coherent positive correlation dominates over equatorial Atlantic and tropical North Africa. The upper-level correlation structure confirms the Atlantic Zonal Circulation, the principal circulation that causes high predictability of climate in tropical North Africa and tropical South America. The Walker Circulation also plays a pivotal role

for stability of the equatorial Pacific Ocean zonal wind. This is further examined through studying the upper-level divergent circulation. Low-level winds have more prediction potential (by 16% variance) than the upper-level particularly at 9 and 6-m lead-time. At 12-month, the upper-level is better and explains 30% more variance.

The upper-level velocity potential is considered in the lagged correlation along with West Sahel rainfall. The lagged correlation pattern shows a wave-number one pattern with negative correlation from tropical North Africa to the Pacific, and North America. The other centre of action (positive) is observed over the Indian Ocean at 3- to 9-month lead. There are two main points that come from this analysis. The climate system over tropical North Africa and South America / East Pacific is not only generating polarity in divergent flow at zero-lag but up to one year in advance. The other point is that a meridional dipole (in lagged correlation) is evident between tropical North Africa and southern Africa countries (south of the equator).

All the variables used in the lagged correlation pattern analysis converge into one consolidated notion that the Atlantic Zonal Circulation is a very stable system that has 'long memory' and gives ground for high predictability of climate variability over tropical North Africa and tropical South America.

A schematic diagram is shown to conceptualise the process involved in the relationship between the predictors and targets (Fig 8.13). In this schematic diagram, the primary kinematics predictors are equatorial Atlantic and Pacific zonal winds. The westerly low-level winds and cold SST over the equatorial Atlantic, and La Nina episode and easterly wind over Pacific lead to increased rainfall and high stream flow. As a result, a high production in agriculture and hydropower over tropical North Africa occurs. As a result of an optimum condition for economic and industrial development arises and employment increases.

8.5 Conclusion

In this Chapter, multivariate models for climate, stream flow, and agricultural production for tropical North Africa and tropical South America are developed via pair-wise correlation and results found in the preceding Chapters. Claims of model performance are penalised through tests to check the chaotic nature of the predictor-target relationships. For example, the rainfall over the equatorial regions of Africa appears to be stochastic in nature; as a result the predictability of rainfall of these regions is low. A cross-validation is used to assess skill at different lags. Tercile hit rates and correlation coefficients are computed between the observed and prediction timeseries. The results surpass current (2002) operational practice in prediction at longer lead-time. The high rate of predictability of the climate system is somewhat dependent on the multi-decadal oscillation, to which the current 50-year data sets are confined.

The physical mechanism involves the zonal overturning circulations over the Atlantic and Pacific oceans. The coherent and consistent nature of the Atlantic Circulation in time and space makes the equatorial Atlantic zonal wind the best and most stable predictor.

The results obtained in this Chapter enhance the capability of ameliorating the adverse effect of climate variability over tropical North Africa in the mitigation strategy in early warning systems.

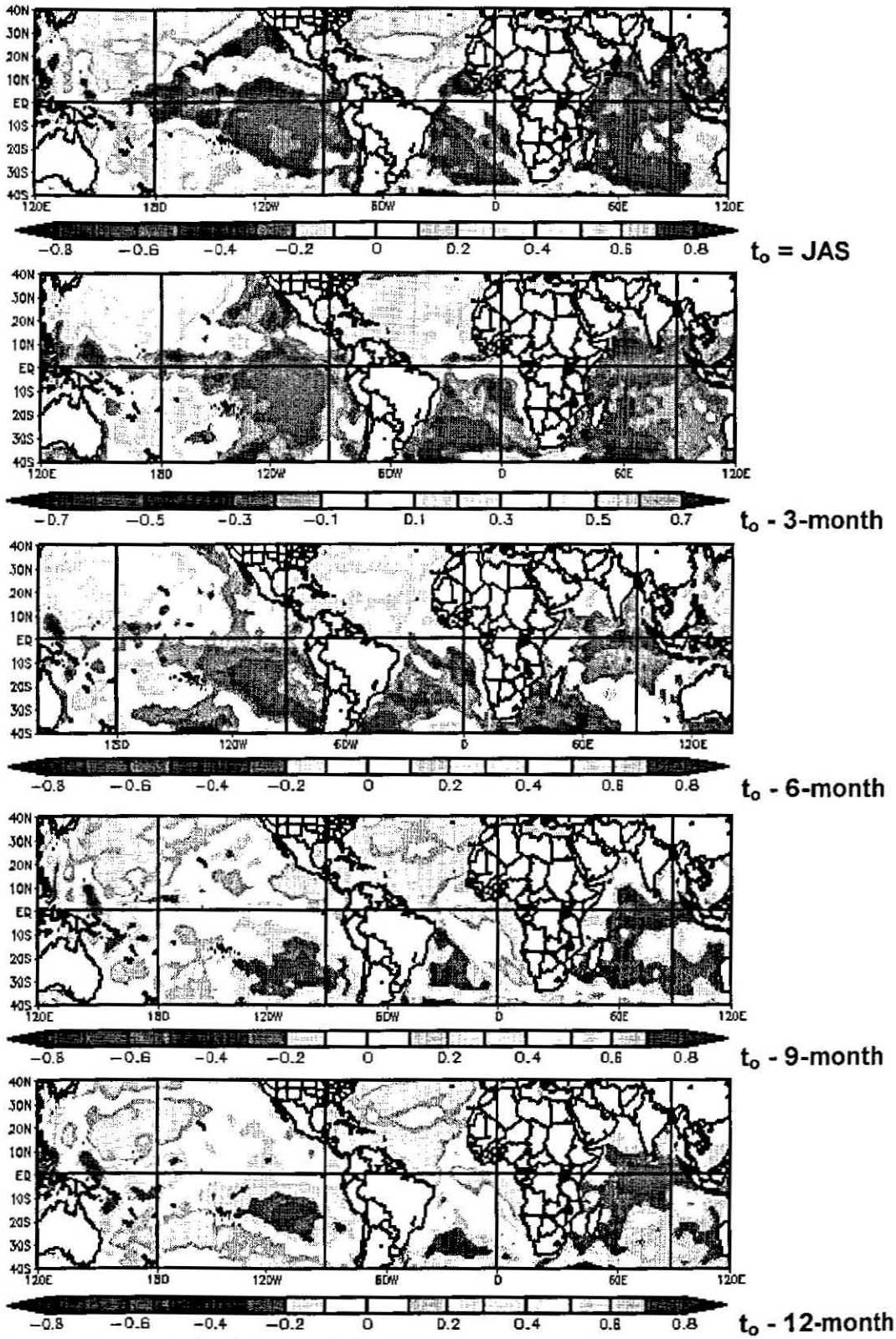

Fig. 8.1 Lagged correlation between West Sahel rainfall and sea surface temperature (black: negative and light black: positive).

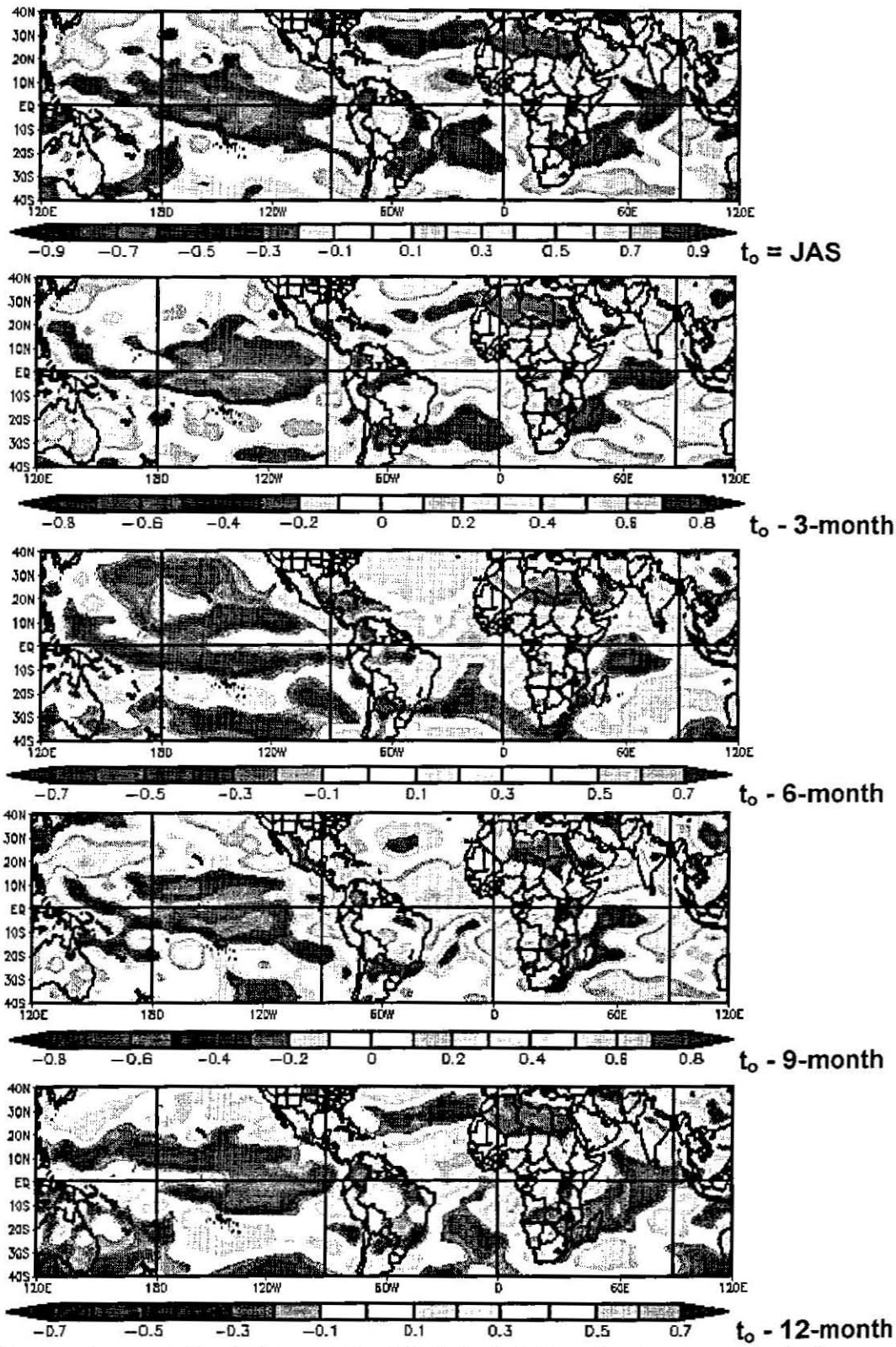

Fig. 8.2 Lagged correlation between West Sahel rainfall and surface zonal wind (black: negative and light black: positive).

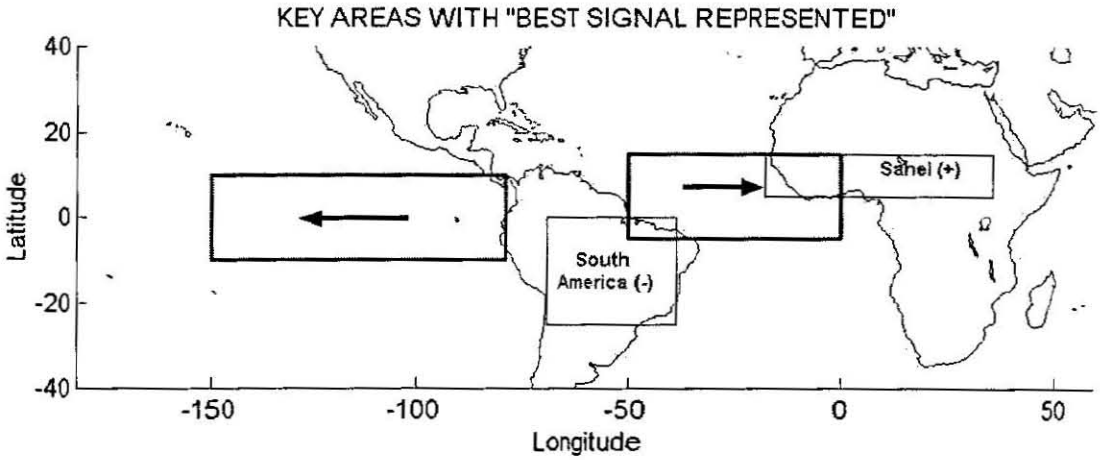

Note: The plus in Sahel and minus in South Americ represent the responses to westerly and easterly winds in Atlantic and Pacific winds in that order.

Fig. 8.3 Key predictors signal and convection responses. The arrows represent the low-level flows in equatorial east Pacific and Atlantic that induce enhanced convection in Sahel (+) and suppresses in South America (-).

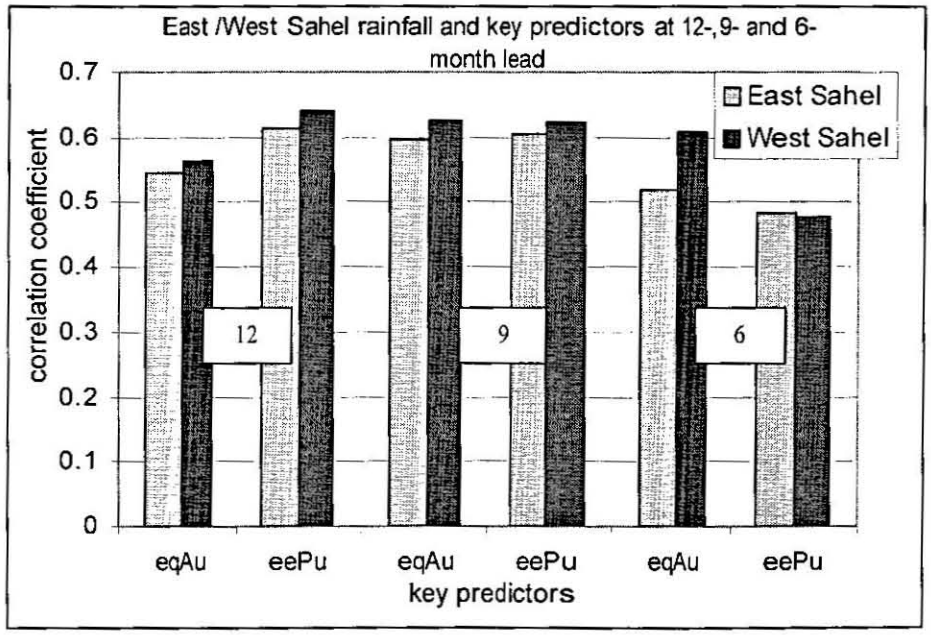

Fig. 8.4 Correlation between Sahel rainfall and key predictors at 12, 9 and 6-month lead. The equatorial east Pacific wind is reversed. The number in the box represents lead-time

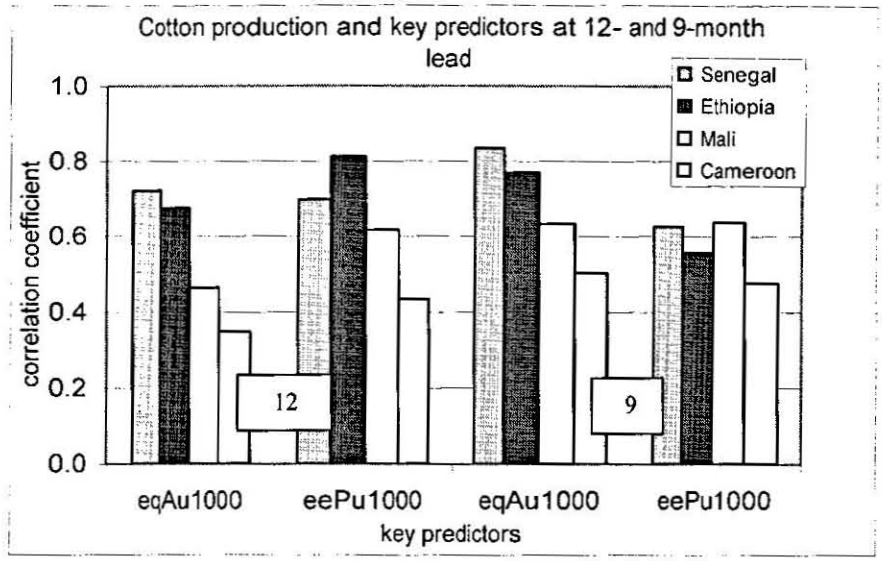

Fig. 8.5 Correlation between cotton production in certain tropical North Africa countries and key predictors at 12- and 9-month leads. Note that the sign of eqAu1000 is reversed and the number in box represents the lead-time.

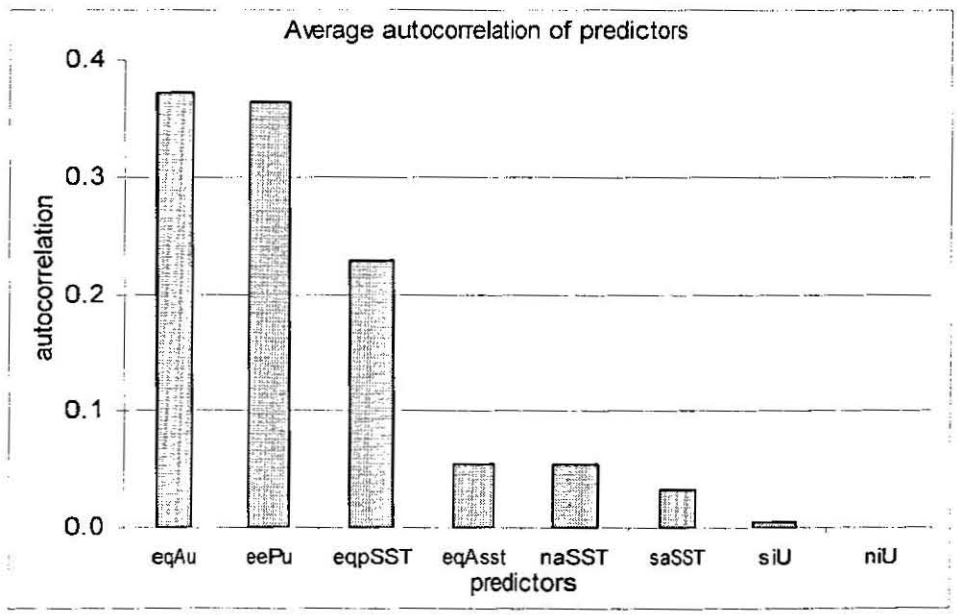

Fig. 8.6 Average autocorrelation computed based on continuous data from 1950-1998. The average is taken from 1 to 12-month lag.

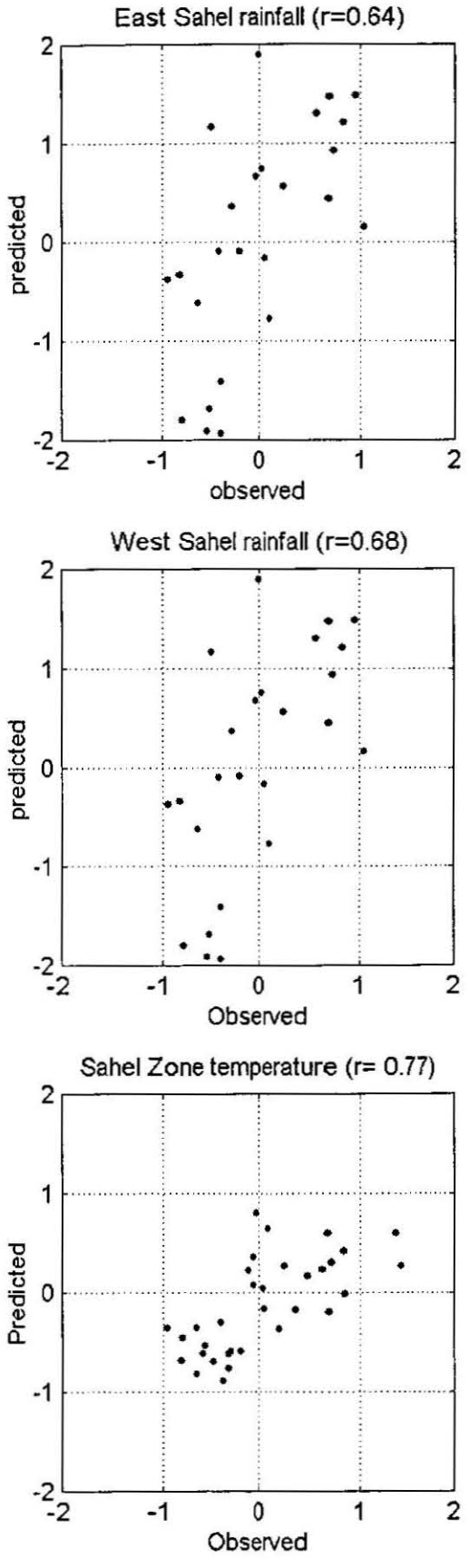

Fig. 8.7 Scatter plots of observed against predicted rainfall and temperature over tropical North Africa at 6-month lag.

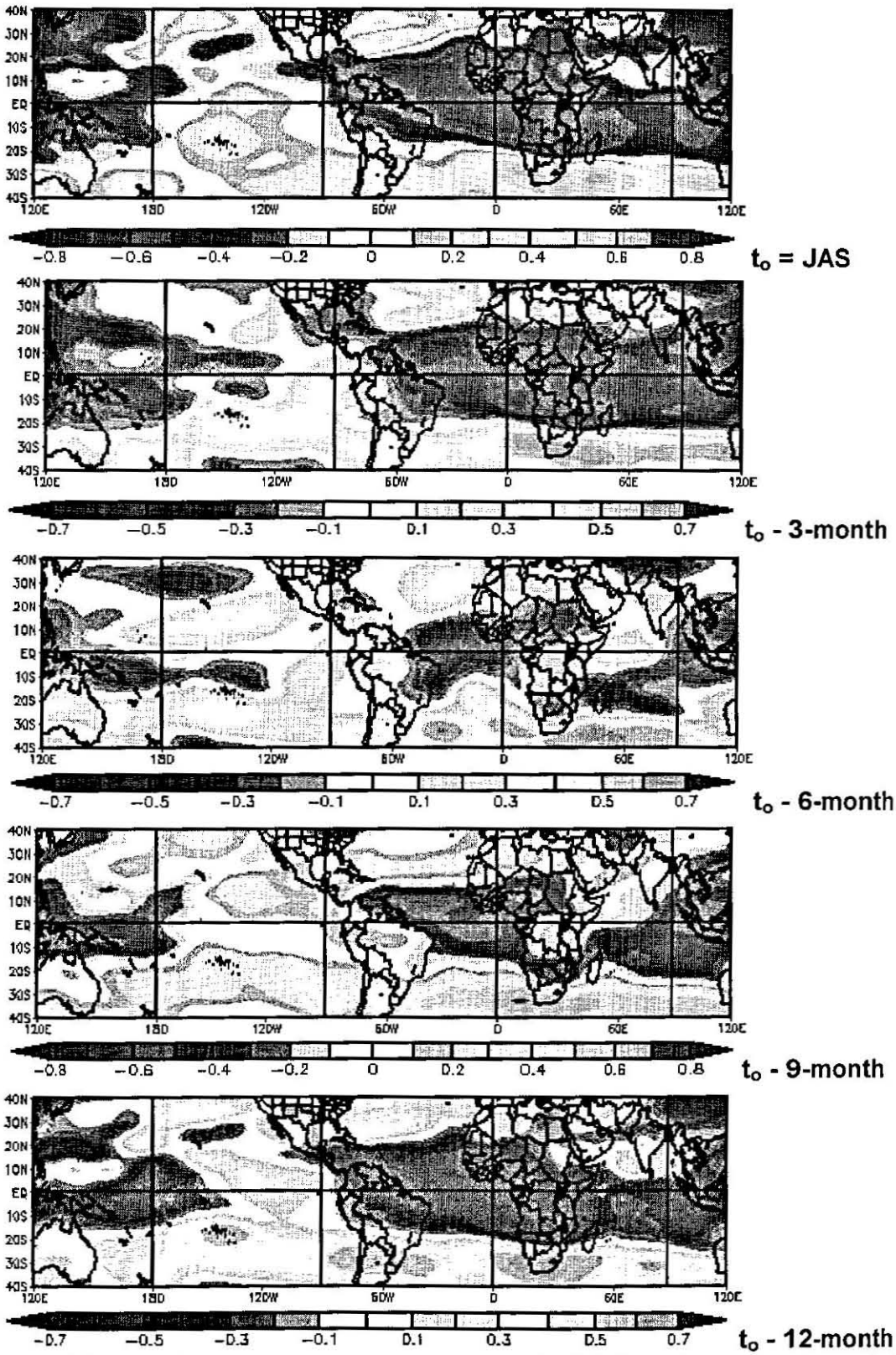

Fig. 8.8 Lagged correlation between West Sahel rainfall and 200-hPa zonal wind (black: negative and light black: positive).

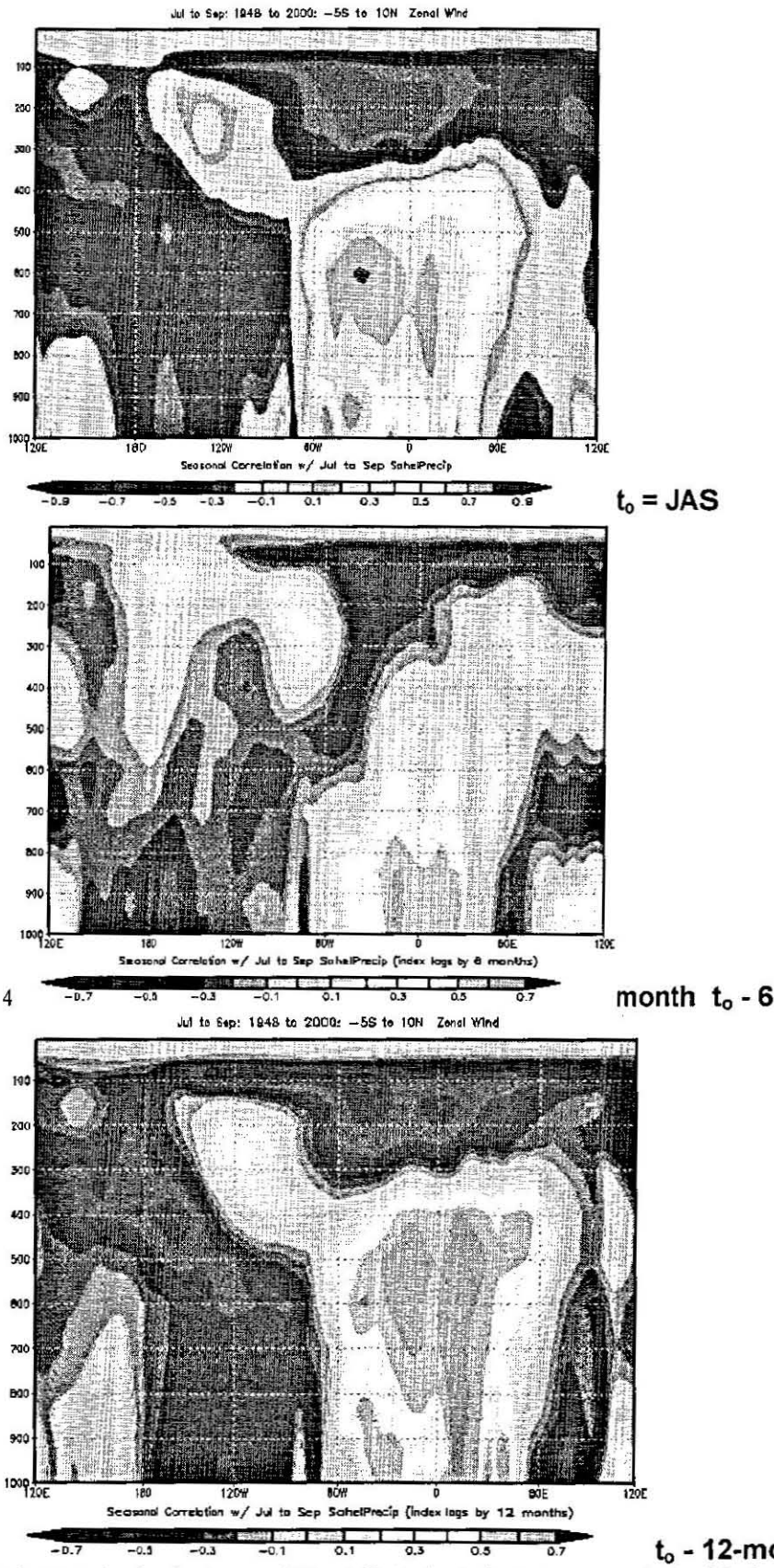

Fig. 8.9 Lagged correlation between West Sahel rainfall and zonal wind in longitude-height cross-section (dark: negative, light dark: positive).

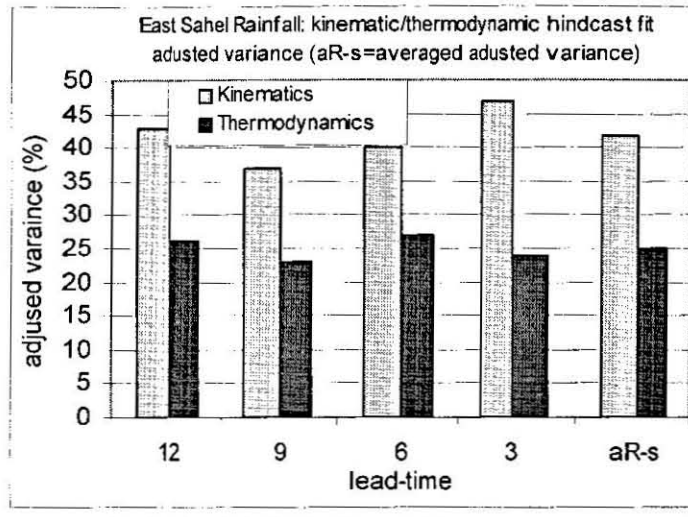

a) East-Sahel rainfall hindicast fit.

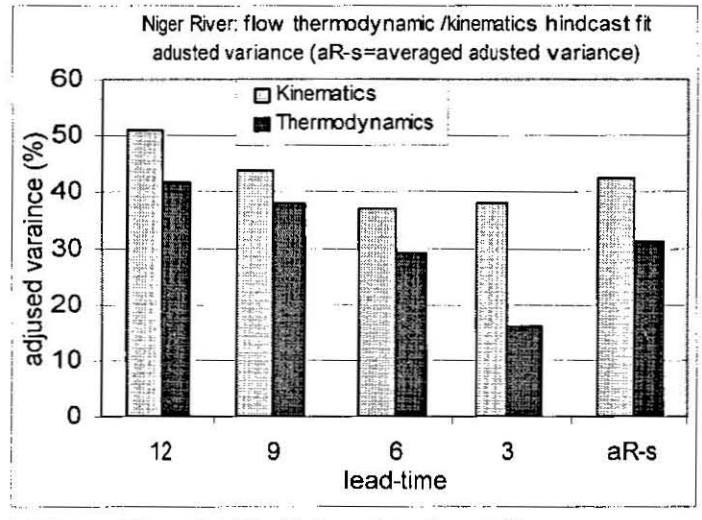

b) Niger River (at Mali) flow hindicast fit.

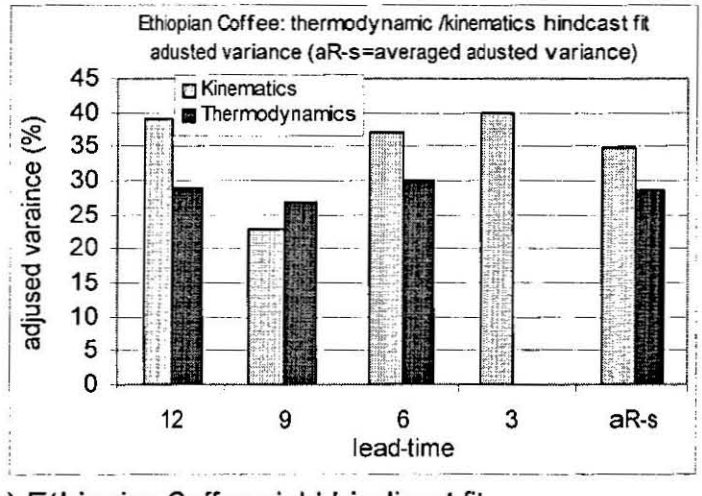

c) Ethiopian Coffee yield hindicast fit.

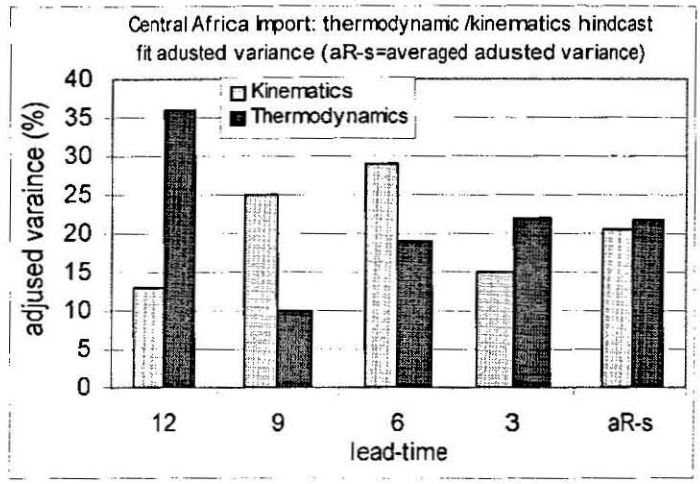

d) Central Africa import hindcast fit.

Fig. 8.10 Comparison of the hindcast skills of thermodynamic and kinematic predictors in hindcast fitting the East-Sahel rainfall, Niger River flow, Ethiopian Coffee production and Central Africa import (at different lead-time).

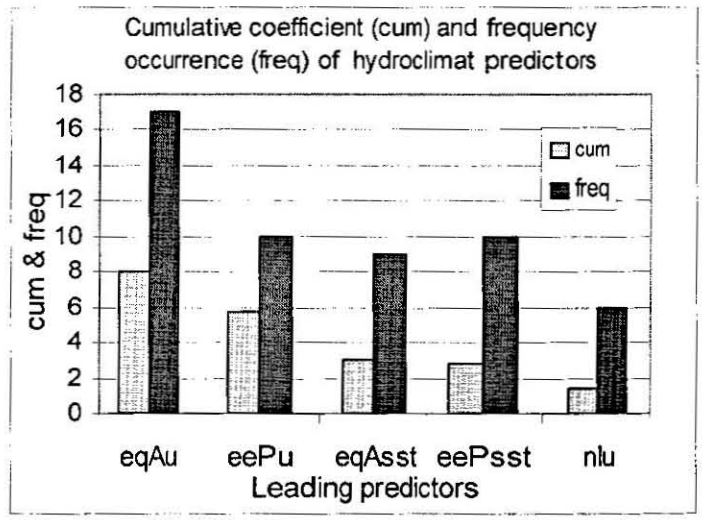

Fig. 8.11 Cumulative coefficients of the leading predictors and frequency of occurrence in prediction models for hydroclimate. The most frequent coefficients with same signs are considered.

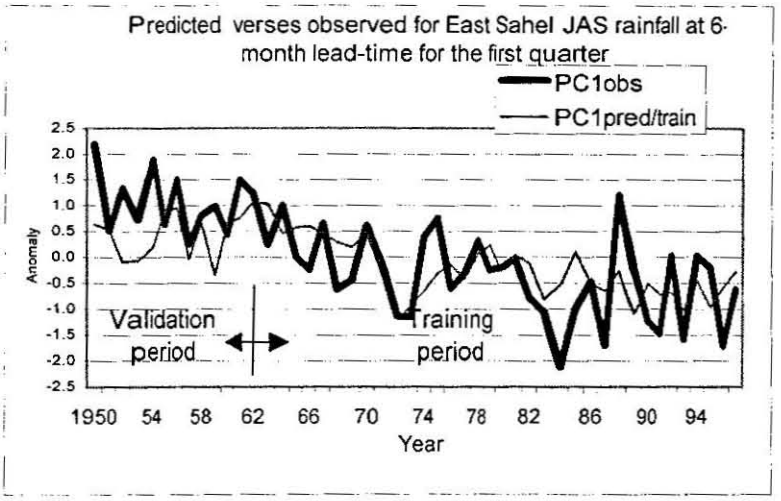

a) Prediction and observed rainfall of East Sahel for the first quarter (1950-1962).

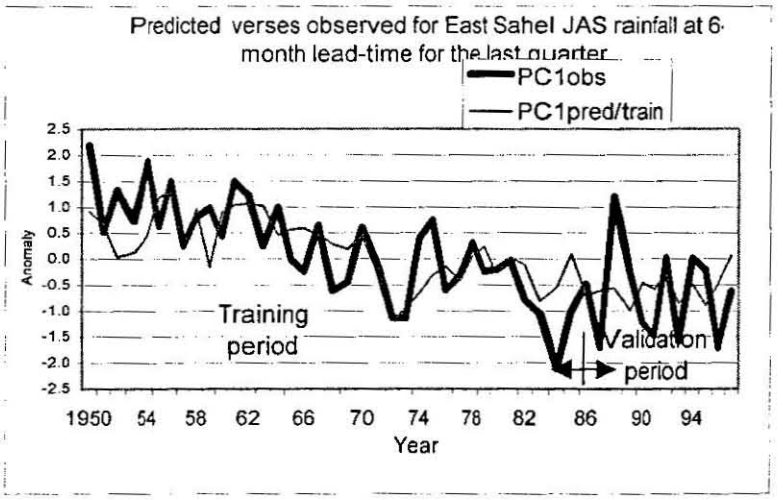

b) Prediction and observed rainfall of East Sahel for the last quarter (1986-1997).

Fig. 8.12 Plots of predicted and observed of East Sahel rainfall. The training period is shown.

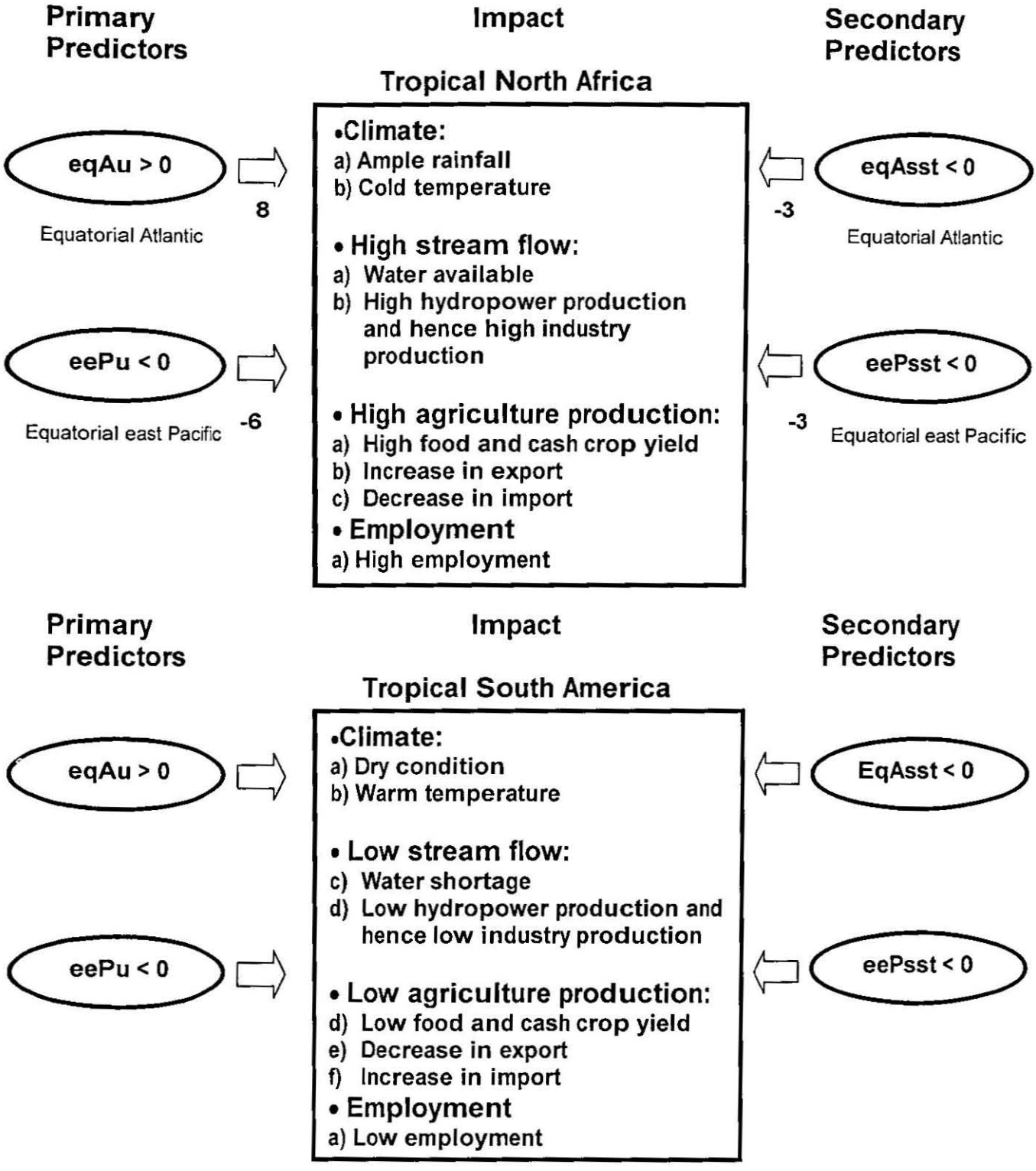

Fig. 8.13 Impacts of the leading predictors based on models constructed on tropical North Africa and South America. Number shows cumulative coefficient values. Note that tropical South Atlantic SST predicts better and longer lead-time Sahel rainfall than equatorial Atlantic SST when considered individually but the latter is much more important than tropical North Atlantic SST.

Table 8.1 Targets

No.	Predictant	Region
1	Climate: a) Rainfall b) Temperature	Tropical North Africa regions: West Sahel, East Sahel, Ethiopia, and Guinea Coast. Ditto above and central South America.
2	Stream flow	Nile, Senegal, Niger (Tropical Africa rivers) and Parana (Brazil)
3	Agricultural activity	
3.1	Maize yield	Egypt, Ethiopia, Mauritania, Mali, and Sudan
3.2	Wheat yield	Egypt, Sudan and Ethiopia
3.3	Coffee (Arabica) yield	Cameron, Ethiopia, Ghana, Colombia, Paraguay and Peru
3.4	Cotton yield	Cameroon, Central Africa, Egypt, Ethiopia, Mali, Niger, Senegal, Colombia, Peru, Venezuela, and Brazil
3.5	Agricultural Import	Central Africa, Ethiopia, Mali, Mauritania, Niger, Nigeria, and Sudan
3.6	Agricultural export	Cameroon, Egypt, Ethiopia, Ghana, Mali, Mauritania, Niger, Nigeria, and Sudan

Note: Air temperature is predicted for Sahel [(18°W, 40°E), (10°N, 20°N)], Guinea Coast [(18°W, 15°E) (4°N, 10°N)] and Central South America [(75°W, 0°W), (20°S, 5°S)].

Table 8.2 Candidate predictors: representation and their domains.

No.	Parameter	Variables	Acronym	DOMAIN
1	SST	North Atlantic SST	nAsst	(60°W, 20°W),(5°N,20°N)
2	SST	South Atlantic SST	sAsst	(40°W,10°E),(30°S,10°S)
3	SST	Equatorial Atlantic SST	eqAsst	(30°W,10°E), (10°S,5°N)
4	SST	West Indian Ocean SST	wIsst	(50°E,80°E),(10°S,10°N)
5	SST	East Indian Ocean SST	eIsst	(90°E,110°E),(10°S,10°N)
6	SST	East Pacific SST	eePsst	(150°W,80°W),(10°S, 5°N)
7	SST	Northwest Pacific SST	nwPsst	(150°E,160°W),(10°N,30°N)
8	SST	Southeast Pacific SST	sePsst	(150°W,90°W),(30°S,10°S)
9	Zonal wind	Atlantic zonal wind	eqAu	(55°W,0°),(5°S,15°N)
10	Zonal wind	East Pacific zonal wind	eePu	(150°W, 80°W), (10°S,10°N)
11	Zonal wind	North Indian zonal wind	nIu	(50°E,70°E), (5°N,20°N)
12	Zonal wind	Southern Indian zonal wind	sIu	(50°E,70°E), (15°S,0°)
13	Meri. wind	Atlantic meridional wind	Av	(15°W,10°E),(15°S,5°N)
14	Meri. wind	Indian meridional wind	Iv	(40°E,55°E), (15°S,5°N)
15	Meri. wind	Pacific meridional wind	Pv	(95°W,75°W),(15°N,5°N)

Note: Meri. Denotes meridional.

Table 8.3 Response of climate, stream flow and agricultural yield predictor to kinematic and thermodynamic predictors.

predictors	Climate	Stream flow	Coffee	wheat	Maize	Import value	Export value
eqAsst	√	√	√		√	√	√
SAsst	√				√	√	√
nAsst	√			√	√	√	√
elsst	√	√	√	√			√
wlsst	√	√		√	√	√	√
swlsst		√					
eePsst	√	√	√	√			√
nwPsst			√	√	√	√	
sePsst		√	√	√	√		√
eqAu	√	√	√	√	√	√	√
nlu	√	√		√	√	√	
slu	√		√	√	√	√	
eePu	√	√	√	√	√		
Av	√	√	√	√	√	√	√
lv	√		√		√	√	√
eePv		√				√	√

Table 8.4 Multivariate linear prediction models for tropical North Africa rainfall.

Target	Multivariate algorithms	Lead (month)	R^2_{adj} fit (%)	df
East Sahel	-0.25(nlu)-0.59(eePu)	12	43	15
East Sahel	-0.61(eePu)	9	36	15
East Sahel	-0.33(sAsst)+0.24(nlu)+ 0.34(eqAu)	6	42	15
East Sahel	-0.41(sAsst)-0.48(eePu)	3	40	15
East Sahel	-0.43(eqaAsst)-0.28(eePsst)+0.44(eqAu)	0	59	15
West Sahel	-0.22(nlu)-0.62(eePu)	12	38	15
West Sahel	-0.31(slu)-0.54(eePu)	9	39	15
West Sahel	-0.33(slu)+0.50(eqAu)	6	38	15
West Sahel	-0.36(eqAsst)+0.64(eqAu)	3	49	15
West Sahel	-0.25(eqAsst)-0.33(wlsst)+0.55(eqAu)	0	67	15
Ethiopia	+0.38(Av)-0.52(eePsst)	3	26	47
Ethiopia	-0.24(eqAsst)-0.63(eePsst)-0.21(slu)	0	49	47
Guinea Coast	-0.31(nlu)-0.49(Av)-0.50(eePu)	3	30	47
Guinea Coast	+0.54(eqAsst)+0.44(eqAu)	0	30	47

* represents insignificant. Colinearity has been screened out to the level $r^2 < 10\%$.

Table 8.5 Objective multivariate linear prediction models for tropical North Africa and tropical South America air temperature

Target	Multivariate algorithms	lead (month)	R^2_{adj} fi (%)
a) Tropical North Africa			
Target season: JAS			
Sahel	+0.17(nAsst)-0.29(eqAu)+0.16(nlu)	12	38
Sahel	+0.12(nAsst)+0.13(eePsst)-0.31(eqAu)	9	39
Sahel	+0.19(eqAsst)+0.18(nAsst)-0.27(eqAu)	6	43
Sahel	+0.28(eqAsst)+0.20(eePsst)-0.15(eqAu)	3	47
Sahel	+0.26(sAsst)+0.20(eePsst)-0.15(eqAu)	0	47
Target season: JAS			
Sahel	-0.76(nwPsst)-1.0(sePsst)	12	33
Sahel	+0.34(eePsst)	9	30
Sahel	+0.30(eePsst)	6	33
Sahel	+0.59(sAsst)-0.54(nwPsst)	3	24
Sahel	+0.94(wlsst)+0.28(nlu)	0	36
Guinea Coast	+0.20(sePsst)	12	22
Guinea Coast	+0.17(sePsst)+0.10(slu)	9	22
Guinea Coast	+0.09(nAsst))+0.22(sePsst)	6	31
Guinea Coast	+0.20(sAsst)+0.22(nAsst)-0.17(nlu)	3	51
Guinea Coast	+0.23(eqAsst)+0.20(eePsst)	0	60
Target season: AMJ			
Guinea Coast	+0.27(eePsst)	12	27
Guinea Coast	+0.30(eePsst)	9	34
Guinea Coast	+0.30(eePsst)	6	37
Guinea Coast	+0.36(eqAsst)	3	24
Guinea Coast	+0.63(wlsst)	0	18
b) Tropical South America			
Target season: JFM			
Central	-0.59(nwPsst)-0.53(nlu)	12	18
Central	+0.43(eePsst)+0.93(nwPsst)	9	63
Central	-0.40(eePsst) -0.36(sAsst)+0.79(nwPsst)	6	67
Central	+0.41(eePsst)+0.28(eqAu)	3	72
Central	+0.40(eePsst)	0	55

Table 8.6 Objective multivariate linear prediction models for tropical North Africa and Brazil stream flows.

Targets	Multivariate algorithms	Lead(month)	R^2_{adj} fit (%)	df
Nile	-0.26(Iv)+0.49(eqAu)	12	30	20
Nile	+0.38(eqAsst)+0.23(nlu)-0.62(eePu)	9	38	20
Nile	+0.56(eePv)	6	27	20
Nile	+0.27(nlu)+0.330(Av)+0.47(eqAu)	3	33	20
Nile	+0.64(eePsst)+0.51(eqAu)	0	64	20
Niger	-0.32(Iv)-0.66(eePu)	12	57	13
Niger	-0.23(wlsst)-0.60(eePu)	9	57	13
Niger	-0.33(eqAsst)-0.33(slu)+0.40(eqAu)	6	55	13
Niger	-0.40(eqAsst)-0.33(Iv)+0.45(eqAu)	3	55	13
Niger	-0.40(eqAsst)-0.30(Iv)+0.51(eqAu)	0	65	13
Senegal	-0.51(eePu)	12	34	13
Senegal	+0.51(eqAu)	9	35	13
Senegal	+0.51(eqAu)	6	33	13
Senegal	-0.27(eqAsst)+0.52(eqAu)	3	41	13
Senegal	-0.37(eqAsst)+0.46(eqAu)	0	56	13
Parana	+0.28(Iv)+0.66(sePsst)	12	46	20
Parana	+0.33(eePsst)+0.42(eePu)	9	33	20
Parana	+0.67(eePu)	6	46	20
Parana	0.23(Iv)+0.28(nlu)+0.78(eePu)	3	56	20
Parana	+0.51(Iv)-0.45(eqAu)	0	44	20

Table 8.7 Objective multivariate linear prediction models for tropical North Africa agricultural yields. Note model is developed after linearly detrended.

Target	Multivariate algorithms	Lead (month)	R^2_{adj} fit (%)
a) Coffee			
Cameroon	+0.37(nAsst)-0.32(slu)	12	23
Cameroon	+0.55(nAsst)	9	18
Ethiopia	+0.34(nAsst)-0.56(slu)	12	55
Ethiopia	+0.41(nAsst)+0.30(eqAu)	9	34
Ghana	+0.41(Av)+0.29(Iv)-0.39(slu)	12	45
Ghana	+0.50(Av)+0.30(eqAu)	9	35
Guinea	-0.36(slu)	12	15
Guinea	+0.39(nAsst)+0.41(eqAu)	9	34
b) Maize			
Ethiopia	-0.27(sAsst)+0.37(slu)	12	15
Mauritania	-0.51(sAsst)+0.28(Iv)	12	27
Mauritania	-0.36(sAsst)+0.38(nAsst)	9	26
Mali	+nAsst(0.27)-0.48(Iv)	12	17
Sudan	-0.35(sAsst)-0.25(Iv)	12	13
Sudan	+0.19(nAsst)-0.36(eqAsst)	9	34
c) Wheat			
Ethiopia	-0.30(eqAsst)+0.29(Av)+0.35(Iv)	12	21
Ethiopia	-0.30(sAsst)+0.15(Av)-0.37(nlu)	9	13
Sudan	+0.38(Av)	12	13
Sudan	+0.34(Av)+0.32(slu)-0.45(nlu)	9	34

Table 8.8 Objective multivariate linear prediction models for tropical North Africa agricultural import and export. Linear trends have been removed prior to the construction of the models.

a) Import

Target	Multivariate algorithms	Lead (month)	R^2_{adj} fit(%)
Central Africa	-0.62(Av)	12	36
Central Africa	-0.45(nAsst)	9	25
Ethiopia	+0.34(eqAsst)+0.48(Av)	12	25
Ethiopia	-	9	-
Mali	+0.61(sAsst)-0.26(nAsst)	12	34
Mali	+0.48(sAsst)-0.23(nAsst)	9	23
Mauritania	+0.28(eePsst)+0.37(Av)	12	17
Mauritania	-	9	-
Niger	+0.45(sAsst)+0.23(slu)	12	27
Niger	-	9	-
Nigeria	-0.31(eqAsst)+0.36(slu)	12	20
Nigeria	-	9	-
Sudan	+0.17(eqAsst)+0.36(sAsst)-0.43(wlsst)	12	15
Sudan	-	9	-

b) Export

Target	Multivariate algorithms	Lead (month)	r^2_{adj} fit (%)
Cameroon	+0.27(nAsst)-0.57(slu)	12	
Cameroon	+0.25(nAsst)-0.21(eePsst)+0.23(eqAu)	9	18
Egypt	-0.32(eqAsst)+0.45(nwPsst)	12	20
Egypt	-	9	-
Ethiopia	+0.60(sAsst)-0.39(sePsst)	12	28
Ethiopia	+0.59(sAsst)-0.45(nAsst)-0.37(eePsst)	9	41
Ghana	+0.40(nwPsst)-0.26(slu)	12	27
Ghana	+0.35(nwPsst)+0.48(Av)	9	31
Guinea	-0.42(eqAsst)+0.22(eePsst)+0.51(nwPsst)	12	30
Guinea	+0.43(nAsst)-0.40(nwPsst)-0.37(lv)	9	28
Mali	0.23(eePsst)+0.26(Av)+0.35(lv)	12	17
Mali	-	9	-
Mauritania	-0.31(eqAsst)-0.45(Av)-0.33(lv)	12	39
Mauritania	-0.46(eqAsst)-0.41(eqAu)	9	31
Niger	+0.24(nAsst)-24(sAsst)-0.41(slu)	12	32
Niger	+0.42(nAsst)+0.37(eqAu)	9	34
Nigeria	+0.36(nAsst)-0.31(sAsst)-0.43(slu)	12	42
Nigeria	+0.35(nAsst)+0.33(eqAu)	9	24
Sudan	-0.43(sAsst)+0.24 (sePsst)	12	12
Sudan	-0.45(slu)	9	15

Table 8.9 Objective multivariate linear prediction models for tropical North Africa and tropical South America climate and stream flow after linearly de-trended.

Target zones / regions	Multivariate algorithms boreal summer rainfall	Lead (month)	R^2_{adj} fit (%)
East Sahel	+0.37(eqAsst) +0.27 (eqAu)	12	15
East Sahel	+0.41(eqAsst)+0.21(eqAu)	9	16
East Sahel	-0.42(eePsst)	0	18
West Africa	+0.49(eqAsst)+0.34(eqAu)	12	26
West Africa	+0.52(eqAsst)+0.30(eqAsst)	9	27
West Africa	+0.30(eqAu)	3	9
West Africa	-0.27(eePsst) + 0.39(eqAu)	0	29
Northern Congo	+0.35(eqAsst) + 0.23(eqAu)	12	12
	Boreal Summer Temperature		
Sahel Region	-0.32(eqAsst)	12	10
Sahel Region	-0.42(eqAsst) -0.38(nlu)	9	21
Sahel Region	+0.32(sePsst)	6	10
Sahel Region	+0.38(eePsst)	3	15
Sahel Region	+0.57(eePsst)	0	33
Guinea Region	+0.33(sePsst)	6	10
Guinea Region	+0.37(nAsst)+0.29(eqAu)-0.39(nlu)	3	31
Guinea Region	+0.34(eqAsst)+0.41(eePsst)	0	32
	Boreal Winter Temperature		
Central South America	-0.92(sAsst) +0.82(eePsst)	9	35
Central South America	+0.88(eePsst)	6	52
Central South America	+0.87(eePsst)+0.70(eqAu)	3	76

Note: Models are not shown for no model hindcast fit (e.g. for East Sahel rainfall, there is no model for 6- and 3-month lead-times).

Table 8.10 Autocorrelation function of zonal wind and SST indices based on continuous standardised raw data from 1950-1998.

Lead (month)	eqAu1000	nlu1000	slu1000	eqPu1000	eqAsst	aSSTd	pSSTi
0	1.00	1.00	1.00	1.00	1.00	1.00	1.00
1	0.68	0.84	0.78	0.53	0.86	0.86	0.76
2	0.32	0.46	0.42	0.39	0.51	0.50	0.37
3	0.10	-0.03	-0.02	0.29	0.04	0.02	0.11
4	0.19	-0.48	-0.43	0.32	-0.42	-0.45	0.15
5	0.47	-0.80	-0.72	0.38	-0.75	-0.79	0.35
6	0.59	-0.91	-0.82	0.40	-0.87	-0.92	0.41
7	0.44	-0.79	-0.71	0.34	-0.76	-0.79	0.19
8	0.15	-0.48	-0.43	0.27	-0.44	-0.46	-0.14
9	0.03	-0.03	-0.02	0.24	0.01	0.00	-0.30
10	0.24	0.45	0.40	0.29	0.46	0.46	-0.15
11	0.59	0.82	0.74	0.44	0.80	0.81	0.14
12	0.77	0.96	0.87	0.46	0.93	0.93	0.28

Table 8.11 Autocorrelation function of zonal wind and SST indices based on continuous filtered (1.5-16-year) data from 1950-1998.

Lead (month)	eqAu1000	nlu1000	slu1000	eqPu1000	eqAsst	aSSTd	pSSTi
0	1.00	1.00	1.00	1.00	1.00	1.00	1.00
1	0.99	0.98	0.98	0.99	0.98	0.98	0.98
2	0.95	0.92	0.92	0.96	0.93	0.93	0.93
3	0.90	0.83	0.84	0.92	0.87	0.86	0.86
4	0.84	0.72	0.75	0.86	0.78	0.77	0.76
5	0.76	0.60	0.63	0.79	0.68	0.67	0.64
6	0.68	0.47	0.51	0.72	0.58	0.56	0.51
7	0.59	0.34	0.40	0.64	0.48	0.44	0.38
8	0.51	0.21	0.28	0.55	0.38	0.33	0.25
9	0.43	0.10	0.18	0.47	0.29	0.23	0.12
10	0.37	0.00	0.10	0.39	0.21	0.14	0.00
11	0.31	-0.08	0.03	0.32	0.15	0.07	-0.10
12	0.27	-0.14	-0.30	0.26	0.10	0.01	-0.18

Table 8.12 Cross-validation of prediction for rainfall, temperature and stream flow using hit rate (%) and correlation coefficient (multiplied by 100) based on independent (non-training) data.

A) target season and variable: boreal summer rainfall			
Target area	Lag (month)	Hit rate (%)	Correlation *100
East Sahel	12	76	77
	9	88	70
	6	77	64
	3	70	63
West Sahel	12	85	80
	9	71	78
	6	77	68
	3	70	67
b) Target season and variable: Boreal summer temperature			
Sahel Region	12	70	67
	9	80	65
	6	70	77
	3	68	43
Guinea Region	12	67	33
	9	75	36
	6	67	48
	3	74	71
c) Target season and variable: Stream flow			
Niger at Mali	12	67	45
	9	55	70
Parana in Brazil	12	57	75
	9	55	85

Note: Independent validation data for rainfall: 1950-65 and 1981-1996; for temperature1950-165 and 1981-1996; for stream flow: 1950-1959 and 1980-1989.

CHAPTER 9

DISCUSSION, CONCLUSION AND RECOMMENDATION

In this Chapter, the main results are summarised. The main contribution of this study to the understanding of climate variability and prediction in tropical North Africa is documented.

9.1 Discussion

Sahelian rainfall has been studied in characterisation and possible mechanisms using observation and numerical studies. The Sahel mode of rainfall variability is characterised by a decadal oscillation (Lamb 1978a,b; 1979; 1980; 1982a,b; 1983; Nicholson 1981, 1993, 1998; Ward, 1998). This characterisation can be revealed using wavelet analysis by filtering variability < 1.5-years.

The source of this variability of Sahel is related to the Atlantic SST dipole (Lough, 1986; Palmer, 1986; Semazzi et al., 1996; Fontaine et al., 1998; Folland et al., 1986, 1991), ENSO (Palmer et al., 1992; Ward, 1992; Janicot et al., 1998; Camberlin et al., 2001; Hastenrath, 200; Gist and Nicholson, 2001), and meridional gradient of entropy (Eltahir and Gong, 1996). But, the modes of transmission of these signals to Sahel climate are not sufficiently covered. In this study, it found ENSO, Atlantic SST and IOD transmit influences to African Monsoon through the Atlantic Zonal Circulation. The Pacific Walker Circulation and Atlantic Zonal Circulation work in anti-phase to enhance convection in South America and East Pacific and suppress convection in tropical North Africa and West Pacific during El Nino episodes and vice versa. ENSO and Atlantic SST dipole influence the local climate of Sahel and Guinea Coast through meridional Overturning. Warming in east Pacific and/or Atlantic SST dipole reversal (cold north) results in subsidence over west Sahel and rising motion along the Guinea Coast. Here it is found that ENSO damps other local east-west or north-south

SST modulation during peak activity. As a result, the equatorial Atlantic SST is a damped mode in relation to its impact on tropical North Africa climate, despite operating with similar air-sea interaction as east the Pacific (Zebiak, 1993; Xie, 2001; Ruiz-Barradas et al., 2000). But, when ENSO teleconnection is weak or absent, the Atlantic SST modes exert their influence on African climate.

The mutidecadal-drying trend of Sahel climate has been simulated using coupled climate-vegetation feedback simulation (Xue et al, 1990; Xue et al., 1993) based on Charney (1975) and Charney et al. (1977) albedo-rainfall-vegetation theory. Zeng et al (1999) reproduced the Sahel rainfall using coupled-ocean-atmosphere-land-vegetation model, where atmosphere-ocean coupling is responsible for the low-frequency variability while the land-surface feedback is found to increase the interannual Sahel rainfall variability.

A phenomenon that comes closest to exhibiting periodic characteristics in the mean zonal winds of the equatorial stratosphere is the quasi-biennial oscillation (QBO). This oscillation has zonally symmetric easterly and westerly wind regimes (easterly and westerly phases) that alternate regularly with a period varying from 24 to 30 months. It is depicted at 50-30-hPa levels. QBO derives its energy and momentum from the tropical troposphere through mixed-Rossby-gravity waves and Kelvin waves. The energy of these gravity waves leaks through the tropopause.

The west phase of QBO appears to be in-phase with the Pacific SST and Atlantic SST dipole. This QBO-ocean coupling results in suppressed convection over tropical North Africa.

When the Pacific SST signal is weak and a reversal of tropical Atlantic dipole mode occurs, then the Atlantic dipole modulates the surrounding regions through the meridional Overturning shifting the centres of convection (the ITCZ) to

mode of variability of this index during boreal summer is identified. The wet minus dry years is selected for composite analysis. The composites reveal the Atlantic Zonal Circulation with dipole structure in moisture, vertical velocity, velocity potential, and convection between tropical North Africa and tropical South America. The SST reveals a cold tongue over the east Pacific (La Nina signal) and a feeble anomaly over the equatorial Atlantic. The composite analysis unravels principal mechanisms that are responsible for the tropical North Africa climate variability. The interplay between the Atlantic-Walker circulations determines the large-scale velocity potential dipole and convection polarity between tropical North Africa and tropical South America. The swing of these large-scale upper-level divergent and convection modes govern the climate variability of tropical North Africa and South America. The variability of these modes is attributable to the pulsation and perturbation of the Atlantic Zonal Circulation.

Correlation analysis is also performed to investigate the link between East Sahel rainfall and the tropical Circulation. Significant results are found that supports the composite structure. The correlation with SST reveals tropical Atlantic SST dipole (negative in the tropical south Atlantic) that is coherent in time up to 6-month lead. Negative correlation is also established between Northeast Africa hydroclimate and SST over the tropical Pacific Ocean cold tongue region. At longer lead-time, the Pacific SST dipole (positive in Northwest and negative in Southeast) becomes the principal structure and is important for prediction purposes.

In the horizontal wind field, the East Sahel is closely tied to the Atlantic westerlies at lower level/ easterlies at upper level and therefore the Atlantic Overturning. The reverse relationship holds between the rainfall over East Sahel and the Pacific Walker Circulation. The moisture field, the vertical velocity, convection, and precipitable water reveal a wave number one dipole structure between tropical North Africa (positive) and South America / South Atlantic (negative). The

other interesting result is the vertical structure of the vertical velocity in the equatorial latitudes with positive correlation from east Pacific to Atlantic throughout the atmosphere, and negative correlation in west Pacific (150°E to 150°W) and in tropical North Africa. The main point that arises from this representation is the agreement between tropical North Africa and West Pacific and the contrast with the east Pacific and tropical South America convection. The coherency and physical link between the Atlantic velocity potential dipole, ENSO and tropical North Africa rainfall is revealed.

ENSO signals are transmitted to tropical North Africa through the kinematic component of the climate system. An El Nino perturbs the east-west divergent circulation of the Pacific Walker and the Atlantic Zonal Circulation, strengthening of the Africa Easterly Jet (AEJ). Strong AEJ produces a north-south circulation (Hadley Circulation) with rising motion and enhanced convection over Guinea Coast and suppressed convection in West Sahel. Warm episodes in the equatorial Atlantic also influence tropical North Africa in a similar way. The combined effect of warm equatorial east Pacific and cold equatorial Atlantic on tropical North Africa is also investigated using a GCM simulation. The result is that the ENSO signal dominates the equatorial Atlantic SST signal. In this relation, the equatorial Atlantic SST is a 'slave' to equatorial east Pacific SST. The result has enormous practical implication in analysing and predicting tropical North Africa climate. If the equatorial Atlantic SST shows optimal condition for rainfall production over tropical North Africa, it does not necessary mean that wet condition prevails in this region if the kinematic influences of ENSO are on the scene. The tropical North Africa is also sensitive to one of the most important mode of variability of the tropical Atlantic SST: the tropical Atlantic SST dipole. Positive SST in the north and negative in south in tropical Atlantic enhances convection the Sahel at the expense of the Guinea Coast.

The principal modes of global east-west divergent circulations are studied in search of teleconnections with the Atlantic Zonal Circulation. The stability and

coherency of tropical North Africa climate is examined in this context. The result reveals that years with a strong equatorial Atlantic low-level wind and transverse Monsoon Circulation concur to reproduce the large-scale velocity potential structure and the convection polarity between tropical North Africa and South America. The anti-phase relationship between the east-west circulations of the Pacific and Atlantic is the main feature.

QBO and globally integrated angular momentum also modulates the tropical North Africa climate variability together with ENSO. Positive angular momentum suppresses convection over tropical North Africa, as does a QBO west phase.

Modes of equatorial subsurface ocean temperature are investigated using global ocean data assimilation model interpolated fields. The most dominant modes of variability are identified using singular value decomposition for the first 250-m depth of Pacific, Atlantic and Indian Ocean. The temporal component is decomposed into seasonal / annual cycles and interannual timescales using wavelet transform. The interannual timescale of the subsurface temperature is also analysed co-spectrally using cross-wavelet modulus with Atlantic, Pacific and Indian Ocean east-west divergent modes. The ENSO signal in the subsurface thermocline temperature is also identified. The part of subsurface thermocline temperature that is sensitive to ocean-atmosphere is found.

Stable and skilful linear multivariate models are developed for rainfall, temperature, stream flow, and agriculture production for tropical North Africa that surpass current (2002) operational practice with longer lead-times and higher hit rates. Predicting the tropical climate at a year ahead is attained owing to the memory and stability of the equatorial Ocean winds associated with the Atlantic Overturning teleconnection to the Pacific. A cautionary note is provided on the impact of the "step" in global climate in the late 1970s that appears to bias some of the predictability.

The main contribution of this study is that the tropical North Africa climate swing is governed by Atlantic Zonal Circulation through coupling with the Pacific ENSO and its Walker Circulation. The Atlantic velocity dipole is related to the subsurface temperatures in all equatorial oceans. An understanding of the heat content of tropical oceans therefore contributes to the understanding of ocean-atmosphere coupling in relation to tropical North African climate.

9.3 Extension to theoretical framework: Baroclinic and coupled Rossby waves in Pacific Ocean

Baroclinic Rossby wave equation (e.g., White, 2000) is given as:

$$\frac{\partial \eta}{\partial t} + C_R \frac{\partial \eta}{\partial x} = -\left(\frac{\rho_0'}{\rho_0}\right) \text{curl}\left[\frac{\tau}{f\rho_0}\right]$$

where η represents the sea level height (SLH), C_R represents the westward phase speed for free oceanic baroclinic Rossby waves and τ represents wind stress. ρ_0 is the mean density of thermocline and ρ_0' reduced density (anomaly from the mean) and curl represents the derivative for vorticity.

The phase speed for baroclinic Rossby wave is

$$C_R = -\frac{\beta g' H}{f^2} \qquad (9.1)$$

where $\beta = \frac{2\Omega \cos(\phi)}{a}$ $f = 2\Omega \sin(\phi)$, g' is reduced gravity (0.04 m s^{-2}) and H (160 m) is thermocline temperature.

Eqn. 9.1 gives the theoretical value of the free Rossby Wave phase speed. Its phase speed at 10°S in the Pacific Ocean is computed using the values shown in Table 9.1. This speed happens to be -0.22 m s^{-1}. Killworth et al. (1997) found a phase speed of -0.23 m s^{-1} for free baroclinic Rossby at the same latitude.

Observed coupled Rossby Wave

An observed Rossby wave phase speed is computed in the equatorial Pacific using the basic wave characteristic (phase speed = period/wavelength). The period is determined from its wavelet modulus (Fig. 7.29) and is taken to be 4 years. The half wavelength is obtained from the EOF1 of equatorial subsurface temperature (Fig. 7.13a) and is 4500 km (full wavelength = 9000 km). This allows a computation of wave speed, 0.07 m s^{-1}. This phase speed is one-third of the theoretical phase speed of the free baroclinic Rossby Wave speed. The deceleration of the observed wave is due to coupling with the Pacific Walker Cell that generates a preferred longitude for maximum thermocline changes and maximum convective coupling that slows or anchors the propagating of the wave. When decoupling occurs, it is speculated that a tendency of the angular momentum associated with the Walker Cell is produced and as a result the phase speed of the Rossby Wave increases. In short, ocean-coupling in Pacific slows the Rossby Wave.

White (2000) found a zonal phase speed of -0.13 m s^{-1} at 10°S in the Pacific Ocean for tropical coupled Rossby Waves in the longitude limit (8000 km) based on the dispersion relation of tropical coupled Rossby Wave. Based on the slope of distance-time plots of SLH, SST and meridional surface wind at the same latitude, he obtained -0.15 ± 0.03 m s^{-2} at 10°S phase speed, two-thirds of the free wave speed and twice of the 'observed' coupled phase speed found in this study. This difference between the result elicited here and that of White (2000) is accounted for the latitude considered.

9.4 Recommendation

a) The simulation with CCM3 failed to reveal the Atlantic Zonal Circulation but was capable of reproducing the ENSO signal and its influences within the tropical Pacific Ocean. A further study is required using coupled general circulation models with full physics to understand the mechanisms responsible for maintaining Atlantic and Pacific Circulation zonal overturning circulations.

b) Tropical subsurface thermocline and heat content require a comprehensive study to find additional signals beside ENSO that will assist to climate prediction and understanding of ocean-atmosphere interaction.

c) The transverse Monsoon Circulation appears to play a vital role in the tropical North Africa climate variability through the Tropical Easterly Jet. This circulation deserves further investigation to understand the physical mechanisms of this teleconnection in relationship to tropical North African climate.

d) The results obtained in this study should be incorporated into the West Africa Climate Outlook Forum Training Programme.

Table 9.1 Constants and values used in computing free baroclinic Rossby wave.

Universal constants	Value
Angular momentum of the earth (Ω)	$7.25*10^{-11}$ s^{-1}
Radius of the Earth (a)	6378000 m
Theoretical computation	
Coriolis parameter f^2 at 10°S	f= 2Ωsin (latitude) $f^2 = 2.24*10^{-11}$ s^{-1}
β at 10°S	$2.25*10^{-11} m^{-1} s^{-1}$
Depth (H) from Fig. 7.13a	160 m
Reduced gravity from: http://iridl.ldeo.columbia.edu/expert/SOURCES/.LEVITUS94/.ANNUAL/.rhoa/	0.04 m s^{-2}
Free baroclinic Rossby Wave phase speed at 10°S	-0.22 m s^{-1}

REFERENCES

Afifi, A.A., and V. Clark, 1996: Computer aided multivariate analysis. Third edition. Texts in Statistical Science. Chapman & Hall. 455 pp.

Amarasekara, N. A., R. F. Lee, E.R. Williams, and E. A. B Eltahir, 1997: ENSO and the natural variability in flow of tropical rivers. J. Hydrol., 200, 24-39.

Barnston, A. G., and Y. He, 1996: Still of canonical correlation analysis forecasts of 3-month mean surface climate in Hawaii and Alaska. J. Climate, 9, 2579 - 2605.

Barnston, A. G and T, M. Smith, 1995: Specification and prediction of global surface temperature and prediction from global SST using canonical correlation analysis. Part 11. Prediction. J. Climate, 9, submitted.

Barnston, A. G, 1994: Linear statistical short-term climate predictive skill in the Northern Hemisphere. J. Climate, 7, 1513 - 1564.

Barnston, A. G and C.F. Ropelewski, 1992: Prediction of ENSO episodes using canonical correlation analysis. J. Climate, 5, 1316-1245.

Battisti, D.S. and E.S. Sarachik, 1995: Understanding and predicting ENSO. Rev. *Geophys.*, **33**, Suppl.

Bliss, E. W., 1925: The Nile flood and world weather. Mem. Roy. Meteoro. Soc., 4, 36, 53-84.

Björnsson, H. and S. A. Venegas, 1997: A manual for EOF and SVD analyses of climatic data. Centre for Climate and Global Change Research, McGill University, Canada. 52 pp.

Bretherton, C. S., C. Smith and J. M. Wallace, 1992: An intercomparison of methods for finding coupled patterns in climate data. J. Climate, 5, 541-560.

Burpee, R.W., 1992: The origin and structure of easterly waves in the lower troposphere. J. Atmos. Sci., 29,77-90.

Camberlin, P., S. Jaincot and I. Poccard, 2001: Seasonal and atmospheric dynamics of the teleconnection between African rainfall and tropical seas-surface temperature: Atlantic vs. ENSO. Int. J. Climatol., 21, 973-1005.

Camberlin, P., 1997: Rainfall anomalies in the source region of the Nile and their connection with Indian summer monsoon. *J. Climate*, **10**,1380-1392.

Camberlin, P.,1995: June-September rainfall in Northeast Africa and atmospheric signals over the tropics: A zonal perspective. Int. J. Climatol.,15, 773-783.

Carton, J.A., G. Chepurin, X. Cao, and B.S. Giese, 1999: A simple ocean data assimilation retrospective analysis of the global ocean 1950-1995, J. Phys. Oceanogr., (accepted).

Carton, J. A., X. Cao, B. S. Giese, and A. M. da Silva, 1996: Decadal and interannual SST variability in the tropical Atlantic. Phys. Oceanogr., 26, 1165-1175.

Carton, J. A., and B. Huang, 1994: Warm events in the tropical Atlantic. J. Phys. Oceanogr., 24, 888-903.

Chang, P., R. Ji, and H. Li, 1997: A decadal climate variation in the tropical Atlantic Ocean from thermodynamics air-sea interactions. Nature, 385, 516-518.

Charney, J.G., W.J. Quirk, S. -H. Chow, and J. Kornfield, 1977: A comparative study of the effects of albedo change on drought in semi-arid regions. J. Atmos. Sci., 34, 1366-1385.

Charney, J.G, 1975: Dynamics of desert and drought in the Sahel. Quart. J. Roy. Meteor. Soc., 101, 193-202.

Cunnington C., and P.R. Rowntree, 1986: Simulation of the Saharan atmosphere-dependence on moisture and albedo. Quart. J. Roy. Meteor. Soc., 112, 971-999.

Curtis, S. and Hasternrath, 1995: Forcing of anomalous sea surface temperature evolution in the tropical Atlantic during Pacific warm events. J. Geophys. Res., 100, 15835-15847.

Delecluse, P., J. Servain, C. Levy, K. Arpe, and L. Bengtsson, 1994: On the connection between the 1984 Atlantic warn event and the 1982-1983 ENSO. Tellus, 46A, 448-464.

Dirmeyer, P.A., and J. Shukla, 1996: The effect on regional and global climate of expansion of the world's deserts. Quart. J. Roy. Meteor. Soc., 122, 451-482.

Duing, W., and A. Leetmaa, 1980: Arabian Sea cooling: A preliminary heat budget. J. Phys. Oceanogr., 10, 307-312.

Eltahir, E A B, and Wang. G. 1999: Nilometers, El Nino and climate variability. Geophys. Res. Letters, 26, 4, 489 - 492.

Eltahir, E A B, 1996: El Nino and the natural variability in the flow of the Nile. Water Resources Research, 32, 131-137.

Eltahir, E A B, C. Gong, 1996: Dynamics of wet and dry years in West Africa. J. Climate, 9, 1030-1042.

Enfield, D. B., and D. A. Mayer, 1997: Tropical Atlantic SST variability and its relation to El Nino-Southern Oscillation. J. Geophys. Res., 102 C1, 929-945.

FAO, 2002: http://apps.fao.org/page/collections.

Folland C. K., J. A. Owen, and M. N. Ward: 1991: Prediction of seasonal rainfall in Sahel region of Africa using empirical and dynamical methods. J. Forecasting, 10, 21-56.

Folland C. K., Palmer, T. N. and D. E. Parker, 1986: Sahel rainfall and world-wide sea temperature, 1901-85: Nature, 320, 602-607.

Fontaine B., Trzaska, and Janicot, 1998: Evolution of the relationship between near global and Atlantic SST mode and the rainy season in West Africa: Statistical analyses and sensitivity experiments. Climate Dynamics, 14, 353-368.

Fontaine B. and S. Janicot, 1992: Wind-field coherence and its variation over West Africa. J. Climate, 5, 512-524.

Fontaine B., S. Janicot and V. Moron, 1995: Rainfall anomaly patterns and wind field signals over West Africa in August(1958-1989). J. Climate, 8, 1503-1510.

Glanz, M. H., R. W. Katz, N. Nicholls, 1991: Teleconnection Linking Worldwide climate anomalies: scientific basis and societal impact. Cambridge University Press: Cambridge.

Glanz, M. H., 1996: Currents of change: El Nino's impact on climate and society. Cambridge University Press: Cambridge.

Grist, J. P, S. E. Nicholson, and A. I. Barcilon, 2002: Easterly waves over Africa. Part 11: Observed and modeled contrasts between wet and dry years. Mon. Wea. Rev., 130, 212-225.

Grist, J. P, S. E. Nicholson, 2001: A study of the dynamic factors influencing the rainfall variability in the West Africa Sahel. J. Climate, 14, 1337-1359.

Goddard L., S. J. Mason., S. E. Zebiak, C. F. Ropelewski, R. Basher and M. A. Cane, 2001: Current approaches to seasonal-to-interannual climate prediction. Int. J. Climatol., 21, 1111-1152.

Hack, J. J., B. A. Boville, J. T. Kiehl, P. J. Rasch, and D. I. Williamson, 1994: Climate statistics from the National Centre for Atmospheric Research Community Climate Model. CCM2. Gephys. Res., 99, 20785-20813.

Hammer, G.L., N. Nicholls, and C. Mitchell, 2000. Applications of Seasonal Climate Forecasting in Agricultural and Natural Ecosystems: The Australian Experience. Edited by G. L. Hammer et al, pp. 149-160. The Netherlands: Kluwer Academic Publishers.

Hastenrath, S., 2000: Interannual and longer-term variability of upper-air circulation over the tropical Atlantic and West Africa in Boreal Summer. Int. J. Climatol., 20, 1415-1430.

Hastenrath, S, L. Greischer and van Heerden, 1995: Prediction of summer rainfall over South Africa. J. Climate, 8,1511-1518.

Hastenrath, S, and P. J. Lamb, 1977: Some aspect of circulation and climate over eastern equatorial Atlantic. Mon. Wea. Rev., 106, 1280-1287.

Hirst, A.C., 1986: Unstable and damped equatorial modes in simple coupled ocean-atmosphere models. J. Atmos. Sci., 43, 606-630.

Hirst A.C., and S. Hastenrath, 1983: Atmospheric-ocean mechanisms of climate anomalies in the Angola-Tropical Atlantic sector. J. Phys. Ocean, 13, 1146-1157

Hirst, A.C., 1986: Unstable and damped equatorial modes in simple coupled ocean-atmosphere models. J. Atmos. Sci., 43, 606-630.

Hisard, P., 1980: Observation de réponses de type <<El Nino>> dans l'Atlantique tropical oriental Golfe de Guinea. Oceanol. Acta, 3, 69-78.

Holton, J. R., 1979: An Introduction to Dynamic Meteorology. Second edition. International Geophysical Series, Vol. 23, Academic Press, 391 pp.

Horel, J. D. and J. M. Wallace, 1981: Planetary scale atmospheric phenomena associated with the Southern Oscillation. Mon. Wea. Rev., 109, 813-829.

Hsieh, W.W. and B. Tang, 1998: Applying neural network models to prediction and data analysis in meteorology and oceanography. Bull. Am. Meteorol. Soc. 79: 1855-1870.

Huang, B. and J. Shukla, 2002: The interannual variability in the tropical Indian Ocean and its decadal modulation. Extended Abstract. American Meteorological Society 13th Symposium on Global Change and variations, 2002 Annual Meeting.

Hurrell, 2000: Observations of tropical Atlantic variability. Http://www.asp.ucar.edu/colloquium/2000/Lectures/hurrell2.html.

Iizuka, S., 2001: Simulation of an air-sea interaction in the Indian Ocean with a coupled GCM. Symposium on " the Ocean-Atmosphere Coupled Dynamics in the Indian Ocean". Abstracts. December 17-18, 2001, Tokyo Prince Hotel.

Janicot, S., A. Harxallah, B. Fontaine, and V. Moron, 1998: West African monsoon dynamic and eastern equatorial Atlantic and Pacific SST anomalies (1970-1988). J. Climate, 11, 1874-1882.

Jury, M.R., 2002: Thermocline oscillation across the Indian Ocean as a key mechanism of southern Africa climate variability (abstract). South African Society for Atmospheric Sciences (SASAS) 2002 Conference (26 to 28 August 200).

Jury, M.R, and A. Philipp, 2002: Regionalisation of African rainfall and application to interannual prediction. Submitted to Journal.

Jury, M.R, 2001a: The off-equatorial Rossby wave as the dominant mechanism of Indian Ocean Variability. Symposium on " the Ocean-Atmosphere Coupled Dynamics in the Indian Ocean". Abstracts. December 17-18, .2001, Tokyo Prince Hotel.

Jury, M.R, 2001b: Development of optimum statistical long-range forecast models of summer climate and hydrological resources over Southern Africa. A report to the Water Research Commission, based on research in the period 1997-2002.

Jury, M.R, 2001c: Economic impacts of climate variability in South Africa-development of models to predict growth rate. Paper presented in SASAS (South Africa Society of Atmospheric Science), 607 September 2001, Cape Town, South Africa.

Jury, M.R, 2001d:A review of research on African climate variability and avenues for further exploration. Submitted to Climate Research.

Jury, M. R., H. Mulenga and H. Rautenbrach, 2000: Tropical Atlantic variability and Indo-Pacific simulation. The Global Atmosphere and Ocean System, 7, 107-124.

Jury, M.R and J.-L. Melice, 2000: Analysis of Durban rainfall and Nile river flow 1871-1999. Theor. Appl. Climatol., 67,161-169.

Jury, M.R, 1999: Interannual variability of Africa river flows and associated climate structure. Preprint volume of the Eight Conference on Climate Variation, 13-17 September 1999, Denver, CO. by the AMS, Boston, MA.

Jury, M.R, H. M. Mulenga, and S. J. Mason: 1999: Exploratory long-range models to estimate summer climate variability over South Africa. J. Climate, 12, 1892-1899.

Jury, M.R, H. M. Mulenga, and S. J. Mason and A. Brandao 1997: Development of objective statistical system to forecast summer rainfall over southern Africa. WRC Report No. 672/1/97.

Jury, M.R., 1996: South-east Atlantic warm events: composite evolution and consequences for southern Africa climate. S. Afr. J. Marine Science, 17, 21-28.

Jury, M.R, 1993: Regional teleconnection patterns associated with summer rainfall over South Africa, Namibia and Zimbabwe. Int. J. Climatol., 16, 135-153.

Kalnay, E., M. Kanamitsu, R. Kistler, W. Collins,D. Deaven, L. Gandin, M. Iredell, S. Saha, G. White, J. Woollen, Y. Zhu, A. Leetmaa, R.Reynolds, M. Chelliah, W. Ebisuzaki, W.Higgins, J. Janowiak, K. C. Mo, C. Ropelewski, J. Wang, Roy Jenne, and D. Joseph,1996: The NCEP/NACR reanalysis 40-year project. Bull. Amer. Meteor. Soc., 77, 437-471.

Kiehl, J. T., B. Boville, B. Briegleb, J. Hack, P. Rasch, and D. Williamson, 1996: Description of the NCAR Community Climate Model (CCM3). NCAR Technical Note, NCARE/TN-420+STR, Boulder, Colorado.

Killworth, P .D, D. B. Chelton, and R. A. deZoeke, 1997: The speed of observed and theoretical long extratropical planetary waves. J. Phys. Oceanogr., 27,1946-1966.

Kirtman, B. P., 1996: Ocean Rossby Waves and the ENSO period in a coupled model. Centre for Ocean-Land-Atmosphere Studies (COLA), COLA Report 28. Http://grads.iges.org/reps/rep28/colarep28.html.

Kistler, E. Kalnay, W. Collins, S. Saha, G. White, J. Woolen, M. Chelliah, W. Ebisuzaki, M. Kanamitsu, V. Kousky, H. van den Dool, R. Jenne, and M. Fiorino, 2000: The NCEP/NCAR 50 year reanalysis. Submitted to the Bull. Amer. Meteo. Soc.

Koteswaram, P., 1958: The easterly jet stream in the tropics. Tellus, 43-57.

Krishnamurti, T. N., 1971: Observational study of tropical upper tropospheric motion field during the Northern Hemisphere summer. J. App. Meteor., 10, 1066-1096.

Krishnamurti, T. N., 1979: Tropical meteorology, compendium of meteorology. Ed. by A. Wan-Nielsen, WMO No., 364. 428 pp.

Kwon, H. J., 1989: A reexamination of the genesis off African waves. J. Atmos., Sci., 46, 3521-3631.

Lamb, P. J. and R. A. Pepper, 1992: Further case studies of tropical Atlantic surface atmospheric and oceanic patterns associated with sub-Saharan drought. J. Climate, 5, 476-488.

Lamb, P. J., 1983: West Africa water vapor variations between contrasting Sub-Saharan rainy seasons. Tellus, 35A, 198-212.

Lamb, P. J., 1982b: Comments on "West African Rainfall variations and tropical Atlantic sea surface temperature". Climate Monitor., 11, 46-49.

Lamb, P. J., 1982a: Persistence of Sub-Saharan drought. Nature, 299, 46-48.

Lamb, P. J., 1980: Sahelian drought. New Zealand J. Geogr., 68, 12-16.

Lamb, P.J., 1979: Some perspective on climate and climate and dynamics. Progress Phys. Geogr., 3, 215-235.

Lamb, P. J. and R. A. Pepper, 1978: Further case studies of tropical Atlantic surface atmospheric and oceanic patterns associated with sub-Saharan drought. J. Climate, 5, 476-488.

Lamb, P. J., 1978a: Case studies of tropical Atlantic surface circulation patterns during recent Sub-Saharan weather anomalies: 1967 and 1968. Mon. Wea. Rev., 106, 482-491.

Lamb, P. J., 1978b: Large-scale tropical Atlantic circulation patterns associated with Sub-Saharan weather anomalies. Tellus, 30, 240-251.

Landsea, C.W, W. M. Gray, P. W. Mielke, Jr. K. J. Berry, and R. K. Taft, 1998: June to September rainfall in North Africa: Verification of our 1998 forecast. http:// tropical.atmos.colostate.edu/forecasr/1998/.

Lau, K. -M., and H. -Y Weng, 1995: Climate signal detection using wavelet transform: How to make a time series sing. Bull. Amer. Meteor. Soc., 76, 2391-2402.

Latif, M., and T.P. Barnett, 1995: Interaction of the tropical oceans. J. Climate, 8, 952-964.

Lau, N. -C., and M. J. Nath, 1996: The role of the atmosphere: bridge in making tropical Pacific ENSO events to extratropical SST anomalies. J. Climate, 9, 2036-2057.

Li, T, C. P. Chang, B. Wang, Y. -S Zhang, and H . Annamalai, 2001: A theory for the Indian Ocean dipole mode. Symposium on " the Ocean-Atmosphere Coupled Dynamics in the Indian Ocean". Abstracts. December 17-18, 2001, Tokyo Prince Hotel.

Lorenz, E. N., 1990: Can chaos and intransitivity lead to interannual variability? Tellus, 42A, 378-389.

Lorenz, E. N., 1984: Irregularity; a fundamental property of the atmosphere. Tellus, 36A, 98-110.

Lorenz, E. N., 1963: Deterministic non-periodic flow. J. Atm. Sci., 20, 130-141.

Lough, J. M., 1986: Tropical Atlantic seas surface temperatures and rainfall variations in Sub-Saharan Africa. Mon. Wea. Rev., 114, 561-570.

Markham, C. G., and D. R. McLain, 1977: Sea surface temperature related to rain in Ceara, Brazil. J. Appl. Meteor., 13, 176 -179.

Mason S.J., 2000: Definition of technical terms in forecast verification scores. Available in the International Research Institute for Climate Prediction web site http://iri.ideo.Columbia.edu/outreach/publication/ seminar/ Quality.

Mason, S. J., A. M. Joubert, C. Cosijin, and S. J. Crimp, 1996: Review of the current state of seasonal forecasting techniques with application to South Africa. WaterSA, 22,203-209.

Matitu, M. R,2001: Response of tropical Africa rainfall to zonal circulations over adjacent oceans. MSc Thesis, University of Zululand.

Matsuno T., 1966: Quasi-geostrophic motions in the equatorial area. J. Met. Soc. Japan, 44, 25-42.

Merle, J., 1980a: Seasonal heat budget in the equatorial Atlantic Ocean. J. Phys. Oceanogr., 10, 464-469.

Merle, J., 1980b: Variabilité themique annulle et interannuelle de l'océan Atlantique equatorial Est L. 'hypothésed'un é <<El Niño>> Atlantique. Oceanol. Acta, 3, 209-220.

Meyers, G., Dongug, J. R., and Reed, R. K., 1986: Evaporative cooling of the western equatorial Pacific Ocean by anomalous winds. Nature (London), 323, 523-526.

Molinari, R. L., Festa, J. F., and Marmolejo, E., 1985: Evolution of sea surface temperature in the tropical Atlantic Ocean during FGGE, 1979, II. Oceanographic fields and heat balance of the mixed layer. J. Mar. Res., 43, 67-81.

Morelet, 1983. J., 1980b: Sampling theory and wave propagation. NATO ASI Series, FI, Springer, pp 233-261.

Moura A. D., E. S. Sarachik, 1997: Seasonal-to-interannual climate prediction and applications: new institutions, new possibilities. WMO Bulletin, 46(4), 342-347.

Moura, A. D. and J. Shukla, 1981: On the dynamics of droughts in Northeast Brazil: Observation, theory, and numerical experiments with a general circulation model. J. Atmos. Sci., 38, 2653-2675.

Mulenga, H. M., 1998: Southern Africa climatic anomalies, summer rainfall and Angola low. PhD Thesis, Oceanography Department, University of Cape Town (Cape Town, South Africa), 261 pp.

Murtugudde, R., and A. J. Busalacchi, 1999: Interannual variability of the dynamics and thermodynamics of the tropical Indian Ocean. J. Climate, 12, 2300-2326.

Nicholson S. E. and J. P. Grist, 2001: A conceptual model for understanding rainfall variability in the West African Sahel on interannual and inter-decadal timescale. Int. J. Climatal., 21, 1733-1757.

Nicholson, S. E. and I. M. Palao, 1993: A re-evaluation of rainfall variability in the Sahel. Part I: Characteristics of rainfall fluctuations. Int. J. Climatol., 13, 371-289.

Nicholson, S. E., 1998: Interannual and decadal variability of rainfall over the Africa continent during the last two centuries. Water resources variability in Africa during XXth century. Proceeding of the Abidjan'98 Conference held at Abidjan, Cote D'Ivoire, November 1998, 107-116, IAHS Publ. No. 252.

Nicholson S. E., and D. Entekhabi, 1987: The nature of rainfall variability in equatorial and Southern Oscillation. Archiv fur Meteor. Geophys., Bioklimatologie, A 34, 311-348.

Nicholson, S. E., 1981: Rainfall and atmospheric circulation during drought periods and wetter years in West Africa. Mon. Wea. Rev., 109, 2191-2208.

Norquist, D. C., E. E. Recker, R. J. Reed, 1977: The energetics of African waves disturbances as observed during Phase III of Gate. Mon. Wea. Rev., 105, 334-342.

Palmer, T. N., 1999: The influence of the Atlantic, Pacific and Indian Ocean on Sahel rainfall. Nature, 322, 251-253.

Palmer, T. N., and D. L. T. Anderson, 1994: The prospects for seasonal forecasting. Quart. J. Roy. Meteor. Soc., 120, 755-793.

Palmer, T. N., C. Brankovic, P. Viterbo, and M. J. Miller, 1992: Modeling the interannual variation of summer monsoon. J. Climate, 5, 299-417.

Palmer 1986: Influence of Atlantic, Pacific, and Indian Oceans on Sahel rainfall. Nature, 322, 251-253.

Philander, S. G., 1990: El Niño, La Niña, and the Southern Oscillation. International Geophysical Series, vol. 46, Academic Press, 293 pp.

Poccard, I., S. Janicot, and P. Camberlin, 2000: Comparison of rainfall structures between NCEP/NCAR reanalysis and observed data over Tropical Africa. Climate Dynamics, 16,897-915.

Preisendorfer, R. W., 1988: Principal component analysis in meteorology and oceanography. Development in Atmospheric Science, 17. Elsevier, 425 pp.

Quinn, W. H., 1992: A study of southern oscillation-related climate activity 622-1990 incorporating Nile river flood data. In "El Nino: Historical and paleoclimate aspects of Southern Oscillation" ed. Diaz, H. F., and V. Markgraf, V, 119-142.

Reinhold, B. B., 1987: Weather regimes: the challenge: the challenge in the extended-range forecasting. Science, 235, 437-441.

Rowell, D. P., C.K. Folland, K. Maskell, J. A., and M. N. Ward, 1995: Variability of summer rainfall over tropical North Africa (1906-92): Observation and modelling. Quart. J. Roy. Meteor. Soc., 121, 669-704.

Rowell, D. P., C.K. Folland, and K. Maskell, J. A., and M. N. Ward, 1992: Modelling the influence of global sea surface temperatures on the variability and predictability of seasonal Sahel rainfall. Geophys. Res. Lett., 19, 905-908.

Ropelewski, C. F., and M. S. Halpert, 1987: Global and regional scale precipitation patterns associated with El Nino / Southern Oscillation. Mon. Wea. Rev., 115, 1606-26.

Ropelewski, C. F., and M. S. Halpert, 1989: Precipitation patterns associated with the high index phase of the Southern Oscillation. J. Climate, 2,268-284.

Rosati, A., K. Miyakoda and R. Gudgel, 1997: The impact of ocean initial conditions on ENSO forecasting with a coupled model. Mon. Wea. Rev., 125, 754-772.

Ross, R. S., 1991: Energetics of African wave disturbances derived from the FSU global spectral model. Meteor. Atmos. Phys., 45, 139-158.

Ruiz-Barradas, A., J. A. Carton and S. Nigam, 2000: Structure of interannual-to-decadal climate variability in the tropical Atlantic sector, J. Climate, 13, 3285-3297.

Saji, N.H., B.N. Goswami, P.N. Vinayachandran, and T. Yamagata, 1999: A dipole mode in the tropical Indian Ocean. Nature, 401, 360-363.

Saravanan, R., and P. Chang, 2000: Interaction between tropical Atlantic variability and El Nino-Southern Oscillation. J. Climate, submitted.

Schiller, A., J. S. Godfrey, P. C. McIntosh, G. Meyers, and R. Fielder, 2000: Interannual dynamics and thermodynamics of the Indo-Pacific Oceans. J. Phys. Oceanogr., 30,987-1012.

Seleshi, Y., 1996:Stochastic prediction of summer rainfall amount over the Northeast African Highlands and Indian Ocean. PhD thesis, Laboratory of

Sutton, R. T., S. P. Jewson, and D. P. Rowell, 2000: The elements of climate variability in the tropical Atlantic region. J. Climate, 13, 3261-3284.

UNEP, 2000: The GEO-2000 Global Environmental Outlook. http://www.grida.no/geo2000/english/0051.htm.

Vautard, R., G. Plaut, R. Wang, and G. Brunet, 1999: Seasonal Prediction of North American Surface air Temperatures using space–Time principal Components. J. Climate, 12, 380–394.

Venegas, S. A., 2001: Statistical methods for signal detection in climate. Danish Centre for Earth System Science, Niels Bohr Institute for Astronomy, Physics and Geophysics, University of Copenhagen, Denmark. 96 pp.

Venzke, S. M., M. Latif, and A Villwock, 2000: The coupled GCM ECHO-2. Part II: Indian Ocean Response to ENSO. J. Climate, 13, 1371-1387.

von Storch, H., and A. Navarra, 1995: Analysis of climate variability- Applications of statistical techniques. Springer-Verlag, 334 pp.

Tang, Y. and W.W. Hsieh, 2002: Neural-dynamic hybrid coupled model forecasts of the tropical Pacific sea surface temperatures. Experimental Long-Lead Forecast Bulletin, Vol. 11, Number 2, June, 2002.

Tang, T., W. W. Hsieh, A.H. Monahan and F.T. Tangang, 1998: Seasonal predictions of sea surface temperatures in the tropical Pacific - Comparing neural networks and canonical correlation analysis. J. Climate, submitted.

Tangang, F.T., B. Tang, A.H. Monahan, and W. W. Hsieh, 1998: Forecasting ENSO events: a neural network - extended EOF approach. J. Climate,11, 29-41.

Thorncroft, C. D., M. Blackburn, 1999: Maintenance of the African easterly jet Quart. J. Roy. Meteor. Soc., 125,763-786.

Thorncroft, C. D, and D. P. Rowell, 1998: Interannual variability of African wave activity in a GCM. Int. J. Climtol., 18, 1305-1323.

Thorncroft, C. D., 1995: An idealised study of African easterly waves. III. More realistic basic states. Quart. J. Roy. Meteor. Soc., 121, 1589-1614.

Thorncroft, C. D., and B. J. Hoskins, 1994: An idealised study of African easterly waves. I: A linear view. Quart. J. Roy., 120, 953-982.

Thompson, P. D., 1957: Uncertainty of initial state as a factor in the predictability of large-scale atmospheric flow patterns. Tellus, 9, 275-295.

Tourre, Y. M., B. R. Rajagopalan, and Y. Kushnir, 1999: Dominant patterns of climate variability in the Atlantic Ocean during the last 136. J. Climate, 12, 2285-2299.

Tourre, Y. M., and W. B. White, 1995: ENSO signals in global upper-ocean temperature. J. Phys. Oceanogr., 25, 1317-1332.

Tourre, Y. M., M.Decqué and J. F. Royer, 1985: Atmospheric response of a general circulation model forced by a sea surface temperature distribution analogous to winter 1982-1983 El Nino. Coupled Ocean-Atmosphere Models. J. C. J. Nihoul, ed.., Elsevier Publishers, 479-490.

Tseng, L., 1999: Interannual Variability of the Tropical Atlantic Climate and Its Relations to El Nino-Southern Oscillation. http://iri.columbia.edu/ outreach /meeting/TWWS1999/Li_san/Li_San.htm.

Tyson, P.D., W. Karlen, K. Holmgren and G. A. Heiss, 2000: The little Ice Age and medieval warming in South America. South African Journal of Science, 96, 121-126.

Tyson, P.D, 1991: Climatic change in Southern Africa: Past and present conditions and possible future scenarios. Climate Change, 18,241-258.

Wang G. and E. A. B. Eltahir, 1999: Use of information in the medium-and long-range forecasting of the Nile floods. J. Climate, 12, 1726-1737.

Wang, B., and Y. Wang, 1996: Temporal structure of southern oscillation as revealed by waveform and wavelet analysis. J. Climate, 9, 1586-1598.

Wanger, R. G., and A. da Silva,1994: Surface conditions associated with anomalous rainfall in the Guinea Coastal region. Int. J. Climatol., 14, 179—199.

Ward, M. N., 1998: Diagnosis and short-lead time prediction of summer rainfall in tropical North Africa at interannual and multi-decadal timescales. J. Climate, 11, 3167-3191.

Ward, M. N., C. K. Folland, K. Maskell, A. W. Colman, D. P. Rowell, K. B. Lane: 1997, Experimental seasonal forecasting of tropical rainfall at the U. K.

Meteorological Office. In "Prediction of Interannual climate variations" (Ed. Shukla). Springer-Verlag, Berlin.

Ward, M. N., 1992: Provisionally corrected surface wind data, worldwide ocean-atmosphere surface fields and Sahelian rainfall variability. J Climate, 5, 454-475.

WCRP, 1999: Climate research for Africa. World climate research programme, CLIVAR. WRCP Informal Report No. 16/1999. ICPO Publication Series No. 29.

WCRP, 1997: CLIVAR: A research programme on climate variability and predictability for the 21st Century. WCRP No. 101, WMO/TD No. 853, ICPO No. 10.

Webster, P. J., 2001: A general theory of monsoon regulation in the context of a coupled ocean-atmosphere-land system. Symposium on the Ocean-atmosphere Coupled Dynamics in Indian Ocean. Abstract. December 17-18, 2001. Tokyo Prince Hotel. Japan.

Webster, P.J., V.O. Magana, T.N. Palmer, J. Shukla, R.A. Tomas, M. Yanai, and T. Yasunari, 1998: Monsoons: Processes, predictability, and the prospects for prediction J. Geophys. Res., 103, no. c7.

Webster, P., 1983: Large-scale structure of the tropical atmosphere. 235-275. In "Large-scale Dynamical Processes in the Atmosphere" ed. B. J. Hoskins and R. P. Pearce. Academic Press.

Weickmann, K.M., W.A. Robinson and M.C. Penland, 2000: Stochastic and oscillatory forcing of global atmospheric angular momentum. J. Geophys. Res., 105, D12, 15543-15557.

Wells, N., 1988: The Atmosphere and Ocean: a physical introduction. Second edition, Jon Wiley & Sons Ltd., 394 pp.

White, W. B., 2001: Evidence of coupled Rossby Waves in the annual cycle of the Indo-Pacific Ocean. J. Phys. Oceanogr., 31, 2944-2957.

White, W. B., 2000: Coupled Rossby waves in the Indian Ocean on interannual timescale, J. Phys. Oceanogr., 30, 2972-2988.

Zebiak, S.E., 1993: Air-sea interaction in the equatorial Atlantic region. J. Climate, 6, 1567-1586.

Zeng, N., and J. D. Neelin, 2000: The role of vegetation-climate interaction and interannual variability in shaping the African savanna. J. Climate, 13, 2665-2670.

Zeng, N., J. D. Neelin, K. -M. Lau, and C.J. Tucker, 1999: Enhancement of interdecadal climate variability in the Sahel by vegetation interaction. Science, 286, 1537-1540.

Zeng, X., and E. A. B. Eltahir, 1998: The role of vegetation in the dynamics of West African monsoons. J. Climate, 11, 2078-2096.

Zeng, X., and E. A. B. Eltahir, 1997: The response to deforestation and desertification in a model of West African Monsoons. Geophys. Res. Lett., 24, 155-158.

Zhang, G. L., and N. A. Mcfarlane, 1995: Sensitivity of climate simulations to the parameterisation of cumulus convection on the Canadian Climate Centre general circulation model. Atmosphere-ocean, 33, 407-446.